Title
MATHEMATICAL MODELING AND OPTIMIZATION OF LIQUID-JUNCTION PHOTOVOLTAIC CELLS

Author
Orazem, M.E.

Publication Date
1983-06-01

Lawrence Berkeley Laboratory
UNIVERSITY OF CALIFORNIA

Materials & Molecular Research Division

MATHEMATICAL MODELING AND OPTIMIZATION OF LIQUID-JUNCTION PHOTOVOLTAIC CELLS

M.E. Orazem
(Ph.D. Thesis)

June 1983

Prepared for the U.S. Department of Energy under Contract DE-AC03-76SF00098

DISCLAIMER

Mathematical Modeling and Optimization of Liquid-Junction Photovoltaic Cells

Mark Edward Orazem

(Ph. D. thesis)

Materials and Molecular Research Division
Lawrence Berkeley Laboratory, and

Department of Chemical Engineering
University of California
Berkeley, California 94720

June 1983

To my parents
who fed my curiosity
and taught me to question

CONTENTS

ACKNOWLEDGEMENT

I greatly appreciate the training, support, and encouragement I received from my research director, Professor John Newman. I also appreciate the encouragement of the other members of the chemical engineering faculty at Berkeley, especially Professors Prausnitz, Radke, Hanson, Lynn, and Hess. It was a pleasure to work with Gloria Pelatowski, who traced the figures of this dissertation. I have enjoyed my education at Berkeley, and I leave with fond memories of the friends I have made here.

This work was supported by the United States Department of Energy under Contract Number DE-AC03-76SF00098 through the Director, Office of Energy Research, Office of Basic Energy Sciences, Chemical Sciences Division, and through the Assistant Secretary of Conservation and Renewable Energy, Office of Advanced Conservation Technology, Electrochemical Systems Research Division.

Chapter 1. Introduction

The liquid-junction photovoltaic cell is an electrochemical system with one or two semiconducting electrodes. This system has been studied since the early 1970's as a means of converting solar energy to chemical or electrical energy. Most of these studies have been oriented toward developing an understanding of the semiconductor electrode.

The design of a liquid-junction photovoltaic cell requires selection of an appropriate semiconductor-electrolyte combination as well as an efficient cell configuration. The selection of a semiconductor is based upon the band gap, which provides an upper limit to the conversion efficiency of the device, and the choice of electrolyte is governed by the need to limit corrosion. The objective of this work was to develop a mathematical model of the liquid-junction cell which could predict the effect of design parameters on cell performance. The one-dimensional model of the liquid-junction cell was coupled with primary resistance calculations to predict the effect of cell design on performance.

The one-dimensional mathematical model treats explicitly the semiconductor, the electrolyte, and the semiconductor-electrolyte interface in terms of potentials and concentrations of charged species. The model incorporates macroscopic transport equations in the bulk of the semiconductor and electrolyte coupled with a microscopic model of the semiconductor-electrolyte interface. Homogeneous and heterogeneous recombination of electron-hole pairs is included within the model. Recombination takes place at the semiconductor-electrolyte interface through interfacial sites, which can enhance the recombination rate. Surface sites at the semiconductor-metal interface were not included within

the model. The coupled nonlinear ordinary differential equations of the model were posed in finite-difference form and solved numerically.

The development of the mathematical model is presented in Chapter 2. The model is used to gain insight into the potential distribution of the system under equilibrium conditions and under illumination. The model is also used to show the effect of cell parameters such as kinetic limitations at the semiconductor-electrolyte interface, semiconductor thickness and dopant concentration, electrolyte resistance, and mass-transfer and kinetic limitations to current flow at the counterelectrode.

The design and optimization of photoelectrochemical cells is presented in Chapter 3. The performance of three cell configurations was calculated for operation under AM-2 solar illumination (882 W/m^2). The one-dimensional model of the liquid-junction cell was coupled with calculations of the primary resistance to current flow associated with two-dimensional systems. An economic analysis is presented based upon these results.

The primary resistance calculations for two of the three cell designs presented in Chapter 3 were based on previous work. The primary resistance and current distribution for a cell containing a slotted electrode is presented in Chapter 4. This work involves application of the Schwarz-Christoffel transformation coupled with numerical methods. An analytic approximation to the primary resistance is also presented.

Concepts of potential in electrochemical systems are discussed in Chapter 5. Various definitions of electrical potential are presented, and the use and measurement of these potentials are reviewed.

The equilibrated semiconductor is described in Chapter 6. This work involves development of statistical mechanical models of semiconductors,

with comparison of the Fermi energy to the electrochemical potential of electrons. The concentration dependence of activity coefficients for electrons and holes is developed based on the Fermi-Dirac distribution for electrons. Equilibrium relationships are presented for the semiconductor-electrolyte interface. This work allows calculation of concentration and potential variables under equilibrium conditions.

A review of experimental methods for characterization of photoelectrochemical cells is presented in Chapter 7. This work includes standard semiconductor characterization methods such as Hall, optical, and photodecay measurements.

A comparison of Maxwell's equations and dilute-solution transport equations is presented in Appendix A. The standard relationships for complex permittivity and index of refraction are also presented. The documentation for the computer programs is presented in Appendix B.

Chapter 2. Mathematical Modeling of Liquid-Junction Photovoltaic Cells

The liquid-junction photovoltaic cell is an electrochemical system with one or two semiconducting electrodes. This system has undergone intense study since the early 1970's as a means of converting solar energy to chemical or electrical energy.[1-8] A number of articles review the physics of the liquid-junction cell, the role of the semiconducting electrode, and the literature (see, e.g., references 9-19).

A mathematical model is presented here which treats explicitly all components of the liquid-junction photovoltaic cell. The results of the model, obtained through numerical computation, are used to gain insight into the cell behavior and into the factors influencing cell design.

1. INTRODUCTION

Semiconductors are characterized by the difference in energy between valence and conduction band electrons. Electrons can be transferred from the valence band to the conduction band by absorption of a photon with energy greater than or equal to the transition or band-gap energy. When the electron moves into the higher energy level, it leaves behind a vacancy in the valence band, or hole. Both the negatively charged electrons and the positively charged holes are mobile and can serve as charge carriers (see, e.g., Grove[20] or Sze[21]). In the presence of a potential gradient (or electric field), electrons and holes tend to migrate in opposite directions and thus can carry electrical current. In the absence of a potential gradient, electron-hole pairs produced by illumination recombine with no net flow of electrical current. Photovoltaic devices therefore require an equilibrium

potential gradient in the region of the semiconductor to be illuminated.

The potential gradient in a photovoltaic cell is created by forming an interface or junction with a semiconducting material. Metal-semiconductor, p-n semiconductor, and semiconductor-electrolyte interfaces are used in construction of photovoltaic cells.[22-24]

1.1. The Liquid-Junction Photovoltaic Cell

The interface in a p-n junction photovoltaic cell is constructed by doping the surface of an n or p-type semiconductor with atoms that invert the semiconductor type. These atoms are then thermally diffused into the host semiconductor to an optimal depth.[22-24] Diffusion rates in grain boundaries greatly exceed those in the bulk crystal; thus the need for a distinct boundary limits this technique to single-crystal host semiconductors. The junction between an electrolyte and a semiconductor, in contrast to the p-n junction, is formed spontaneously when the semiconductor is immersed in the electrolyte. The doping and diffusion processes are not needed, and polycrystalline semiconductors can be used.[8] The study of the liquid-junction photovoltaic cell is motivated by the ease of formation of a semiconductor-electrolyte interface and the possible use of relatively inexpensive thin-film polycrystalline semiconductors.

The performance of photoelectrochemical cells constructed with thin-film or polycrystalline semiconductors is strongly dependent upon the method of film formation and upon the surface preparation. Conversion efficiencies (incident solar illumination to electrical power) of 3 to 6.5 percent have been reported for cells using thin-film n-CdSe electrodes,[25-33] and a conversion efficiency of 5.1 percent has been achieved with a pressure-sintered polycrystalline CdSe photoelectrode.[34] A comparable

efficiency of 8.1 percent has been reported for a single-crystal CdSe electrode.[35] Conversion efficiencies of 0.038 to 0.3 percent have been reported for polycrystalline CdS films[36-38] as compared to 1.3 percent for single-crystal CdS.[35] Conversion efficiencies of up to 7.3 percent have been reported for polycrystalline n-GaAs films;[39-41] 12 percent has been reported for the single crystal n-GaAs.[42,43] The lower efficiency of the polycrystalline thin-film semiconductors, as compared to the single-crystal counterparts, is expected to be compensated by their lower cost.

The major disadvantage of the liquid-junction photovoltaic cell as compared to solid-state solar cells is the corrosion of the semiconductor electrode. Efficient conversion of solar energy requires a band gap between 1.0 and 2.0 eV,[11] and most semiconductors near this band gap corrode readily under illumination. Semiconductors with large band-gaps tend to be more stable but cannot convert most of the solar spectrum. Protective films, use of d-band semiconductors (MoS_2, $MoSe_2$, and WSe_2), and use of polychalcogenide redox couples (polysulfide, polyselenide, or polytelluride ions) have been proposed to reduce corrosion of small band-gap semiconductors. This work has been reviewed elsewhere.[5,8,13,14,17-19,44,45]

The principal elements of the liquid-junction photovoltaic cell, as shown in Figure 1, are the counterelectrode, the electrolyte, the semiconductor-electrolyte interface, and the semiconductor. Preferential adsorption of charged species (ionic species from the electrolyte and electrons from the semiconductor) at the semiconductor-electrolyte interface is accompanied by an equilibrium potential gradient in the semiconductor. Sunlight is absorbed within the semiconductor and causes generation of electron-hole pairs which are separated by the potential gradient. This separation leads

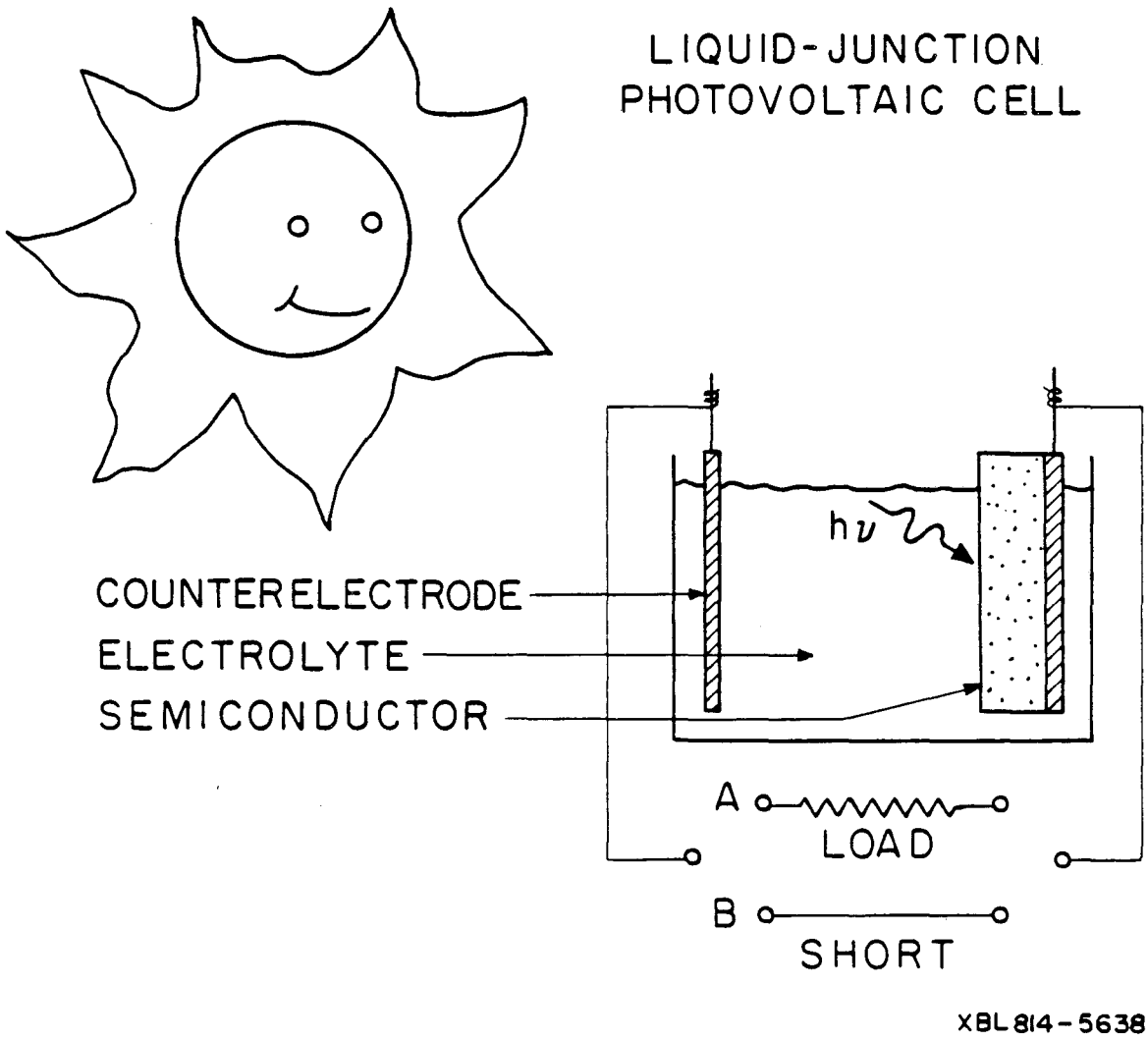

Figure 1. The liquid-junction photovoltaic cell.

to concentration and potential driving forces for electrochemical reactions at the semiconductor-electrolyte interface. The electrochemical reactions allow passage of electrical current through the cell.

1.2. Models of the Liquid-Junction Photovoltaic Cell

Development of a mathematical model constitutes an important step toward understanding the behavior and predicting the performance of the liquid-junction photovoltaic cell. Coupled phenomena govern the system, and the equations describing their interaction cannot, in general, be solved analytically. Two approaches have been taken in developing a mathematical model of the liquid-junction photovoltaic cell: approximate analytic solution of the governing equations and numerical solution.

1.2.1. Analytic approach. The semiconductor electrode is typically divided into three regions. Surface-charge and electron and hole-flux boundary conditions model the semiconductor-electrolyte interface. The region adjacent to the interface is assumed to be a depletion layer, in which electron and hole concentrations are negligible. The potential variation is therefore independent of hole and electron concentration in this region. Far from the interface a neutral region is defined in which the potential is constant; here electron and hole fluxes are driven only by diffusion.

The fundamental governing equations for the semiconductor, presented in section 2.2.1, are Poisson's equation and material balances for holes and electrons. Current-potential relationships are derived in the analytic approach by invoking assumptions appropriate to each region.

Integration of Poisson's equation in the depletion layer, for example, results in a depletion layer thickness W in terms of the voltage drop V

across the layer;

$$W = \left[\frac{2\varepsilon V}{F(N_d - N_a)}\right]^{1/2} \quad (1)$$

The depletion layer thickness is generally assumed to be independent of illumination. This assumption corresponds to an assumption that the potential distribution is independent of illumination and is therefore valid only for small photocurrents (less than 1 mA/cm^2). In addition, the assumption that the semiconductor can be separated into depletion and neutral regions restricts the voltage drop V to values high enough to deplete the majority carriers (electrons in an n-type semiconductor) in a region adjacent to the interface but small enough to avoid formation of an inversion layer (in which the concentration of minority carriers is significant). The assumptions used in the analytic models are invalid under many operating conditions in which the liquid-junction cell may be practical.

Several analytic current-voltage relationships have been derived which use the general approach described above and differ in their treatment of surface reactions and recombination within the depletion and neutral layers. Gartner[46] neglected recombination and thermal generation of carriers in the depletion region and neglected the effect of concentration limitations at the semiconductor-electrolyte interface. The Gartner model is frequently used to analyze experimental results.[47-49] Wilson[50,51] used the same approach but included surface recombinations. Albery *et al.*[52] extended the model of Gartner by including recombination of holes and electrons in the depletion layer. Reichman[53,54] presented a model which included recombination in the depletion region and kinetic limitation at the interface. Reiss[55] presented models for various cases, including within the

model the potential drop across the electrolyte double layer, surface recombination, and surface kinetic limitations. The semiconductor was divided into depletion and neutral regions, and the effect of illumination on cell potential was included as an additive photovoltage. Ahlgren[56] incorporated a Butler-Volmer reaction rate expression into the boundary conditions at the semiconductor-electrolyte interface. McCann and Haneman[57] included enhanced recombination associated with grain boundaries within the bulk of the semiconductor. The photovoltage was included in the calculation of the depletion region width. McCann *et al.*[58] used an analytic model to calculate the current-voltage characteristics of front and back-wall-illuminated liquid-junction cells.

Surface states and crystal imperfections have been found to play an important role in charge-transfer and redox reactions at the semiconductor-electrolyte interface.[59-65] Mathematical and conceptual relationships have been developed which describe electrochemical reactions at the semiconductor-electrolyte interface in terms of surface states and potentials (see, e.g., references 66-76). Electrochemical reaction via surface states has been included within an analytic model,[77] but this model is still limited by the restrictions described above.

Equivalent circuit models of the liquid-junction cell have been presented.[78-80] These models are useful in the analysis of impedance response measurements but suffer from a lack of clear physical interpretation.

1.2.2. Numerical approach. Use of a digital computer in the numerical solution of the equations governing the liquid-junction cell eliminates the need for restrictive assumptions. The numerical approach was taken in this

work and has been used in the modeling of solid-state devices.[81-86] Laser and Bard[87-90] developed a computer program which was used to calculate open-circuit photopotentials, the transient behavior of the system following charge injection, and the time dependence of photocurrents in liquid-junction cells. Time dependent material balances of holes and electrons and Poisson's equation described the semiconductor. The interface was included in terms of charge and flux boundary conditions. The model was limited by lack of convergence for electrode thicknesses greater than that of the space-charge region and did not treat explicitly the electrolyte and counterelectrode.

A number of computer programs related to the liquid-junction photovoltaic cell have been developed. Leary *et al.*,[91] for example, calculated carrier concentrations in polycrystalline films using a numerical solution of Poisson's equation coupled with overall charge neutrality within spherical grains. Their model was used for analysis of semiconductor gas sensors. A computer program has been presented by Davis and colleagues[92-94] which uses simultaneous calculation of surface and solution equilibrium states to obtain the equilibrium condition of electrical double layers.

2. MATHEMATICAL MODEL

The one-dimensional steady-state model presented in this section treats explicitly the semiconductor, the electrolyte, and the semiconductor-electrolyte interface in terms of potentials and concentrations of charged species. The effect of kinetic and mass-transfer limitations at the counterelectrode is included. The model can be used to gain an understanding of the behavior of the liquid-junction photovoltaic

cell and to predict and optimize cell performance.

2.1. Physical Description

A one-dimensional representation of the liquid-junction photovoltaic cell is presented in Figure 2. This model includes macroscopic representations of the counterelectrode, the electrolytic solution, and the semiconductor coupled with a microscopic representation of the interface between the semiconductor and the solution. The semiconductor-electrolyte interface couples the macroscopic equations which govern the adjacent bulk phases.

The interface is represented by four planes, inner and outer Helmholtz planes on the electrolyte side of the interface and inner and outer surface states on the semiconductor side. The outer Helmholtz plane (OHP) is the plane of closest approach for (hydrated) ions associated with the bulk solution. The inner Helmholtz plane (IHP) passes through the center of ions specifically adsorbed on the semiconductor surface. The outer surface state (OSS) represents the plane of closest approach for electrons (and holes) associated with the bulk of the semiconductor. The inner surface state (ISS) is a plane of surface sites for adsorbed electrons.

This model of the semiconductor-electrolyte interface is an extension of the classical diffuse double-layer theory.[95-97] Charge adsorbed onto the IHP and the ISS planes is balanced by charge in the diffuse region of the electrolyte and the space-charge region of the semiconductor. The net charge of the interface, including surface planes and diffuse and space-charge regions, is equal to zero.

Within the model, single-step reactions relate concentrations and potentials at interfacial planes. A continuous spectrum of energy levels at

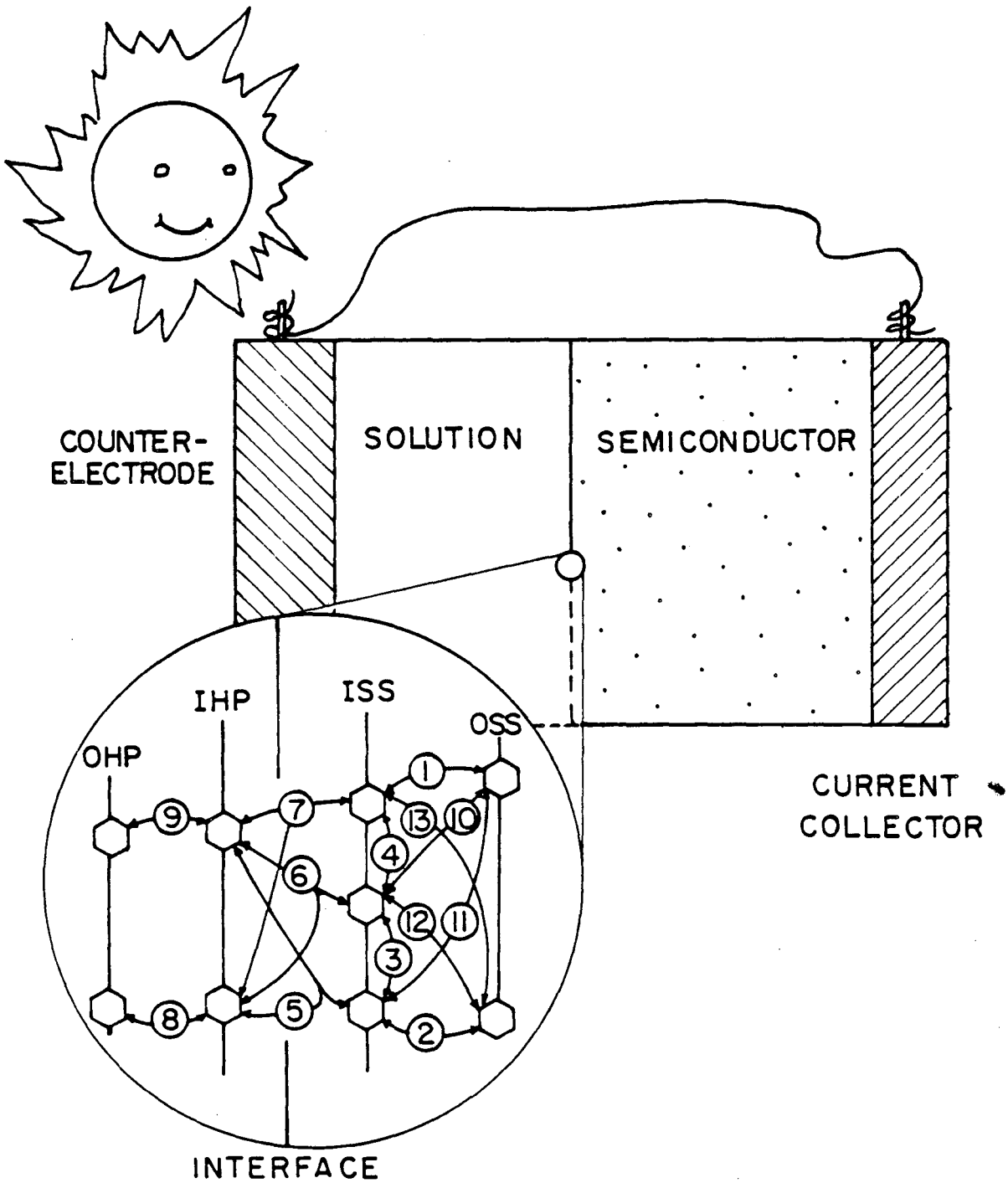

XBL 835-9621

Figure 2. Mathematical model of the liquid-junction photovoltaic cell.

the ISS is represented by three discrete energy levels (designated v, t, and c). Conduction electrons are adsorbed via reaction 1 (see INTERFACE in Figure 2) from the OSS to high-energy sites at the ISS, via reaction 10 to intermediate-energy sites at the ISS, and via reaction 11 to low-energy sites at the ISS. Via reaction 2, low-energy electrons at the ISS can occupy vacancies in the valence band, or holes, at the OSS. Intermediate-energy electrons can transfer from the ISS to the OSS through reaction 12 and high-energy electrons can transfer through reaction 13. Reactions 3 and 4 allow the shifting of electrons from one energy level to another.

Ionic species from the solution are adsorbed onto the IHP by reactions 8 and 9. Two adsorbed species are considered here. It is assumed that other ionic species in the solution do not adsorb and do not participate in the electrochemical reactions. Relaxation of this assumption involves the inclusion of additional ion-adsorption and charge-transfer reactions. Reactions 5, 6, and 7 are the charge-transfer reactions that take place among adsorbed ions at the IHP and adsorbed high, intermediate, or low-energy electrons at the ISS. Charge-transfer reactions allow passage of electrical current from the semiconductor to the solution.

2.2. Theoretical Development

The equations governing the liquid-junction photovoltaic cell in the dark or under steady-state illumination are developed here in terms of the model presented above. The governing relationships can be developed separately for the semiconductor and the electrolyte. The microscopic model of the semiconductor-electrolyte interface couples the equations governing the macroscopic systems.

2.2.1. Semiconductor. The electrochemical potential of a given species can arbitrarily be separated into terms representing a reference state, a chemical contribution, and an electrical contribution.

$$\mu_i = \mu_i^{\phi} + RT\,ln(c_i f_i) + z_i F\Phi\,, \tag{2}$$

where Φ is a potential which characterizes the electrical state of the phase and can be arbitrarily defined. The potential used here is the electrostatic potential which is obtained through integration of Poisson's equation.[98] Equation (2) can be viewed as the defining equation for the activity coefficient, f_i.

The flux of an individual species within the semiconductor is driven by a gradient of electrochemical potential, which corresponds to gradients of potential and concentration (see, e.g., chapter 11 in reference (99) and Gerischer[69]). Under the assumption that the individual ionic activity coefficients are constant with a value of one,* the flux of holes is given by

$$N_{h^+} = -u_{h^+} F\,p\,\frac{d\Phi}{dy} - D_{h^+}\frac{dp}{dy}\,, \tag{3}$$

and the flux of electrons by

$$N_{e^-} = u_{e^-} F\,n\,\frac{d\Phi}{dy} - D_{e^-}\frac{dn}{dy}\,. \tag{4}$$

The concentrations of electrons and holes are represented by n and p, respectively, and the mobilities u_i are related to the diffusivities D_i by the Nernst-Einstein equation

$$D_i = RTu_i\,. \tag{5}$$

Homogeneous reaction takes place in the semiconductor; thus a

* The assumption of constant activity coefficients, valid for dilute solutions, is appropriate for most semiconductors. The carrier concentrations in semiconductors is usually less than 0.0001 M, which is low as compared to dilute aqueous solutions. The assumption of constant activity coefficients is in harmony with a Boltzmann distribution of electrons and holes. Use of Fermi-Dirac distributions for these charged species results in activity coefficients that are functions of concentration (see Chapter 6).

material balance for a given species, say holes,** yields

$$\frac{dN_{h^+}}{dy} = R_{h^+} , \tag{6}$$

where R_{h^+} is the net rate of production of holes under steady-state conditions.

The rate of production of holes is, by stoichiometry, equal to the rate of production of electrons and is governed by three concurrent processes: generation by absorption of light, generation by absorption of heat, and recombination of electrons and holes (i.e., transfer of an electron from the conduction band to the valence band).

$$R_{h^+} = G_L + G_{th} - R_{rec} . \tag{7}$$

Mathematical models of the homogeneous recombination process have been developed which incorporate single-step electron transfer from one energy level to another. They differ in the assumption of the presence or absence of impurities within the semiconductor which allow electrons to have energies between the conduction and valence-band energies.[100,101]

Band-to-band kinetic models (presented in Figure 3) allow electrons to have only valence or conduction-band energies. Absorption of the appropriate amount of thermal or electromagnetic energy creates an electron-hole pair; recombination of an electron and a hole releases energy in the form of heat or light. The band-to-band model yields

$$R_{h^+} = \eta m q_0 e^{-my} - k_{rec}(np - n_i^2) , \tag{8}$$

where η is the fraction of incident photons with energy greater than the

---

** The development presented here, while applicable to p-type semiconductors, is oriented toward analysis of an n-type semiconductor in which holes are the minority carrier. Material balances of holes and electrons are not independent, and conservation of the minority carrier was chosen to improve the numerical computational accuracy.

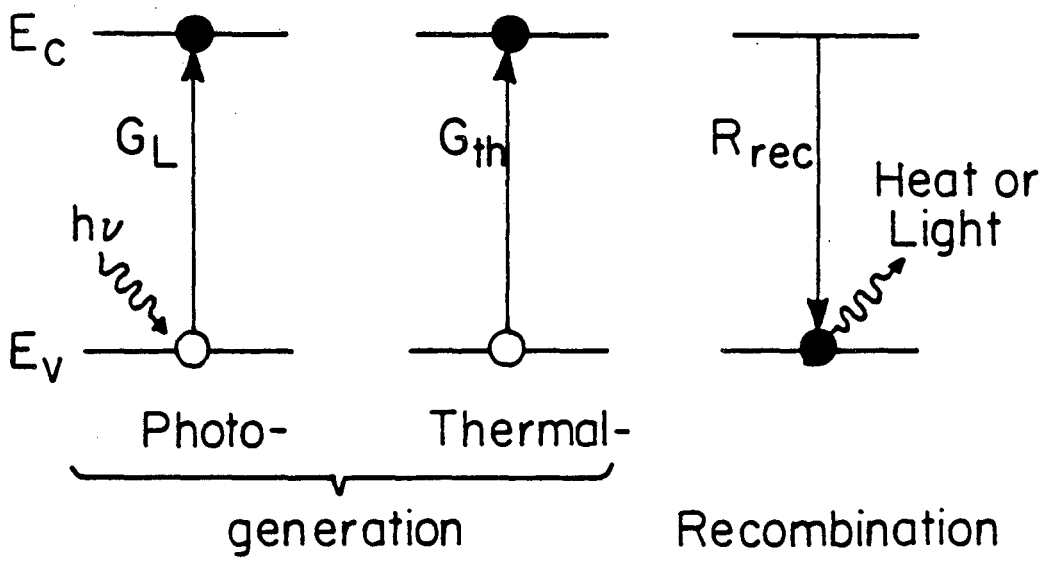

Individual Reaction Rates

$$G_L = \epsilon m q_0 e^{-mx}$$

$$G_{th} = k_{th}(N_c - n)(N_v - p)$$

$$R_{rec} = k_{rec}\, np$$

XBL 831-5023

Figure 3. Schematic representation of band-to-band recombination kinetics in the semiconductor.

band gap energy, m is the absorption coefficient, q_o is the incident solar flux, and n_i is the intrinsic concentration,

$$n_i = \left[\frac{k_{th}(N_c - n)(N_v - p)}{k_{rec}}\right]^{1/2}. \tag{9}$$

The intrinsic concentration is written in terms of N_c and N_v, the number of available conduction and valence-band sites respectively, and k_{th} and k_{rec}, thermal generation and recombination rate constants. Under equilibrium conditions, the rate of thermal generation is equal to the rate of recombination, and $np = n_i^2$.

Most semiconducting materials contain impurities or imperfections within their lattice structure which may be described as fixed sites with valence-band electron energies within the semiconductor band gap. The trap-kinetics model allows recombination to occur through these sites (see Figure 4). Absorbed radiation drives an electron from the valence band to the conduction band, and all recombination and thermal generation reactions are assumed to occur through trap sites. This model results in

$$R_{h^+} = \eta m q_o e^{-my} - \frac{N_t k_2 (np - n_i^2)}{\dfrac{k_1(N_v - p) + k_3(N_c - n)}{k_4} + \dfrac{k_2}{k_4} p + n}, \tag{10}$$

where k_1, k_2, k_3, and k_4 are the rate constants for the corresponding reactions shown in Figure 4. The intrinsic concentration is given by

$$n_i = \left[\frac{k_1 k_3 (N_v - p)(N_c - n)}{k_2 k_4}\right]^{1/2}. \tag{11}$$

The electron and hole concentrations are generally small as compared to the respective conduction and valence-band site concentrations. The intrinsic concentration is therefore constant, and the reaction rate can be characterized with three lumped rate constants ($N_t k_2$, $(k_1 N_v + k_3 N_c)/k_4$, and k_2/k_4). Homogeneous electron-hole recombination was assumed in the

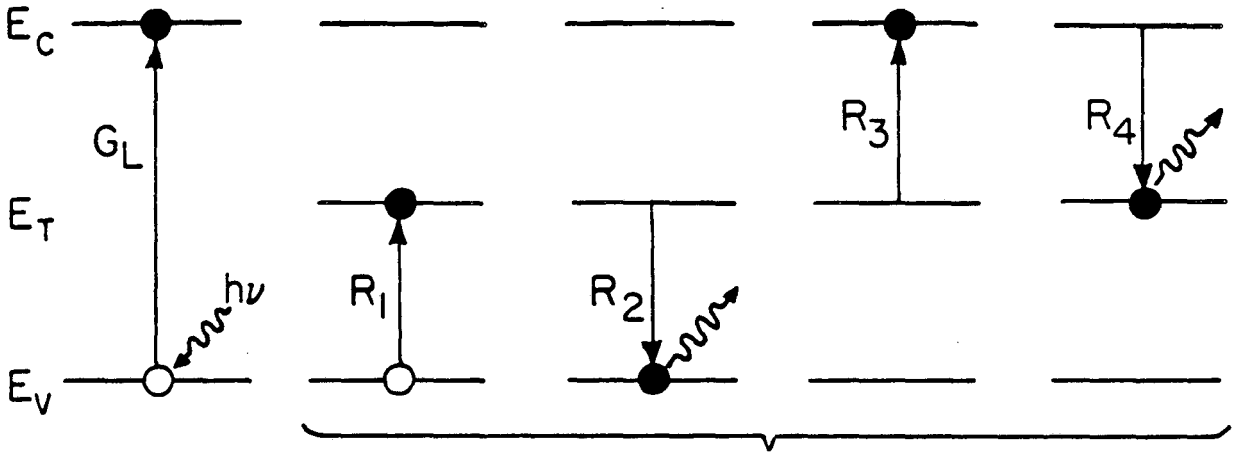

Thermal Generation and Recombination Through Trap Sites

Individual Reaction Rates

$$G_L = \epsilon m q_0 e^{-mx}$$

$$R_1 = k_1(N_V - p)(N_T - n_T)$$

$$R_2 = k_2 n_T p$$

$$R_3 = k_3 n_T (N_C - n)$$

$$R_4 = k_4 n (N_T - n_T)$$

XBL 831-5024

Figure 4. Schematic representation of single-trap recombination kinetics in the semiconductor.

mathematical model to occur through trap sites (equations (10) and (11)).

The expressions for the intrinsic concentration (equations (9) and (11)) are consistent with the expression derived through statistical-mechanical models (see equation (32) of Chapter 6). The intrinsic concentration can be considered to be a constant for a given semiconductor only if the ratios n / N_c and p / N_v are negligibly small as compared to unity. This condition is consistent with the assumption of unity activity coefficients for electrons and holes. The value of the intrinsic concentration derived from statistical-mechanical arguments serves as a relationship among the kinetic parameters in equations (9) and (11).

The divergence of the current is zero at steady state; therefore the fluxes of holes and electrons are related by

$$\frac{dN_{e^-}}{dy} - \frac{dN_{h^+}}{dy} = 0 \,. \tag{12}$$

A material balance on electrons, analogous to equation (5), could be used to replace equation (12).

Poisson's equation,

$$\frac{d^2\Phi}{dy^2} = - \frac{F}{\varepsilon_{sc}}[\, p - n + (N_d - N_a)] \,, \tag{13}$$

relates the potential to the charge distribution. The concentrations of ionized electron donors and acceptors are represented by N_d and N_a, respectively. The Debye length,

$$\lambda_{sc} = [\varepsilon_{sc} RT / F^2 (N_d - N_a)]^{1/2} \,,$$

characterizes the distance over which the potential varies in the semiconductor. It typically has a value of 1×10^{-6} to 2×10^{-5} cm.

The degree of ionization of donors or acceptors is dependent upon the concentrations of charged species within the semiconductor and upon the

temperature. Complete ionization has been assumed in this work. This assumption is reasonable at room temperatures and is consistent with the assumption of unity activity coefficients.

2.2.2. Electrolyte. For a one-dimensional case, neglecting convective effects, the flux of an ionic species is governed by potential and concentration gradients.

$$N_i = - z_i u_i c_i F \frac{d\Phi}{dy} - D_i \frac{dc_i}{dy} . \tag{14}$$

Under the assumption that homogeneous reactions do not take place, conservation of mass yields a uniform flux at steady-state, i.e.,

$$\frac{dN_i}{dy} = 0 . \tag{15}$$

The potential and concentrations of charged species are related by Poisson's equation,

$$\frac{d^2\Phi}{dy^2} = - \frac{F}{\varepsilon_{sol}} \sum_i z_i c_i . \tag{16}$$

Electroneutrality of the electrolyte is not assumed here because the diffuse region near the interface plays an important role in the microscopic model of the interface. The Debye length in the solution is given by

$$\lambda_{sol} = [\varepsilon_{sol} RT / F^2 \sum_i z_i^2 c_{i,\infty}]^{1/2}$$

and typically has a value of 1×10^{-8} to 1×10^{-7} cm.

The relationships presented above are sufficient to describe the electrolytic solution. An additional relationship yields the current density as a function of the ionic fluxes,

$$i = F \sum_i z_i N_i . \tag{17}$$

Within the semiconductor, this can be regarded as an integrated form of equation (12).

2.2.3. Semiconductor-electrolyte interface. A general interfacial reaction can be expressed as

$$\sum_i s_i M_i^{z_i} \rightarrow ne^- , \tag{18}$$

where s_i is the stoichiometric coefficient of species i, M_i is a symbol for the chemical formula of species i, and n is the number of electrons transferred. (See chapter 8 in reference (99).) For single-step reactions, n is equal to one.

The rate of a single-step reaction l at the interface is given by

$$\begin{aligned} r_l = k_{f,l} \exp\left[\frac{(1-\beta_l)F\Delta\Phi_l}{RT}\right] \prod_i c_i^{p_{i,l}} \\ - k_{b,l} \exp\left[\frac{-\beta_l F\Delta\Phi_l}{RT}\right] \prod_i c_i^{q_{i,l}} , \end{aligned} \tag{19}$$

where β_l is a symmetry factor (usually assumed to be equal to 1/2), $k_{f,l}$ and $k_{b,l}$ are forward and backward reaction rate constants, respectively, and $\Delta\Phi_l$ is the potential driving force for the given reaction, l. The potential driving force enters into reactions involving charge transfer from locations of one potential to locations of another.

The reaction orders for a given species i in the forward and reverse directions are $p_{i,l}$ and $q_{i,l}$ respectively. They are determined from the stoichiometric coefficients, $s_{i,l}$:

$$\begin{aligned} &\text{If } s_{i,l} = 0; \quad p_{i,l} = 0, \quad \text{and } q_{i,l} = 0. \\ &\text{If } s_{i,l} > 0; \quad p_{i,l} = s_{i,l}, \text{ and } q_{i,l} = 0. \\ &\text{If } s_{i,l} < 0; \quad p_{i,l} = 0, \quad \text{and } q_{i,l} = -s_{i,l}. \end{aligned}$$

The reaction rates are written in terms of the equilibrium constants as

$$r_l = k_{b,l}\left\{K_l \exp\left[\frac{(1-\beta_l)F\Delta\Phi_l}{RT}\right]\prod_i c_i^{p_{i,l}} - \exp\left[\frac{-\beta_l F\Delta\Phi_l}{RT}\right]\prod_i c_i^{q_{i,l}}\right\}. \tag{20}$$

The equilibrium constant used here is the ratio of the forward and backward rate constants:

$$K_l = \frac{k_{f,l}}{k_{b,l}}. \tag{21}$$

Six of the thirteen equilibrium constants are independent and can be calculated as functions of equilibrium interfacial concentrations and potentials.

$$K_l = \exp[-\frac{F}{RT}\Delta\Phi_l]\prod_i c_i^{-s_{i,l}}. \tag{22}$$

A discussion of the calculation of equilibrium concentrations and potentials and the subsequent calculation of equilibrium constants is presented elsewhere (see Chapter 6). The remaining constants can be calculated from equation (22) or from the following identities:

$$K_4 = \frac{K_3(N_d - N_a)^2}{K_1 K_2 n_i^2}, \tag{23a}$$

$$K_6 = K_5 / K_3, \tag{23b}$$

$$K_7 = K_6 / K_4, \tag{23c}$$

$$K_{10} = K_1 K_4, \tag{23d}$$

$$K_{11} = K_{10} / K_3, \tag{23e}$$

$$K_{12} = K_2 / K_3, \tag{23f}$$

and

$$K_{13} = K_{12} K_4. \tag{23g}$$

Within the parametric studies which follow, one independent rate constant is assumed to be characteristic of each of four groups of interfacial reactions. The four groups, shown in Figure 2, are reactions 1, 2, 10, 11, 12, and 13 (OSS-ISS), reactions 3 and 4 (ISS), reactions 5, 6, and 7 (ISS-IHP), and reactions 8 and 9 (IHP-OHP). The individual rate constants for each reaction l are related to the characteristic rate constant by

$$k_{b,l} = k_l^0 K_l^{-\beta} \tag{24}$$

and

$$k_{f,l} = k_{b,l} K_l = k_l^0 K_l^{1-\beta}, \tag{25}$$

where k_l^0 is the pre-exponential part of the rate constant, with a characteristic value for a given reaction type, and β was given a value of one half. These equations are consistent with equations (20) and (21).

Material balances govern the interface under steady-state conditions. These are expressed by continuity of flux at the OSS and the OHP,

$$N_{e^-}\Big|_{oss} = \sum_l -s_{e^-,l} r_{l,iss}\ , \tag{26}$$

$$N_{h^+}\Big|_{oss} = \sum_l -s_{h^+,l} r_{l,iss}\ , \tag{27}$$

and

$$N_i\Big|_{ohp} = \sum_l -s_{i,l} r_l\ ; \tag{28}$$

and material balances for each adsorbed species i at the ISS and the IHP,

$$\sum_l s_{i,l} r_{l,iss} = 0\ , \tag{29}$$

and

$$\sum_l s_{i,l} r_{l,ihp} = 0\ . \tag{30}$$

Gauss's law can be applied to the region between the OSS and ISS:

$$(\Phi_{oss} - \Phi_{iss}) = \frac{\delta_1}{\varepsilon_{sc}} \left[\frac{\varepsilon_2}{\delta_2}(\Phi_{iss} - \Phi_{ihp}) + F(\sum_{iss}\gamma_i - q^+_{iss}) \right], \quad (31)$$

and between the ISS and the IHP:

$$(\Phi_{iss} - \Phi_{ihp}) = \frac{\delta_2}{\varepsilon_2} \left[\frac{\varepsilon_{sol}}{\delta_3}(\Phi_{ihp} - \Phi_{ohp}) - F(\sum_{ihp} z_i \gamma_i) \right]. \quad (32)$$

The evaluation of Gauss's law in the region between the OSS and the ISS includes a term for a fixed positive charge at the ISS, q^+_{iss}, which was set equal to zero in this study.

2.2.4. Boundary conditions. The semiconducting electrode is bounded at one end by the electrolyte and at the other end by a metallic current collector. The boundary conditions at the semiconductor-electrolyte interface are incorporated into the model of the interface. The boundary conditions at the semiconductor-current collector interface are that the potential is zero, the potential derivative is equal to a constant, determined by the charge assumed to be located at the semiconductor-current collector interface (this constant was set equal to zero in this study), and all the current is carried by electrons (the flux of holes is zero). The boundary conditions in the electrolytic solution are set a fixed distance (10 Debye lengths) from the interface. This distance may be considered to be a diffusion layer. The boundary conditions are that the potential gradient is continuous and that all concentrations have their bulk value.

2.2.5. Counterelectrode. In the region sufficiently far from the interface that electroneutrality holds, the potential distribution is linear and is a function of current density. The potential drop in the region between the counterelectrode and the outer limit of the diffusion layer is given by

$$V_{IR} = \frac{Li}{\kappa}, \tag{33}$$

where κ is the solution conductivity and L is the distance between the counterelectrode and the outer edge of the diffusion layer. The conductivity of dilute solutions is related to ionic mobilities and concentrations by

$$\kappa = F^2 \sum_i z_i^2 u_i c_i . \tag{34}$$

The potential drop across the counterelectrode-electrolyte interface is given by

$$V_{CE} = V_{CE}^0 + \eta_{CE} , \tag{35}$$

where V_{CE}^0 is the equilibrium potential drop across the interface and η_{CE} is the total counterelectrode reaction overpotential. The total overpotential is related to the current density through the Butler-Volmer reaction model;[99,102]

$$i = i_o \left\{ \left[1. - \frac{i}{i_{4,lim}} \right] \exp\left[\frac{(1-\beta)nF}{RT} \eta_{CE} \right] - \left[1. + \frac{i}{i_{3,lim}} \right] \exp\left[- \frac{\beta n F}{RT} \eta_{CE} \right] \right\}, \tag{36}$$

where i_o is the exchange current density associated with the bulk concentrations of reactants, $i_{k,lim}$ is the diffusion-limited current density associated with species k, and n is the number of electrons transferred in the counterelectrode reaction.

2.2.6. Numerical method. The coupled, nonlinear equations presented for the liquid-junction cell were solved numerically for the cell under equilibrium and steady-state conditions.[103] The equations were properly linearized, posed in finite-difference form, and solved using Newman's BAND

method,[104] coupled with Newton-Raphson iteration. Calculation of a current-potential curve involved iterative solution of the system of coupled equations for input values of solar illumination and current density.

3. RESULTS

Computed results for the mathematical model of the liquid-junction photovoltaic cell are presented in the following section. The parameter values chosen for the model are consistent with an n-type GaAs anode in contact with an 0.8 M K_2Se, 0.1 M K_2Se_2, 1.0 M KOH solution. The redox couple was assumed to be Se_2^{2-}/Se^{2-}, and the semiconductor was illuminated at the semiconductor-electrolyte interface. Input parameter values are as presented in Tables 1 through 3 unless stated otherwise. Dependent parameters calculated from the input data are presented in Table 4.

The n-type GaAs system was chosen for analysis to allow comparison to the experimental work of Heller and Miller.[8,42,43] Their cell achieved a 12 percent power efficiency based upon incident radiation, an open circuit potential of 0.7 volts, and a closed circuit current of 24 mA/cm^2. A description of their experimental electrodes, cell, and measuring techniques is presented in reference (35). The counterelectrode area was 50 times that of the semiconductor. The Se_2^{2-}/Se^{2-} redox couple was chosen to limit the corrosion of GaAs under 1000 W/m^2 illumination to a few micrometers per year (approximately 0.04 mA/cm^2).[105-107]

The discussion of the effect of kinetic, bulk semiconductor, and interfacial parameters does not include the effect of IR drop in the electrolyte or kinetic and mass-transfer limitations at the counterelectrode (see section 2.2.5). The contribution of these phenomena is discussed in section 3.4.1.

Table 1. Input Parameters for the Semiconductor

Semiconductor: n-GaAs		
Valence band site concentration	N_v	1.16×10^{-5} mol/cm^3
Conduction band site concentration	N_c	7.80×10^{-7} mol/cm^3
Band gap	E_g	1.4 eV
Dopant concentration	$N_d - N_a$	9.96×10^{-8} equiv/cm^3
Electron diffusivity	D_{e^-}	222.0 cm^2/s
Hole diffusivity	D_{h^+}	6.46 cm^2/s
Permittivity	ε_{sc}	1.06×10^{-12} C/V-s
Solar absorption coefficient	m	4.40×10^{-5} cm^{-1}
Solar spectrum efficiency	η	0.3735
Total incident radiation (AM-2)	q_o	7.139×10^{-7} mol/cm^2-s
Homogeneous recombination rate constants:	$N_t k_2$	1.89×10^9 s^{-1}
	$(k_1 N_v + k_3 N_c)/k_4$	100.
	k_2/k_4	2.56×10^{-3} cm^3/mol

Table 2. Input Parameters for the Semiconductor-Electrolyte Interface

ISS site	k	v	t	c	
ISS site energy	E_k	1.3	1.4	1.5	eV
ISS site density	γ_k	0.3334	0.3333	0.3333	

Total ISS site concentration	Γ_{iss}	4.019×10^{-12} mol/cm^2
Total IHP site concentration	Γ_{ihp}	1.200×10^{-13} mol/cm^2
IHP adsorption energy	ΔE_3	0.0 J/mol
	ΔE_4	0.0 J/mol
Equilibrium OSS potential	Φ_{oss}	5.93 mV
Equilibrium charge on interface		-0.1298 μC/cm^2
Distance between OSS and ISS	δ_1	1.0×10^{-8} cm
Distance between ISS and IHP	δ_2	2.0×10^{-8} cm
Distance between IHP and OHP	δ_3	2.0×10^{-8} cm
Permittivity between ISS and IHP	ε_2	6.93×10^{-12} C/V-cm
Rate constants:		
(OSS-ISS)	k_{etr}	1.0×10^{25} cm^3/mol-s
(ISS)	k_{sft}	1.0×10^{29} cm^2/mol-s
(ISS-IHP)	k_{cht}	1.0×10^{29} cm^2/mol-s
(IHP-OHP)	k_{ads}	1.0×10^{23} s^{-1}

Table 3. Input Parameters for the Electrolyte

Electrolyte: 0.8 M K_2Se, 0.1 M K_2Se_2, 1.0 M KOH						
Species index	k	1	2	3	4	
Species		K^+	OH^-	Se_2^{2-}	Se^{2-}	
Charge number	z_k	+1	-1	-2	-2	
Bulk concentration	$c_{k,\infty}$	0.0028	0.0010	0.0001	0.0008	mol/cm^3
Diffusivity (x10^5)	D_k	1.957	5.260	1.000	1.000	cm^2/s
Permittivity		ε_{sol}			6.930x10^{-12}	C/V-cm
Conductivity		κ			0.3	$(\Omega\text{-cm})^{-1}$
Temperature		T			300.	K

Table 4. Values Calculated from Input Parameters

Semiconductor:		
Fermi level	E_f	1.347 eV
Intrinsic concentration	n_i	5.228×10^{-18} mol/cm^3
Minority carrier diffusion length	L_p	5.846×10^{-4} cm
Debye length	λ_{sc}	1.689×10^{-6} cm
Electrolyte:		
Debye Length	λ_{sol}	1.967×10^{-8} cm

3.1. Interfacial Kinetic Limitations

The values of the interfacial rate constants can affect the open-circuit cell potential, the value of the limiting current, and the shape of the current-potential curve. Most (>99 percent) of the recombination under open-circuit illumination occurs at the interface. Homogeneous recombination is included in the model but does not play a major role for the range of parameters studied.

3.1.1. Ion-adsorption reactions. Current-potential curves are presented in Figure 5 with the interfacial rate constant for adsorption and desorption of ions onto the inner Helmholtz plane as a parameter (reactions 8 and 9 in Figure 2). In each case the cell potential is a maximum at open circuit (700.5 mV) and decreases as the anodic current increases. A limiting current is observed due to limitations of mass transfer and generation of holes in the semiconductor.

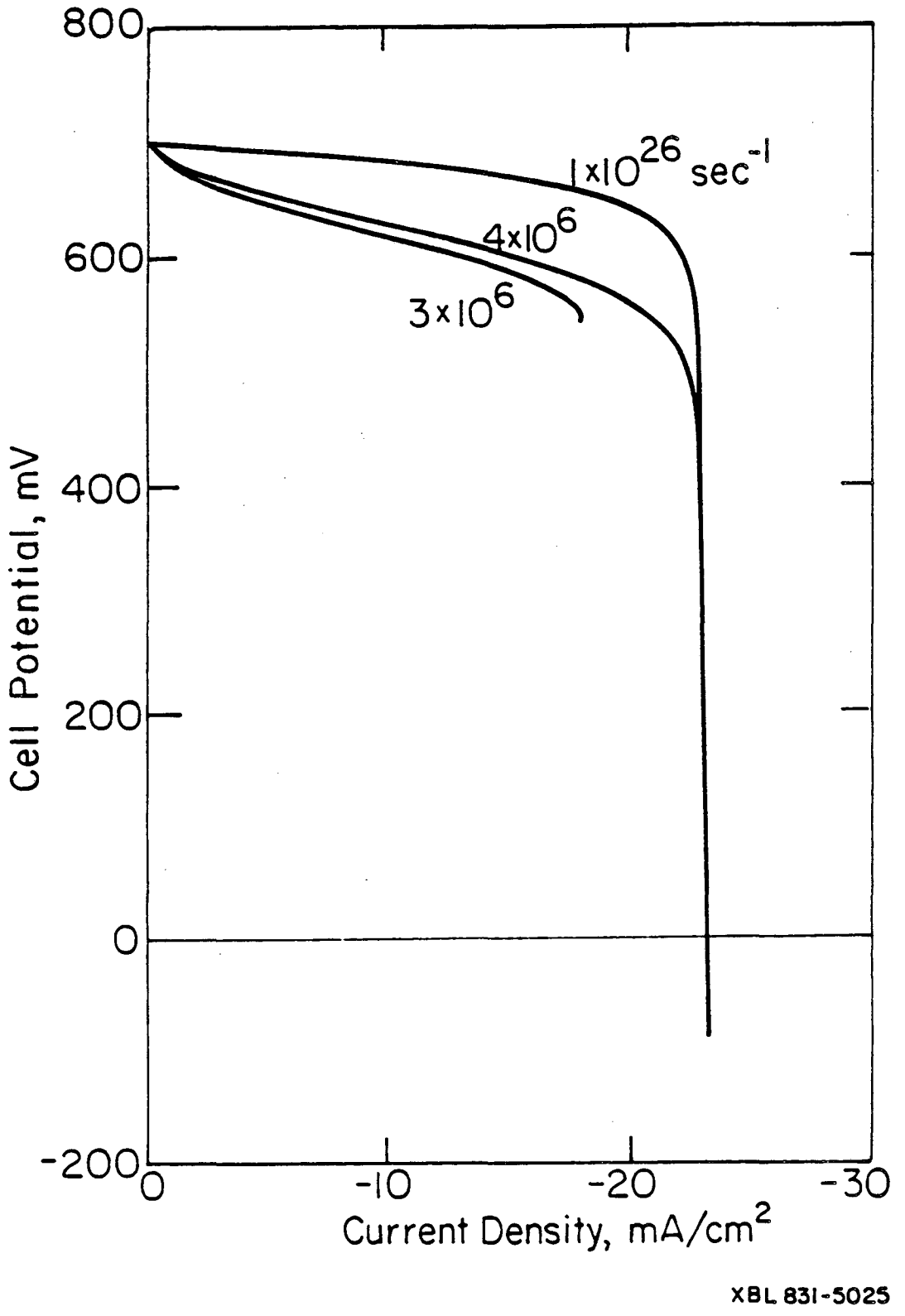

Figure 5. Computer current-potential curves for an n-type GaAs Anode with ion-adsorption rate constant as a parameter.

The ion-adsorption rate constant influences the limiting current and the shape of the current-potential curve. A dramatic decrease in the maximum power obtained from this system is observed for the cases with small ion-adsorption rate constants. Kinetic limitations to ion adsorption are seen to have a major effect on cell performance. Insight into the effect of these kinetic limitations can be obtained by comparing the potential distribution at several points along the current-potential curve for a system with no kinetic limitations (large rate constants) to the related potential distributions for a system with kinetic limitations to ion adsorption.

The potential distribution for the case with no kinetic limitations is presented in Figure 6. In the dark, at open-circuit, (curve a) the system is equilibrated. The potential is nearly constant throughout the solution and the interfacial planes (OHP, IHP, ISS, and OSS). The potential varies in the semiconductor in response to charge distributed in the semiconductor. This variation of electrical potential in the equilibrated semiconductor is termed "band-bending." The difference in potential between the front (semiconductor-electrolyte interface) and the back (current collector-semiconductor interface) of the semiconductor is the "flat-band potential." (This is the potential that would need to be applied in order to achieve uniform potential in the semiconductor.)

Under illumination at open circuit (curve b) the concentrations of electrons and holes increase, and the variation of potential in the semiconductor decreases. The decrease in potential variation in response to illumination is referred to as the "straightening of the bands." The charges of holes and electrons, generated by the illumination, tend to go in opposite directions under the influence of the electric field. Their

Figure 6. Potential distribution for the liquid-junction cell with no kinetic limitations ($k_{ads} = 1.0 \times 10^{26}\ s^{-1}$). Curve a, open circuit in the dark; curve b, open circuit under illumination; and curve c, near short circuit ($i = -23.1\ mA/cm^2$) under illumination. $\lambda_{sc} = 1.689 \times 10^{-6}$ cm, and $\lambda_{sol} = 1.967 \times 10^{-8}$ cm.

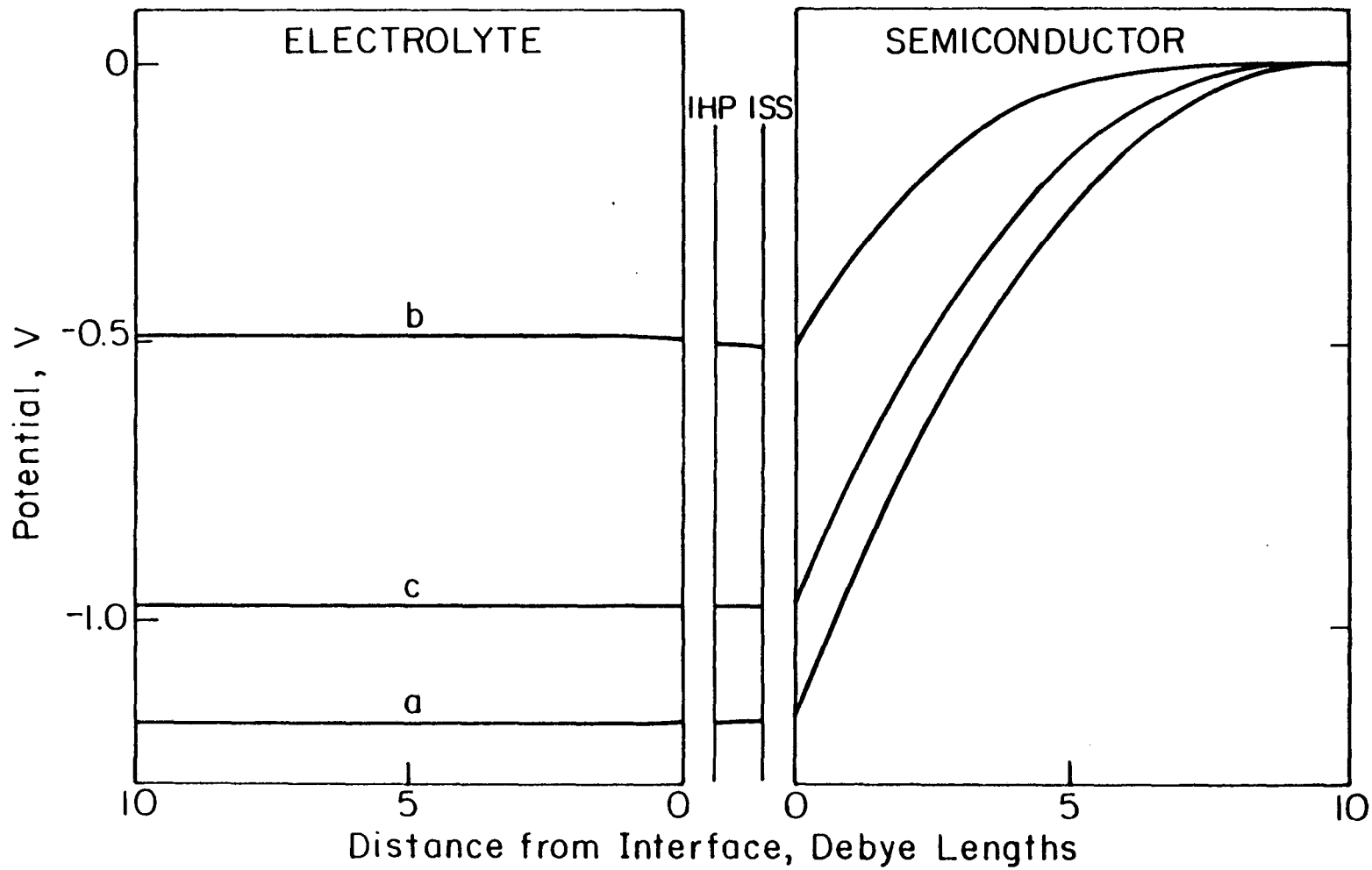
ELECTROLYTE
SEMICONDUCTOR
IHP ISS
0
-0.5
-1.0
Potential, V
b
c
a
10
5
0
0
5
10
Distance from Interface, Debye Lengths

XBL 831-5026

accumulation, at open circuit, at various locations creates an electric field which tends to cancel that existing in the dark and leads to this straightening of the bands. The difference between the potential in the dark and under illumination represents a driving force for flow of electrical current. The potential distribution near the short-circuit condition (curve c) approaches the equilibrium distribution.*** All the variation in potential (from open circuit in the dark to open circuit under illumination to limiting current under illumination) takes place in the semiconductor. The potential drop across interfacial planes is comparatively small and invariant.

The potential distribution for the system under kinetic limitations to ion adsorption is presented in Figure 7. The open-circuit potential distribution in the dark and under illumination (curves a and b, respectively) are equivalent to those shown in Figure 6. The potential distribution near short circuit (curve c), however, does not approach the equilibrium distribution. A significant part of the potential drop occurs across the interface, providing a potential driving force which allows adsorption reactions to proceed.

Concentration distributions of holes and electrons in the semiconductor are presented in Figures 8 and 9 for a system with no interfacial kinetic limitations and for a system with kinetic limitations to ion adsorption, respectively. The equilibrium and illuminated open-circuit concentration distributions for the two cases are identical. Under equilibrium conditions the concentration of holes (curve a) is essentially zero in the bulk of the semiconductor and increases near the negatively

*** Short-circuit is defined as the condition of a zero cell potential. The description presented here neglects electrolyte resistance and counterelectrode mass-transfer and kinetic effects in determining the condition of short circuit. These effects will be treated later; inclusion of electrolyte and counterelectrode effects cause the short-circuit potential distributions discussed here to occur at a negative cell potential.

Figure 7. Potential distribution for the liquid-junction cell with kinetic limitations to ion adsorption ($k_{ads} = 4.x10^{6}\ s^{-1}$). Curve a, open circuit in the dark; curve b, open circuit under illumination; and curve c, near short circuit ($i = -23.1\ mA/cm^2$) under illumination. $\lambda_{sc} = 1.689x10^{-6}$ cm, and $\lambda_{sol} = 1.967x10^{-8}$ cm.

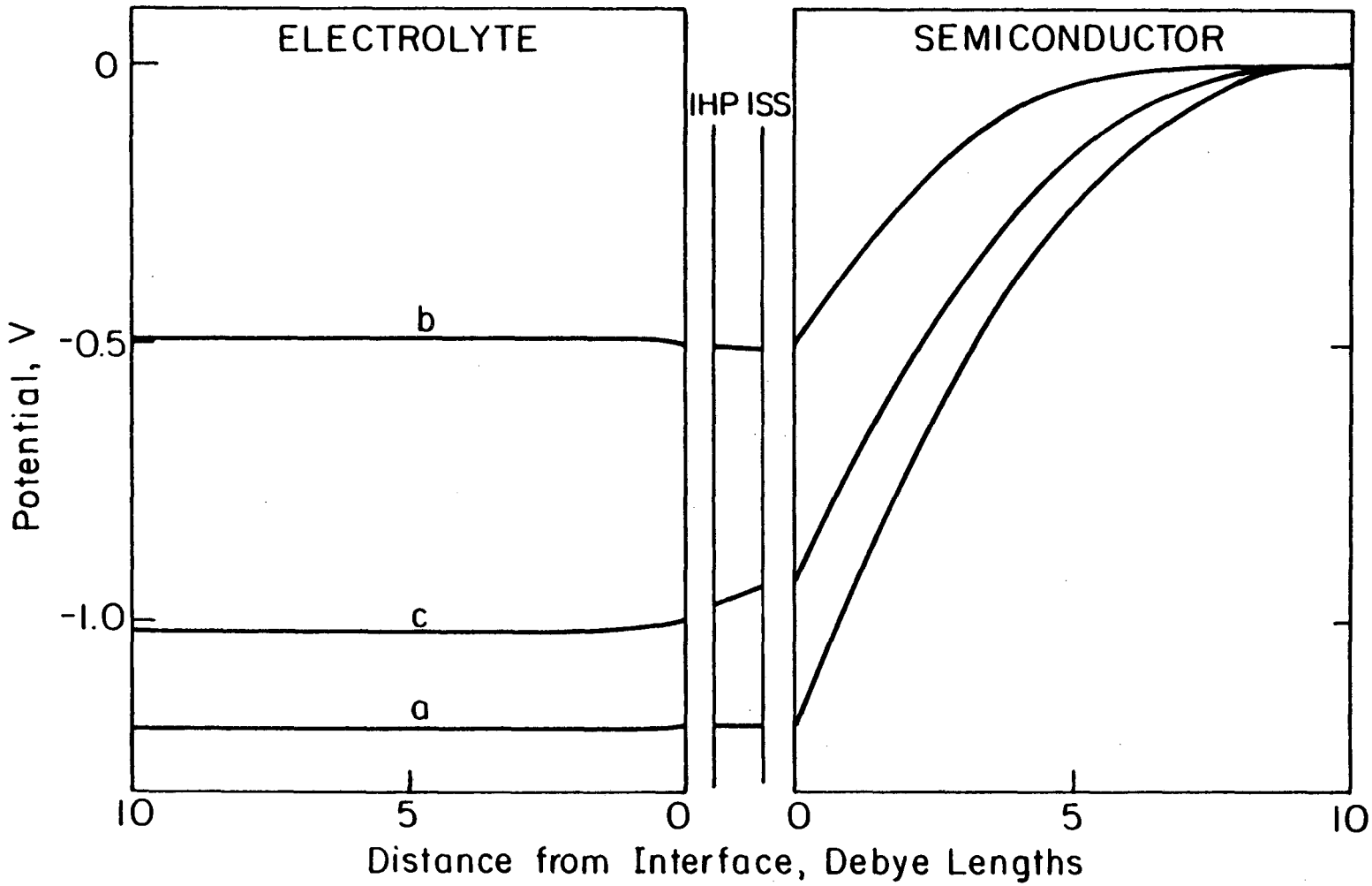
ELECTROLYTE
SEMICONDUCTOR
IHP
ISS
0
-0.5
-1.0
b
c
a
Potential, V
10
5
0
0
5
10
Distance from Interface, Debye Lengths

XBL 831-5027

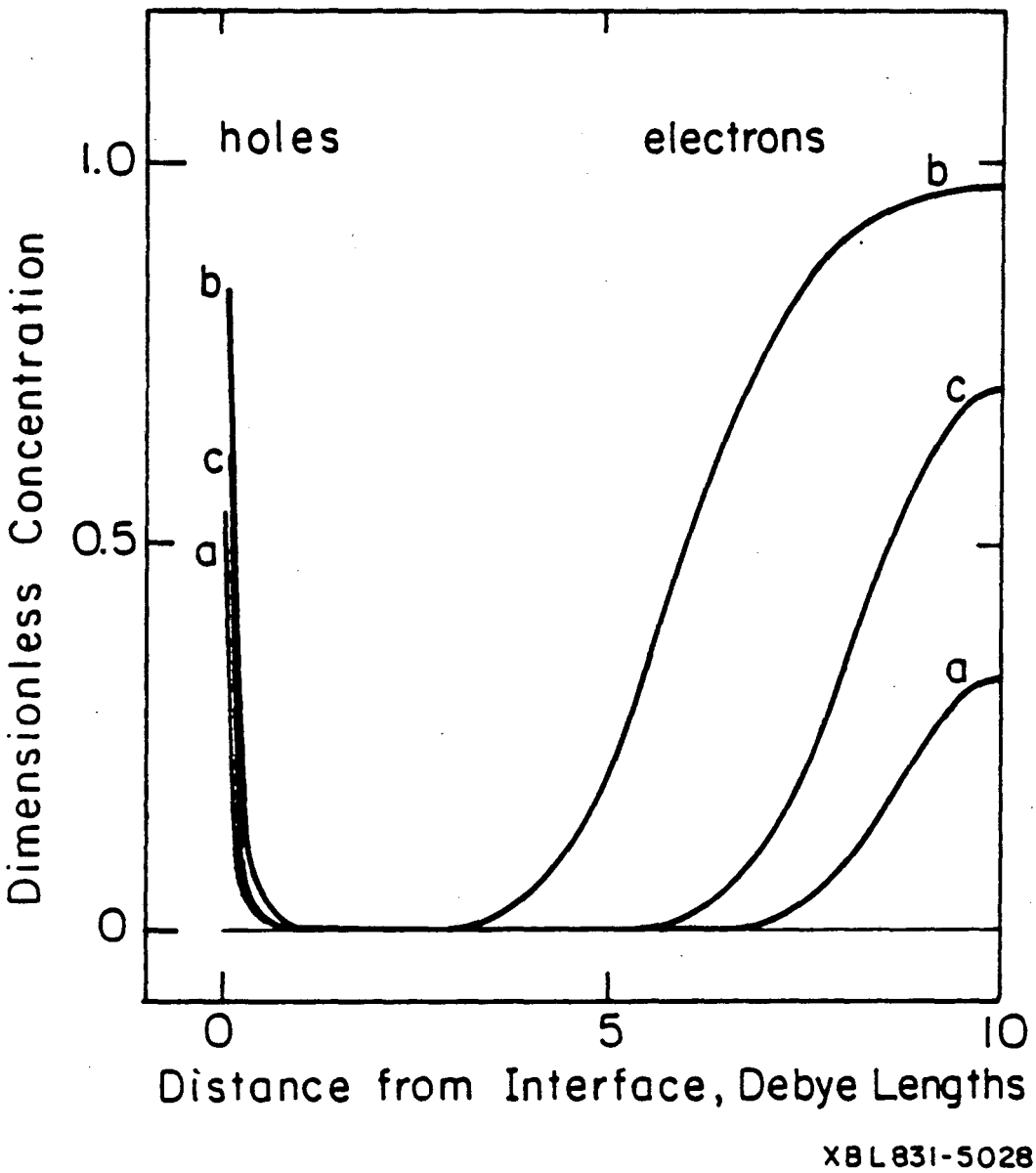

Figure 8. Concentration distribution for the liquid-junction cell with no kinetic limitations (k_{ads} = 1.0x10^{26} s^{-1}). Curve a, open circuit in the dark; curve b, open circuit under illumination; and curve c, near short circuit (i = -23.1 mA/cm^2) under illumination.

Figure 9. Concentration distribution for the liquid-junction cell with kinetic limitations to ion adsorption ($k_{ads} = 4.x10^{6}\ s^{-1}$). Curve a, open circuit in the dark; curve b, open circuit under illumination; and curve c, near short circuit ($i = -23.1\ mA/cm^2$) under illumination.

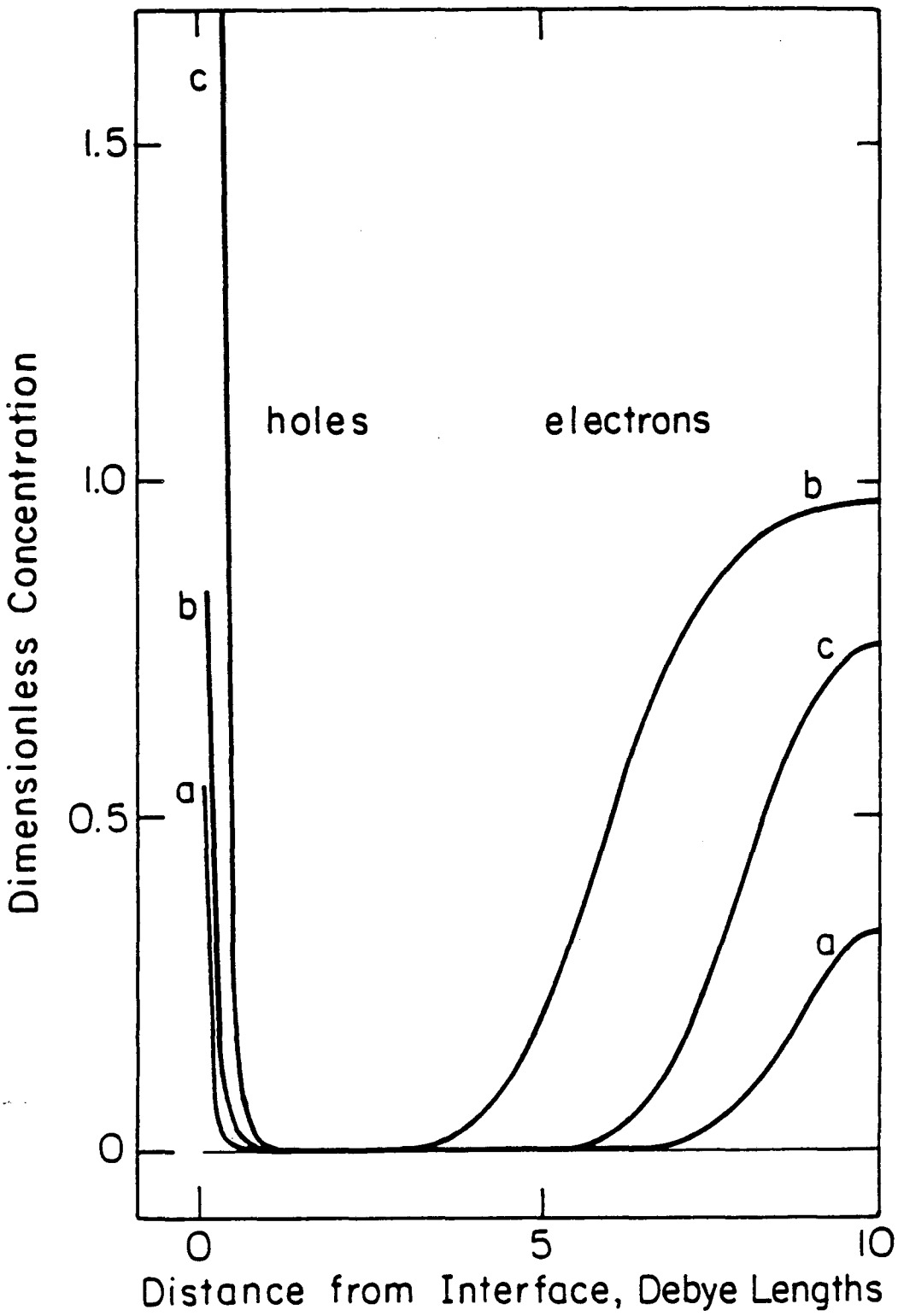
c
b
a
holes
electrons
b
c
a
1.5
1.0
0.5
0
0
5
10
Dimensionless Concentration
Distance from Interface, Debye Lengths

XBL831-5029

charged interface. Conduction electrons are depleted near the interface and reach a value of 0.328 dimensionless units at the current collector, where the concentrations are scaled by the dopant concentration ($N_d - N_a$). The electron concentration in a neutral region of the semiconductor would have a value essentially equal to 1.0. The equilibrated semiconductor of Figure 8 can therefore be described as having an inversion region extending from the semiconductor-electrolyte interface to 0.5 Debye lengths from the interface and a depletion region extending to the current collector.

The positive background charge density has a value of 1.0; the semiconductor has a net positive charge which is balanced by charge associated with the diffuse region of the electrolyte and the interface. System electroneutrality is maintained. The potential gradient, the driving force for migration of charged species, is balanced by the concentration gradient, which drives diffusion. The net flux of each species in the semiconductor is equal to zero at equilibrium.

Illumination under open-circuit conditions produces electron-hole pairs, which are separated by the potential gradient (see Figures 6 and 7). The concentration of holes increases near the interface, and the concentration of electrons increases near the current collector (curve b). As the system without kinetic limitations approaches short circuit (curve c in Figure 8), the concentrations of holes and electrons approach the equilibrium distributions. The system under kinetic limitations to ion adsorption, in contrast, experiences an increase in hole concentration at large current densities (curve c in Figure 9).

A small ion-adsorption rate constant is therefore compensated by increased potential and concentration driving forces at the interface. In

this way, kinetic limitations influence the cell performance.

3.1.2. Charge-transfer reactions. Current-potential curves are presented in Figure 10 with the rate constant for charge transfer from the inner surface states of the semiconductor to the inner Helmholtz plane as a parameter (reactions 5, 6, and 7 in Figure 2). The cell potential has a maximum value under open-circuit illumination and decreases as the anodic current increases. Kinetic limitations to charge transfer adversely influence the power performance of the cell.

The potential distribution for a system with kinetic limitations to charge transfer is presented in Figure 11 and can be compared to the potential distribution for the system with no kinetic limitations (Figure 6). The open-circuit potential distribution in the dark (curve a) and under illumination (curve b) are equivalent to those presented in Figure 6. The potential distribution at large current densities (-23.1 mA/cm^2) shows a large potential drop across the interface. This potential drop, as for the case with kinetic limitations to ion adsorption, provides a potential driving force which allows the kinetically-limited reaction to proceed.

Hole-concentration distributions are presented in Figure 12 for the case with kinetic limitations to charge transfer. These distributions may be compared to those in Figure 8 for the system with no kinetic limitations. A large concentration driving force (331.6 dimensionless units at the outer surface states) is developed near limiting current. A small charge-transfer rate constant is compensated by increased potential and concentration driving forces.

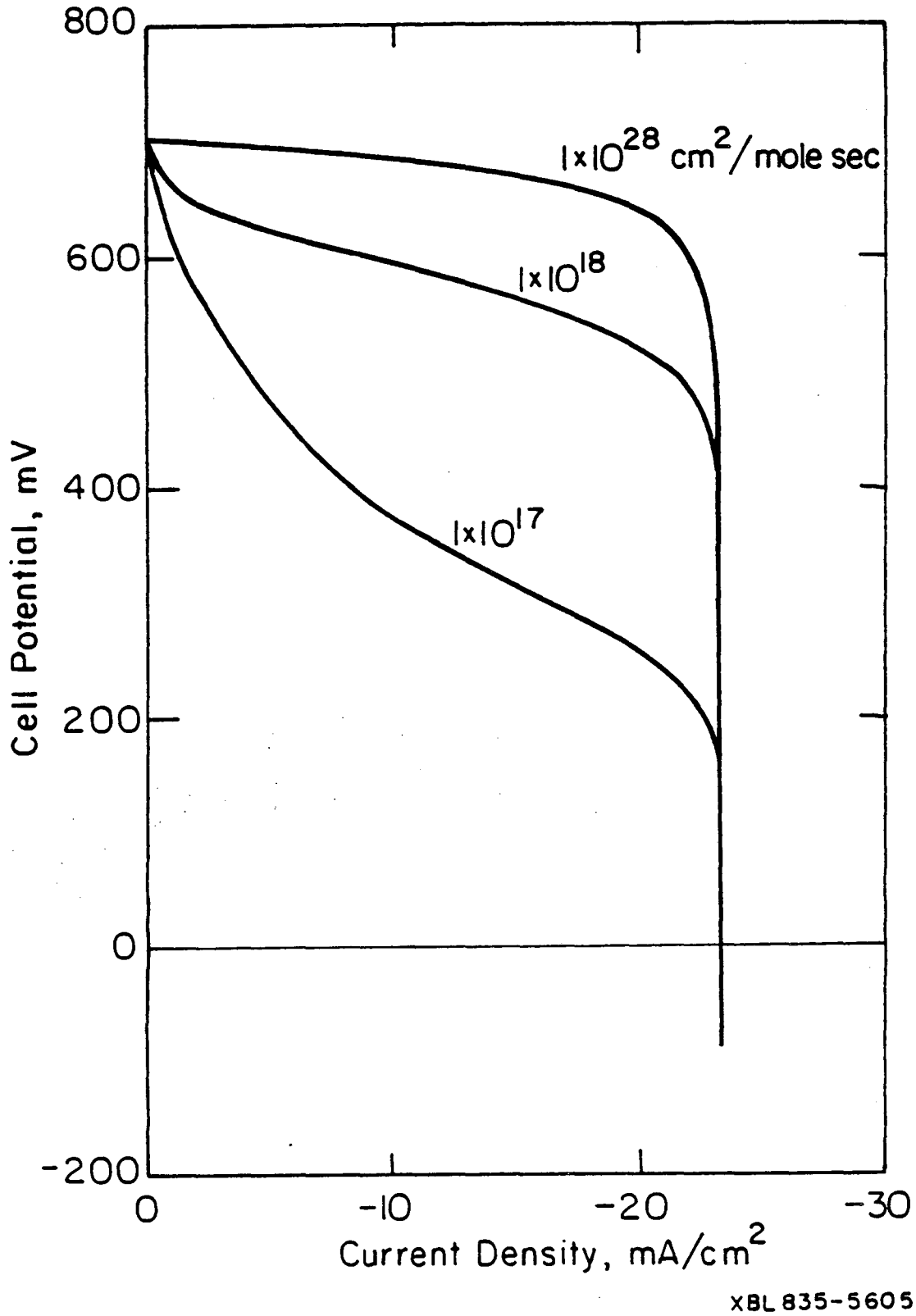

Figure 10. Computer current-potential curves for an n-type GaAs Anode with charge-transfer rate constant as a parameter.

Figure 11. Potential distribution for the liquid-junction cell with kinetic limitations to charge transfer (k_{cht} = 1.x10^{17} cm^2/mol-s). Curve a, open circuit in the dark; curve b, open circuit under illumination; and curve c, near short circuit (i = -23.1 mA/cm^2) under illumination. λ_{sc} = 1.689x10^{-6}, and λ_{sol} = 1.967x10^{-8} cm.

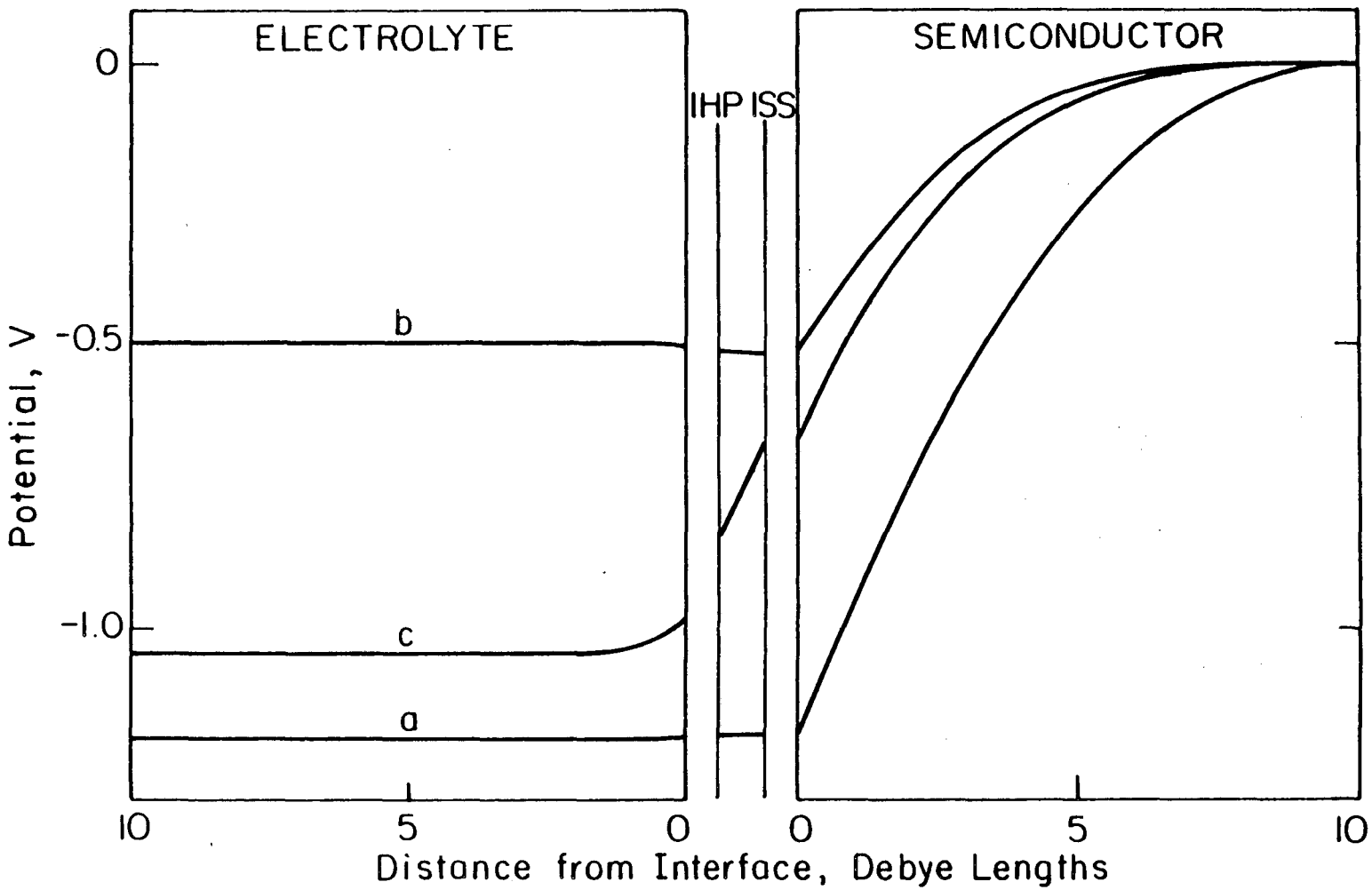
ELECTROLYTE
SEMICONDUCTOR
IHP
ISS
0
-0.5
-1.0
b
c
a
Potential, V
10
5
0
0
5
10
Distance from Interface, Debye Lengths

XBL 831-5030

Figure 12. Concentration distribution for the liquid-junction cell with kinetic limitations to charge transfer ($k_{cht} = 1.x10^{17}$ $cm^2/mol-s$). Curve a, open circuit in the dark; curve b, open circuit under illumination; and curve c, near short circuit ($i = - 23.1$ mA/cm^2) under illumination.

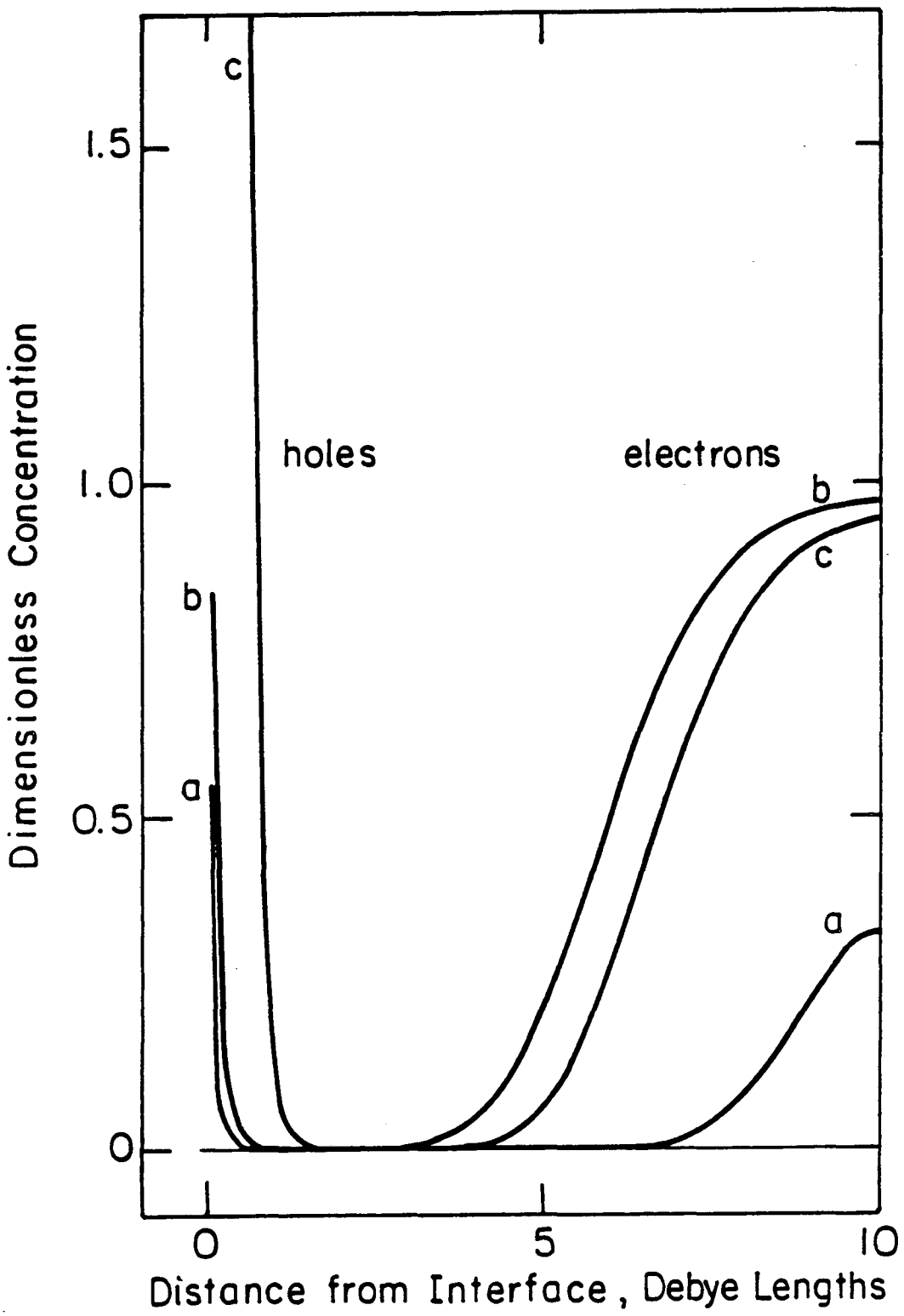
c
1.5
holes
electrons
1.0
b
c
b
a
0.5
a
0
0
5
10
Dimensionless Concentration
Distance from Interface, Debye Lengths

XBL831-5031

3.1.3. Electron-adsorption reactions. The influence of electron-adsorption rate constants (reactions 1, 2, 10, 11, 12, and 13 in Figure 2) upon the current-potential curve is presented in Figure 13. A small electron-adsorption rate constant reduces the net rate of recombination of holes and electrons at the surface and thus increases both the cell potential and the value of the limiting current.

3.1.4. Surface-shift reactions. The rate constants for reactions which allow electrons to move from one energy level at the interface to another (reactions 3 and 4 in Figure 2) do not have any independent effect upon the cell potential or the value of the limiting current. These rate constants affect only the path by which recombination may take place.

3.2. Bulk Semiconductor Properties

Bulk semiconductor properties can greatly influence the performance of the liquid-junction photovoltaic cell. Some properties which can be controlled in semiconductor manufacture and cell design are the dopant concentration, the thickness of the semiconductor, the solar absorption coefficient, and the amount of light absorbed in the semiconductor.

3.2.1. Dopant concentration. Current-potential curves are presented in Figure 14 for concentrations of positive background charge ranging from 2.500×10^{-7} to 0.0396×10^{-7} equivalents/cm^3 and for a semiconductor thickness of 10 Debye lengths. The cell performance is strongly dependent upon doping level. The "straightening of the bands" under illumination is greatest with a small dopant concentration; thus in this case a large open-circuit cell potential is observed. The low concentration of charge-carrying species in the neutral region is associated with a large resistance to current

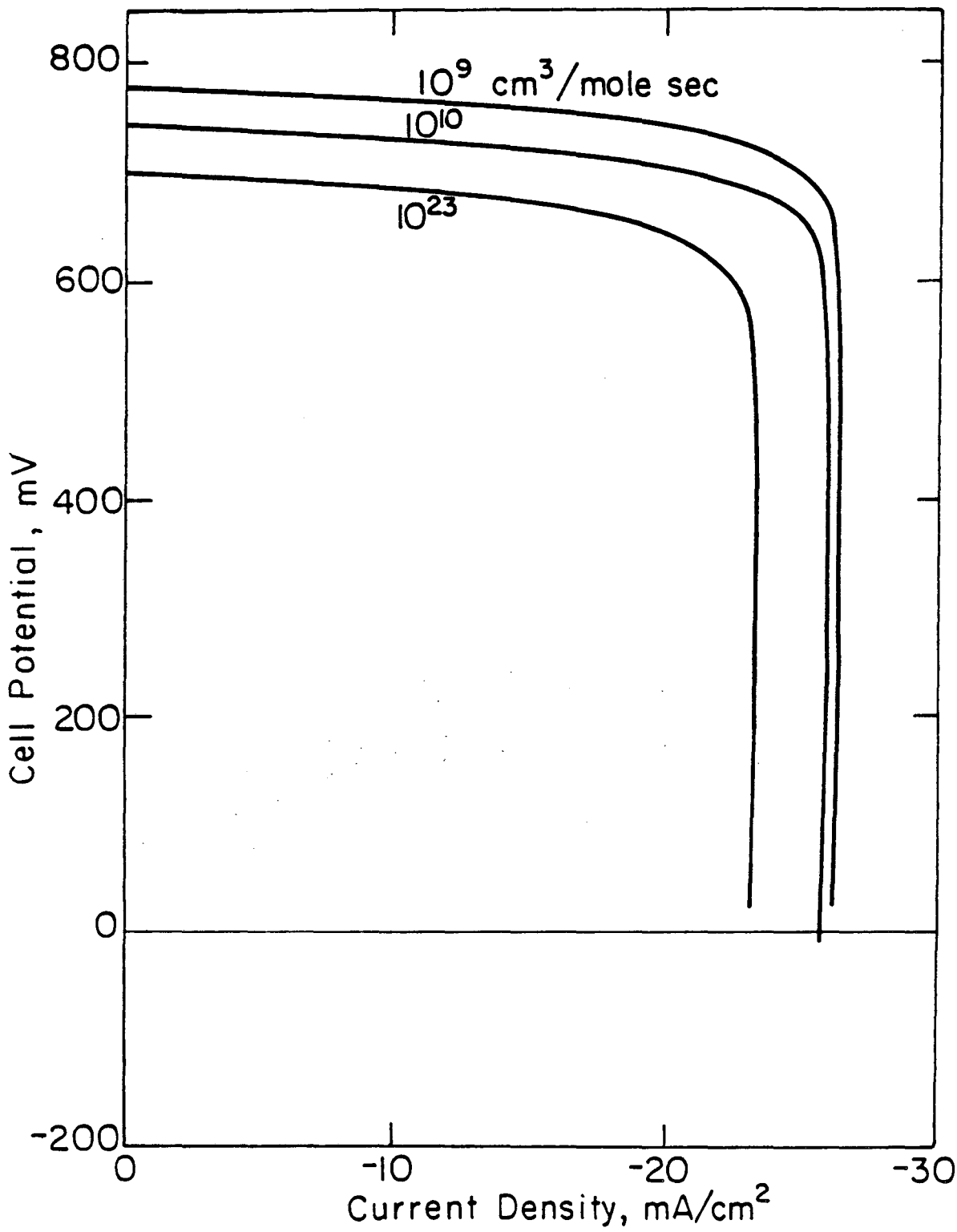

Figure 13. Computer current-potential curves for an n-type GaAs anode with electron-adsorption rate constant as a parameter.

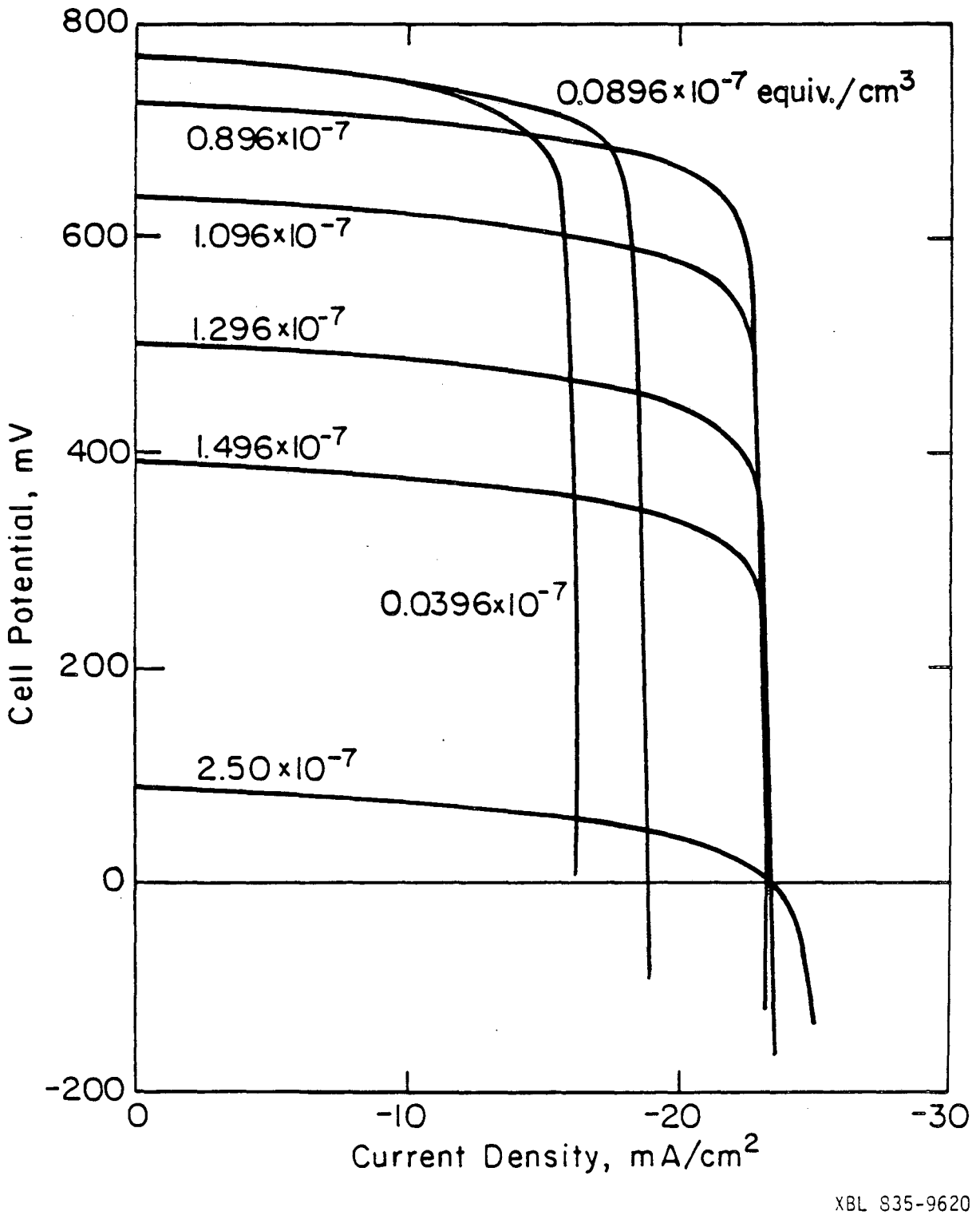

Figure 14. Computed current-potential curves for an n-type GaAs anode with dopant concentration as a parameter.

flow in the semiconductor and with enhanced homogeneous recombination of electron-hole pairs; thus a small limiting current is observed. Conversely, a large dopant concentration is characterized by a small open-circuit potential and a large limiting current.

The semiconductor Debye length is inversely proportional to the square root of the dopant concentration. If the semiconductor thickness were held constant at a value of 1.69×10^{-5} cm, as opposed to 10 Debye lengths, similar results would be observed for high dopant concentrations. At low dopant concentrations, the semiconductor thickness would be smaller than the space-charge region thickness, and the cell potential would be reduced (see section 3.2.2). A change in the Debye length influences the utilization of the incident radiation (see section 3.2.3.), but the change in cell performance due to this effect is small.

Maximization of power density yields an optimal dopant concentration for the n-GaAs system of about 9.0×10^{-8} equivalents/cm^3. The donor concentration in the work presented by Heller and Miller[42,43] was 6×10^{18} carriers/cm^3 (or 9.96×10^{-8} equivalents/cm^3).

3.2.2. Semiconductor thickness. The effect of semiconductor thickness on the cell performance is presented in Figure 15 for a characteristic depth of light adsorption of 228.2 A (corresponding to 1.35 Debye lengths). The cell potential increases as the thickness increases from 5 to 13 Debye lengths. The current-potential curve is essentially unchanged for an increase in thickness from 13 to 30 Debye lengths. A very thick semiconductor is expected to decrease the system performance because of resistive losses in the semiconductor. A thin semiconductor limits the cell performance because of saturation of charge in the semiconductor. All mobile electrons

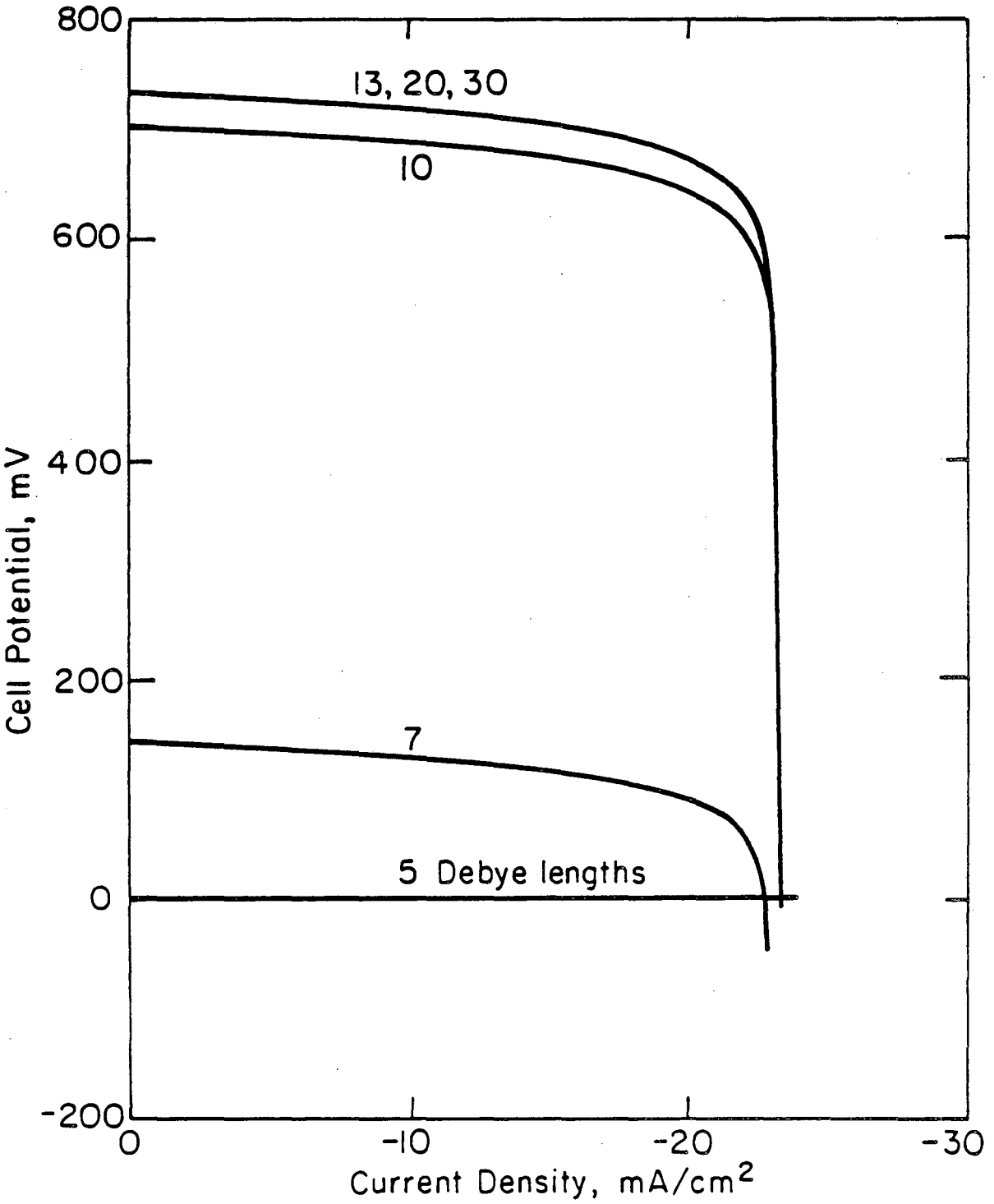

XBL 835-9619

Figure 15. Computed current-potential curves for an n-type GaAs anode with semiconductor thickness as a parameter.

are driven from the semiconductor in response to the negatively charged interface, and a large potential gradient across the semiconductor cannot be sustained.

3.2.3. Solar absorption coefficient. The characteristic length for absorption of light can be compared to the Debye length by the dimensionless absorption coefficient $m\lambda_{sc}$. The open circuit cell potential is presented in Figure 16 as a function of the dimensionless absorption coefficient. A maximum in cell potential is observed in the region where the characteristic length for absorption of light is of the same order as the Debye length. The cell potential is relatively insensitive to the dimensionless absorption coefficient within the range of 0.2 to 3.0. The optimal value for the dimensionless absorption coefficient was around 0.425, where the characteristic length for light absorption is 2.4 Debye lengths. The absorption coefficient for single crystal GaAs, averaged over photons with energy greater than the band gap energy, is 4.4×10^{-5} cm. This value corresponds to a dimensionless absorption coefficient of 26 and to a characteristic absorption depth of 0.0038 Debye lengths.

3.2.4. Solar flux. The amount of light absorbed within the semiconductor has a strong effect on cell performance. As seen from Figure 17, light scattering or reflective losses can reduce the limiting current from -23.2 mA/cm^2 under full AM-2 irradiation (modeled here with a single mean absorption coefficient) to -14.0 mA/cm^2 under 60 percent of AM-2 irradiation. The 40 percent decrease in limiting current is accompanied by a 1 percent decrease in open-circuit cell potential. The amount of light absorbed within the semiconductor is directly related to the generation of the limiting species, holes, and therefore primarily affects the limiting

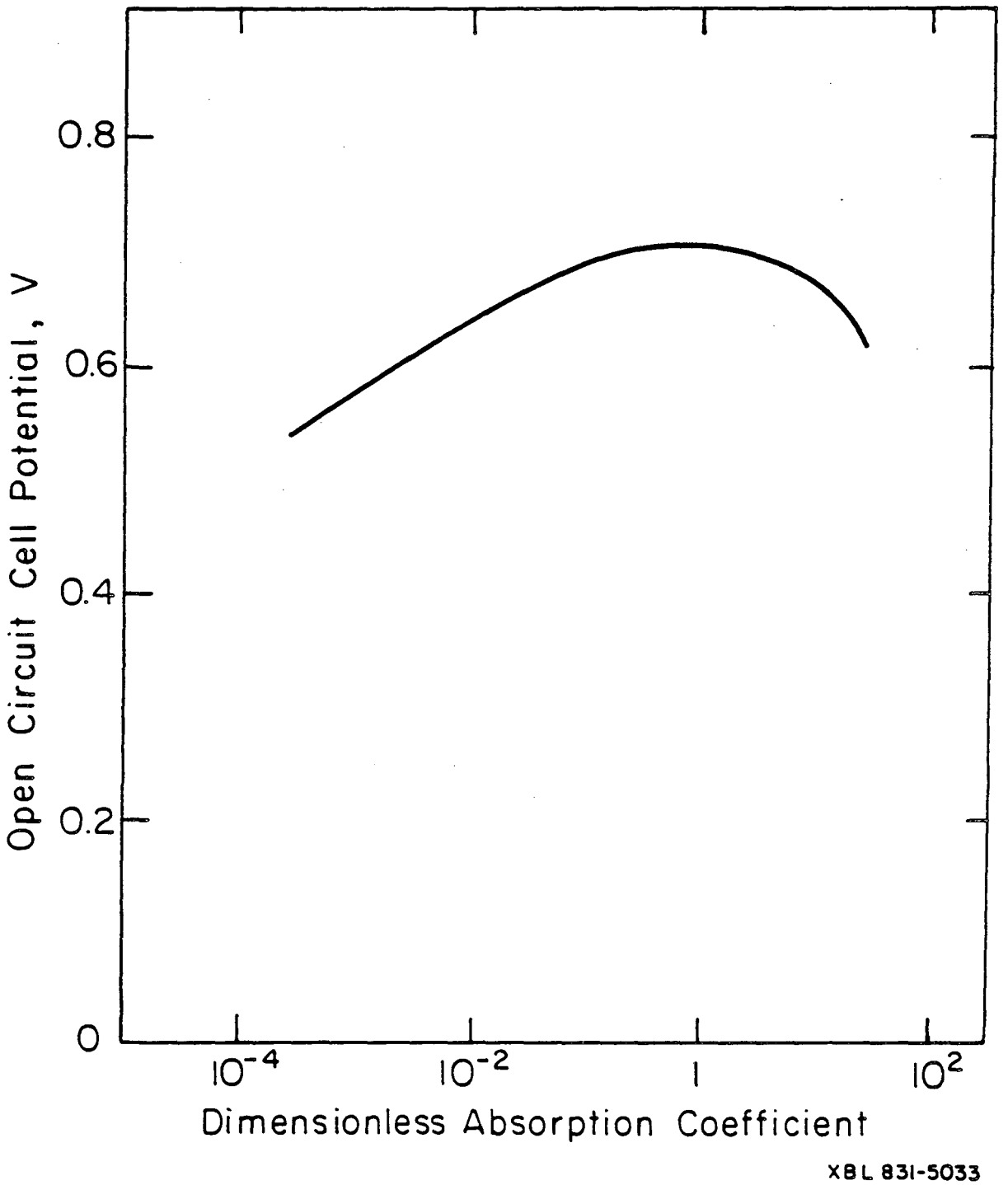

Figure 16. Open-circuit cell potential as a function of dimensionless solar absorption coefficient.

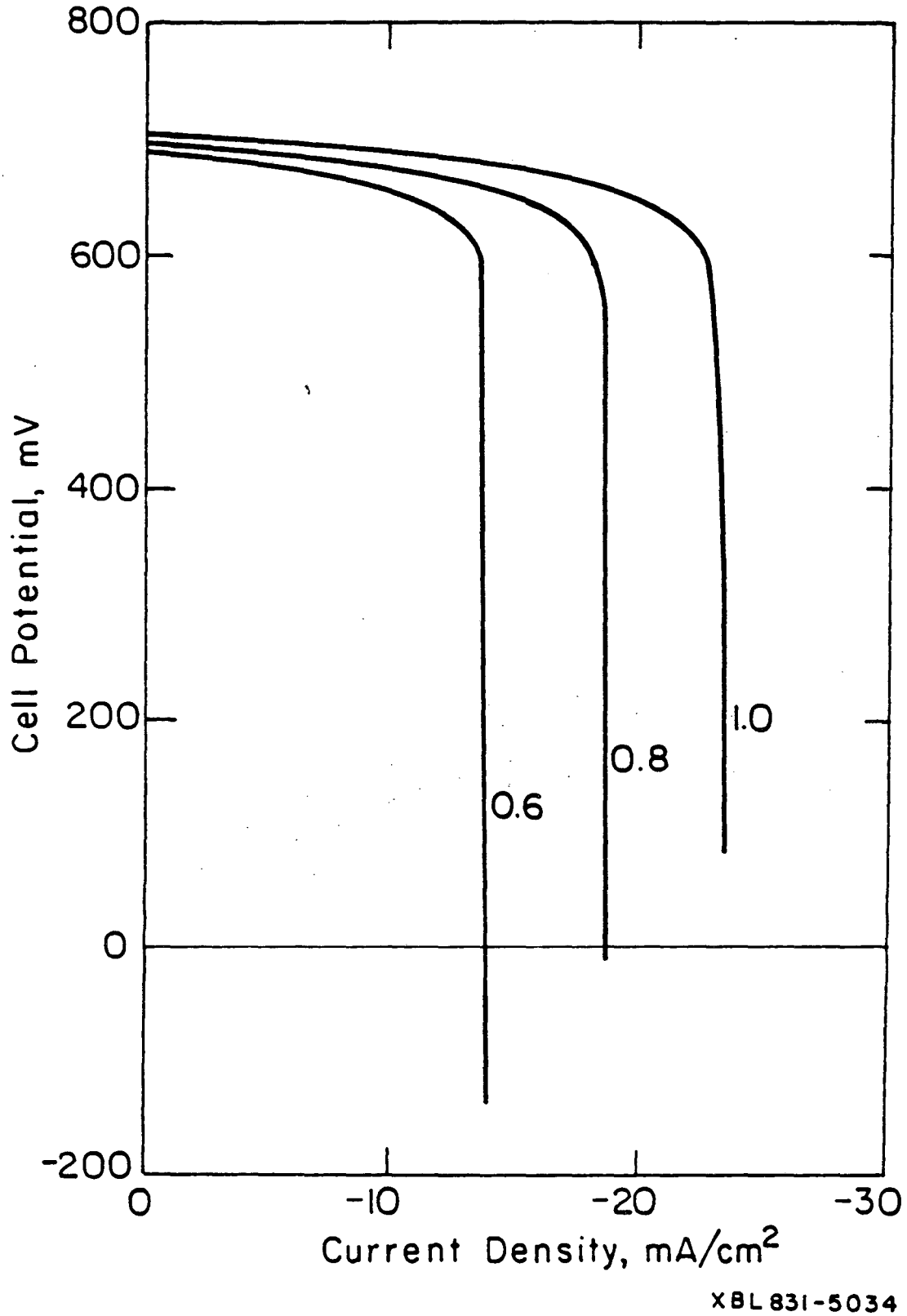

Figure 17. Computed current-potential curves for an n-type GaAs anode with fractional absorption of incident AM-2 radiation as a parameter.

current.

3.3. Interfacial Parameters

Model parameters that are characteristic of the interface cannot, in general, be independently measured. The results of the model can be used, however, to gain insight into the importance and influence of these parameters. The total equilibrium charge adsorbed onto the surface was held constant in the studies presented below by adjusting the total ISS site concentration in response to changes in equilibrium energies of adsorbed species

3.3.1. Surface electron-energy levels. Charge-transfer and surface recombination reactions at the interface are assumed to take place through surface electron sites; these sites have associated with them energy levels which may differ from the conduction and valence-band energy levels. A possibly continuous distribution of electron energy levels is represented in the model by three discrete energy levels.

Recombination paths under open-circuit illumination are presented in Figures 18, 19, and 20 for three individual distributions of surface electron-energy levels. The width of the arrows representing the direction of electron transfer is proportional to the flux carried along that path. The conduction band energy at the OSS is 2.6 eV when expressed on the same basis as the ISS energy levels. The valence band energy at the OSS is 1.2 eV.

The energy levels of ISS sites influence the open-circuit cell potential under illumination and the path taken by electrons in surface recombination. The majority of recombination occurs through the site with the most favored energy level. A continuous distribution of energy levels is

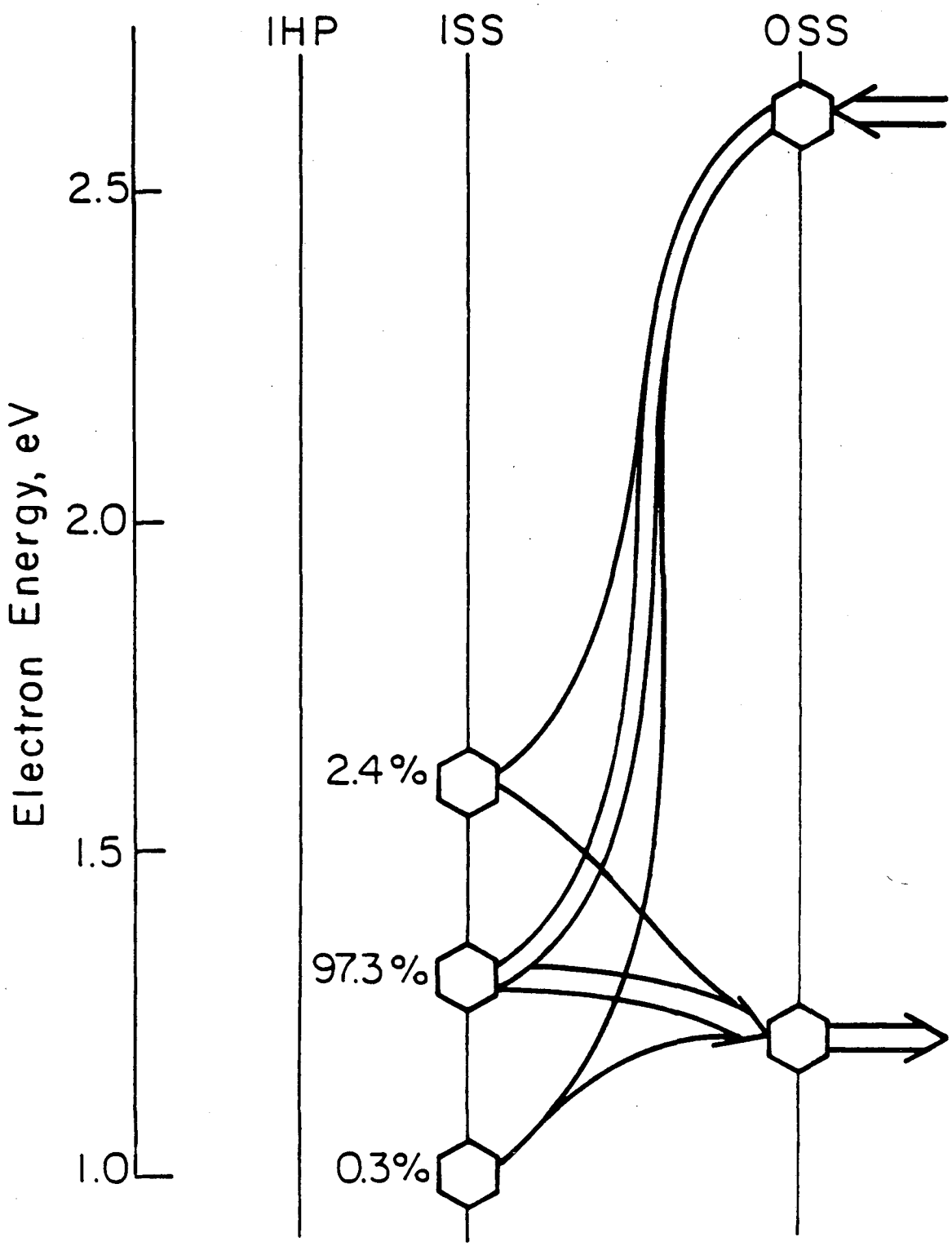

Figure 18. Interfacial recombination reaction distribution under open-circuit illumination for inner surface state electron energy levels of 1.0, 1.3, and 1.6 eV (cell potential = 704.0 mV).

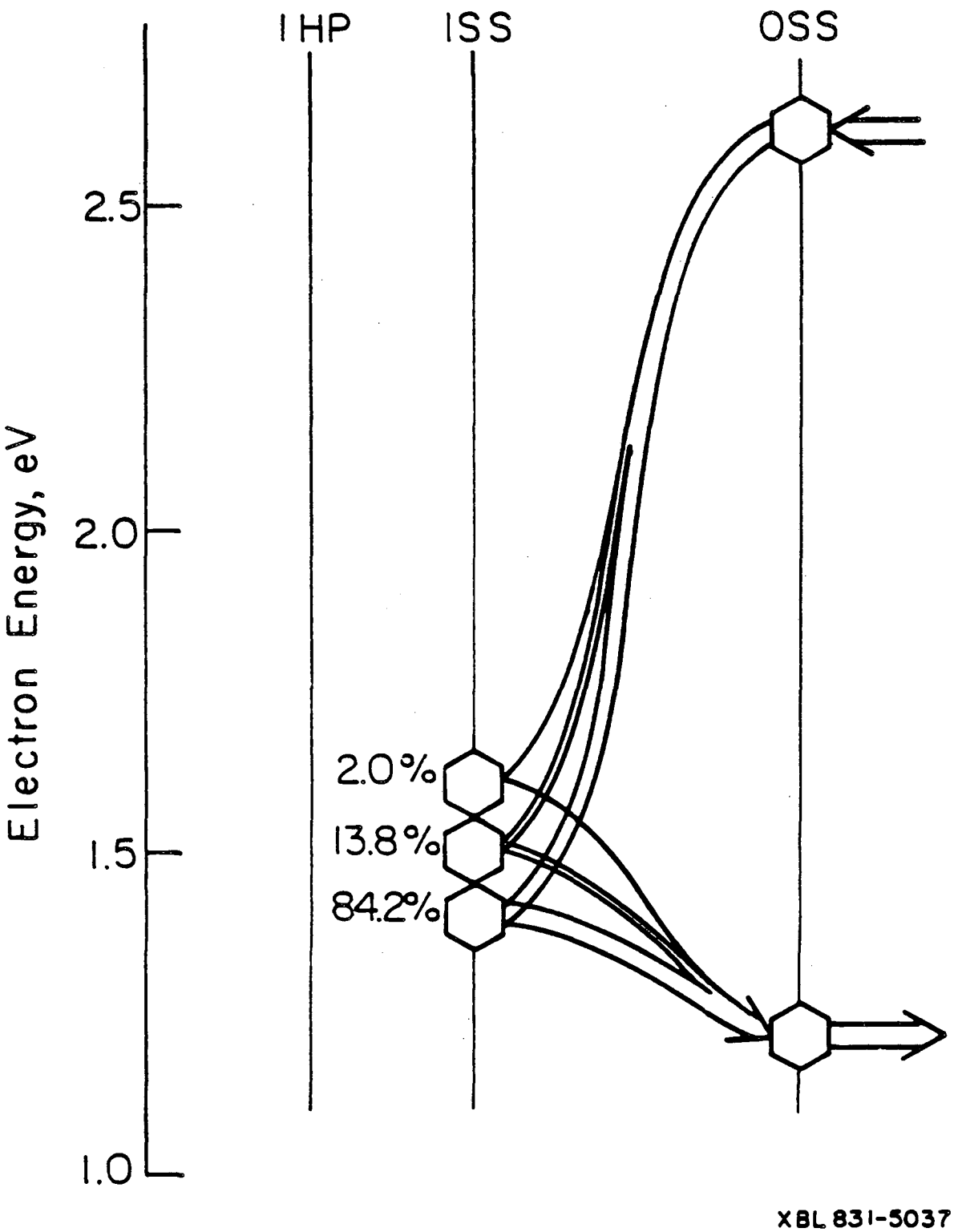

Figure 19. Interfacial recombination reaction distribution under open-circuit illumination for inner surface state electron energy levels of 1.4, 1.5, and 1.6 eV (cell potential = 693.0 mV).

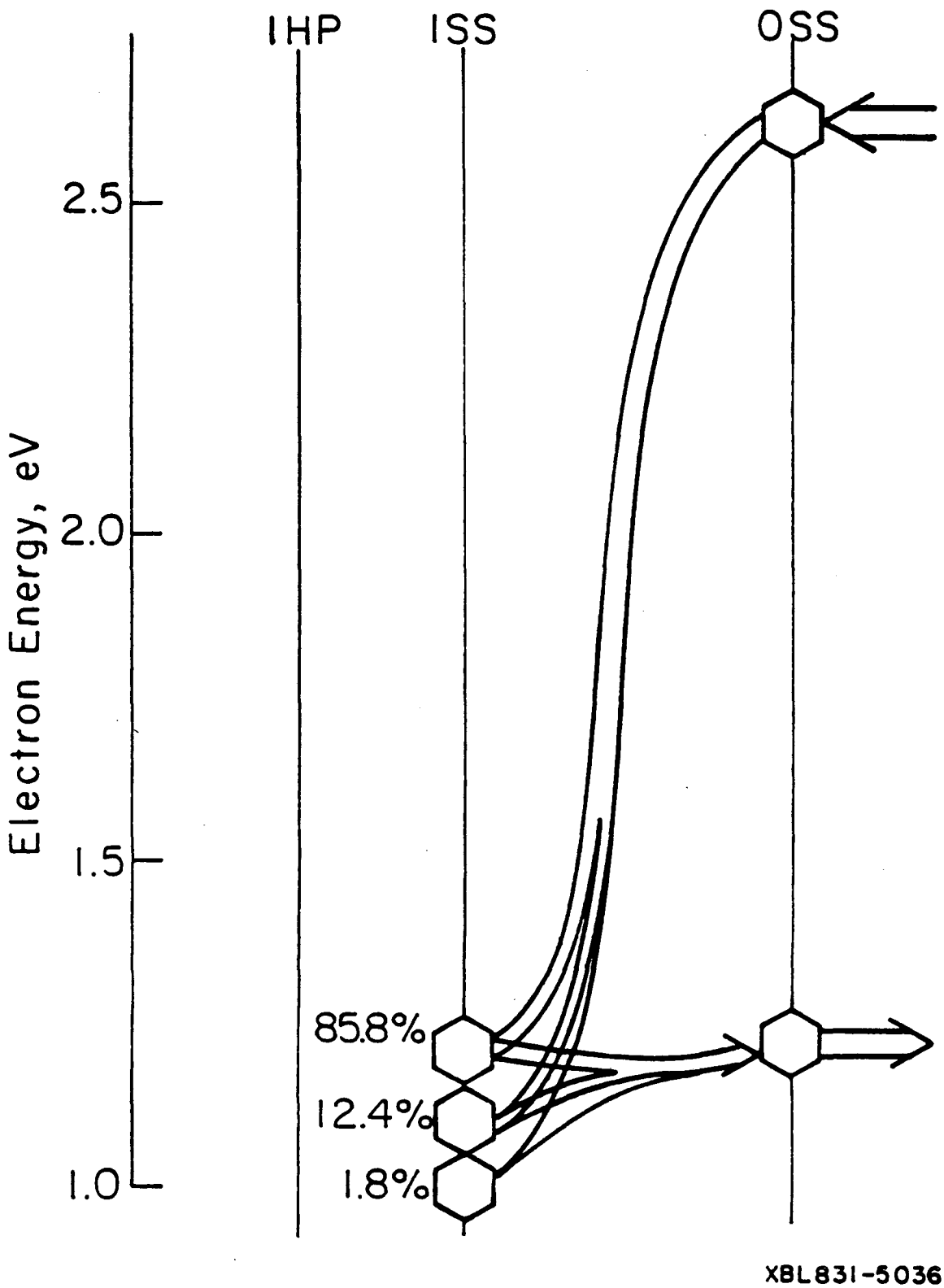

Figure 20. Interfacial recombination reaction distribution under open-circuit illumination for inner surface state electron energy levels of 1.0, 1.1, and 1.2 eV (cell potential = 705.1 mV).

therefore well modeled by a set of three discrete energy levels that include the favored energy level.

3.3.2. Ion-adsorption energy. The adsorption energy for an ionic species i is related to kinetic parameters for the respective ion-adsorption reaction by (see Chapter 6)

$$\Delta E_i = - z_i F \Delta\Phi_l + RT \ln\left[\frac{k_{f,l}}{k_{b,l}}\right], \tag{37}$$

where l represents the adsorption reaction and $\Delta\Phi_l$ is the equilibrium potential drop from the inner Helmholtz plane to the outer Helmholtz plane.

The effect of ion adsorption energy on the current-potential curve is presented in Figure 21. A negative energy of adsorption increases the concentration of the ion at the surface and decreases the cell potential. A positive energy of adsorption decreases the concentration of the ion at the surface and increases the cell potential. The concentration of adsorbed ions at the IHP does not affect the limiting current because holes are the current-limiting species.

3.4. Cell Design

Under electrolyte-side illumination and without interfacial kinetic limitations, electrolyte resistance, and counterelectrode effects, the maximum power efficiency of the cell was calculated to be 15.0 percent. This is the value that one might observe if the power density is calculated using a potential drop measured between the semiconductor electrode and a reference electrode reversible to the redox reaction and located just outside the diffusion region. The resistance of the electrolyte, mass-transfer and kinetic limitations at the counterelectrode, and the choice of front or back-illumination will affect this value.

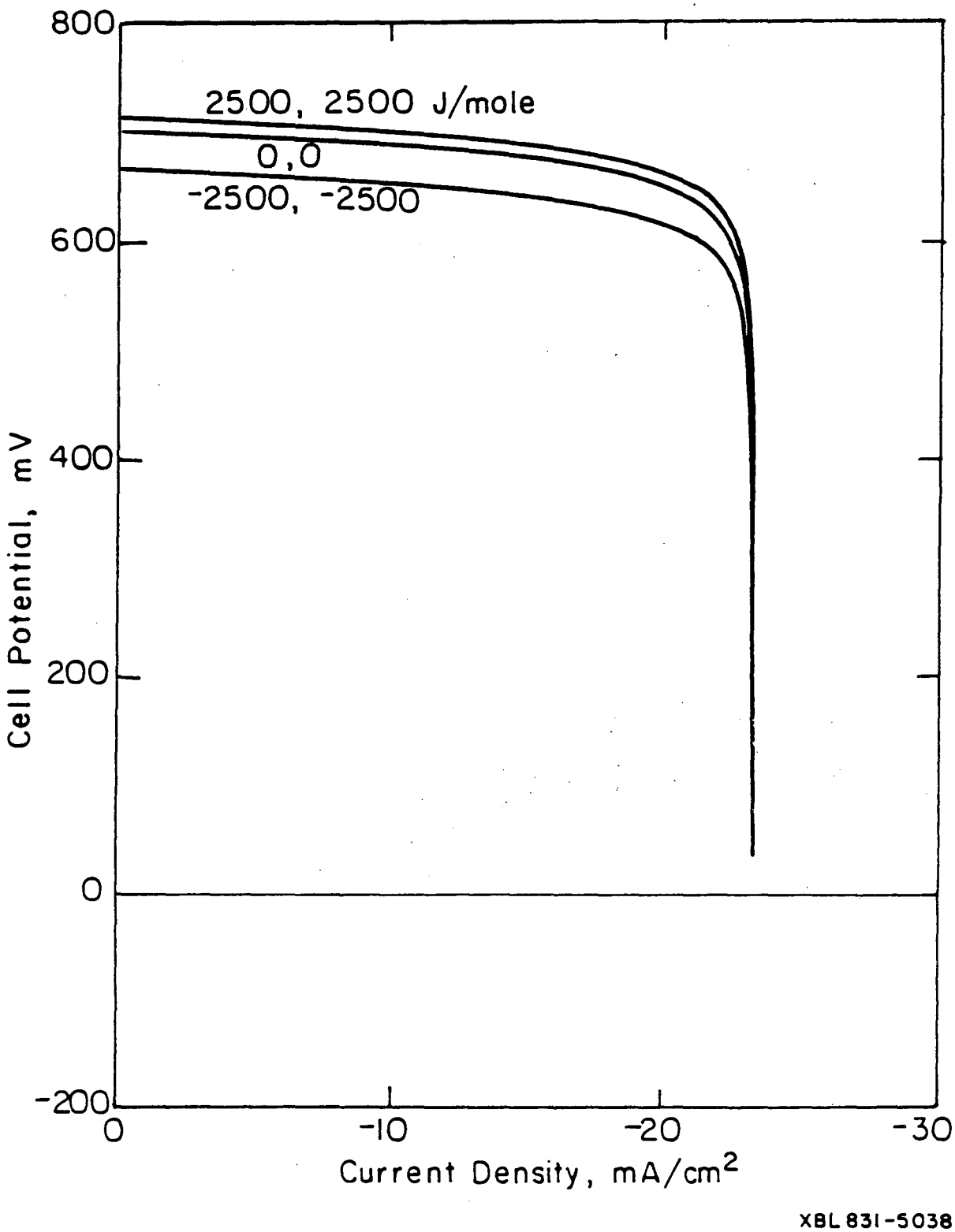

Figure 21. Computed current-potential curves for an n-type GaAs anode with interfacial ion-adsorption energy as a parameter.

3.4.1. Electrolyte and counterelectrode. Resistance in the electrolyte and kinetic and mass-transfer effects at the counterelectrode decrease the maximum power-density of the liquid-junction photovoltaic cell. The current-potential curve for a system with no interfacial kinetic limitations (see Figure 5) is presented in Figure 22 with electrolyte resistance included. The conductivity of the electrolyte was assumed to be 0.3 $\Omega^{-1}cm^{-1}$. The cell potential at a given current is reduced by an amount which is proportional to the current density and to the distance L between the counterelectrode and the semiconductor. A 10 cm separation between the counterelectrode and the semiconductor reduces the maximum power efficiency of the cell to 4.0 percent.

The same base current-potential curve is presented in Figures 23 and 24 with the effect of kinetic and mass transfer limitations at the counterelectrode included. The reaction

$$2Se^{2-} \rightarrow Se_2^{2-} + 2e^- \tag{38}$$

was assumed to follow the sequence

$$Se^{2-} \rightarrow Se^-_{ads} + e^-, \tag{39a}$$

$$2Se^-_{ads} \rightarrow Se_2^{2-}. \tag{39b}$$

Under the assumption that the second step is equilibrated, the current density at the counterelectrode can be expressed by

$$i = i_o\left\{\left[1. - \frac{i}{i_{4,lim}}\right]\exp\left[\frac{(1-\beta)F}{RT}\eta_{CE}\right] - \left[1. + \frac{i}{i_{3,lim}}\right]^{1/2}\exp\left[-\frac{\beta F}{RT}\eta_{CE}\right]\right\}, \tag{40}$$

where i_o is the exchange current density associated with the bulk concentrations of reactants,

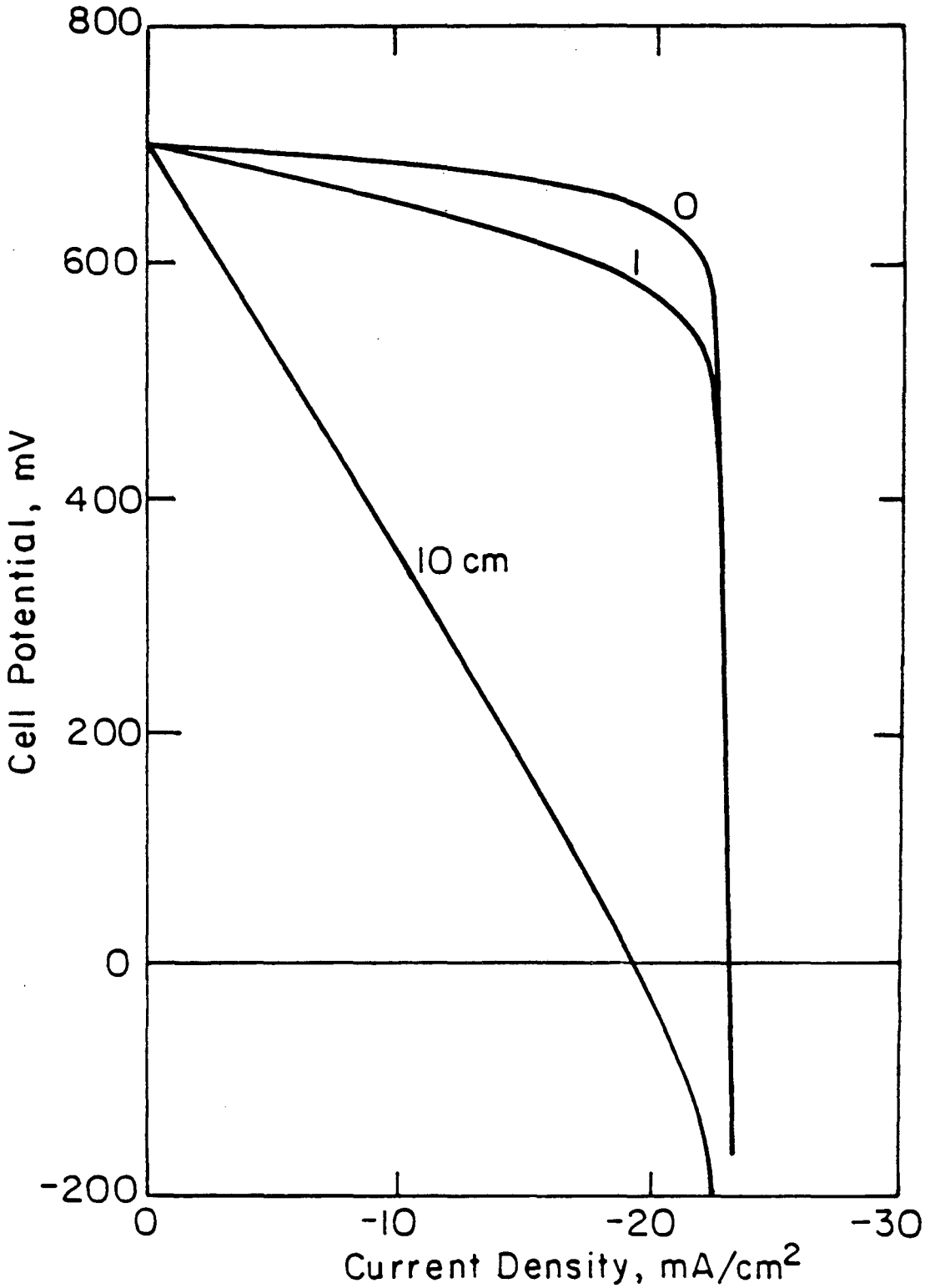

Figure 22. Computed current-potential curves for an n-type GaAs anode with the separation between the counterelectrode and the semiconductor as a parameter. Solution resistance has been included.

Figure 23. Computed current-potential curves for an n-type GaAs anode with diffusion-limited current density at the counterelectrode as a parameter. Curve a, counterelectrode effects not included; curve b, $i_{lim,3}$=20 mA/cm^2 and $i_{lim,4}$=80 mA/cm^2; curve c, $i_{lim,3}$=10 mA/cm^2 and $i_{lim,4}$=40 mA/cm^2; curve d, $i_{lim,3}$=5 mA/cm^2 and $i_{lim,4}$=20 mA/cm^2.

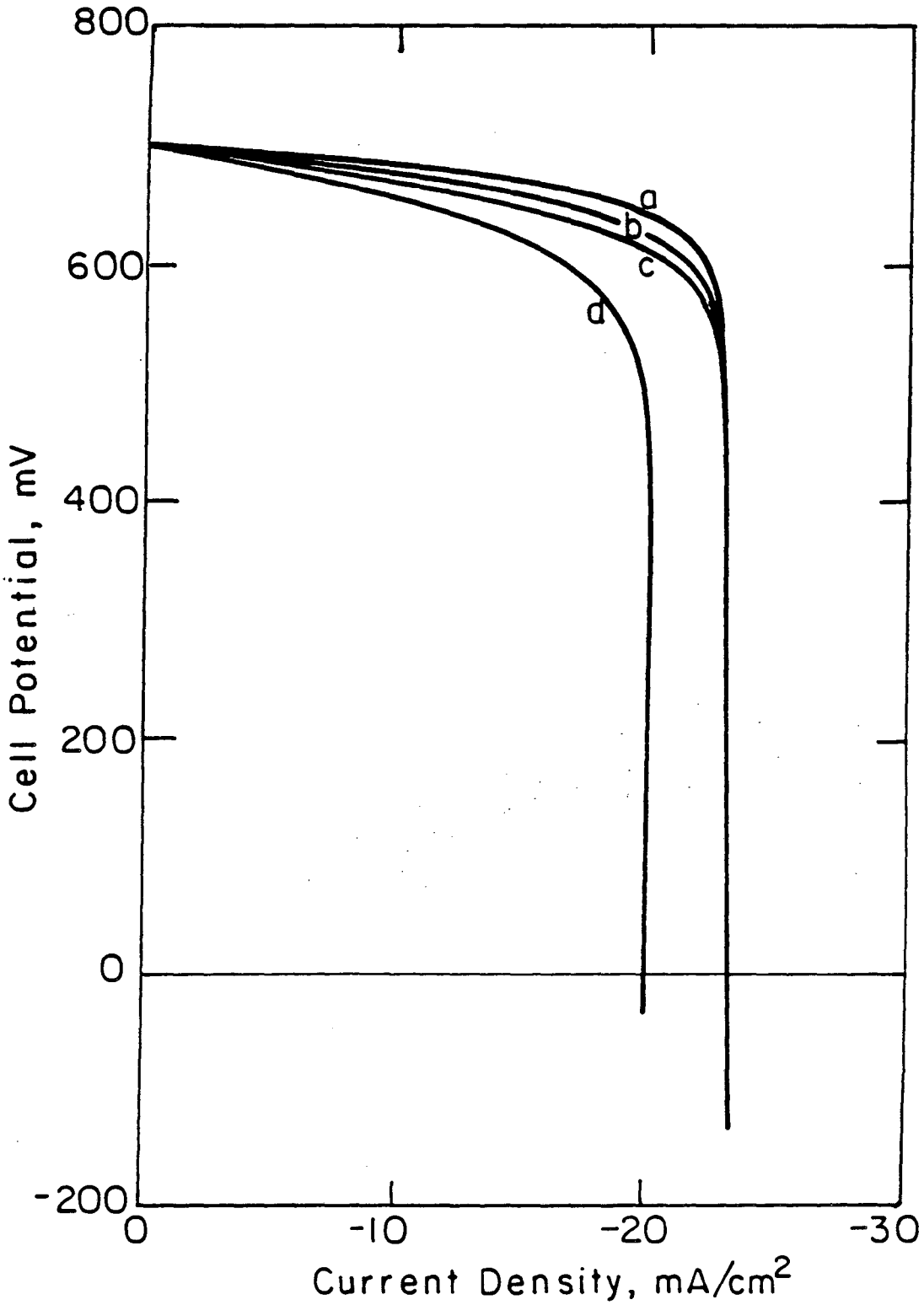
800
600
400
200
0
-200
0
-10
-20
-30
Cell Potential, mV
Current Density, mA/cm²
a
b
c
d

XBL 831-5041

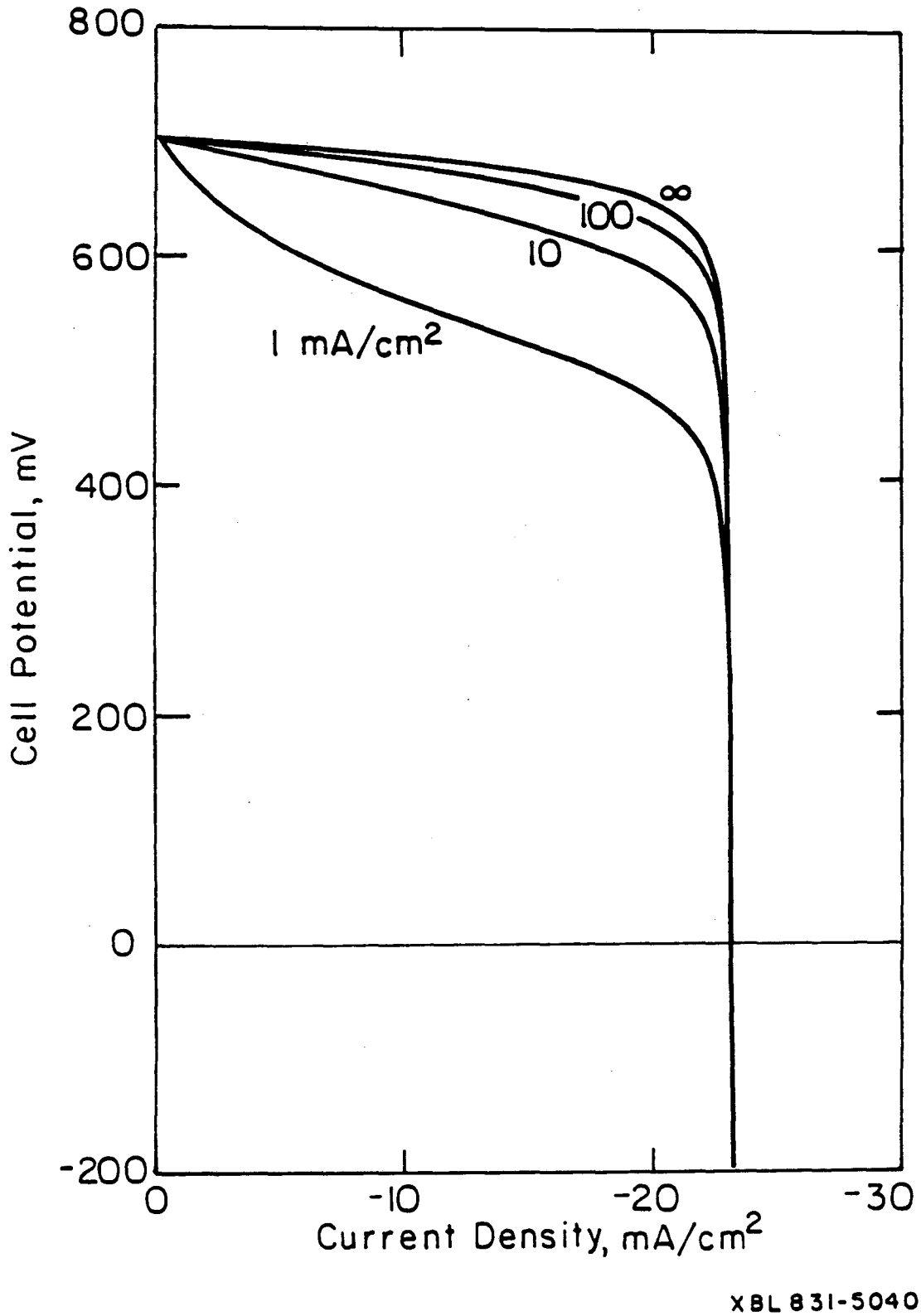

Figure 24. Computed current-potential curves for an n-type GaAs anode with counterelectrode exchange-current density as a parameter. Kinetic and mass-transfer effects at the counterelectrode have been included.

$$i_o = Fk_{a,f}^{\beta} c_{4,\infty}^{\beta} \left[\frac{k_{a,b} k_{b,b}^{1/2}}{k_{b,f}^{1/2}} c_{3,\infty}^{1/2} \right]^{(1-\beta)} ,$$

$i_{3,lim}$ is the diffusion-limited current density associated with species Se_2^{2-}, $i_{4,lim}$ is the diffusion-limited current density associated with species Se^{2-}, and n is equal to one.

The effect of diffusion limitation to currents at the counterelectrode is presented in Figure 23 with diffusion-limited current density at the counterelectrode as a parameter. Diffusion-limited current densities of 20 mA/cm^2 for Se_2^{2-} and 80 mA/cm^2 for Se^{2-} correspond to a Nernst stagnant diffusion layer thickness of about 0.010 cm. An exchange-current density of 100 mA/cm^2 was assumed. The influence of the exchange current density on the current-potential curve is presented in Figure 24. Diffusion-limited currents of 20 mA/cm^2 and 80 mA/cm^2 were assumed for the Se_2^{2-} and the Se^{2-} species, respectively. Kinetic limitations, either at the counterelectrode or the semiconductor, cause an inflection point in the current-potential curve.

The calculated maximum power efficiency is 11.8 percent for a cell with a 1.0 cm gap between the semiconductor and the counterelectrode, an exchange current density of 100 mA/cm^2, and diffusion limited currents of 20 mA/cm^2 and 80 mA/cm^2 at the counterelectrode for the Se_2^{2-} and the Se^{2-} species, respectively. Reduction of illumination due to absorption in the electrolyte and reflection were not included.

3.4.2. Front and back illumination. The semiconductor can be illuminated at the semiconductor-electrolyte interface (front illumination) or at the semiconductor-current collector interface (back illumination). The influence of the direction of illumination is strongly dependent upon the relative rates of recombination in the bulk and at the interfaces involved.

Under the conditions of a negligible surface recombination at the semiconductor-current collector interface and of a small rate of homogeneous recombination as compared to the rate of recombination at the semiconductor-electrolyte interface, back-illumination increases the power output. This effect is illustrated in Figure 25, where current-potential curves for the case with no interfacial kinetic limitations are presented for the semiconductor under front and back-illumination. The limiting current under back-illumination is -25.6 mA/cm^2 and the maximum power efficiency is 17.0 percent. The limiting current under front-illumination is -23.2 mA/cm^2 and the maximum power efficiency is 15.0 percent. Generation of electron-hole pairs in regions where recombination is facilitated reduces the power output.

4. DISCUSSION

Experimental results reported in the literature show the general shape of the current-potential curves presented in this chapter. Small scale systems are generally designed with large counterelectrode areas (to minimize any limitation to current flow at the counterelectrode) and a small depth of electrolyte over the semiconductor surface (to minimize losses of illumination by absorption in the electrolyte). Current-potential curves thereby obtained include effects of electrolyte resistance and illumination losses.

Inflection points are observed for many experimental systems, e.g., TiO_2 in 1.0 M NaOH,[108] TiO_2 in 0.1 M Na_2SO_4 at pH less than 10 (adjusted with NaOH and H_2SO_4),[109] $PbFe_{12}O_{19}$, $Hg_2Ta_2O_7$, $CdFe_2O_4$, and $Pb_2Ti_{1.5}W_{0.5}O_{6.5}$ in 0.2 M NaOH,[110] n and p-type GaP in liquid ammonia,[111] p-GaP in 0.5 M H_2SO_4,[112] WO_3 in 1 M sodium acetate,[113] $KTaO_3$ in 8.6 M NaOH,[114] CdS in 0.1 M NaOH,[115] CdS

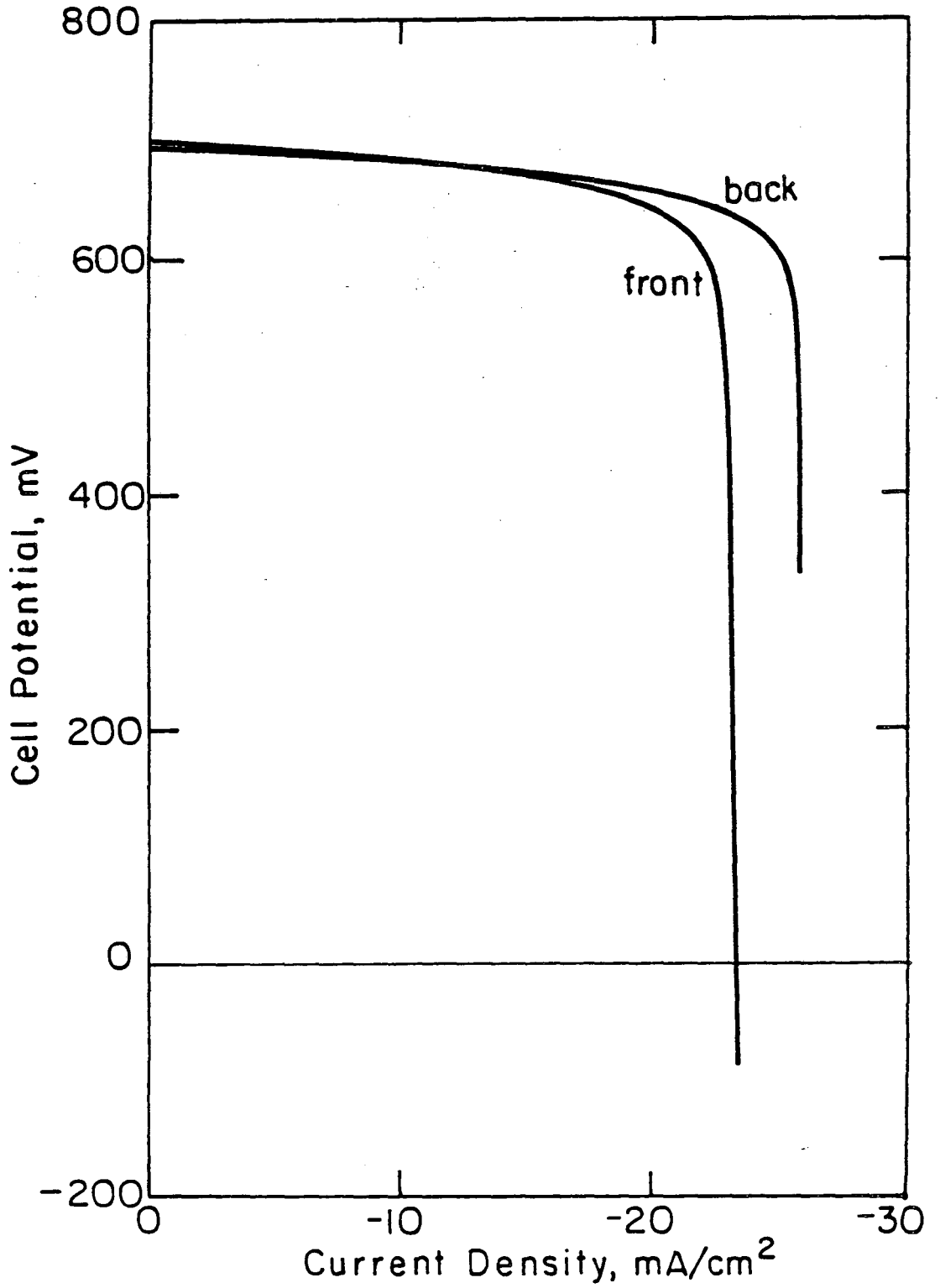

Figure 25. Computed current-potential curves for an n-type GaAs anode with the direction of illumination (front or back illumination) as a parameter.

in 1.0 M NaI, 1.0 M $Na_2S_2O_3$, and 0.1 M I_2,[116] and untreated polycrystalline GaAs with a selenium redox couple.[8] These inflection points are indicative of kinetic limitations to charge-transfer or to ion-adsorption reactions at the semiconductor-electrolyte interface (as shown by the parameter variation in Figures 5 and 10 in section 3.1). Other systems, e.g., ruthenium-treated polycrystalline GaAs[8,40] and single-crystal GaAs[44] in contact with a selenium redox couple, CdS and Bi_2S_3 in contact with a sulphide-polysulfide redox couple[36], CdS in 1M KCl, 0.8M CH_3COOH, and 0.2 M CH_3COOHa,[117] and p-InP in contact with a vanadium redox couple,[8] do not exhibit inflection points. The interfacial reactions are equilibrated for these systems.

The results of the mathematical model presented in this chapter are compared to experimental results in Figure 26. The solid line represents the experimental current-potential curve for a ruthenium-treated n-GaAs photoanode in contact with a selenium redox couple.[42,43] The dashed lines are calculated results in which interfacial reactions were assumed to be equilibrated. Both calculated curves include a seven percent loss of illumination; the lower curve includes an electrolyte resistance of 3 Ω cm^2. The model parameters are presented in Tables 1, 2, and 3. Bulk transport properties were obtained from the literature; values were assumed for properties characteristic of the semiconductor-electrolyte interface. The model agrees with the experimental results near open circuit but exhibits a sharper limiting-current plateau than the experimental results indicate. An increase in the homogeneous recombination rate constants decreases the sharpness of the potential drop near limiting current but also decreases the cell potential. This change in parameter must be accompanied by an increase in the equilibrium OSS potential (see chapter 6). The computer program did not converge at large values of Φ_{oss}.

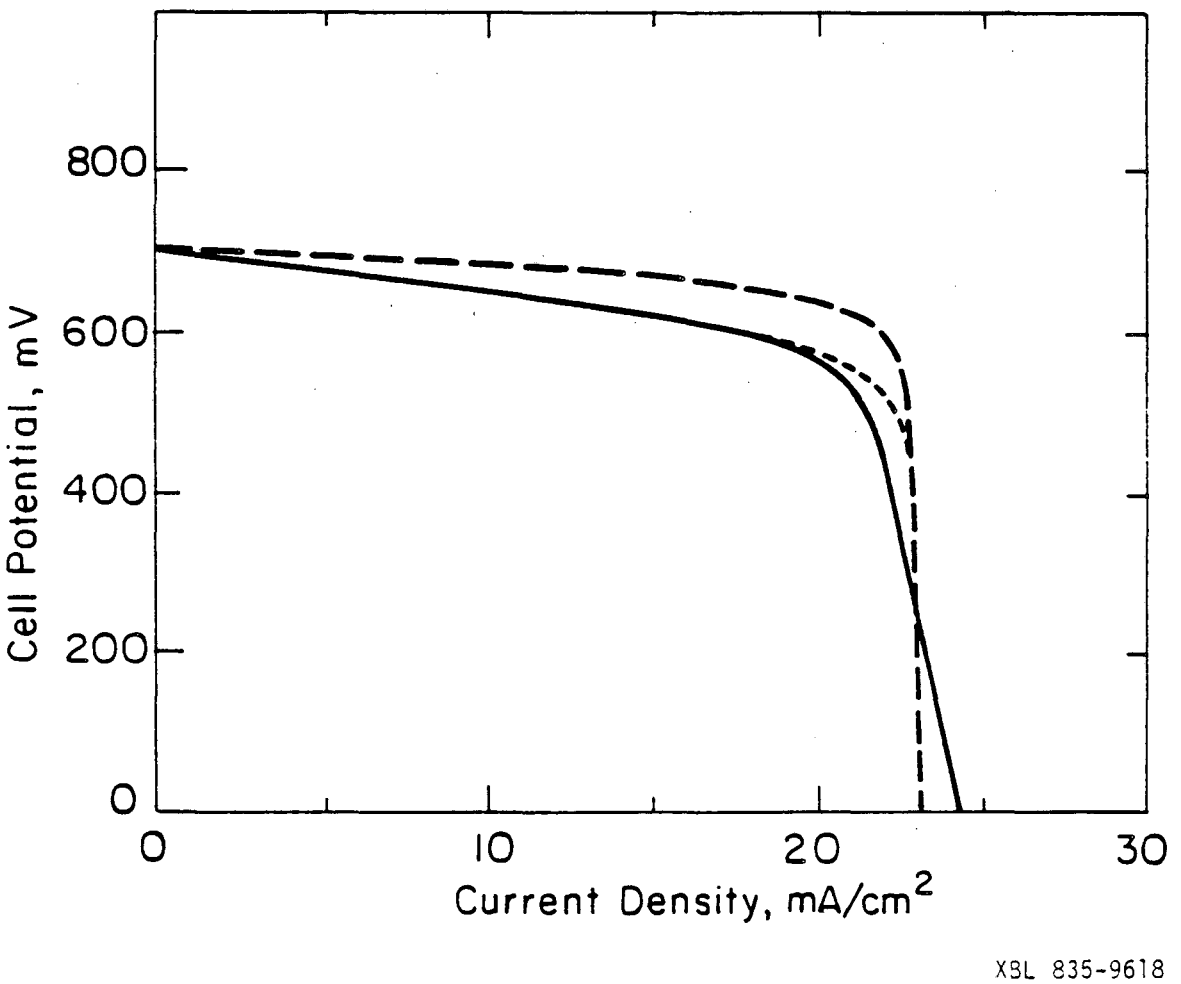

Figure 26. Comparison of computed current-potential curves (dashed lines) to experimental results (solid line) for an n-type GaAs anode in contact with a selenium redox couple.

Some of the model parameters are associated with characteristics of the current-potential curve. In the absence of counterelectrode effects, the magnitude of the limiting current is determined by the intensity of illumination, and the shape of the curve is determined by kinetic parameters. Kinetic limitations to charge-transfer and to ion-adsorption reactions result in an inflection point. Kinetic limitations at the counterelectrode can also cause an inflection point. The magnitude of the open-circuit potential is a function of the equilibrium potential difference between the semiconductor and the solution. Within the model, this parameter is represented by the equilibrium OSS potential. The surface site energy distribution also influences the open-circuit cell potential. These parameters could be varied by selection of different semiconductor-electrolyte combinations. The open-circuit cell potential is also affected by semiconductor properties such as band-gap energy and absorption coefficient.

Analytic models of the liquid-junction cell are described in section 1.2.1 These models can match experimental current-potential curves but show maxima in electron and hole concentrations near the boundary between space-charge and neutral regions. These maxima were not seen in the results of the mathematical model and are probably due to imposition of boundary or matching conditions between those regions.

5. CONCLUSIONS

Kinetic limitations to interfacial charge-transfer and ion-adsorption reactions drastically reduce the power output of the liquid-junction cell. A small interfacial rate constant is compensated by increased potential and concentration driving forces, thus influencing the cell performance.

The cell performance is strongly influenced by bulk-semiconductor and cell-design properties such as the dopant concentration, the semiconductor thickness, and the amount of light adsorbed in the semiconductor. An optimal dopant concentration and semiconductor thickness can be calculated for a given semiconductor system. The resistance of the electrolyte and kinetic and mass transfer limitations at the counterelectrode influence cell performance and may play an important role in the optimal design of a liquid-junction photovoltaic cell.

Chapter 3. Design and Optimization of the Liquid-Junction Photovoltaic Cell

Most studies of the liquid-junction photovoltaic cell have been oriented toward developing an understanding of the semiconducting electrode which characterizes the cell (see, e.g., Chapter 2 and references 1-19). This work describes the design and optimization of liquid-junction photovoltaic devices. The advantages and problems inherent in the liquid-junction cell are reviewed, and a mathematical model of the liquid-junction cell is used to predict the optimal performance of various cell configurations. An economic analysis is presented based upon these results.

1. INTRODUCTION

The liquid-junction photovoltaic cell has appeal because, in contrast to solid-state junctions, the junction between electrolyte and semiconductor is formed easily and allows use of polycrystalline semiconductors. The electrochemical nature of the cell allows both production of electricity and generation of chemical products which can be separated, stored, and recombined to recover the stored energy. These features could make the liquid-junction cell an economical alternative to solid-state photovoltaic devices for solar energy conversion.

Liquid-junction cells also have the advantages that are attributed to other photovoltaic devices. Photovoltaic power plants can provide local generation of power on a small scale. The efficiency and cost of solar cells is independent of scale, and overall efficiency is improved by locating the power plant next to the load. Nuclear and fossil-fuel burning plants, in contrast, are economical only if built on a large scale (on the order of 1000

megawatts).[118]

The design of a liquid-junction photovoltaic cell requires selection of an appropriate semiconductor-electrolyte combination and design of an efficient cell configuration. The selection of a semiconductor is based upon the band gap, which provides an upper limit to the conversion efficiency of the device, and the choice of electrolyte is governed by the need to limit corrosion. The optimal design of the liquid-junction photovoltaic cell is aided by use of mathematical models.

1.1. Band Gap

Photovoltaic cells rely on the unique properties of semiconductors to convert incident radiation to electrical current. The semiconductor property of interest is the moderate gap between the valence and the conduction-band energy levels. Incident photons of light with energy greater than or equal to the band-gap energy transfer their energy to valence-band electrons, producing conduction-band electrons and vacancies in the valence band.

An upper limit to the efficiency of photovoltaic devices can be established, based upon the band gap and the solar spectrum, without consideration of cell configuration. This "ultimate efficiency" is given by[11]

$$\eta_{ult} = \frac{\int_{E_g}^{\infty} N(E)\, dE}{\int_{0}^{\infty} E\, N(E)\, dE} \qquad (1)$$

where E_g is the semiconductor band-gap energy, E is the photon energy, and $N(E)$ is the number density of incident photons with energy E. The fraction of the power in the solar spectrum that can be converted to electrical power is a function of the band gap of the semiconductor.

Photons with energy less than the band gap cannot produce electron-hole pairs. Photons with energy greater than the band gap yield the band gap energy.[119-121]

The "ultimate efficiency" of Equation (1) is presented in Figure 1 as a function of band gap.[11,122,123] The value presented represents an upper limit to conversion of solar energy; factors such as reflection and absorption losses of sunlight, kinetic and mass transfer limitations, and recombination will reduce the efficiency. These effects are included in section 2.2. A band gap between 1.0 and 1.5 eV is generally considered to be appropriate for efficient conversion of solar energy.

1.2. Corrosion

The application of liquid-junction technology to photovoltaic power conversion is limited by problems associated with the semiconductor-electrolyte interface. Primary among these problems is corrosion. Efficient conversion of solar energy requires a band gap between 1.0 and 1.5 eV, and most semiconductors near this band gap corrode readily under illumination. Semiconductors with large band-gaps (4 to 5 eV) tend to be more stable but cannot convert most of the solar spectrum.

Among the approaches taken to solve this problem, the most successful concern the matching of an electrolyte to the semiconductor. The rate of corrosion is reduced if the semiconductor is in equilibrium with the corrosion products. The rate of corrosion can also be reduced by using a redox couple which oxidizes easily. The oxidation of the redox couple Se_{x+1}^{2-}/Se_x^{2-}, for example, has been shown to compete successfully with photocorrosion reactions for holes in n-type GaAs electrodes.[8,105]

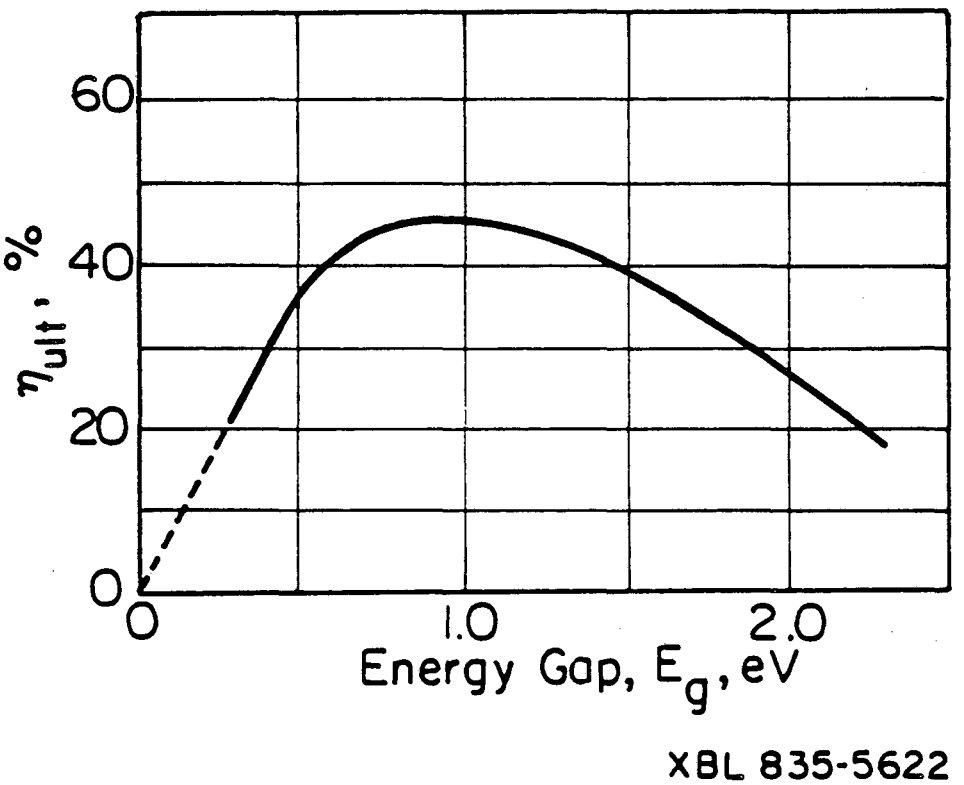

Figure 1. The fraction of the solar energy which can be utilized in electron-hole pair generation as a function of semiconductor band-gap.

P-type semiconductors used as cathodes are more stable than the more common and generally more efficient n-type semiconducting anodes. The inefficiency of p-type photocathodes has been attributed to the presence of surface states near the valence band energy. A stable p-type photocathode has been developed, however, with a solar conversion efficiency of 11.5 percent.[124] Protective films have been proposed to be a solution to electrode corrosion. The electrode, in this case, would be a small band-gap semiconductor covered by a film composed of either a more stable large band-gap semiconductor, a conductive polymer, or a metal. A large Schottky barrier is frequently present at such semiconductor-metal and semiconductor-semiconductor interfaces which blocks the flux of holes from the semiconductor to the electrolyte. In cases where the photocurrent is not blocked, corrosion can take place between the semiconductor and the protective film.[17,45] Menezes *et al.*[125] discuss the difficulties in avoiding absorptive losses in the metal film while maintaining sufficient integrity to serve the semiconductor corrosion protection function. Frese *et al.*[126] have, however, reported a measurable improvement in the stability of GaAs with less than a monolayer gold metal coverage. Thin conductive polypyrrole films appear to be successful in inhibiting corrosion in some electrolytes.[127-132] In addition, insulating polymer films deposited on grain boundaries can improve the performance of polycrystalline semiconductors by reducing surface recombination rates.[133]

1.3. Mathematical Model

Development of a mathematical model constitutes an important step toward design and optimization of the liquid-junction photovoltaic cell. A one-dimensional mathematical model has been developed (see Chapter 2)

which treats explicitly the semiconductor, the electrolyte, and the semiconductor-electrolyte interface in terms of potentials and concentrations of charged species. The model incorporates macroscopic transport equations in the bulk of the semiconductor and electrolyte. Homogeneous and heterogeneous recombination of electron-hole pairs is included within the model. Recombination takes place at the semiconductor-electrolyte interface through interfacial sites, which can enhance the recombination rate. Surface sites at the semiconductor-metal interface were not included within the model.

The coupled nonlinear ordinary differential equations of the model were posed in finite-difference form and solved numerically. The mathematical model can be used to gain insight into the operation of cells with semiconducting electrodes, and to optimize their design. The model was used here to calculate the effect of cell design on the performance of an n-type GaAs semiconducting anode in contact with an 0.8 M K_2Se, 0.1 M K_2Se_2, 1.0 M KOH electrolytic solution. The choice of this semiconducting electrode system was based upon the work of Heller and associates.[8,42,43,105] Cell design parameters are presented in Table 1, and the parameters used in modeling

Table 1. Counterelectrode Parameters

Diffusion-Limited Current Density	$i_{3,lim}$	20.0 mA/cm^2
	$i_{4,lim}$	80.0 mA/cm^2
Exchange Current Density	i_o	100.0 mA/cm^2

the liquid-junction cell are presented in Chapter 2.

2. CELL CONFIGURATION

The optimal design of liquid-junction photovoltaic cells shares constraints with solid-state photovoltaic cells.[22,134] Current collectors cast shadows and can reduce the amount of sunlight absorbed in the semiconductor. A constraint unique to the liquid-junction cell is the placement of the counterelectrode relative to the semiconductor-electrolyte interface. Mass-transfer and kinetic limitations at the counterelectrode and resistance of the electrolyte can play important roles in the optimal design of the liquid-junction photovoltaic cell. These considerations are treated qualitatively by Parkinson.[135]

Under electrolyte-side illumination and without illumination losses, interfacial kinetic limitations, electrolyte resistance, and counterelectrode limitations, the maximum power efficiency of the cell was calculated to be 15.3 percent. The corresponding value under back (or current-collector) side illumination was calculated to be 17.2 percent. These are the values that one might calculate using a potential drop measured between the semiconductor electrode and a reference electrode reversible to the redox reaction and located just outside the diffusion region. The resistance of the electrolyte, illumination losses, and mass-transfer and kinetic limitations at the counterelectrode affect these values and are influenced by cell design. The difference between front and back illumination is due to the assumption that facilitated recombination does not take place at the semiconductor-current collector interface.

The performance of three cell configurations was calculated for operation under AM-2 solar illumination (882 W/m^2). The semiconductor was

assumed to be in the form of a thin film (see Mitchell for a review of thin-film photovoltaic technologies[136]). Interfacial kinetic limitations were not included. The physical parameters were the same as presented in Chapter 2. The one-dimensional model of the liquid-junction cell was coupled with the resistance to current flow associated with the two-dimensional systems. Some methods for calculation of this resistance were reviewed by Fleck *et al.*[137]

2.1. System 1: Wire Counterelectrode

The liquid-junction photovoltaic cell with a wire-grid counterelectrode is presented in Figure 2a. The cell consists of a semiconductive film supported on a metallic current collector, a wire-grid counterelectrode, and a transparent glass cover plate. The space between the cover plate and the semiconductor is filled with the electrolyte. The glass plate is an essential part of the cell because it keeps the system clean and allows optimal orientation of the cell for optimal collection of sunlight. This cell is designed for conversion of solar energy into electrical energy; no provision is made for separation of chemical products. A two-dimensional representation of the cell is presented in Figure 2b.

Sunlight absorbed in the semiconductor must pass through the cover plate, past the counterelectrode, and through the electrolyte. Reflection at each of the interfaces (air-glass, glass-electrolyte, and electrolyte-semiconductor), absorption in the glass and electrolyte, and screening by the counterelectrode decrease the amount of light which can be used for generation of electron-hole pairs. Absorption losses in the electrolyte can be limited by maintaining a small gap between the counterelectrode and the semiconductor. A wide spacing of counterelectrode elements reduces the

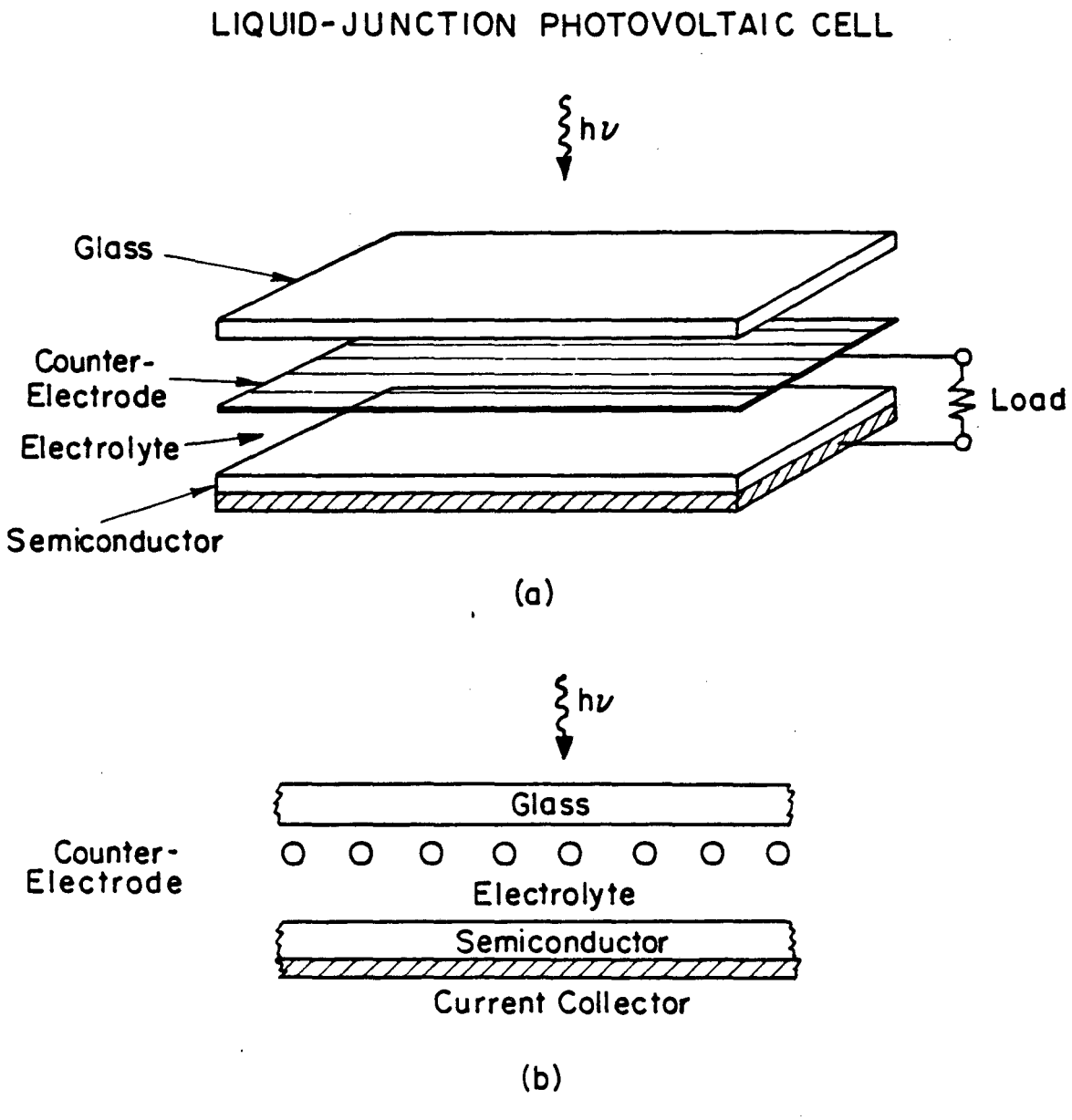

XBL 835-9622

Figure 2. Design of the liquid-junction photovoltaic cell.
System 1: wire counterelectrode.

screening of the semiconductor but also increases the influence of kinetic and mass-transfer effects at the counterelectrode.

The one-dimensional model of the liquid-junction photovoltaic cell was used with averaged uniform current density and solar flux. The shadow of the counterelectrode was implicitly assumed to be diffuse. Resistive losses in the electrolyte were calculated from a two-dimensional solution of Laplace's equation.[138-142] The potential drop in the electrolyte was given by equation (14) in reference (35). The current density at the counterelectrode was assumed to be uniform and was related to the semiconductor current density by

$$i_{ce} = i_{sc} \left(\frac{L}{\pi D}\right), \tag{2}$$

and the counterelectrode shadow was assumed to reduce the magnitude of incident light by a factor of $(1-D/L)$. The effective solar flux was therefore given by

$$\begin{aligned} q_{sc} = q_o\left(1 - \frac{D}{L}\right)(1 - \rho_{air-glass})e^{-(mx)_{glass}} \\ (1 - \rho_{glass-soln})e^{-(mx)_{soln}}(1 - \rho_{soln-sc}), \end{aligned} \tag{3}$$

where ρ_{j-k} is the reflectance associated with the interface $j-k$ and m is the extinction coefficient for a given phase of depth x.

The design parameter for this cell design is the ratio of the counterelectrode element spacing to the counterelectrode element diameter, L/D. When L/D has a value of one, the semiconductor is completely shaded from illumination; when L/D is very large, counterelectrode limitations dominate.

The power density of the cell with a counterelectrode radius of 0.05 cm is presented in Figure 3 as a function of current density with L/D as a parameter. The maximum power density is presented in Figure 4 as a

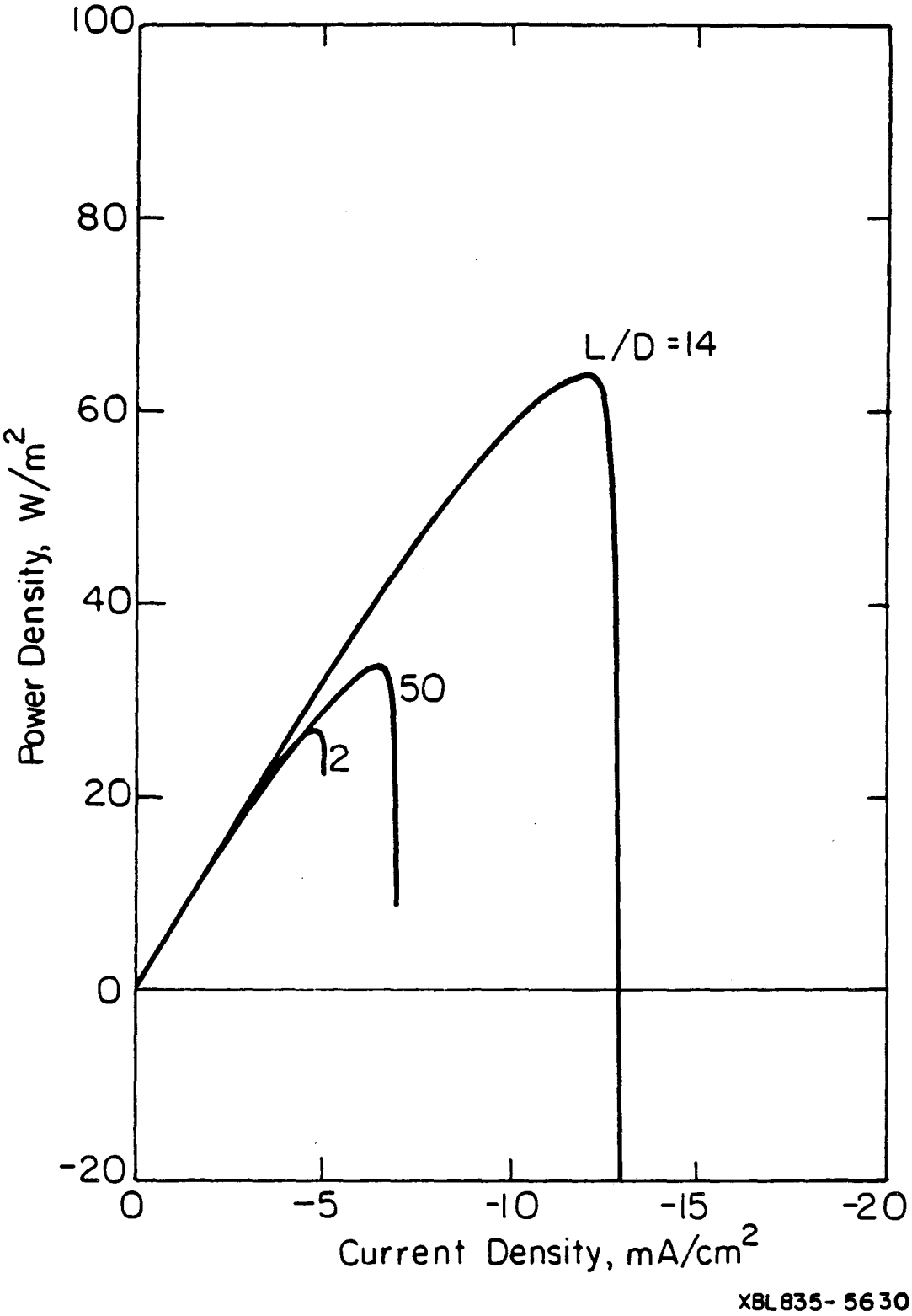

Figure 3. Power density as a function of current density for system 1 with a counterelectrode element diameter of 0.10 cm.

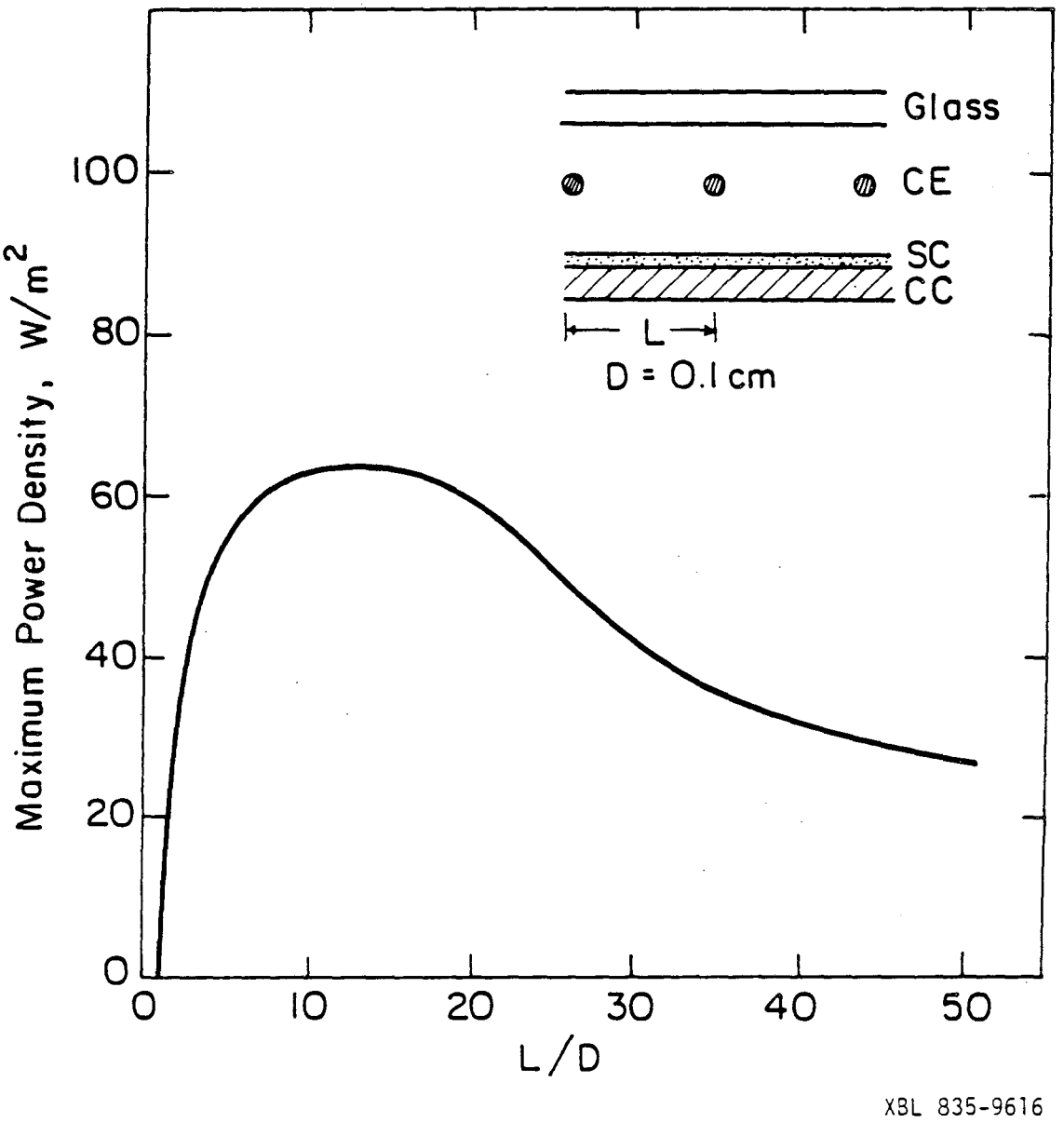

Figure 4. Maximum power density as a function of L/D for system 1 with a counterelectrode element diameter of 0.10 cm.

function of L/D. The separation between the cover plate and the counterelectrode was 0.5 cm, and the separation between the semiconductor and the counterelectrode was 0.5 cm. The electrolyte depth was therefore 1.1 cm. The optimal value of L/D is 14., and the maximum power density obtained is 63.5 W/m^2. The current density under the optimal condition is 11.8 mA/cm^2 delivered at a cell potential of 538.7 mV. The maximum power efficiency of the wire counterelectrode cell was 7.2 percent.

Kinetic limitations at the counterelectrode further reduce this efficiency. An exchange current density of 1 mA/cm^2 leads to a 5.5 percent power efficiency at an optimal L/D of 10.

2.2. System 2: Slotted Semiconductor

The liquid-junction cell configuration with a slotted-semiconductor electrode is presented in Figure 5. A glass cover plate protects the cell. Sunlight passes through the cover plate and the electrolyte and illuminates the semiconductor surface. Electrical current passes between the semiconductor and the counterelectrode through slots cut in the semiconductor. This configuration has the advantage that no shadows are cast upon the semiconductor; furthermore reaction products could be separated if a membrane were placed between the semiconductor and the counterelectrode.

The primary current distribution and the resistance of a cell containing a slotted electrode were calculated using numerical methods coupled with the Schwarz-Christoffel transformation (see chapter 4). The cell resistance is a function of three geometric ratios, chosen to be t/G, h/G, and L/h (see Figure 2a of chapter 4), where L is the half-length of the protruding electrode assembly, t is the thickness of the protruding electrode assembly,

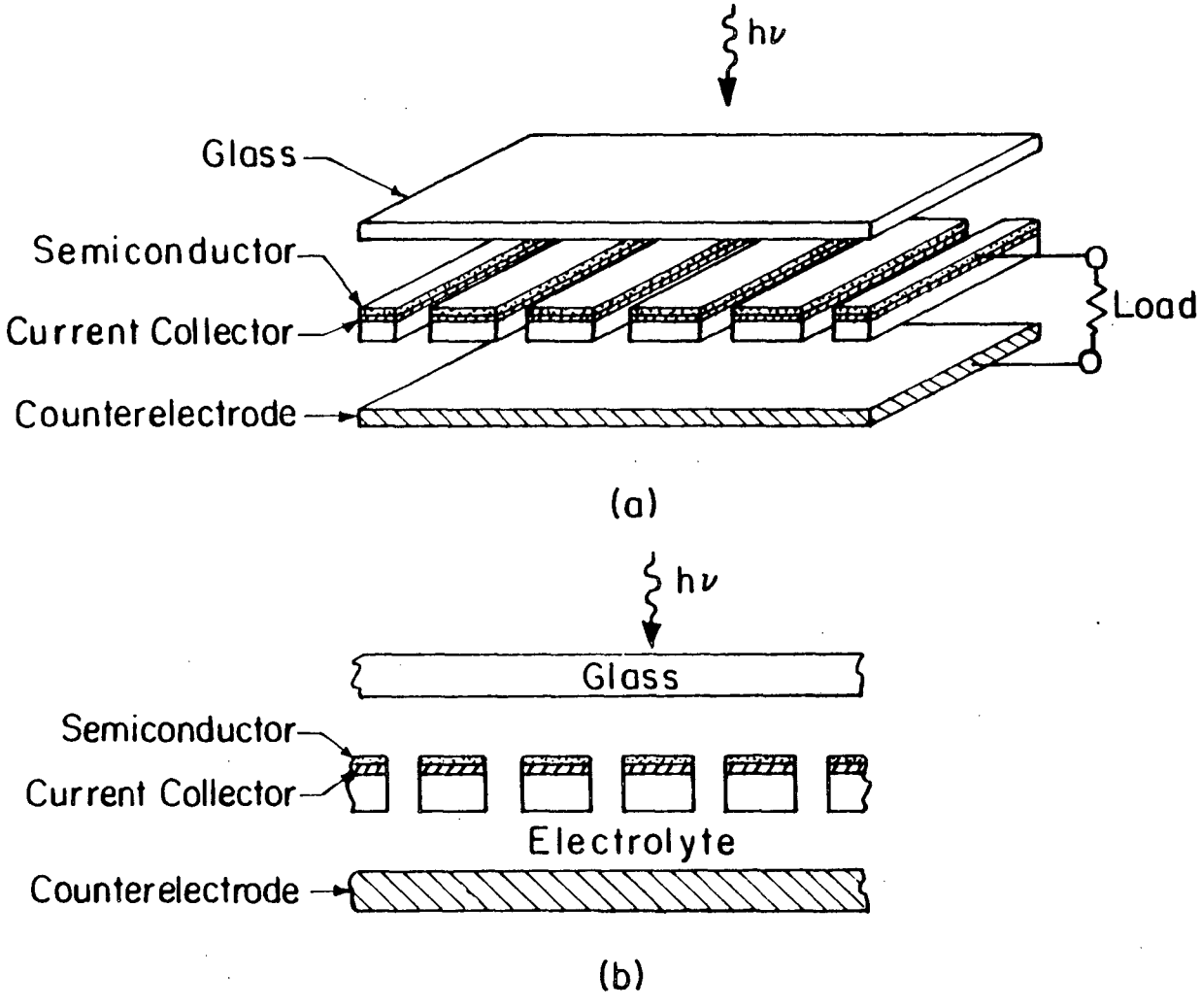

XBL 831-7974

Figure 5. Design of the liquid-junction photovoltaic cell. System 2: slotted semiconductor.

G is the half-gap between the electrode assemblies, and h is the separation between the electrode and the upper insulating wall. h is also the separation between the counterelectrode and the lower edge of the semiconductor-electrode assembly.

The performance of this cell is a function of four geometric parameters. The distance between the counterelectrode and the semiconductor assembly was chosen to be 0.5 cm, and the semiconductor assembly thickness was assumed to be 0.1 cm. The primary resistance for this system is presented in Figure 6 as a function of L/D with h/G as a parameter. The maximum power density is presented in Figure 7 as a function of L/h with h/G as a parameter. L/h was varied by varying the half-length; h/G by varying the half-gap. The maximum power density for this system is obtained with a small gap. For h/G=0.5 (G=1cm), the maximum power density was 47.8 W/m^2, and the maximum power efficiency was 5.4 percent. The current density under maximum power conditions was 15 mA/cm^2 delivered at 477.6 mV. For h/G=10 (G=0.05cm), the maximum power density was 67.7 W/m^2, and the maximum power efficiency was 7.7 percent. At maximum power the current density was 15.2 mA/cm^2 delivered at 534.6 mV.

2.3. System 3: Back-Illuminated Semiconductor

A cell design is presented in Figure 8 in which the semiconductor is illuminated from the current-collector side. The semiconducting film is deposited on a pane of transparent conducting glass. A current-collecting grid is used to offset the low conductivity of the glass. The semiconductor is separated from the counterelectrode by a gap filled with electrolyte. This design could be used with a membrane within the gap, which would allow

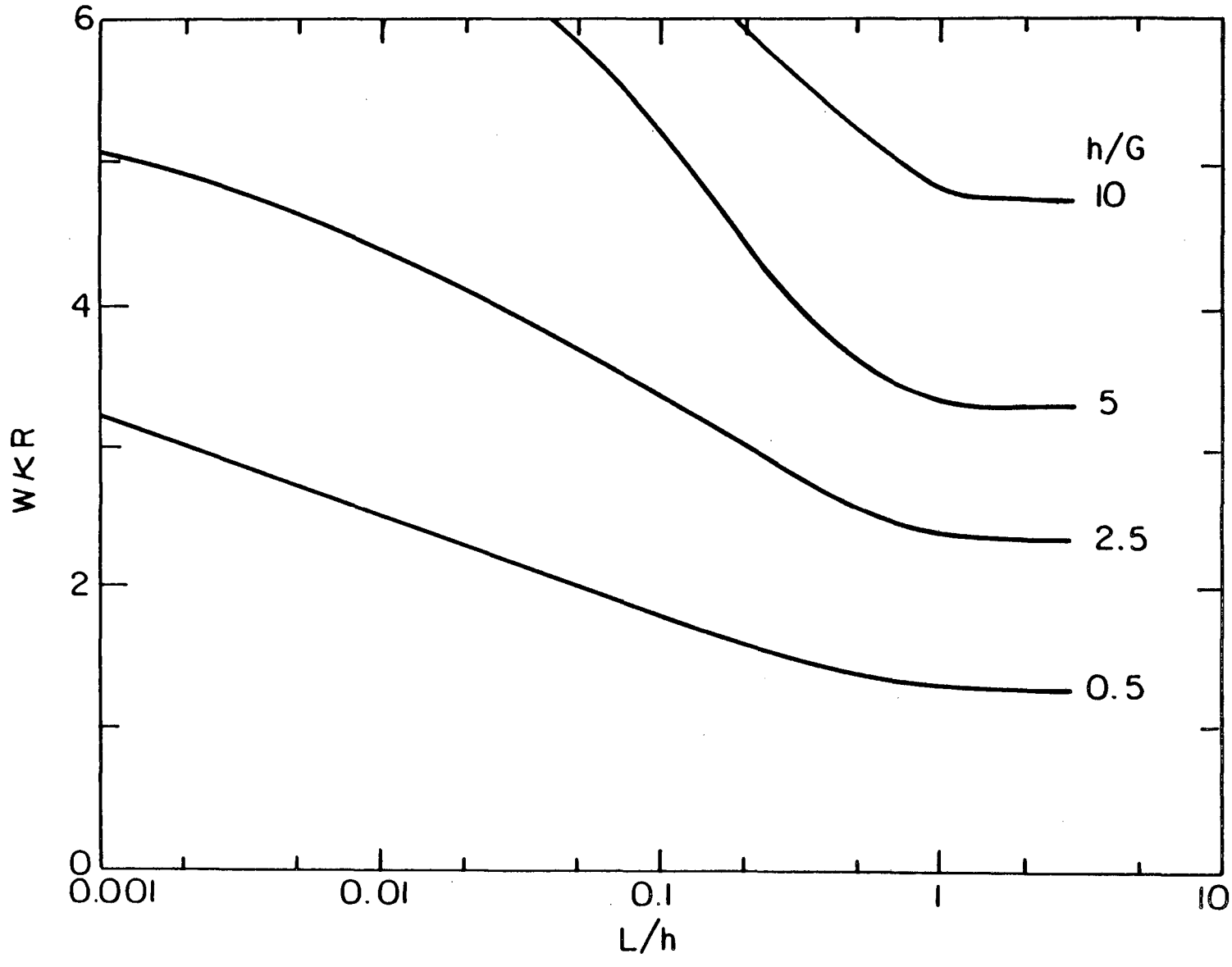

XBL 835-5618

Figure 6. Primary cell resistance as a function of L/h for system 2 with h/G as a parameter.

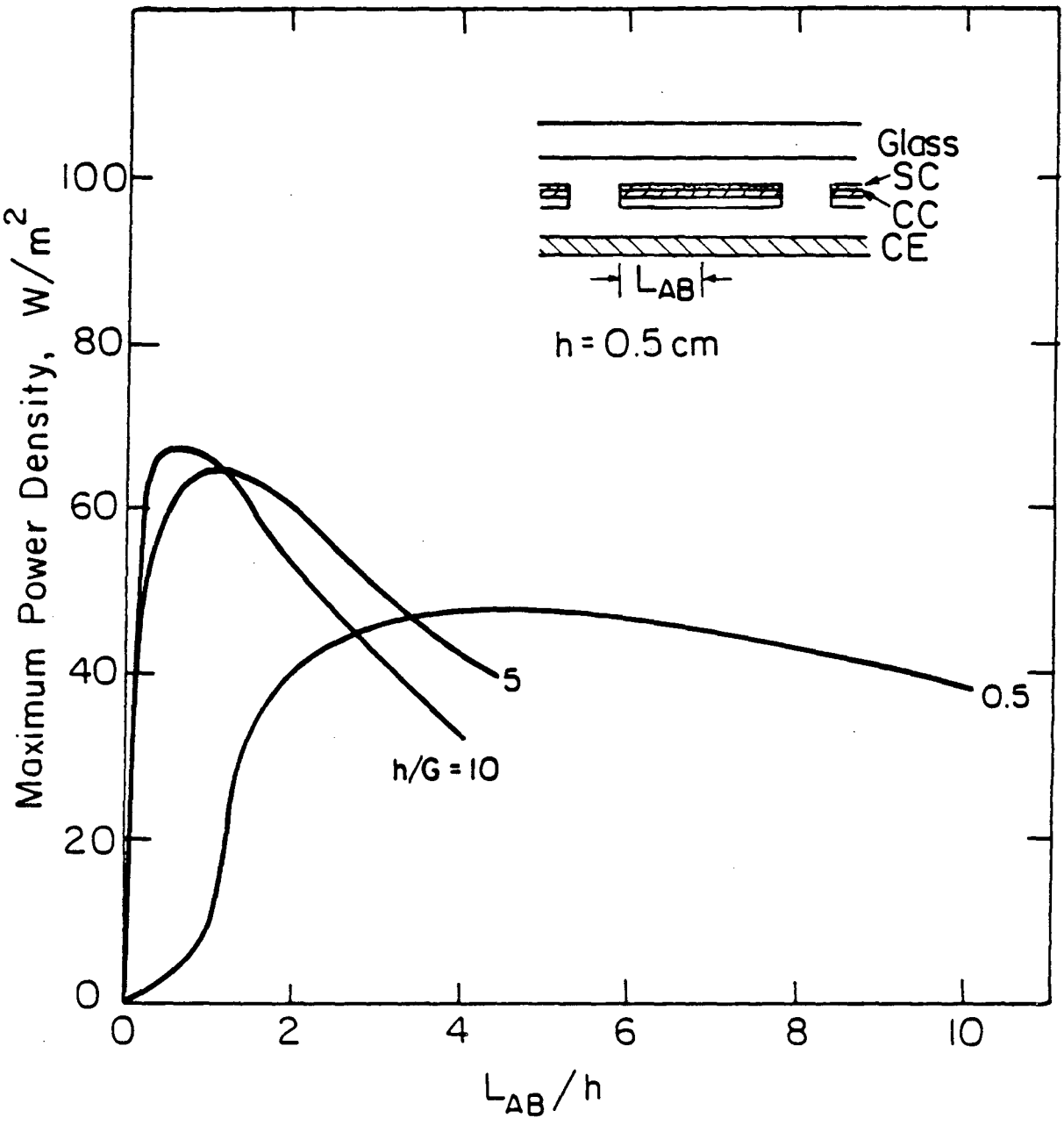

XBL 831-7975 A

Figure 7. Maximum power density as a function of L/h for system 2 with h/G as a parameter.

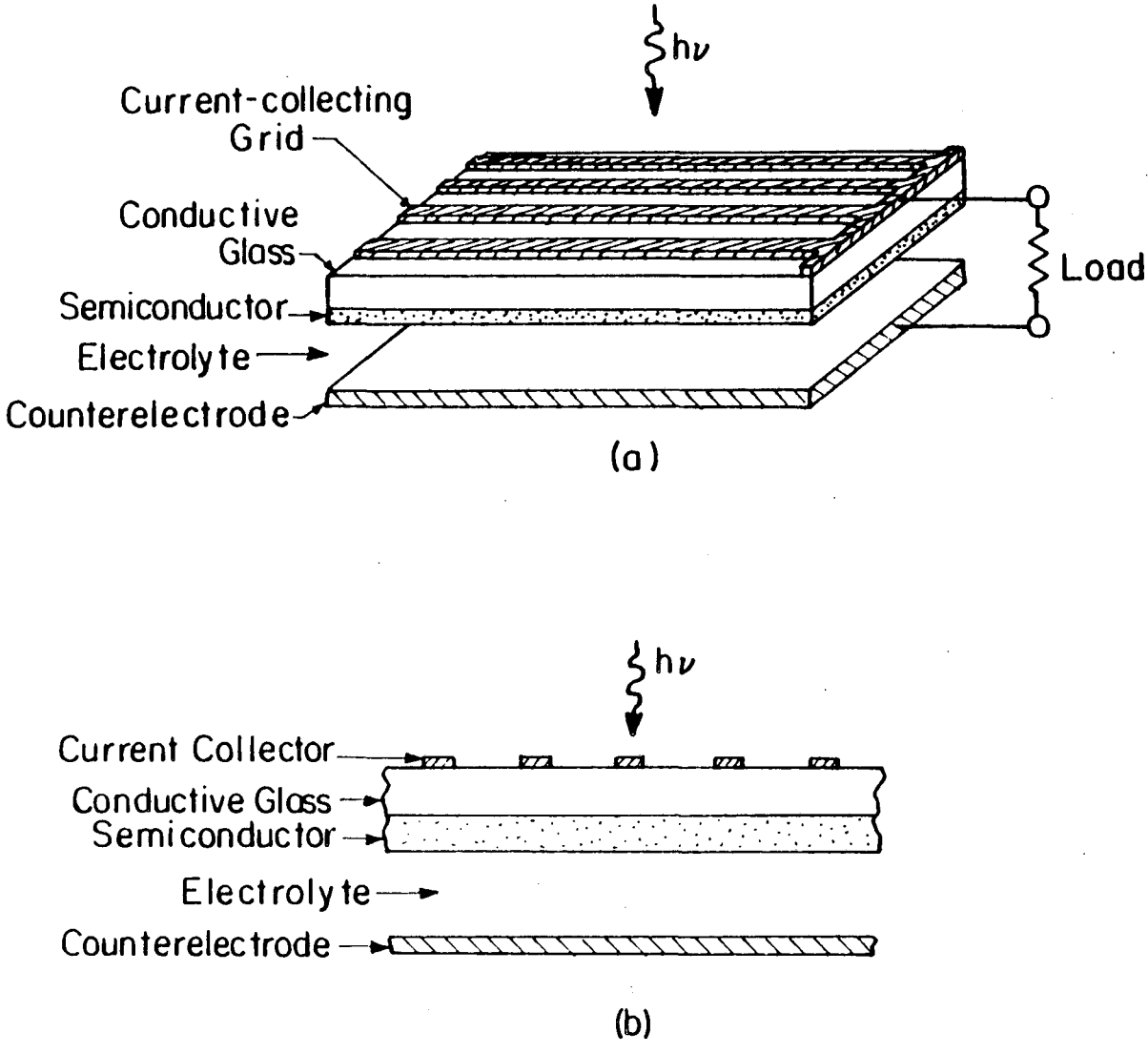

XBL 835-9615

Figure 8. Design of the liquid-junction photovoltaic cell. System 3: back-illuminated semiconductor.

separation of reaction products at each of the electrodes.

The potential drop between the semiconductor and the current-collecting grid can be obtained through application of the general solution to the resistance of a rectangular conductor with arbitrarily placed electrodes presented by Moulton.[143,144] The region between the semiconductor and the grid is presented in Figure 9a in a complex coordinate system where $z = x + iy$. The rectangular conductor is given by $OABC$, the semiconductor by PQ, and the grid element by RS. The Schwarz-Christoffel transformation[144-146] is used to map the coordinate system z, through intermediate half-plane systems (Figures 9b, 9c, and 9d), onto one in which Laplace's equation can be solved easily. This system is shown in Figure 9e, where $\chi = \zeta + i\xi$. The sides of the rectangle, OA and AB, have length l and l' respectively.

The z-coordinate system is related to the w-plane by

$$z = \int_a^w \frac{1}{(w-a)^{1/2}(b-w)^{1/2}(c-w)^{1/2}(d-w)^{1/2}}\, dw \,. \tag{4}$$

A bilinear transformation into the t-plane is made such that when $w = a$, $t = 0$; when $w = b$, $t = 1$; when $w = c$, $t = 1/k^2$; and when $w = d$, $t = \infty$. This transformation is written

$$t = \frac{(d-b)(w-a)}{(b-a)(d-w)} \,, \tag{5a}$$

and

$$\frac{1}{k^2} = \frac{(d-b)(c-a)}{(b-a)(d-c)} \,. \tag{5b}$$

Equation (4) becomes

$$z = \frac{2}{[(c-a)(d-b)]^{1/2}} \int_0^t \frac{1}{[4z(1-z)(1-k^2z)]^{1/2}}\, dt \,. \tag{6}$$

The constants a, b, c, and d are arbitrary quantities which can be chosen

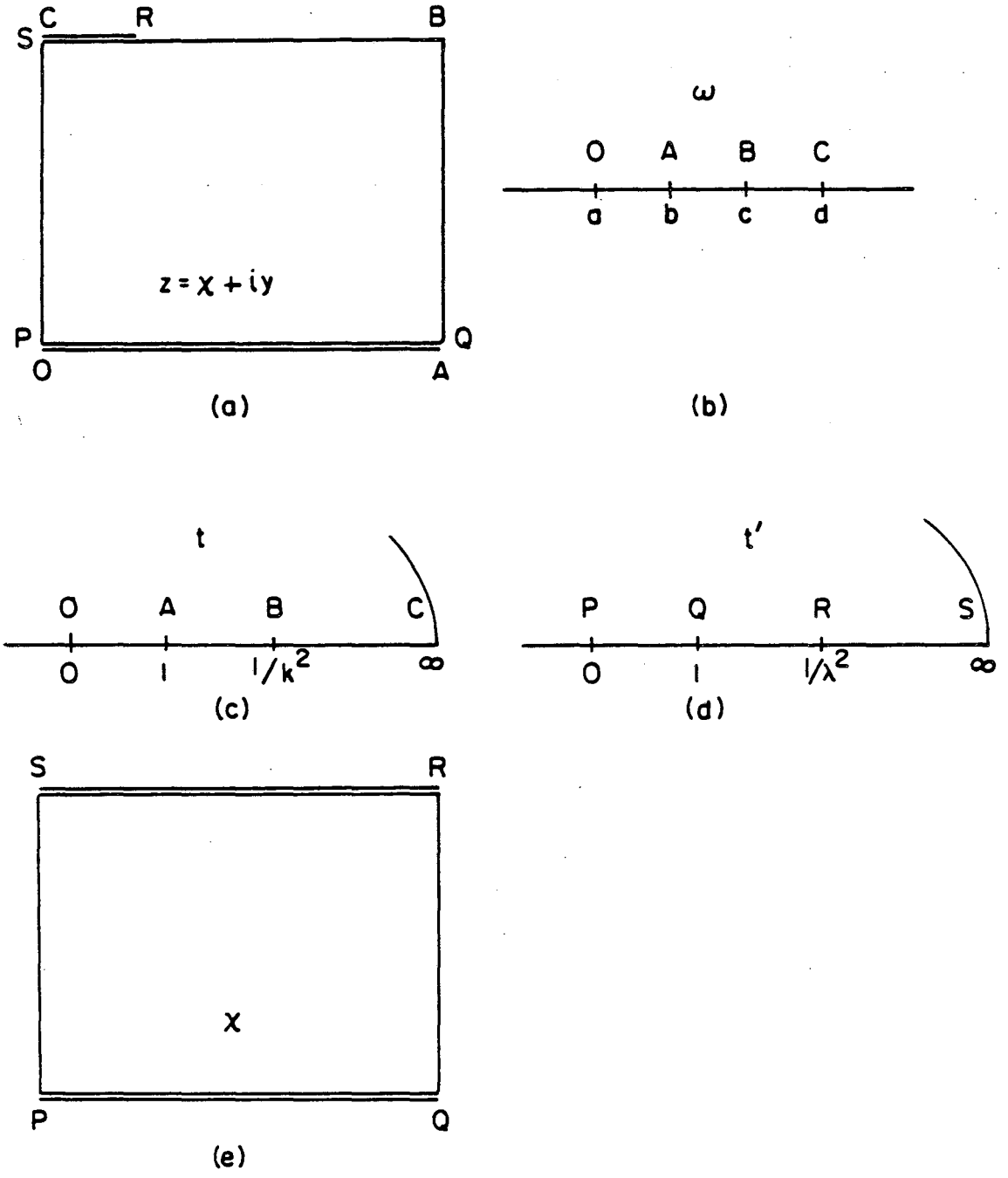

XBL 835-5617

Figure 9. Schematic representation of the mapping of rectangles to planes by the Schwarz-Christoffel transformation.

such that

$$m = \frac{1}{2}\sqrt{(c-a)(d-b)}\,,$$

$$\frac{K'(m)}{K(m)} = \frac{l'}{l}\,,$$

and

$$m = \frac{K'(m)}{l'} = \frac{K(m)}{l}\,.$$

Here, $K(m)$ is the complete elliptic integral of the first kind given by

$$K(m) = \int_0^{\pi/2} \frac{d\varphi}{\sqrt{1 - k^2\sin^2\varphi}}\,,$$

and m is the parameter, related to the modulus k by $m = k^2$. The complementary parameter m_1 is related to the parameter by $m_1 = 1 - m$, and

$$K'(m) = K(m_1)$$

relates $K'(m)$ and $K(m)$. Equation (6) can be expressed as[147]

$$mz = sn^{-1}(\sqrt{t}\,|\,m)\,, \tag{7}$$

or

$$t = sn^2(mz\,|\,m)\,. \tag{8}$$

The positions of the electrodes in the z-space are given by $z = z_1$ at P, $z = z_2$ at Q, $z = z_3$ at R, and $z = z_4$ at S, and in the t-plane by $t = \alpha$ at P, $t = \beta$ at Q, $t = \gamma$ at R, and $t = \delta$ at S. From equation (8), $\alpha = sn^2(mz_1\,|\,m)$, $\beta = sn^2(mz_2\,|\,m)$, $\gamma = sn^2(mz_3\,|\,m)$, and $\delta = sn^2(mz_4\,|\,m)$. The t-plane is transformed to the χ-space through an intermediate t'-plane, described by

$$t' = \frac{(\delta-\beta)\,(t-\alpha)}{(\beta-\alpha)\,(\delta-t)}\,, \tag{9a}$$

and

$$\lambda^2 = \frac{(\beta-\alpha)\,(\delta-\gamma)}{(\delta-\beta)\,(\gamma-\alpha)}\,. \tag{9b}$$

The constants α, β, γ, and δ are chosen such that

$$\mu = \lambda^2 = \frac{1}{2}\sqrt{(\gamma-\alpha)(\delta-\beta)}\,,$$

$$\frac{L'(\mu)}{L(\mu)} = \frac{QR}{PQ}\,,$$

and

$$\mu = \frac{L'(\mu)}{QR} = \frac{L(\mu)}{PQ}\,.$$

Under this transformation, the t'-plane is related to the χ-space by

$$t' = sn^2(\chi|\mu)\,. \tag{10}$$

The quantity $L'(\mu)/L(\mu)$ is a geometric resistance. The resistance of the original system is given by

$$R = l\rho\,\frac{(L'(\mu)}{L(\mu))}\,, \tag{11}$$

where ρ is the resistivity of the rectangular conductor.

Solution of the equations in terms of elliptic functions was performed numerically.[148] The modulus m was obtained from

$$m = 16\exp[-(\pi\,\frac{K'(m)}{K(m)} + \frac{m}{2} + \frac{21}{64}\,m^2)] \tag{12a}$$

for $K'(m)/K(m)$ greater or equal to 1 and by

$$m_1 = 16\exp[-(\pi\,\frac{K(m)}{K'(m)} + \frac{m_1}{2} + \frac{21}{64}\,m_1^2)] \tag{12b}$$

for $K'(m)/K(m)$ less than 1. The error in this approximation is greatest for $K'(m)/K(m)$ equal to 1. and is 0.6 percent, with a corresponding error in the resistance of 0.092 percent. The value of the integrals $K(m)$ and $L(\mu)$ were obtained by the series expansion[148]

$$\begin{aligned} K(m) = {} & 1.38629436112 + 0.09666344259(m_1) + 0.03590092383(m_1)^2 \\ & + 0.03742563713(m_1)^3 + 0.01451196212(m_1)^4 \\ & - ln(m_1)[0.5 + 0.12498593597(m_1) + 0.06880248576(m_1)^2 \\ & + 0.03328355346(m_1)^3 + 0.00441787012(m_1)^4] \end{aligned} \tag{13}$$

For the system of Figure 9a, the positions of the equipotential surfaces are given by $z_1 = 0$, $z_2 = l$, $z_3 = x + il'$, and $z_4 = il'$. Thus, from equation

(9b),

$$\mu = \lambda^2 = m\, sn^2\left(\frac{x}{l} \middle| m\right). \qquad (14)$$

The elliptic function, $sn\left(\frac{x}{l} \middle| m\right)$, was calculated using a series expansion for m close to one,[148] and the Landen transformation[148] was used to improve accuracy for m < 0.9999.

The transparent conducting support for the semiconducting film was assumed to be SnO_2, which is commonly used as a transparent electrode. SnO_2 is a large band-gap semiconductor and is essentially transparent to light with energy below 3.7 eV. The properties of SnO_2 have been reviewed by Jarzebski and Marton.[149-151] The conductivity of the transparent material was assumed to be 50 mho/cm, and the total absorption and reflection losses at the air-SnO_2 interface for a 1/8 inch thick plate were assumed to be 8 percent. The reflectance at the SnO_2-GaAs interface was assumed to be 5 percent. The separation between the counterelectrode and the semiconductor was 0.5 cm.

The maximum power density is presented in Figure 10 as a function of the ratio of the current-collector-element spacing to the element width L/D. When L/D is equal to one, the semiconductor is completely blocked, and the power density is zero. When L/D is large, the resistance of the SnO_2 becomes important. The optimal value of L/D is around 100.; the maximum power density is 118.5 W/m^2, and the power efficiency is 13.4 percent. The current density under optimal operating conditions is 21.0 mA/cm^2 delivered at a cell potential of 564.3 mV.

The excellent performance of this cell design as compared to systems 1 and 2 can be misleading. Facilitated recombination at the semiconductor-metal interface was not included in the model. The back-illuminated system

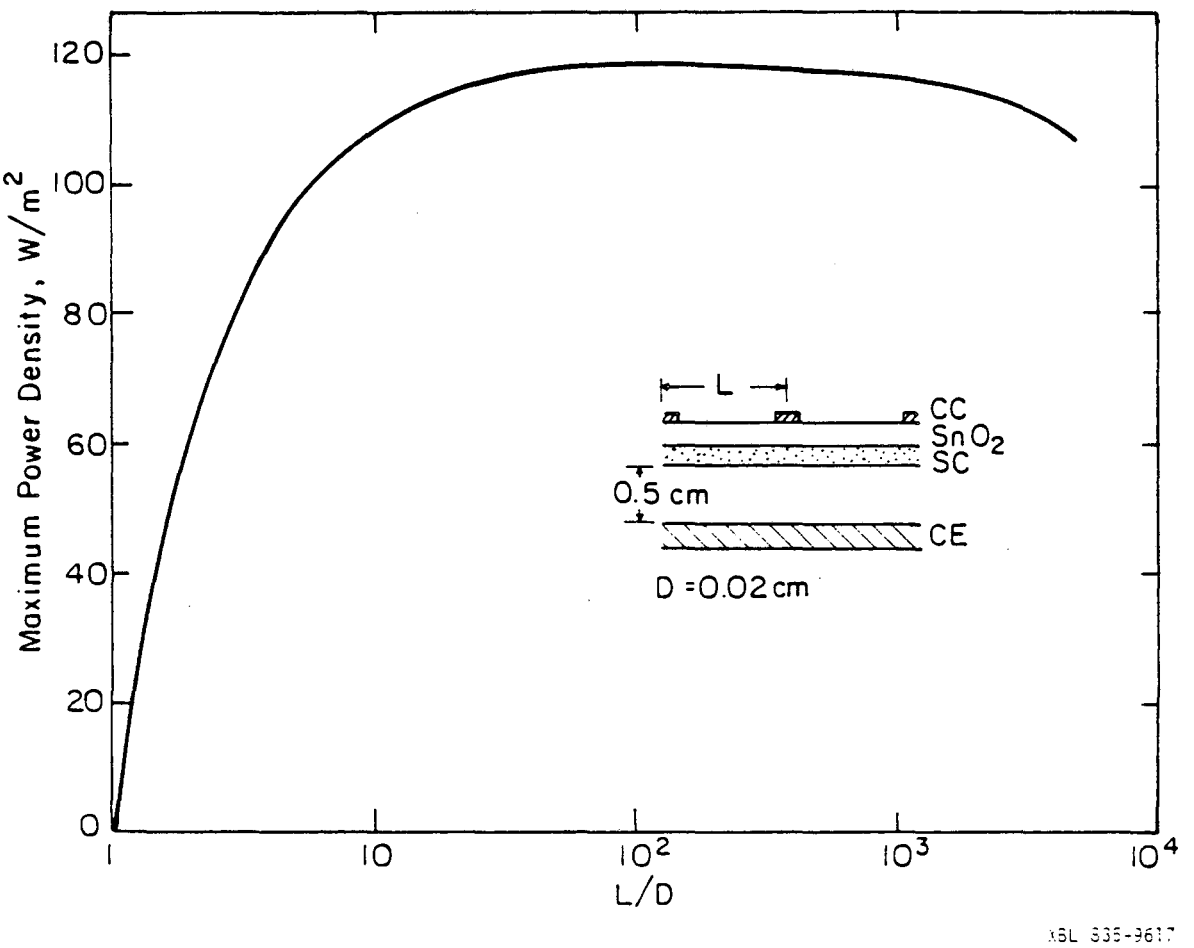

Figure 10. Maximum power density as a function of L/D for system 3 with a current-collector element thickness of 0.01 cm.

does have inherent advantages over front-illuminated cells. Optical losses, for example, can be smaller, and separation of electrochemical products is feasible. The relative rates of electron-hole recombination at the semiconductor-metal and the electrolyte-semiconductor interfaces, however, will influence the relative merit of front and back illumination.

3. INTENSITY OF ILLUMINATION

The intensity of solar illumination varies with location, cloud cover, day of year, and time of day. In addition, mirrors and lenses can be used to concentrate the sunlight and reduce the amount of semiconducting material incorporated into the cell. The prediction of the performance of a given design of the liquid-junction photovoltaic cell must therefore consider the effect of the intensity of illumination.

The maximum power efficiency is presented as a function of illumination intensity in Figures 11, 12, and 13 for systems 1, 2, and 3, respectively. The cells were designed with the design parameters calculated to be optimal under AM-2 illumination. The power efficiency decreases with increasing illumination due to the influence of electrolyte resistance and kinetic and mass-transfer limitations at the counterelectrode. These phenomena become increasingly important as current densities increase, and mass-transfer limitations at the counterelectrode result in an upper limit for cell currents.

The maximum power efficiency for systems 2 and 3 without counterelectrode limitations is also presented in Figures 12 and 13. These results are appropriate for cells with porous counterelectrodes. A porous counterelectrode may not be feasible for system 1 because of the need in this system to pass sunlight through the counterelectrode. The efficiency

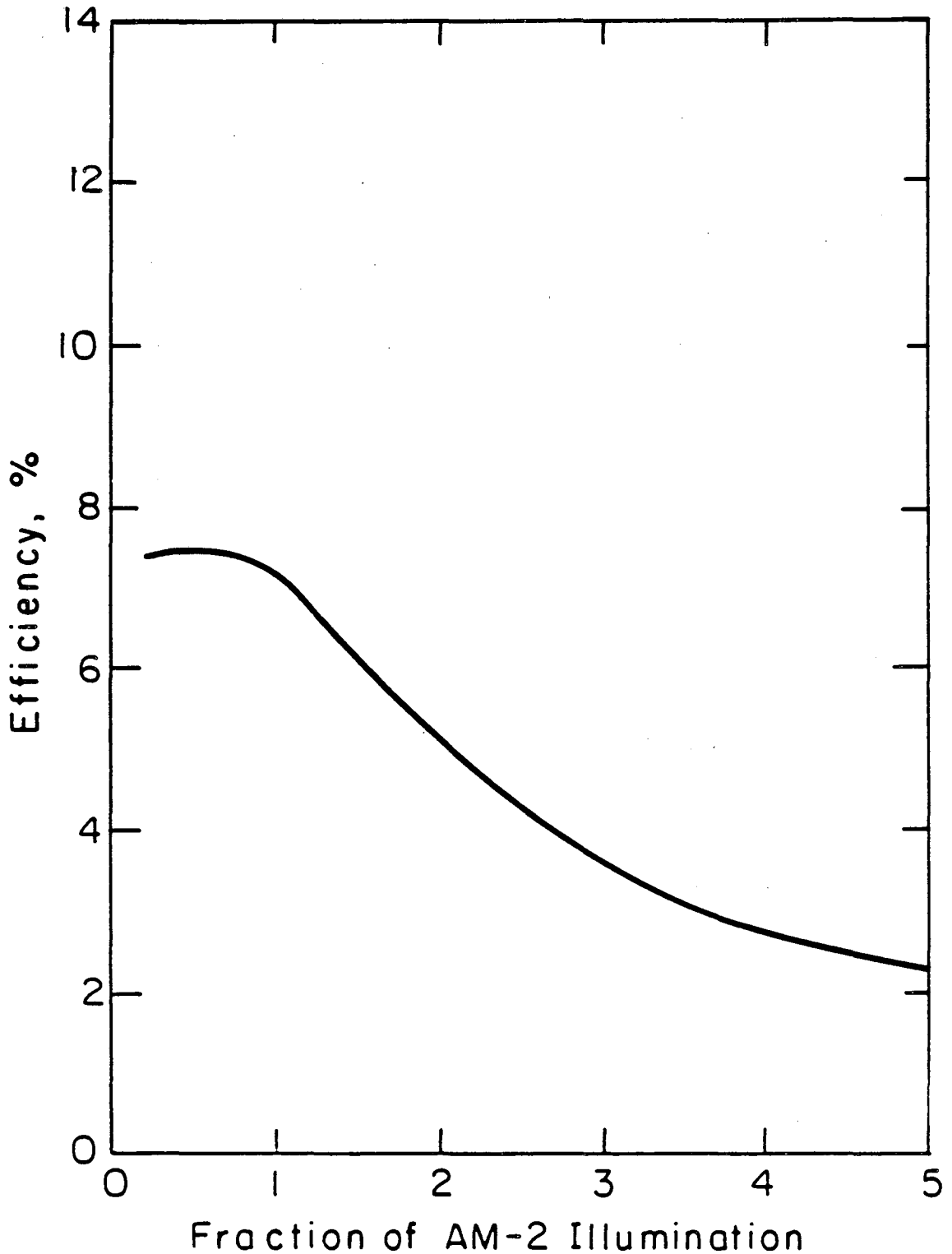

XBL 835-5614

Figure 11. Maximum power efficiency as a function of the fraction of AM-2 illumination (882 W/m^2) for system 1 with L/D = 14.

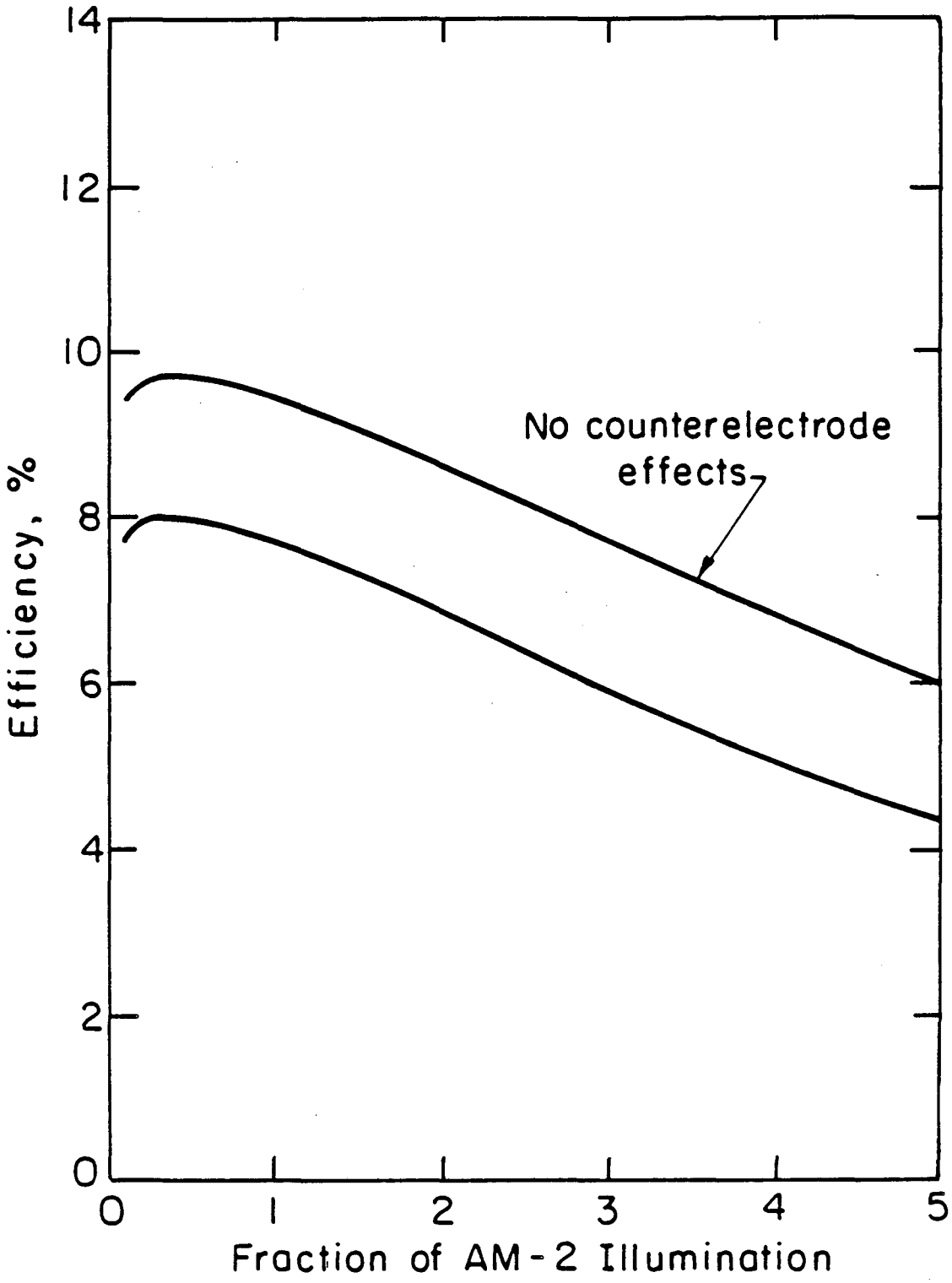

Figure 12. Maximum power efficiency as a function of the fraction of AM-2 illumination (882 W/m^2) for system 2 with h/G = 10 and L/h = 0.5.

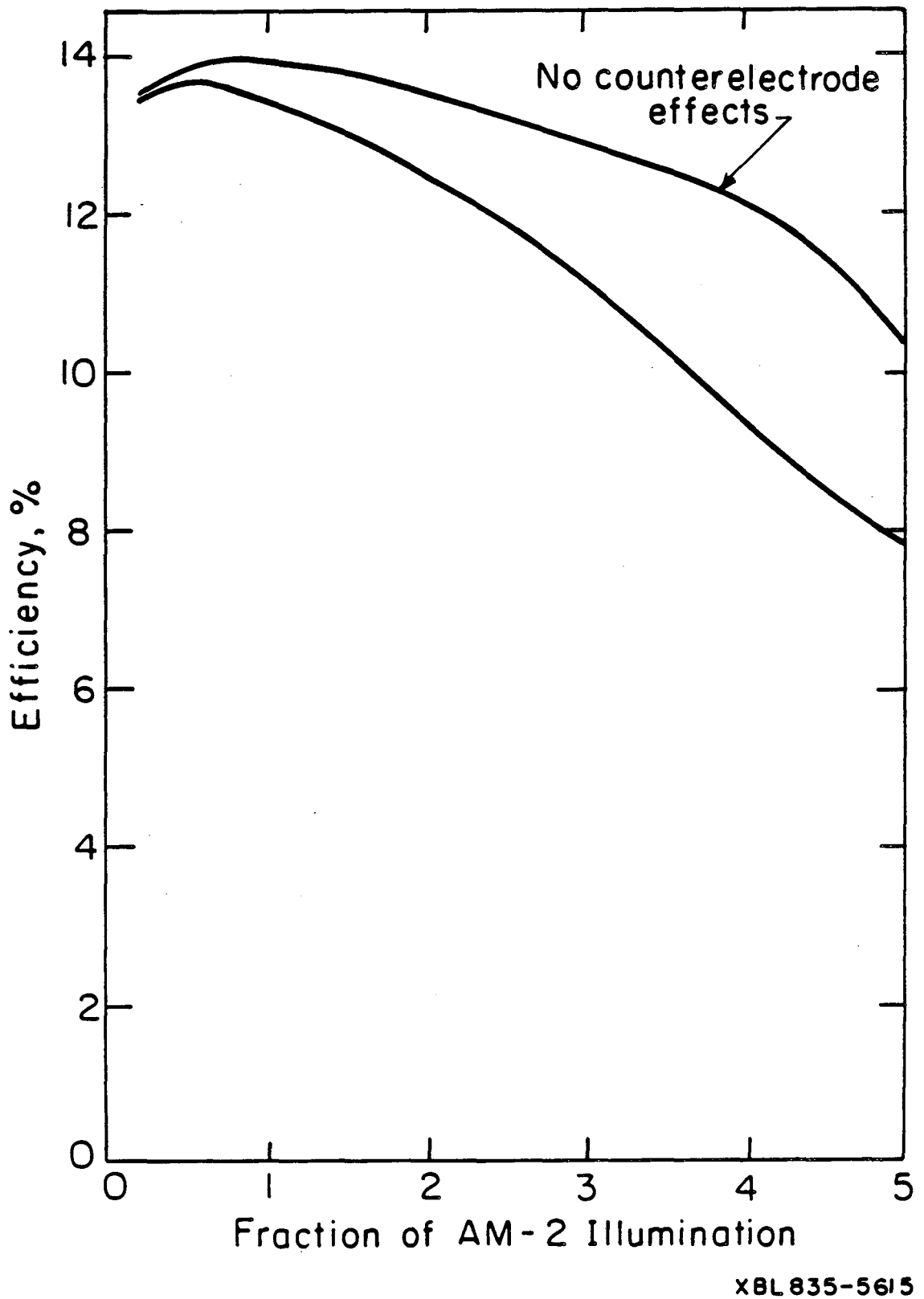

Figure 13. Maximum power efficiency as a function of the fraction of AM-2 illumination (882 W/m^2) for system 3 with a current-collector half width of 0.01 cm and with L/D = 100.

still decreases with illumination intensity due to electrolyte resistance.

The maximum cell current obtained under large magnitudes of illumination depends upon the ratio of the counterelectrode area to the semiconductor area. This ratio must be large for liquid-junction photovoltaic cells designed for large intensities of illumination. Replacement of the flat-plate counterelectrode with a porous electrode[152] can increase the counterelectrode area of systems 2 and 3. Inclusion of a cooling system in the cell design becomes important under these conditions. The electrolyte itself can serve as a heat exchange medium in photoelectrochemical systems.

4. DISCUSSION AND ECONOMIC ANALYSIS

The cells discussed in the previous sections can be divided into two groups, front and back illuminated, within which they can be compared fairly. The comparison of front and back illuminated cells depends upon the relative rates of recombination at the semiconductor-metal and electrolyte-semiconductor interfaces, and these rates will differ from one system to another.

The calculated power efficiencies are presented in Table 2 for the front-illuminated systems. Semiconductor effects, such as recombination, reduce the power efficiency from a value of 37 percent, based solely upon band gap, to 15.3 percent. Reflection losses, with an arbitrarily chosen 80 percent efficiency of illumination, reduce this value to 12.2 percent. This value can be compared to the 12 percent efficiency obtained in the experimental work of Heller and Miller.[8,42,43] The effect of cell design is to reduce the performance to 7.2 percent for system 1 and 7.7 percent for system 2.

Table 2. Power Efficiency under Front-Illummination

	No Illumination Losses	Illumination Losses	Experimental Results
Optimal Band Gap	45	36 (80%)	
GaAs Band Gap	37	32 (80%)	
Semiconductor-Electrolyte Junction	15.3	12.2 (80%)	12.0
Cell Design (1)	10.1	7.2 (55.4%)	
Cell Design (2)	9.8	7.7 (71.6%)	

The calculated power efficiencies are presented in Table 3 for the back-illuminated system. Semiconductor effects reduce the power efficiency from a value of 37 percent, based solely upon band gap, to 17.2 percent. Enhanced recombination at the semiconductor-current collector interface was not included in these calculations. The effect of cell design was to reduce the power efficiency to 13.4 percent.

The calculated performance could be improved by making distances between semiconductor and counterelectrode smaller, reducing the effect of electrolyte resistance. The values chosen for this analysis were based primarily on mechanical considerations. A spacing of 0.5 cm was used between all cell elements. A smaller spacing could result in shorting of counterelectrode and semiconductor and/or trapping of gas bubbles. The

Table 3. Power Efficiency under Back-Illumination

	No Illumination Losses	Illumination Losses
Optimal Band Gap	45	36 (80%)
GaAs Band Gap	37	32 (80%)
Current Collector and Semiconductor-Electrolyte Junction	17.2	13.8 (80%)
Cell Design (3)	15.4	13.4 (86.5%)

influence of the counterelectrode could be reduced by increasing the flow rate or degree of mixing near the counterelectrode, thereby increasing the limiting current. Kinetic limitations at the semiconductor-electrolyte interface were not considered here and may greatly reduce the performance of some semiconductor systems.

Current-potential curves are presented in Figure 14 for the front-illuminated cells. The optimally designed cells of systems 1 and 2 are compared to the cell without interfacial kinetic limitations, counterelectrode limitations, and electrolytic resistance. The cell with a slotted semiconductor has a larger power efficiency than the wire-grid counterelectrode cell and can be designed for separation of chemical products. The analysis of the system designed for separation of chemical products would include the electrical resistance of the membrane.

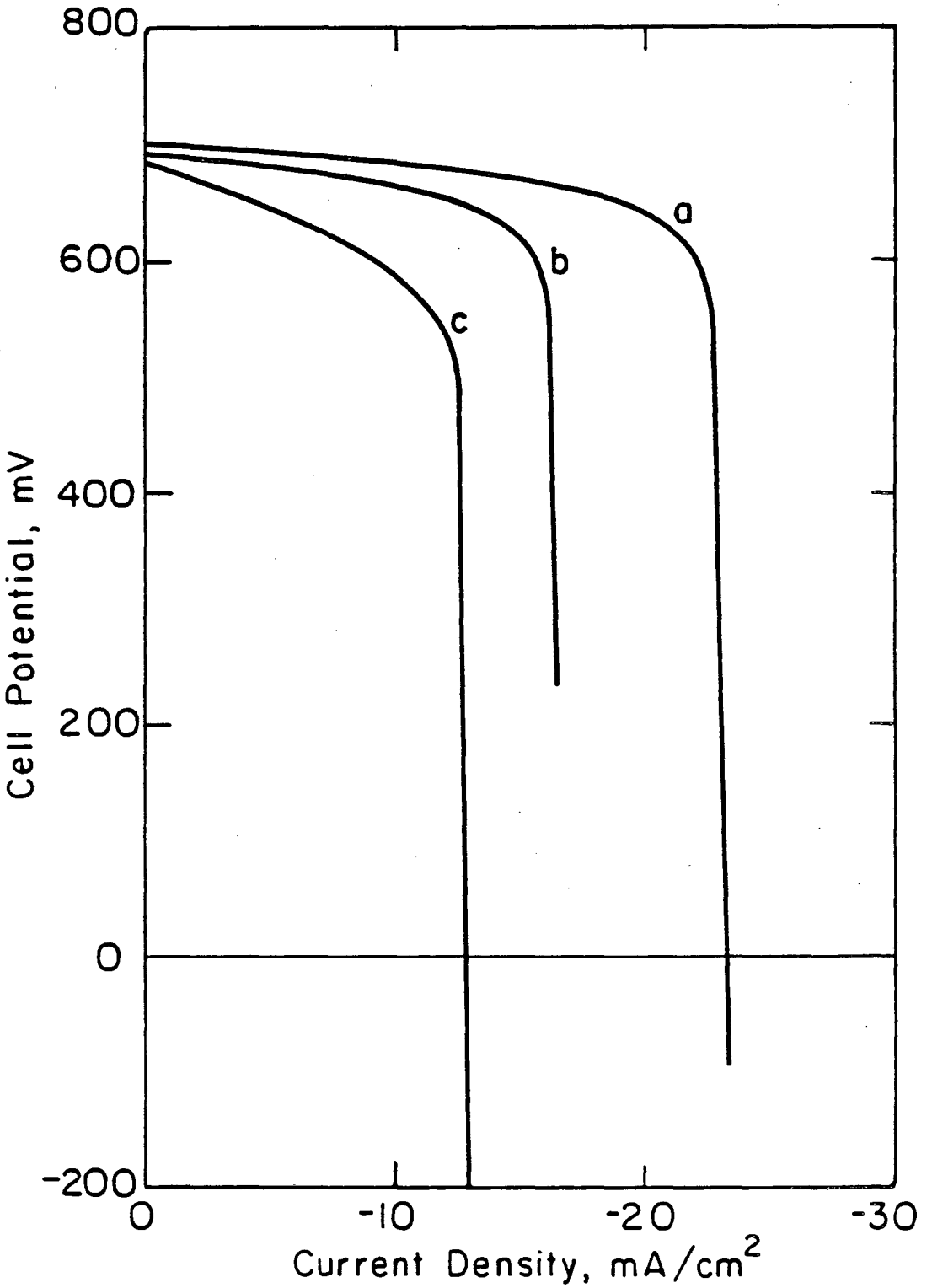

Figure 14. Cell potential as a function of current density for (a) a front-illuminated semiconductor without kinetic, electrolyte-resistance and counterelectrode limitations; (b) system 1 with a counter-electrode element diameter of 0.10 cm and with L/D = 14; and (c) system 2 with h/G = 10 and L/h = 0.5.

Current-potential curves are presented in Figure 15 for the back-illuminated cell. The optimally designed cell of systems 3 is compared to the cell without interfacial kinetic limitations, counterelectrode limitations, and electrolytic resistance. The back-illuminated design is appealing because chemical products can be separated and because of reduced losses of illumination.

The following discussion of cell economics is appropriate for all photovoltaic devices. The allowable capital investment for the cell is given by

$$I = 8.76\ P_{in}\ \eta\ \Delta c\ y_e\ , \tag{15}$$

where P_{in} is the annual incident illumination intensity averaged over 24 hours in W/m^2, η is the cell efficiency, Δc is the difference in selling price and operating cost in dollars/kW-hr, and y_e is the break-even point in years. This equation is presented as a nomogram in Figure 16. The power output of the liquid-junction cell is presented in Figure 16a as a function of the incident solar illumination with the average efficiency of the device as a parameter. The incident solar illumination is averaged over a 24 hour period. On this basis, the average insolation of the continental United States is 200 to 250 W/m^2.[11] Lenses or mirrors could be used to increase the amount of sunlight striking the semiconductor surface. The annual return on investment is presented in Figure 16b as a function of the power output with power cost as a parameter. The total initial investment is presented in Figure 16c as a function of the averaged annual investment with cell break-even period as a parameter.

Based upon a 7.7 percent power efficiency (averaged over 24 hours), 250 W/m^2 incident illumination (averaged over 24 hours), 0.05 dollars/kW-hr

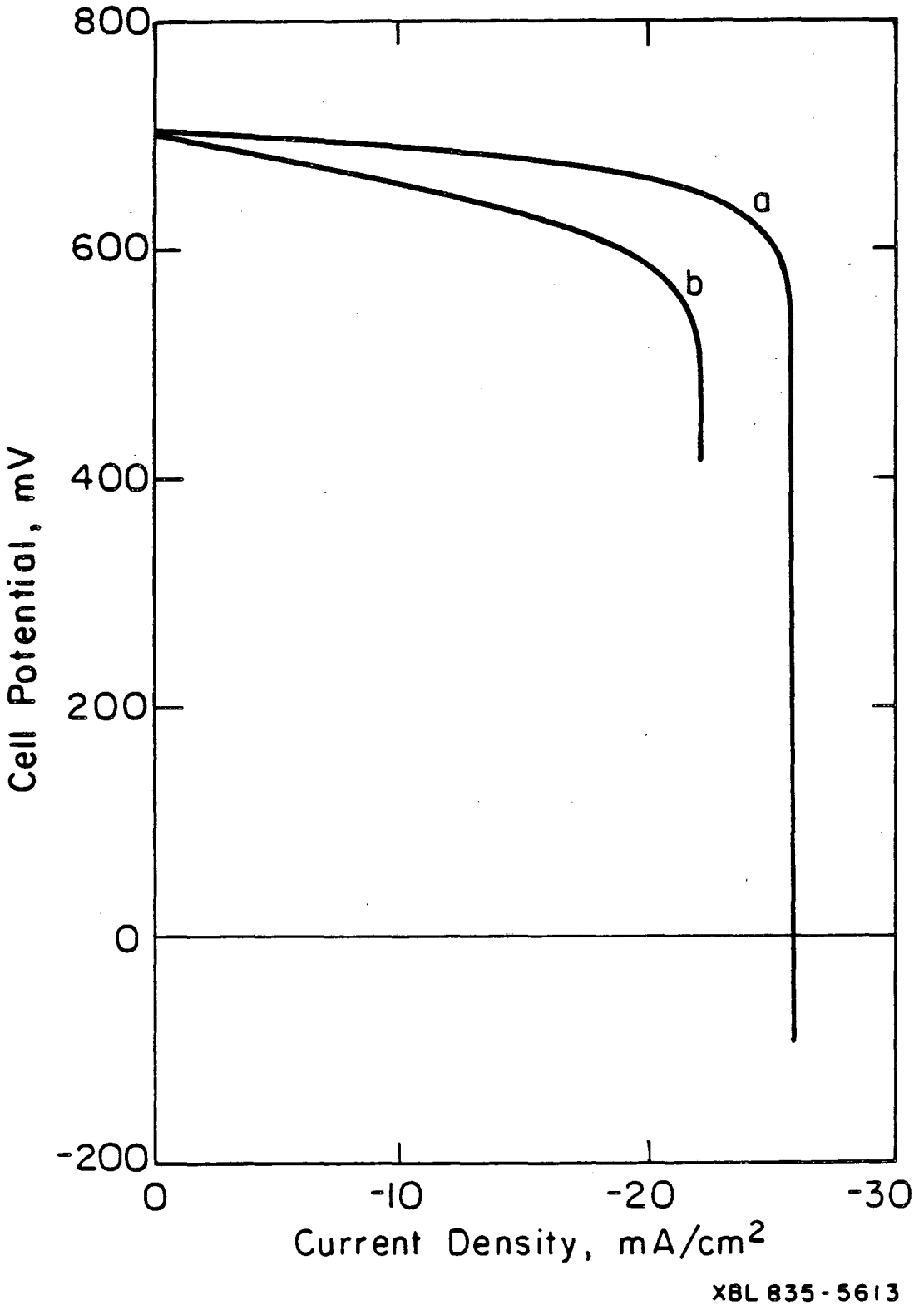

Figure 15. Cell potential as a function of current density for (a) a back-illuminated semiconductor without kinetic, electrolyte-resistance and counterelectrode limitations; and (b) system 3 with a current-collector element half-thickness of 0.01 cm and with L/D = 100.

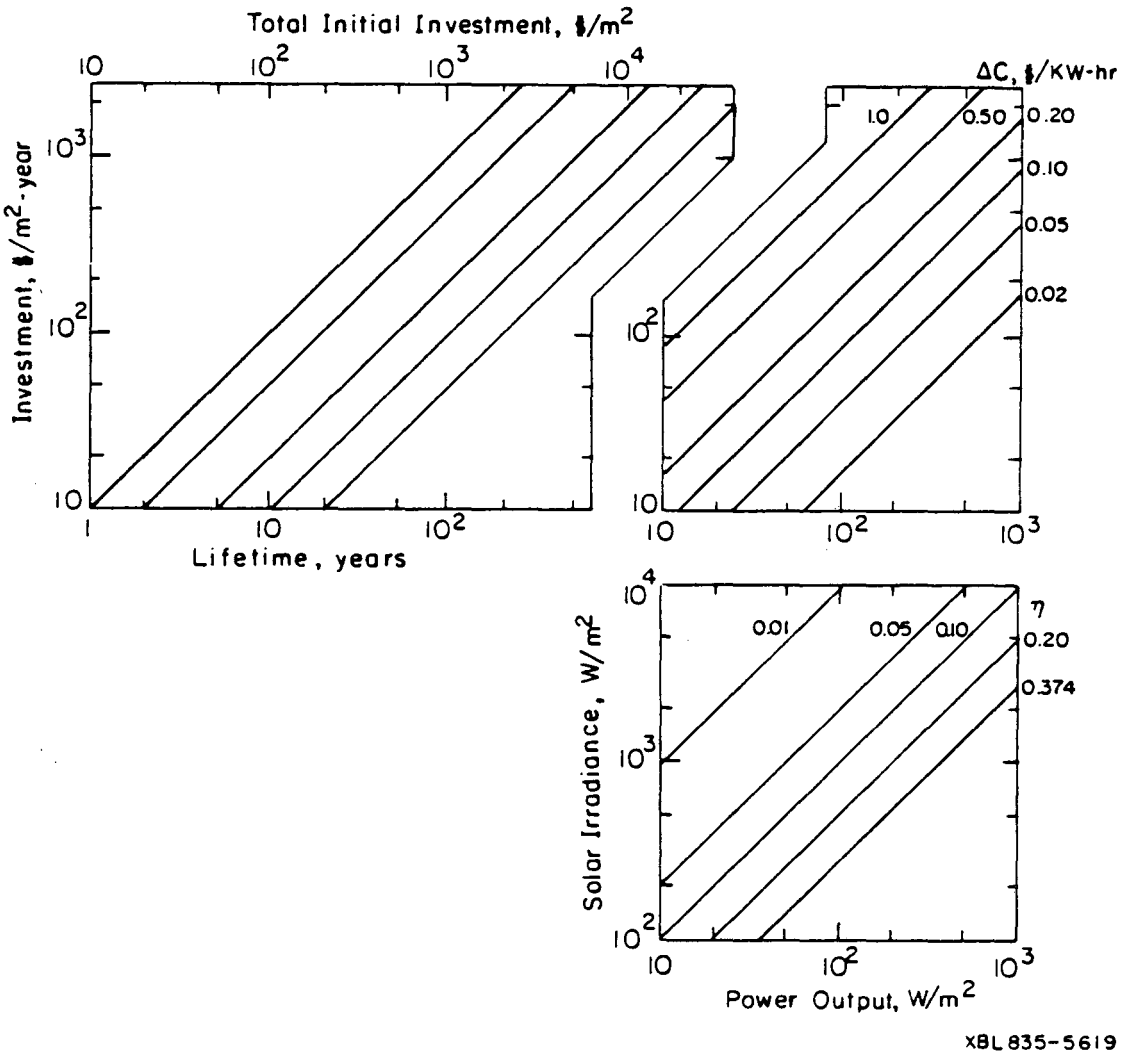

Figure 16. Economic analysis of the liquid-junction photovoltaic cell; (a) power output as a function of the incident solar illumination with power efficiency as a parameter; (b) averaged annual return on investment as a function of the power output with power cost as a parameter; (c) total initial investment as a function of averaged annual return on investment with cell lifetime as a parameter.

profit, and a break-even period of 5 years, an investment of 42 dollars/m^2 is justified for the complete cell. Based upon a 13.4 percent power efficiency (averaged over 24 hours), an investment of 73 dollars/m^2 is justified for the complete cell.

An increase of solar illumination by a factor of five while reducing the efficiency to 6 percent (system 2 with a porous counterelectrode) yields an acceptable initial investment of 164 dollars/m^2. An efficiency of 10.4 percent (system 3 with a porous counterelectrode) yields an acceptable initial investment of 285 dollars/m^2. If the mirrors and lenses needed to concentrate sunlight are cheaper than the semiconducting film, the cell may be most economical under high illumination. Maintenance of a high efficiency under high illumination is possible only with the back-illuminated cell of Figure 8 and the front-illuminated cell of Figure 5, both coupled with porous counterelectrodes.

The values presented here can be compared to the estimate presented by Weaver *et al.*[153] of 0.34 dollars per peak watt. This estimate is based on materials cost and assumes a cell efficiency of 13 percent. Under AM-2 illumination, this value corresponds to 39 dollars/m^2.

5. CONCLUSIONS

The optimization of the liquid-junction photovoltaic cell depends upon the choice of semiconductor, electrolyte, and cell design. The system studied in this work, n-GaAs with a Se_2^{-2}/Se^{-2} redox couple, is close to optimal with respect to utilization of solar irradiation and therefore provides a best-case estimate of liquid-junction cell efficiency. This system, however, exhibits a small rate of corrosion under illumination (a few micrometers per year).[105-107]

The performance of the liquid-junction photovoltaic cell is strongly dependent upon the design, surface area, and placement of the counterelectrode and current collectors. This system may be economical under concentrated illumination or where the power produced has high value.

Chapter 4. Primary Current Distribution and Resistance of a Slotted Electrode Cell

Primary current and potential distributions apply when the surface overpotential can be neglected and the solution adjacent to the electrode can be taken to be an equipotential surface. Calculation of a primary current distribution and resistance represents a first step toward analyzing and optimizing an electrochemical system. The cell resistance calculated can be coupled with calculations including mass-transfer and kinetic effects to optimize approximately a given cell configuration. The objective of this work is to calculate the primary current distribution and resistance of a cell containing a slotted electrode.

1. INTRODUCTION

Calculation of the primary current and potential distributions involves solution of Laplace's equation, $\nabla^2\Phi = 0$, which is not trivial, even for relatively simple geometries. The method of images,[138-142] separation of variables,[154] and superposition[155,156] have been used to solve Laplace's equation for a number of systems. A review of analytic solutions has been presented by Fleck.[137]

The Schwarz-Christoffel transformation[144-146] is a powerful tool for the solution of Laplace's equation in systems with planar boundaries. This method was used by Moulton[143] to derive the current distribution for two electrodes placed arbitrarily on the boundary of a rectangle. Hine *et al.*[157] used this method to describe the primary current distribution for two plane electrodes of infinite length and finite width confined between two infinite insulating planes, perpendicular to but not touching the electrodes. Wagner[158] presented the primary and secondary current distribution for a

two-dimensional slot in a planar electrode. Newman[159] has presented the primary current distribution for two plane electrodes opposite each other in the walls of a flow channel. These solutions made use of the Schwarz-Christoffel transformation.

Application of the Schwarz-Christoffel transformation is generally limited by the ability to generate solutions to the resulting integrals. Analytic solutions allow calculation of the primary current and potential distribution throughout the cell but are possible for a limited number of system geometries. Numerical evaluation of these integrals allows calculation of both the primary current distribution along the electrodes and the cell resistance.

2. CELL GEOMETRY

A cell geometry is presented in Figure 1 which may be well suited for photoelectrochemical applications. This cell contains a slotted semiconductor with the semiconductor-electrolyte interface open to illumination. A glass cover plate protects the cell. Sunlight passes through the cover plate and the electrolyte to illuminate the semiconductor surface. Electrical current passes between the electrolyte and the counterelectrode through the slots of the semiconductor. This configuration has the advantages that no shadows are cast upon the semiconductor, reaction products can be separated, absorption of light by the electrolyte can be minimized, and an enhanced-surface-area counterelectrode (perhaps a porous electrode) can be used.

The slotted electrode cell can be sectioned and, under the assumption that the cell width W is large as compared to the spacing between slots, has the electrochemical characteristics of the two-dimensional cell presented in

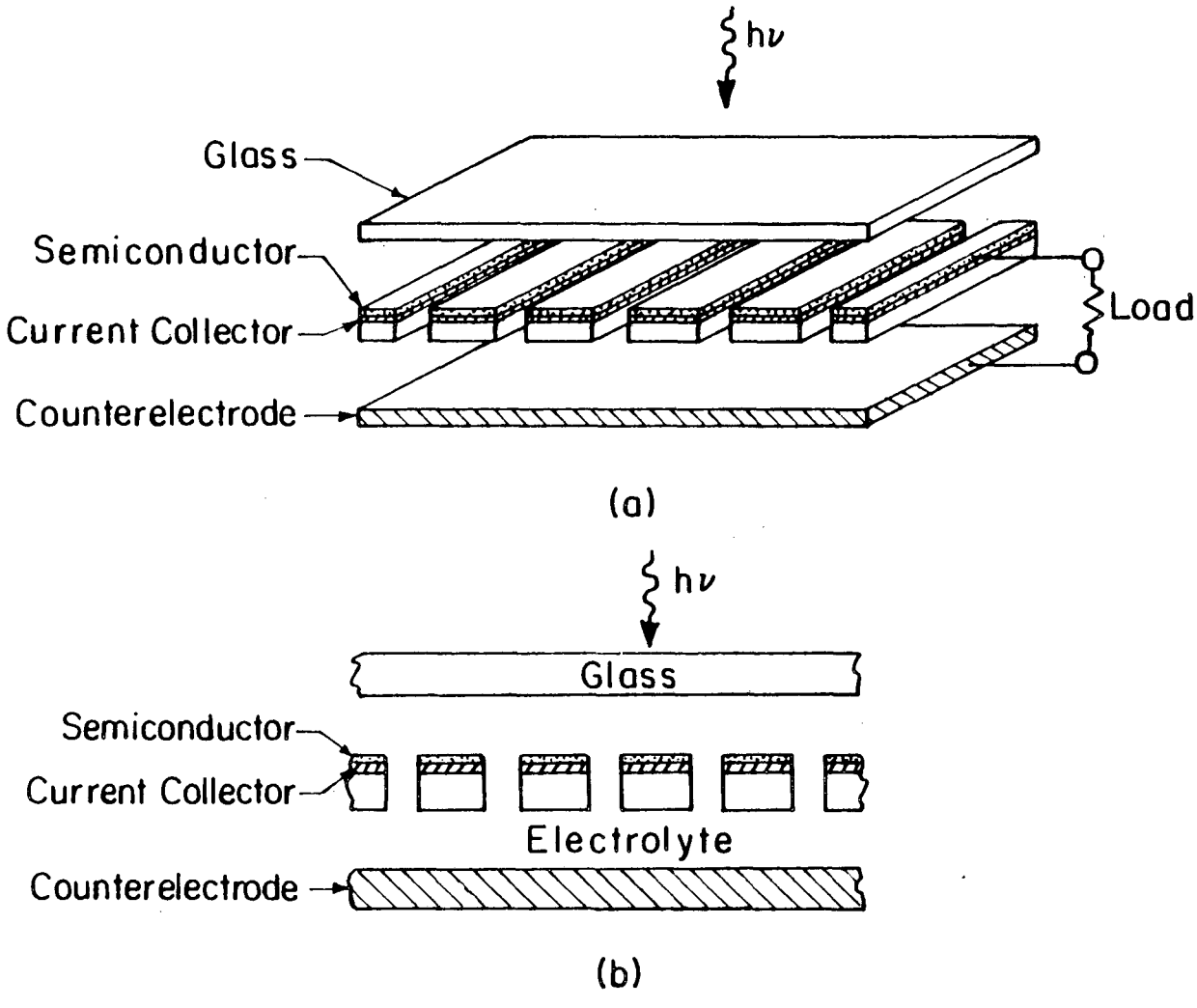

XBL 831-7974

Figure 1. Schematic diagram of the slotted-semiconductor photovoltaic cell.

Figure 2a. The electrodes are represented by AB and EF, and all other boundaries of the cell are considered to be insulators. The coordinate system of Figure 2a is transformed through an intermediate half-plane t (see Figure 2b) to a coordinate system (Figure 2c) in which Laplace's equation can be solved easily.

3. THEORETICAL DEVELOPMENT

The primary current distribution along the electrodes and the cell resistance can be calculated through application of the Schwarz-Christoffel transformation. Complex coordinate systems are used, thus

$$z = z_r + j\, z_i \,.$$

The cell was assumed to be symmetric about $z_r = 0$. The approach presented below, however, could be easily extended to relax this assumption.

The z-coordinate system is related to the t-coordinate system of Figure 2b by

$$z = \int_0^t \frac{(a^2-t^2)^{1/2}}{(b^2-t^2)^{1/2}(c^2-t^2)^{1/2}(d^2-t^2)^{1/2}}\, dt \,. \qquad (1)$$

where a, b, c, and d are the values of t corresponding to z values of A, B, C, and D, respectively. Through the assumption of symmetry about $z_r = 0$, the values $-a$, $-b$, $-c$, and $-d$ correspond to z values of H, G, F, and E, respectively. The electrodes AB and EF correspond to ab and $-c$ --d in the t-plane. Along the electrode AB (ab) this transformation can be expressed by

$$\left.\frac{dz_r}{dt_i}\right|_{ab} = j\, f(t_r) \,, \qquad (2a)$$

where

Figure 2. Schematic diagram of the sectioned cell with coordinate systems:

a) $z = z_r + i\, z_i$,

b) $t = t_r + i\, t_i$, and

c) $\chi = \chi_r + i\, \chi_i$.

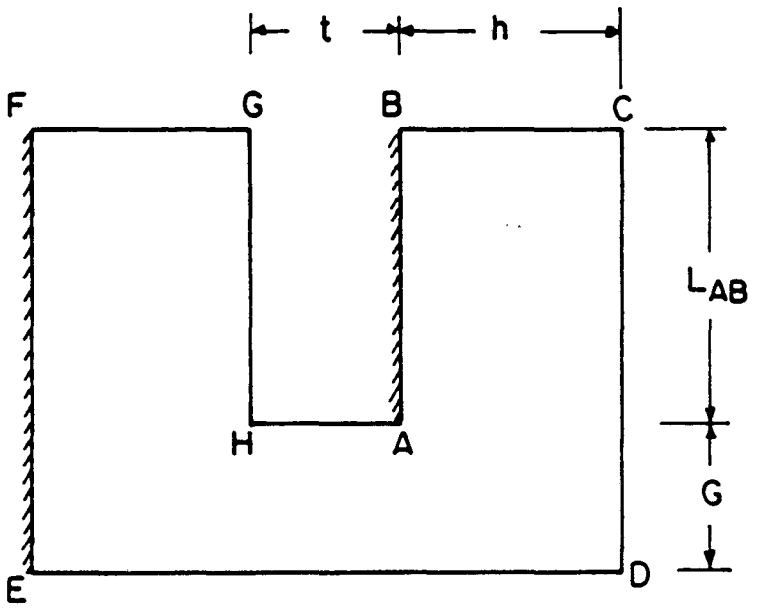

(a)

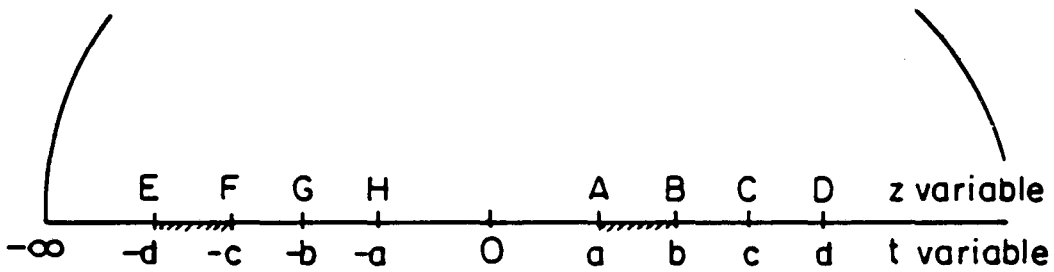

(b)

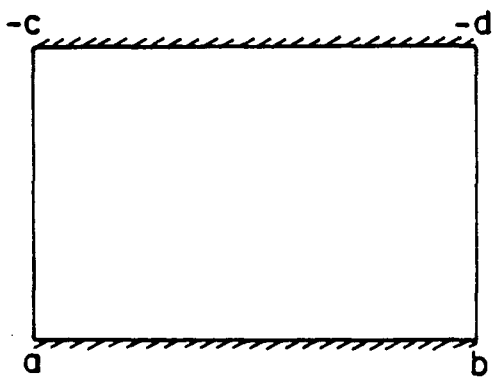

(c)

XBL 832-5205

$$f(t_r) = \frac{(a^2-t_r^2)^{1/2}}{(b^2-t_r^2)^{1/2}(c^2-t_r^2)^{1/2}(d^2-t_r^2)^{1/2}} . \qquad (2b)$$

These equations will be used to calculate the derivative of the potential at the electrodes; z_r is the direction normal to the electrode in the z-plane, and t_i is the direction normal to the electrode in the t-plane.

The variable χ (see Figure 2c) is related to the t-plane by the Schwarz-Christoffel transformation;

$$\chi = \int_a^t \frac{1}{(t-a)^{1/2}(b-t)^{1/2}(-c-t)^{1/2}(-d-t)^{1/2}}\, dt . \qquad (3)$$

Along the electrode ab equation (3) can be expressed as

$$\left.\frac{d\chi_i}{dt_i}\right|_{ab} = g(t_r) , \qquad (4a)$$

where

$$g(t_r) = \frac{1}{(t_r-a)^{1/2}(b-t_r)^{1/2}(c+t_r)^{1/2}(d+t_r)^{1/2}} . \qquad (4c)$$

Equations (2) and (4) are also valid at the electrode EF $(-c-d)$. The variable χ_i is normal to the electrode in χ-space, and t_i is, as above, normal to the electrode in t-space.

The potential in the χ-system is

$$\Phi = \frac{\chi_i}{\chi_{i,max}} V \qquad (5)$$

where V is the cell potential difference and $\chi_{i,max}$ is the separation between electrodes in χ-space. The current density is related to the potential derivative at the electrodes. In the χ system this derivative is given by

$$\left.\frac{\partial\Phi}{\partial\chi_i}\right|_{-c-d} = \left.\frac{\partial\Phi}{\partial\chi_i}\right|_{ab} = \frac{1}{\chi_{i,max}} V . \qquad (6)$$

The potential derivative at the electrode ab in the t-system is

$$\left.\frac{\partial \Phi}{\partial t_i}\right|_{ab} = \left.\frac{\partial \Phi}{\partial \chi_i}\right|_{ab} \left.\frac{\partial \chi_i}{\partial t_i}\right|_{ab}, \tag{7}$$

and the potential derivative in the z system is given by

$$\left.\frac{\partial \Phi}{\partial z_r}\right|_{ab} = \left.\frac{\partial \Phi}{\partial t_i}\right|_{ab} \left.\frac{\partial t_i}{\partial z_r}\right|_{ab}. \tag{8}$$

Substitution of equations (2a), (4a), (6), and (7) into equation (8) and similar manipulations for the $-c-d$ electrode yield the potential derivative along the electrodes ab and $-c-d$ in the original z-coordinate system as functions of t_r;

$$\left.\frac{\partial \Phi}{\partial z_r}\right|_{ab} = \frac{g(t_r)}{f(t_r)} \frac{V}{\chi_{i,max}}, \tag{9a}$$

and

$$\left.\frac{\partial \Phi}{\partial z_r}\right|_{-c-d} = \frac{g(t_r)}{f(t_r)} \frac{V}{\chi_{i,max}}, \tag{9b}$$

respectively.

The current distribution along the electrode AB is therefore given by

$$\frac{i(z_i)}{i_{avg}} = \frac{g(t_r)}{f(t_r) \int_A^B \frac{g(t_r)}{f(t_r)}\, dz_i}. \tag{10}$$

A similar expression results for the electrode EF. The primary cell resistance is

$$W\kappa R = \frac{\chi_{i,max}}{\int_A^B \frac{g(t_r)}{f(t_r)}\, dz_i}. \tag{11}$$

The primary current distribution and the cell resistance for this system are functions of only three geometric ratios and were obtained numerically. Values of A, B, C, and D in the z-plane corresponding to a, b, c, and d in the t-plane were obtained through numerical integration of equation (1). The value of $\chi_{i,max}$ was obtained through numerical integration of equation

(3) between the limits of a and $-d$. The values of t_r corresponding to given values of z were calculated through numerical integration of equation (1) and were used to calculate the values of $f(t_r)$ and $g(t_r)$.

4. RESULTS

The calculated primary current distribution is presented below and compared to current distributions obtained from asymptotic solutions of Laplace's equation. The result most useful for cell design, however, is the cell resistance, presented in section 4.2.

4.1. Primary Current Distribution

The primary current distributions on the AB and EF electrodes are presented in Figures 3 and 4. This distribution is characterized by three geometric ratios, chosen here to be $t/G=4.$, $h/G=1.$, and $L/h=2.5$, where L is the length of the AB electrode, t is the thickness of the protruding electrode assembly, G is the gap between the front edge of the AB electrode and the insulating wall, and h is the separation between the lines AB and CD (and, by symmetry, EF and GH) (see Figure 2). The current distributions of the two electrodes have been superimposed. The current density is infinite at A and is finite at B, E, and F.

Asymptotic forms of the current distribution can be derived and compared to the calculated current distribution. The current distribution close to the edge of an electrode adjoining an insulator with an angle α is

$$\frac{i(z_i)}{i_{avg}} = const\ \frac{\pi}{2\alpha}(Q-z_i)^{\frac{\pi}{2\alpha}-1}, \qquad (12)$$

where Q is the point of intersection of the electrode and insulator. At A, where α is $3\pi/2$, the current density is proportional to $(A-z_i)^{-2/3}$, and at B, E, and F the current density is independent of $(Q-z_i)$. The current density

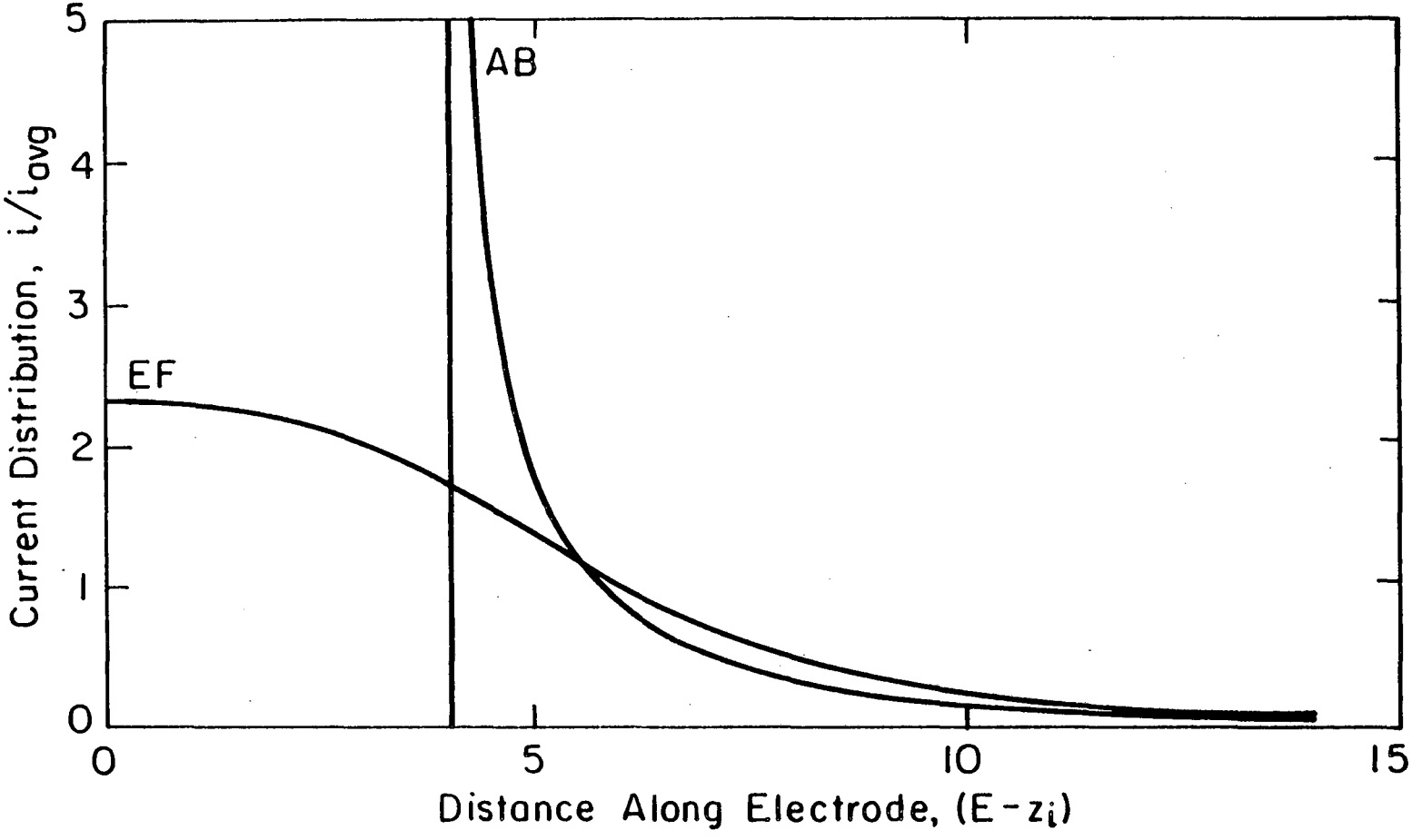

Figure 3. Current distribution along the AB and EF electrodes for L/h = 2.5, t/G = 0.25, and h/G = 1.

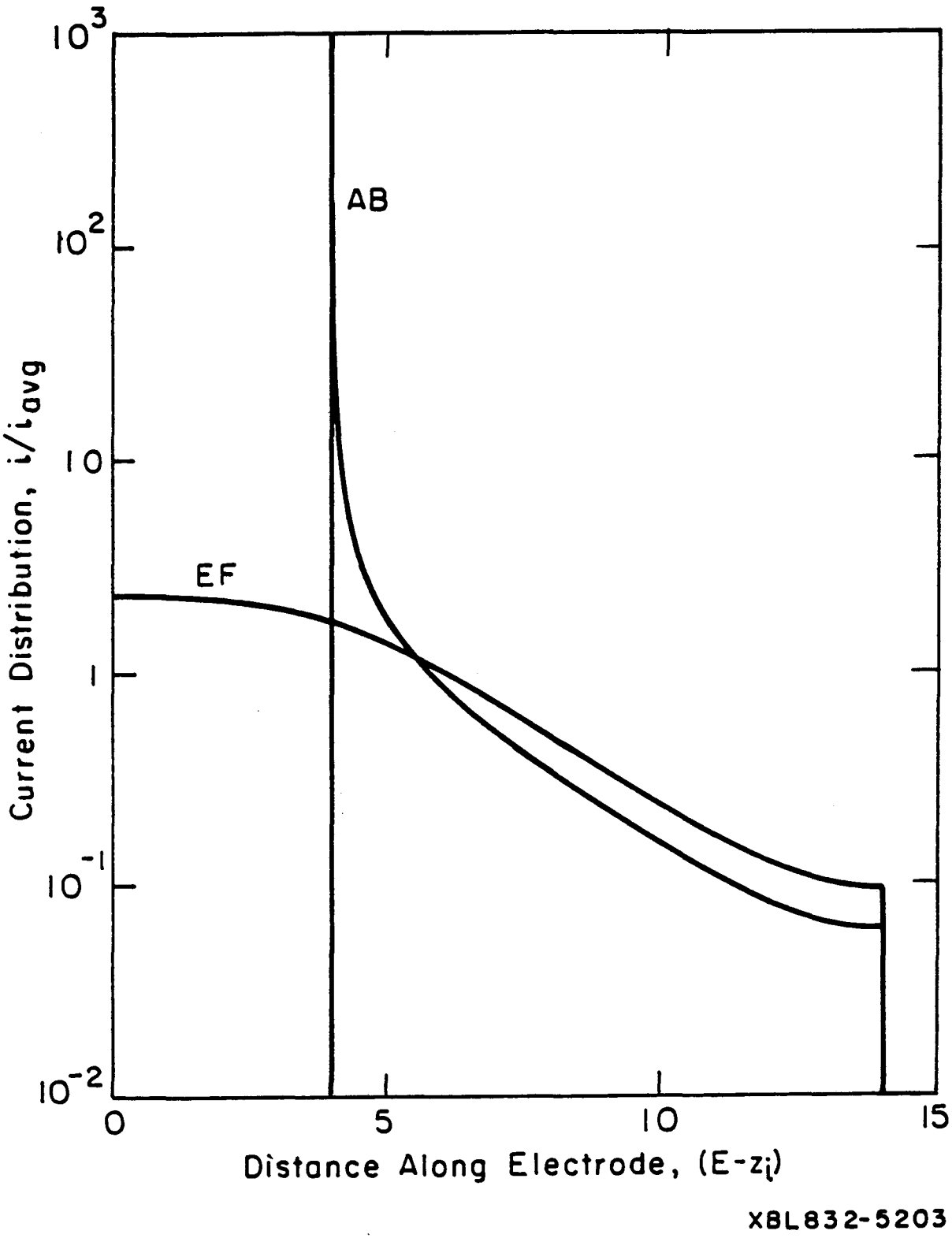

Figure 4. Current distribution along the AB and EF electrodes for L/h = 2.5, t/G = 0.25, and h/G = 1.

is seen in Figures 3 and 4 to approach a constant value at both edges of the EF electrode and at the far edge of the AB electrode. The current distribution along the AB electrode is presented in a log-log format in Figure 5. The behavior close to the edge is emphasized, and the expected -2/3 power dependence on $(A-z_i)$ is observed.

Far from the gap, the asymptotic form for the current distribution is

$$\frac{i(z_i)}{i_{avg}} = const\ \nu \cosh[\nu\ (z_i - z_{i,max})]\ , \tag{13}$$

where

$$\nu = \frac{\pi}{2h}\ .$$

The calculated current distributions for the AB and the EF electrodes are presented along with equation (13) in Figures 6 and 7, respectively. The constant was obtained by matching the asymptotic solution at $z_{i,max}$ to the calculated current distribution. The calculated current distributions match the asymptotic solutions in the region far from the gap.

4.2. Primary Cell Resistance

The primary cell resistance can be expressed as a dimensionless group $W\kappa R$. The dimensionless primary cell resistance for this system is a function of three geometric ratios, as described in the previous section. In the limit that the thickness t approaches zero, the resistance approaches a value that is independent of t/G. The cell resistance can therefore be expressed as the sum of the resistance for t/G equal to 0, $W\kappa R_0$, and a dimensionless correction term, Δ.

$$W\kappa R = W\kappa R_0 + \Delta \tag{14}$$

The resistance $W\kappa R_0$ is presented in Figure 8 as a function of L/h with h/G as a parameter. For all values of h/G, the dimensionless resistance in

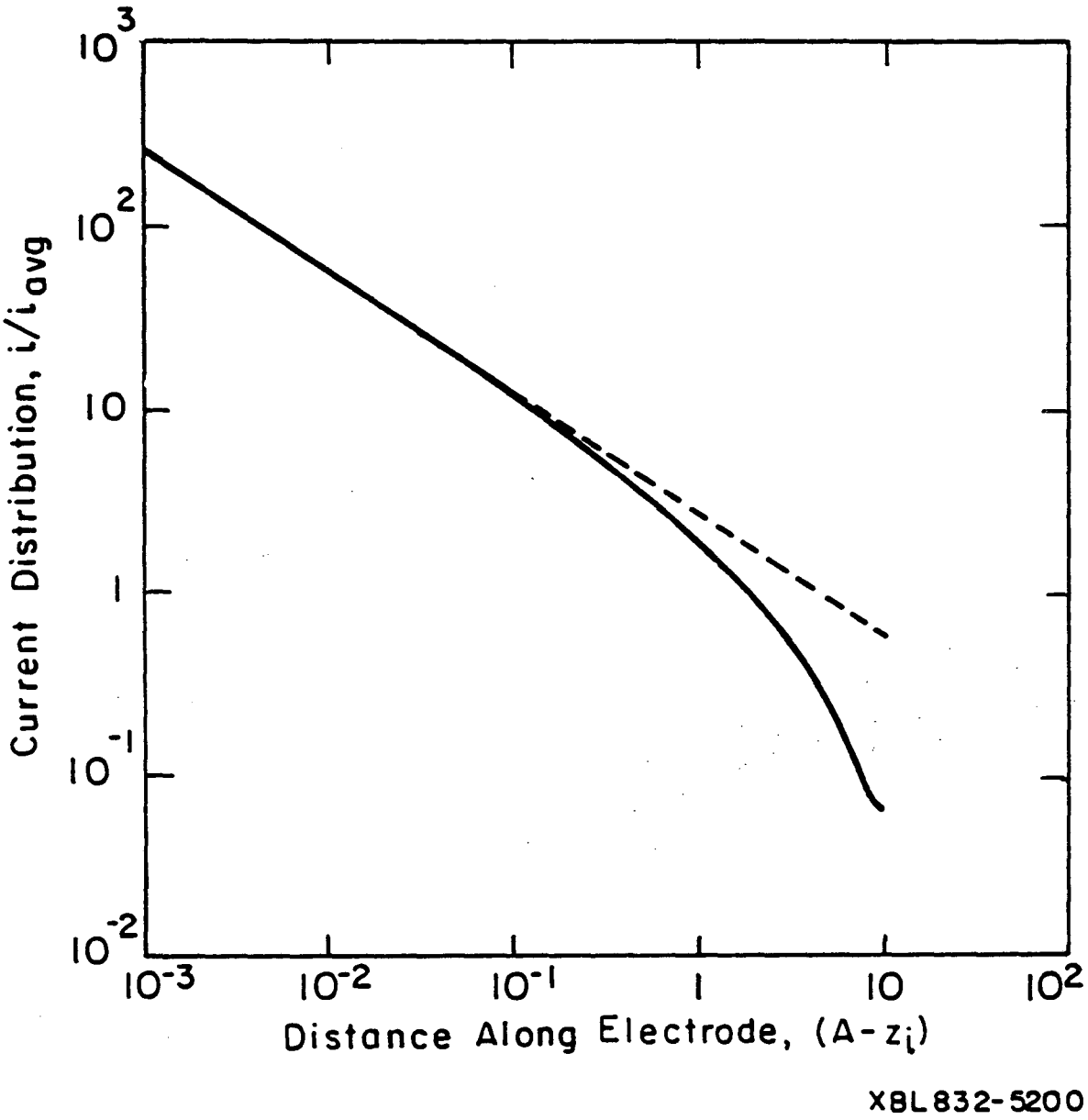

Figure 5. Current distribution along the AB electrode compared to the asymptotic solution for L/h = 2.5, t/G = 0.25, and h/G = 1.

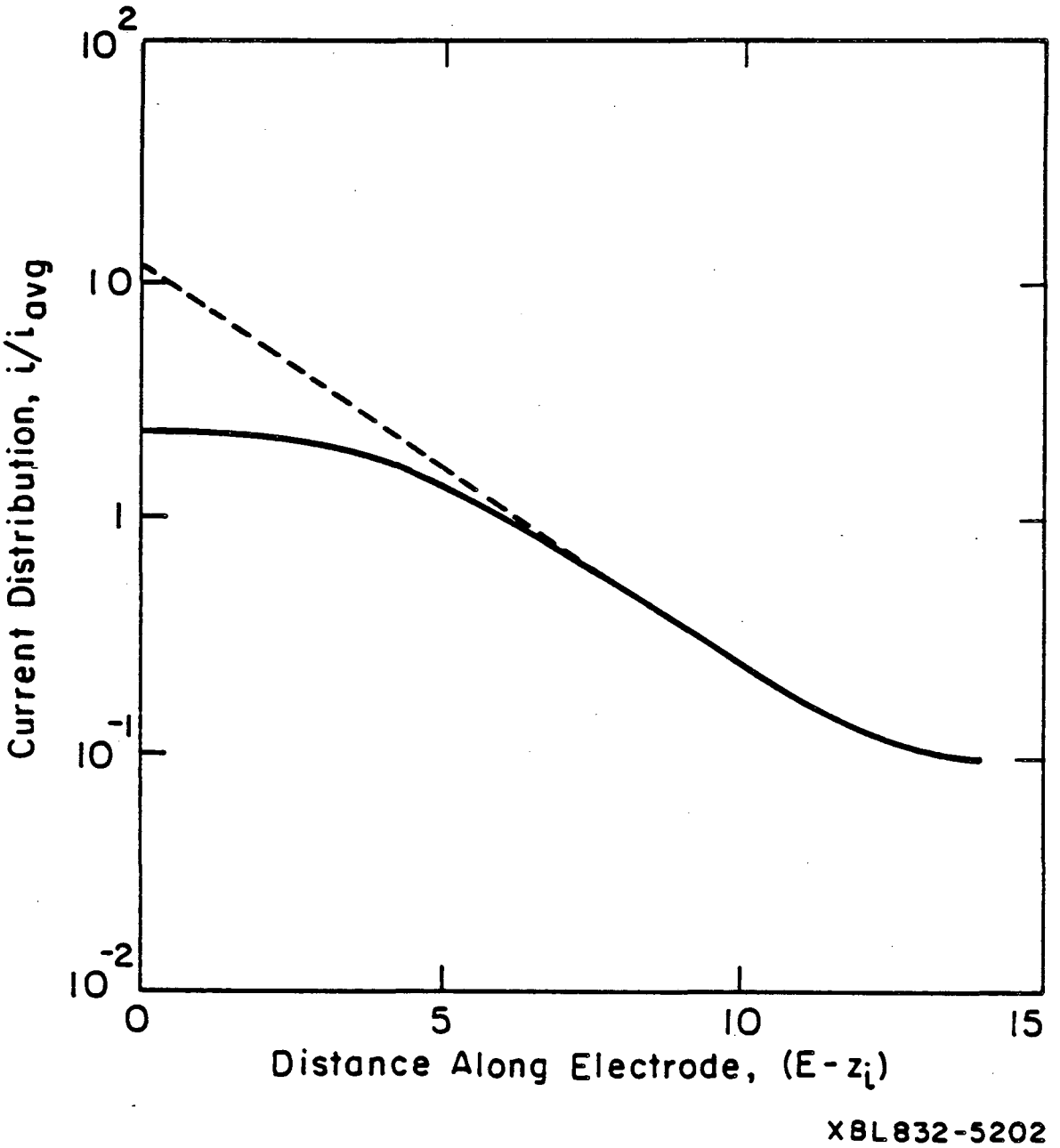

Figure 6. Current distribution along the EF electrode compared to the asymptotic solution for L/h = 2.5, t/G = 0.25, and h/G = 1.

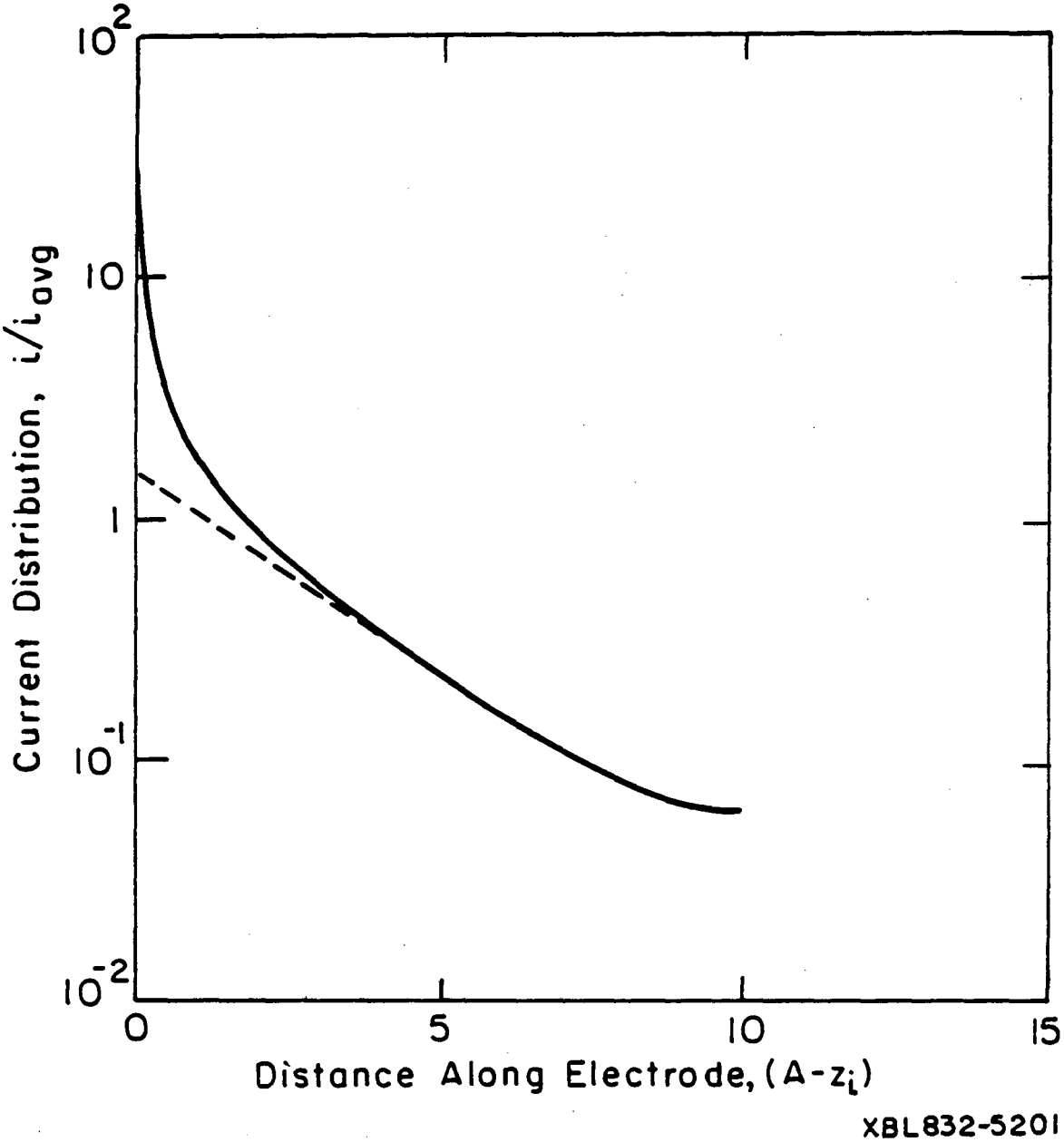

Figure 7. Current distribution along the AB electrode compared to the asymptotic solution for L/h = 2.5, t/G = 0.25, and h/G = 1.

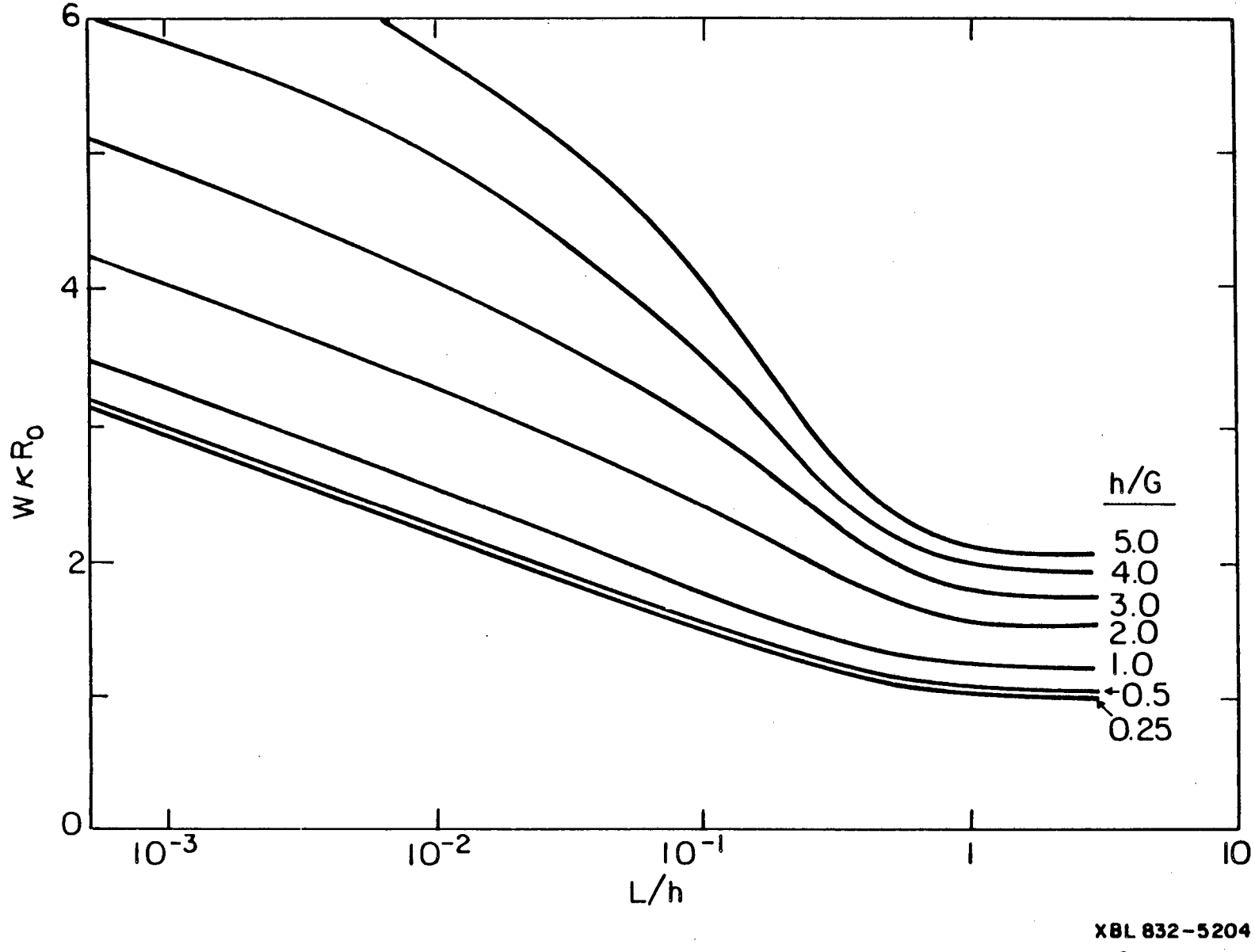

Figure 8. Dimensionless cell resistance with t/G equal to zero as a function of L/h with h/G as a parameter.

Figure 8 approaches a constant value as L/h becomes greater than 2. The additional electrode length is relatively inaccessible and does not contribute much to current flow (see Figures 3 and 4). For all values of h/G and with sufficiently small values of L/h, the resistance approaches infinity with $\left[-\frac{1}{\pi}\ln(L/h)\right]$ as L/h approaches zero.

The resistance correction term, Δ, can be considered to be the additional resistance due to a finite (non-zero) electrode thickness t. Δ is presented in Figure 9 as a function of t/G with L/h as a parameter. This term is independent of h/G and is only a very weak function of L/h. The correction term is given by the upper line in Figure 9 for $L/h>1$ and by the lower line in Figure 9 for $L/h<0.01$. The slope for $t/G>0.5$ has the value 1, as anticipated from the asymptotic solutions for t/G approaching infinity.

The cell resistance for a given configuration can be obtained from Figures 8 and 9 with equation (14). The cell resistance is smallest when the gap (G) is large, the height (h) is small, and the electrode length (L) is large. An approximate analytic expression for the cell resistance can be obtained by interpolation of asymptotic solutions to Equation (11). The correction term for a finite electrode thickness can be expressed by

$$\Delta = t/G + \Delta_1 . \tag{15}$$

The resistance of the cell with a zero electrode thickness is given by

$$W\kappa R_0 = \frac{1}{\pi}\ln\left[\frac{16\left(1+\frac{c}{b}\right)}{\left(1-\frac{c}{d}\right)} - (32 - e^{\pi})\right] + \Delta_0 , \tag{16}$$

where

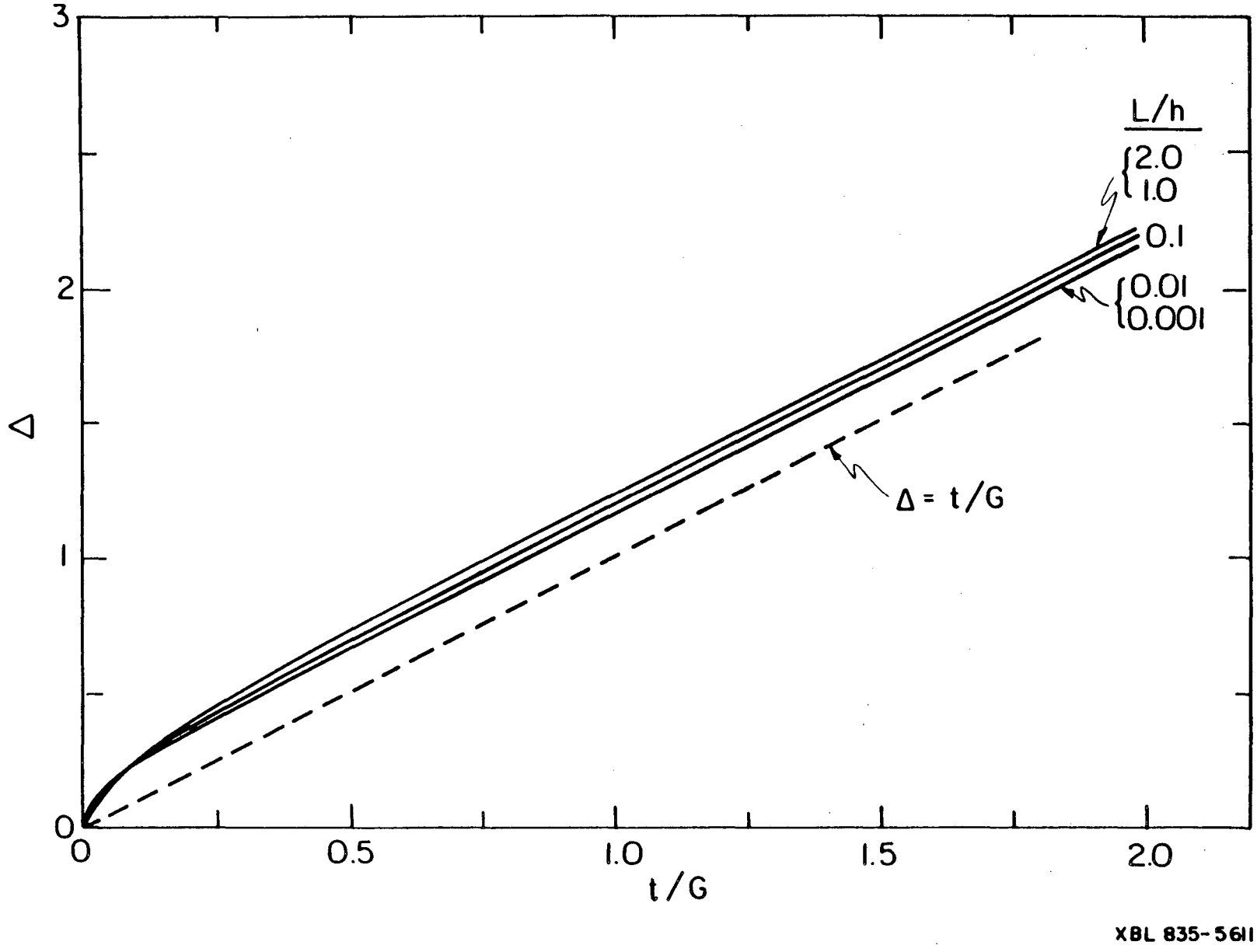

Figure 9. Dimensionless correction to the cell resistance as a function of t/G with L/h as a parameter.

$$\frac{b}{c} = \tanh\left\{\frac{\pi}{2}\left[\frac{\left(\frac{L}{G}\right)^4}{\left(1 + 2\,\frac{L}{G}\right)^2} + \left(\frac{L}{h}\right)^4\right]^{0.25}\right\}, \tag{17}$$

and

$$\left(1 - \frac{c}{d}\right) = 2\,\frac{\sinh^2\left(\frac{x}{2}\right)}{\cosh(x)}, \tag{18a}$$

where

$$x = \frac{4\cos\left(\frac{\pi}{2}\,\frac{L}{L+G}\right) e^{-\frac{\pi}{2}\,\frac{h}{L+G}}}{\cosh\left(0.3\,\frac{\pi}{2}\,\frac{L}{h}\right)} + \frac{\frac{\pi}{2}\,\frac{G}{h}}{\cosh^2\left(1.2\,\frac{\pi}{2}\,\frac{h}{L+G}\right)}. \tag{18b}$$

The error in equation (16) is presented in Figure 10 as a function of L/h. The error is less than five percent and approaches a constant value as L/h approaches infinity and as L/h approaches zero. The error in equation (15) is presented in Figure 11.

The effect of the cell resistance in the photoelectrochemical cell proposed in Section 2 must be balanced with the need for a large semiconductor area open to illumination. Optimal design of this cell requires a large number of narrow slots (see Chapter 3). The resistance of such a cell with $h/G = 10$, $L/h = 0.5$, and $t/G = 20$, can be expressed in terms of equations (14), (15), and (16) as

$$\begin{aligned} W\kappa R &= W\kappa R_o + \Delta_0 + t/G + \Delta_1 \\ W\kappa R &= 2.9891 + 0.0148 + 20. + 0.2 \end{aligned} \tag{19}$$

The error in neglecting the correction terms, Δ_0 and Δ_1, is 0.93 percent.

5. CONCLUSIONS

Numerical integration was coupled with the Schwarz-Christoffel transformation to calculate primary current distributions and cell resistances. Primary current distributions and resistances were presented

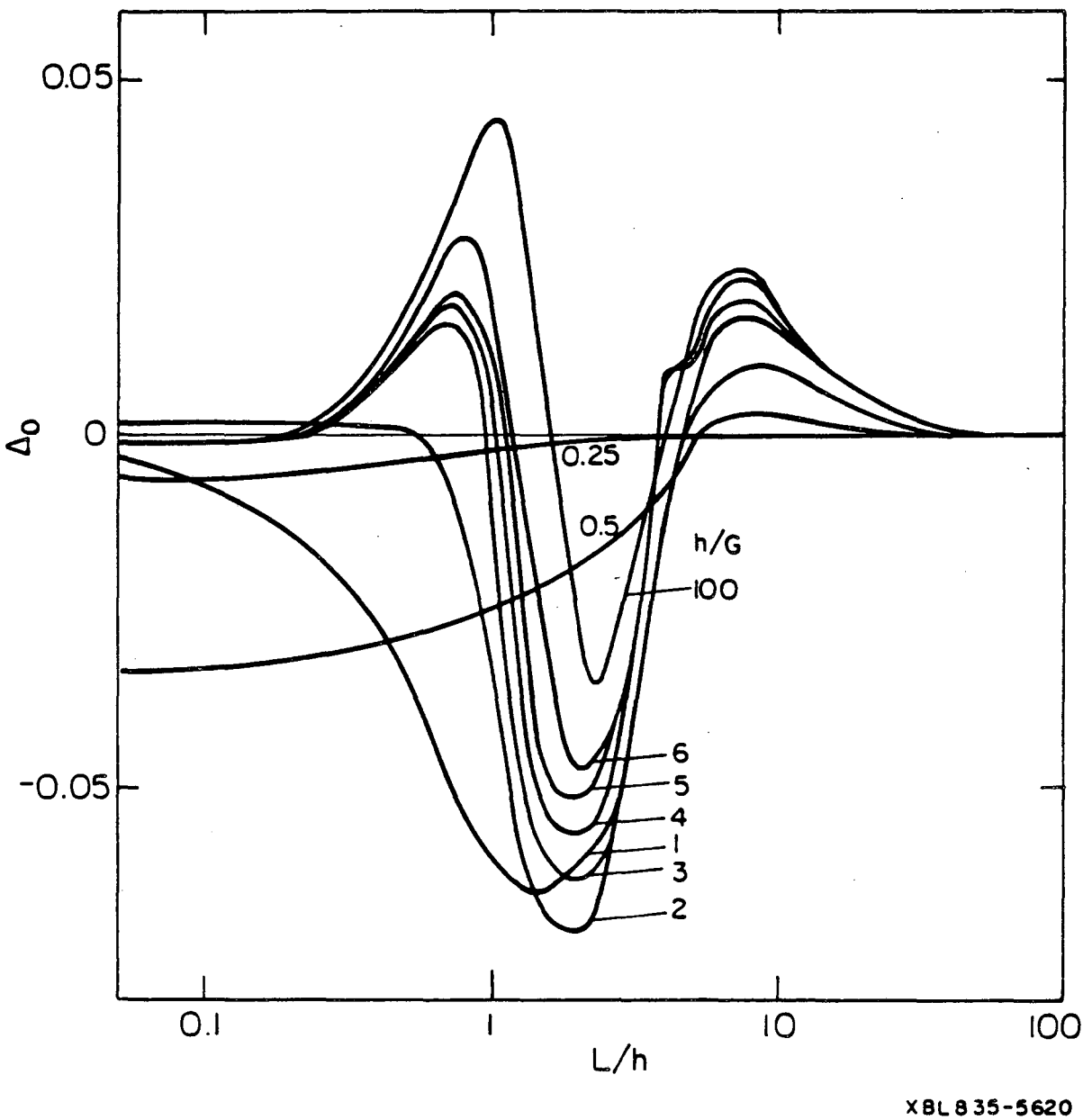

Figure 10. Dimensionless correction to equation (16) for the resistance of a cell with t/G = 0.

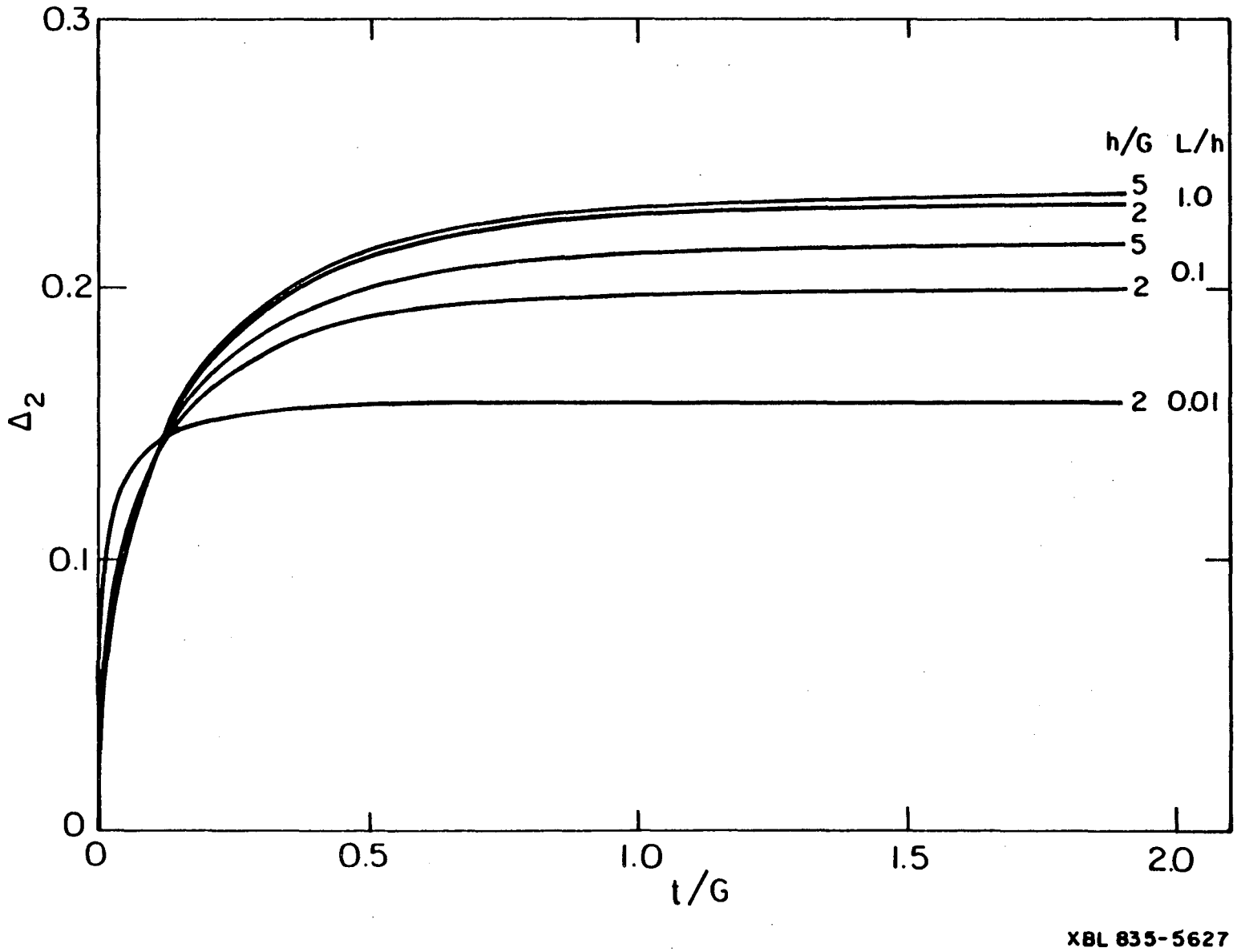

Figure 11. Dimensionless correction to equation (15) for the contribution of t/G to the cell resistance.

for a cell consisting of a slotted electrode over a solid electrode. An approximate analytic expression for the cell resistance was presented.

Chapter 5. Potentials in Electrochemical Systems

Potentials characterize the electrical state of a given location relative to a reference electrical state. Potentials have meaning only in terms of a difference, and this potential difference is proportional to the work of moving a charged test particle from the reference location to the point of interest. The test particle, the physical character of the the locations to and from which the particle is moved, and the nature of the work involved can be chosen in a number of ways. The potential can therefore be defined with a considerable degree of arbitrariness.

1. DEFINITIONS OF POTENTIAL

The *true* or *electrostatic* potential represents an idealization of charged particle interactions.[99] This potential is mathematically well defined to be proportional to the work of moving a point charge against Coulombic forces (which do not include specific chemical forces). The work involved is not reversible in a thermodynamic sense. The test particle used in calculations of electrostatic potential differences is imaginary, and therefore the electrostatic potential difference cannot be measured.

The *cavity* potential, ψ, * (see Maxwell[161]) is proportional to the work required to move a charged test particle from the reference state into a cavity within the phase of interest. The cavity is used to eliminate the effects of external electric fields. In the absence of external electric fields, the cavity potential is referred to as the potential "just outside" the medium. The cavity (also called *Volta* or *outer)* potential represents the electrical state due to long-range interactions. It is independent of the type

* The notation used here to distinguish the various definitions of electrical potentials is consistent with IUPAC recommendations.[160] The symbol Φ will be used when the choice of

of test particle used and is not thermodynamically reversible. The magnitude of the necessary separation between the test particle and the phase depends upon the conductivity of the phase and is of the order of 10^{-5} to 10^{-3} cm.

The cavity potential is closely related to the electrostatic potential with respect to the types of forces involved and, with the appropriate boundary conditions, can be calculated from double integration of Poisson's equation. The cavity potential is well defined and is measurable within macroscopic regions in which a cavity can be formed.

The *Galvani* or *inner* potential, φ, incorporates the effects of both long and short range forces. The Galvani potential difference is proportional to the work of moving a given test particle from the reference state to the point of interest "inside" the phase. It differs from the electrostatic potential in that the test particle is a real species. The Galvani potential is well defined though generally conceded to be unmeasurable because of the experimental difficulty of extracting (or inserting) a real particle from (or into) the interior of a phase.

The Galvani and cavity potentials are related through the *surface* potential, χ, by

$$\varphi = \psi + \chi . \qquad (1)$$

The surface potential represents the change in potential observed in moving a test particle from a cavity "just outside" a phase to a point "inside" the phase. It is unmeasurable and is not thermodynamically reversible.

The *electrochemical* potential of a given species i, μ_i, (or *electron* potential as used by Grahame[95] with electrons as the given species) was

---

definition is not specified.

rigorously defined by Guggenheim[162] to be proportional to the thermodynamically reversible work of moving a test particle of the given species from the reference state to the point in question. This term includes all chemical and potential interactions between particles, short and long range. A consequence of the above definition is that the electrochemical potential of a given species at equilibrium is independent of position.

The electrochemical potential can be separated into two terms: one incorporating chemical interactions (independent of electrical state) and one incorporating the effect of the electrical state.

$$\mu_i = RT \ln(c_i f_i a_i^{\ominus}) + z_i F \Phi . \qquad (2)$$

The chemical potential has been expressed here in terms of variables characteristic of species i: the concentration c_i, the activity coefficient f_i, and a reference state quantity $a_i^{\ominus}$. The potential Φ used to characterize the electrical state can be arbitrarily chosen; therefore this separation is arbitrary and has no physical significance.

The electrochemical potential in equation (2) is thermodynamically defined; the chemical potential and the electrical potential are not. The choice of a potential therefore specifies a choice of chemical potential and, through it, a choice of activity coefficient. This activity coefficient is as well or as poorly defined as the potential is well or poorly defined.

The *real*** potential, α_i, was used by Parsons[98] to identify the chemical potential specified by choosing a cavity potential in the separation of the electrochemical potential into chemical and electrical terms.

** The term "real potential" used here is misleading as it does not distinguish between electrical and chemical potentials. A better choice of terms might be "real chemical potential."

$$\mu_i = \alpha_i + z_i F\psi \,. \tag{3}$$

The chemical potential so specified is independent of long-range electrical interactions.

The arbitrary nature of the definition of an electrical potential is explicitly evident in the following definitions. The potential can be defined as the electrochemical potential of a given ionic species, i.e., referenced to the potential of a suitable reference electrode. This potential is related to a common electrochemical measurement but has the disadvantage that the potential has a value of minus infinity in a phase in which the reference species is absent. The electrochemical potential of electrons, for example, is not useful for characterization of electrical state in electrolytic solutions in which electrons do not exist.

The *quasi-electrostatic* potential introduced by Smyrl and Newman[163] defines the potential in terms of a reference species n through

$$\mu_n = RT \ln(c_n) + z_n F\Phi \,. \tag{4}$$

The electrochemical potential of any other species i is expressed as

$$\begin{aligned} \mu_i = {} & RT \ln(c_i) + RT \left[\ln(f_i) - \frac{z_i}{z_n}\ln(f_n)\right] \\ & + RT \left[\ln(a_i^{\vartheta}) - \frac{z_i}{z_n}\ln(a_n^{\vartheta})\right] \,. \end{aligned} \tag{5}$$

This definition can be used in a solution of vanishing concentration of species n because of the term $RT \ln(c_n)$ in equation (4).

2. PHYSICAL SIGNIFICANCE OF DEFINED POTENTIALS

All the definitions of potential discussed here satisfy the condition that they reduce to

$$z_i F(\Phi^{\alpha} - \Phi^{\alpha'}) = \mu_i^{\alpha} - \mu_i^{\alpha'} \,, \tag{6}$$

where α and α' are phases of identical composition, temperature, and

pressure. The arbitrariness (and the need for careful definition) of the potential therefore cancels in thermodynamic calculations of potential differences between phases of identical composition. These potentials are not equally useful, however, in determining the local electrical state within a given system or potential differences between phases of differing composition.

Consider the electrochemical system shown in Figure 1. The cell potential measured between leads of identical composition (α and α') is related to the difference in electrochemical potential of electrons between the two phases (see equation (6)). Because the leads are of the same composition, this difference also corresponds to the cavity potential difference and the Galvani potential difference (as well as any of the other potential differences defined above).

The electrochemical potential of electrons in the cell at equilibrium is independent of position; thus if all the phases (α, β, γ, δ, ε, and α') were metallic, the electrochemical potential of electrons would be constant throughout the system, and the cell potential would be zero. The cavity potential, however, will vary throughout the system due to the different chemical environments within each phase. The cavity potential of the phase α and the phase α' would be equal.

If one of the phases, say δ, were electrolytic, a nonzero cell potential could ensue. Electrons do not exist within the electrolyte; they must be related to the ionic species in the electrolyte by heterogeneous reactions, e.g., a metal-dissolution reaction:

$$M_\gamma = M_\delta^+ + e_\gamma^- \quad . \tag{7}$$

Each equilibrated reaction yields a relationship among the electrochemical

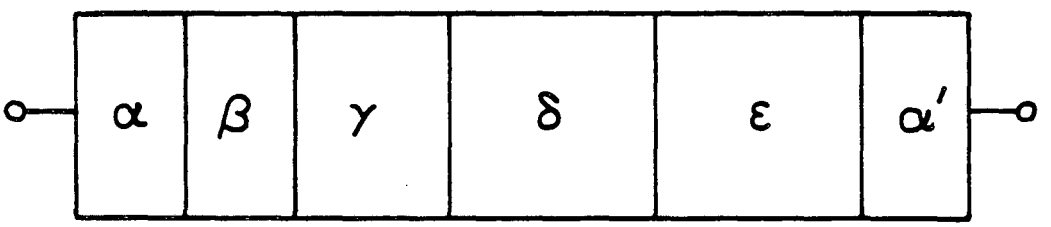

XBL835-5607

Figure 1. Schematic representation of an electrochemical cell.

potentials of the species involved. For the above reaction,

$$\mu_M^{\gamma} = \mu_{M^+}^{\delta} + \mu_{e^-}^{\gamma} . \tag{8}$$

In this way, the cell potential can be related to the electrochemical potentials of the electrolytic species (see section 3 and chapter 2 in reference (1)).

The electrochemical potential of electrons is not a useful measure of the local electrical state throughout an electrochemical system containing non-metallic phases. The cavity potential is a preferred definition of local electrical state because it has meaning in all phases (is not dependent upon the existence of a given species) and (in contrast to the Galvani potential) it can be measured. The cavity potential is not, however, preferred to be made mandatory because the potential of the cell can be calculated and verified without measuring any cavity potentials.

3. CALCULATION OF POTENTIAL DIFFERENCES

Consider the system

$$Pt(\alpha) \mid M \mid soln.(\varepsilon) \mid soln.(\varepsilon') \mid Pt(\alpha') , \tag{9}$$

where M is a metal electrode and ε and ε' represent electrolytic solutions. The cell potential for this system is defined between metals of the same composition in terms of the difference in electrochemical potential of electrons (see equation (6)).

The electrochemical potential of electrons in phase α is equal at equilibrium to the electrochemical potential of electrons in phase M. Electrons in phases M and α' must be related to ionic species in the electrolyte by heterogeneous reactions, e.g., a metal dissolution reaction,

$$M^+ + e^- = M , \tag{10}$$

at the M/ε interface and a hydrogen-evolution reaction,

$$\frac{1}{2} H_2 = e^- + H^+ , \tag{11}$$

at the ε'/α' interface. The cell potential can be written as

$$FU = \mu_{e^-}^{\alpha'} - \mu_{e^-}^{\alpha} , \tag{12}$$

or

$$FU = \frac{1}{2} \mu_{H_2} - \mu_{H^+}^{\varepsilon'} + \mu_{M^+}^{\varepsilon} - \mu_M . \tag{13}$$

Separation of the electrochemical potential into chemical and electrical contributions (equation (2)) yields

$$FU = FU^{\vartheta} + RT \ln\left[\frac{c_{M^+}^{\varepsilon}}{c_{H^+}^{\varepsilon'}}\right] + RT \ln\left[\frac{f_{M^+}^{\varepsilon}}{f_{H^+}^{\varepsilon'}}\right] + \frac{1}{2} RT \ln[P_{H_2}] - F(\Phi^{\varepsilon'} - \Phi^{\varepsilon}) , \tag{14}$$

where

$$FU^{\vartheta} = RT \ln\left[\frac{a_{M^+}^{\vartheta}}{a_{H^+}^{\vartheta}}\right] + \frac{1}{2} \mu_{H_2}^{\circ} - \mu_M^{\circ} . \tag{15}$$

The potential difference $(\Phi^{\varepsilon'} - \Phi^{\varepsilon})$ is referred to as the liquid-junction potential and is not a thermodynamic property. Its magnitude is dependent upon the arbitrary choice of potential definition.[163] Neglect of the liquid-junction potential, coupled with assumption of unity activity coefficients and pressure leads to the Nernst equation.[99]

Equation (13) can be rearranged under the assumption that liquid-junction potentials can be neglected to yield

$$F(\Phi^M - \Phi^{\varepsilon}) = FU - \mu_{e^-}^{M} + (\frac{1}{2} \mu_{H_2}^{\varepsilon'} - \mu_{H^+}^{\varepsilon'}) . \tag{16}$$

Attempts have been made to take advantage of independent calculations and measurements of chemical potentials in order to calculate electrode-electrolyte potential differences via equation (16) for metals in contact with an electrolytic solution.[164,165] This approach is related to the attempted calculation or measurement of individual ionic activity coefficients.[166-168]

Since U can be measured experimentally, the far right-hand term can be calculated by applying a Born-Haber cycle to the electrode reaction, and the electrochemical potential of electrons in the metal phase can be calculated from the electronic theory of metals or obtained from metal/vacuum electron emission experiments, it is argued that an absolute potential difference across the metal-solution interface can be calculated and tabulated.

Calculations of individual chemical potentials for charged species, however, depend upon the choice of individual ionic activity coefficients, which are not specified thermodynamically.[169] This is clear from the definition of chemical potential given in equation (2). The calculation of potential differences between dissimilar phases therefore cannot have an absolute thermodynamic meaning.

Calculation of Galvani potential differences is especially tenuous. The Galvani potential is unmeasurable and must be calculated from assumptions or models which are themselves unmeasurable or unverifiable.

4. MEASUREMENT OF CAVITY POTENTIAL DIFFERENCES

The definition of cavity potentials makes measurement of the potential within a region of changing potential uncertain. Methods have been described, however, to measure the difference in cavity potential between phases characterized by spatially invariant potentials. These phases do not have to be of the same composition. The methods presented here rely on the use of clean surfaces to aid in proper characterization of the interface.

4.1. Gas-Ground Measurements

Maxwell[170] described a way to measure the potential of a point in air relative to ground. A conducting sphere of small radius a, shown in Figure 2, is placed at the point in question and connected to ground by a thin wire. The sphere is then insulated and carried to an electrometer or an electroscope. The charge on the sphere Q is ascertained. The potential V of the sphere relative to ground is given by

$$V = \frac{Q}{a\varepsilon}. \tag{17}$$

It is equal in magnitude and opposite in sign to the potential of the air. The potential measured in this manner is the cavity potential.

Another method described by Maxwell[170] to measure the potential of air relative to ground involves the use of an electrode that loses a continuous stream of conductive material (electrolyte or metallic chips). The potential of the electrode approaches that of the air as the electrode loses its excess charge and can be measured.

4.2. Liquid-Liquid Measurements

A more sophisticated liquid-jet technique is presented by Llopis[171] to measure the cavity potential difference between two liquid phases. A jet of liquid, shown in Figure 3, is directed along the axis of a tube, the inner surface of which is covered with a stream of the other liquid. A potentiostat is used to adjust the potential of one liquid relative to the other until the electric field in the gap between the two liquids has a zero value. This condition exists when movement of the liquid jet relative to the outside tube results in no current flow. Under this condition the cavity potentials in the two phases are equal. The cell potential required to achieve an absence of

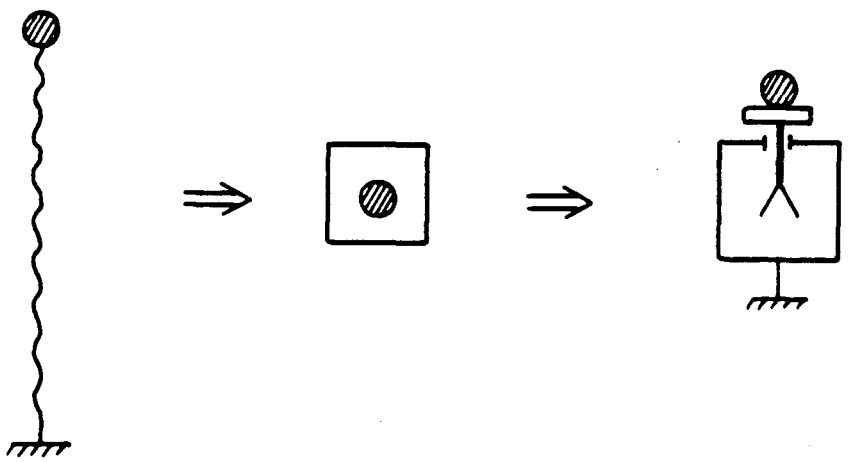

Figure 2. Measurement of cavity potential of a point in air relative to ground:

a) sphere at point connected to ground by wire

b) sphere in isolation being carried to electroscope

c) measurement of charge on sphere by electroscope

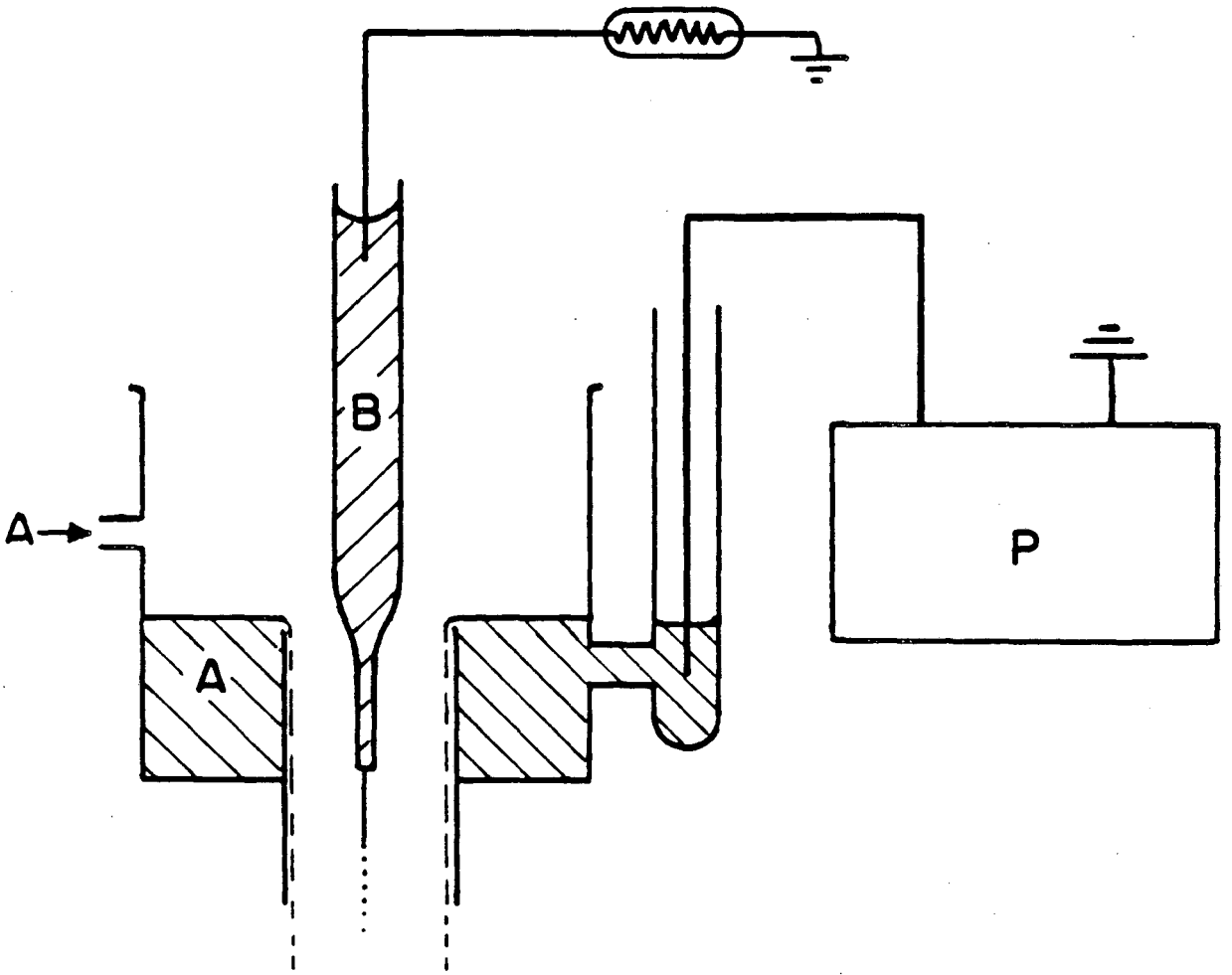

Figure 3. Apparatus for measurement of cavity potential differences between liquid phases.[171]

an electric field is the original cavity potential difference.

This technique was developed by Kenrick[172] and used by Frumkin[173] and Randles.[174] Rapid equilibration of the gas-liquid interfaces is essential in obtaining meaningful results.

4.3. Metal-Metal Measurements

The measurement of cavity potential differences between two metals is presented by Parsons.[98] The experimental setup is presented in Figure 4. Metals α and β are connected through a potentiostat and ammeter with metals of the same composition, α and α'. The region between α and β is evacuated or filled with an inert gas, preferably at low pressure. The potential difference is adjusted with the potentiostat until the electric field E between the two metals is zero. This state exists when a movement of the metal α relative to the metal β produces no current as measured at G. The cavity potentials of the two metals must be equal, and therefore,

$$FE = \alpha^{\alpha}_{e^-} - \alpha^{\beta}_{e^-} \tag{18}$$

If the metals α and β were placed in contact and equilibrated, the cell potential would be equal to zero. The electrochemical potential of electrons in α would be equal to that in β, and

$$\alpha^{\alpha}_{e^-} - F\psi^{\alpha} = \alpha^{\beta}_{e^-} - F\psi^{\beta} . \tag{19}$$

Thus,

$$E = \psi^{\alpha} - \psi^{\beta} . \tag{20}$$

The cell potential required to eliminate the electric field between the two metals is equal to the cavity potential difference between the two metals.

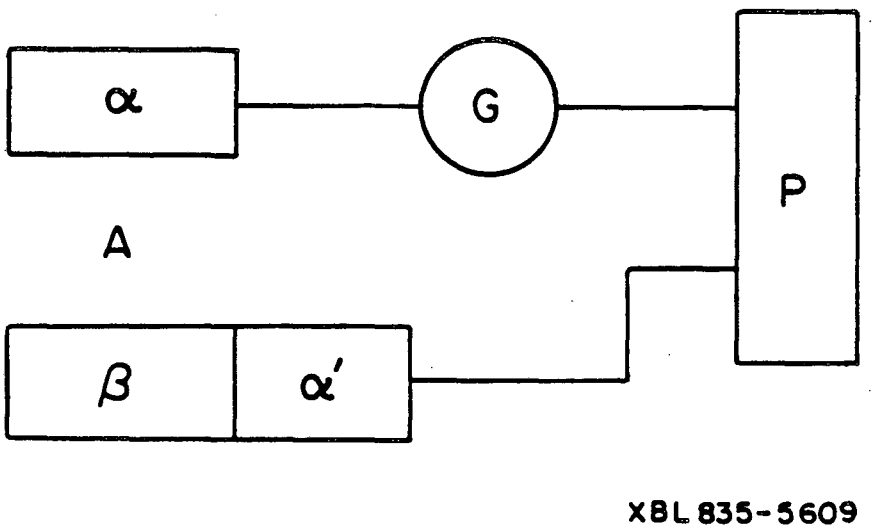

Figure 4. Scheme for measurement of cavity potential differences between a metal α and a metal β.[98]

4.4. Metal-Electrolyte Measurements

A similar measurement can be made for metal/electrolyte systems.[98] The experimental setup is presented in Figure 5; the gap A between the metal of interest δ and the solution δ is either evacuated or filled with an inert gas. The potentiostat is adjusted to eliminate the electric field in the gap. The cell potential is generally related to the cavity potential difference between the two phases by

$$FE = \alpha^{\alpha}_{e^-} - \left[\frac{\mu^{\gamma}_{M} - \alpha^{\delta}_{M^{z_m}}}{z_m} \right] + F(\psi^{\delta} - \psi^{\alpha}), \tag{21}$$

and when the electric field is eliminated within the gap,

$$\psi^{\delta} = \psi^{\alpha} . \tag{22}$$

Thus, under the condition that the electric field is eliminated within the gap,

$$FE = \alpha^{\alpha}_{e^-} - \left[\frac{\mu^{\gamma}_{M} - \alpha^{\delta}_{M^{z_m}}}{z_m} \right] . \tag{23}$$

If the metals β and β' were joined, the cell potential would be zero; therefore

$$\alpha^{\alpha}_{e^-} - \left[\frac{\mu^{\gamma}_{M} - \alpha^{\delta}_{M^{z_m}}}{z_m} \right] = - F(\psi^{\delta} - \psi^{\alpha}) . \tag{24}$$

The cell potential required to eliminate the electric field yields the cavity potential difference between the metal α and the electrolyte δ in contact with a metal γ. If the immersed electrode were of the same composition as α, this experiment would yield the cavity potential difference between the electrolyte and α immersed in the electrolyte.

This technique differs from the metal/metal technique only in that an electrolyte is involved. A similar approach is presented by Bockris and Reddy[175] in which the gap between the metal and the electrolyte contains ionized gas. The use of ionized gasses is also discussed by Llopis.[171]

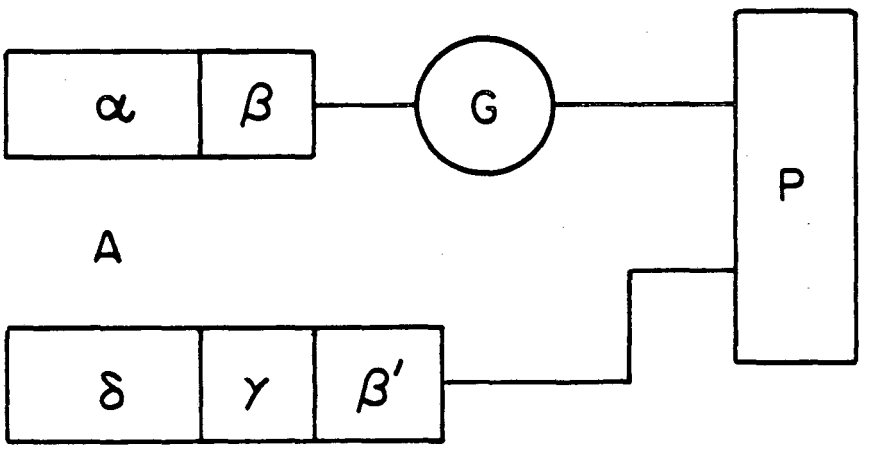

Figure 5. Scheme for measurement of cavity potential differences between a metal α and an electrolyte δ.[98]

4.5. Metal-Vacuum Measurements

The work of extraction of electrons from metals into vacuum by thermionic or photoelectric emission can be measured.[178] When a metal is heated, high energy electrons receive sufficient energy to escape from the surface of the metal. The current density of thermionic emission for a clean surface with no electric field is given by

$$i = A(1-r)T^2 \exp\left(\frac{-e\varphi_w}{kT}\right), \tag{25}$$

where A is a constant, r is the average reflection coefficient for electrons incident to the interface, and φ_w is the work function of the metal.

The emitted current density is measured as a function of temperature, and the work function is obtained from equation (15). The work function presented here is commonly represented to be minus the "real" chemical potential of electrons within the metal (see equation (3)). The association between the work function measured in this way and the "real" chemical potential is, however, not thermodynamically rigorous. Differences in chemical or electrochemical potential between phases at different temperatures are not thermodynamically meaningful. This difference depends upon the arbitrary choice of a secondary reference state for entropy, and this reference state does not cancel. Furthermore, the system is not in a condition of equilibrium.

Photoemission of electrons is an important tool for characterization of electronic solids.[177] The results are generally analyzed through a modified version of the Einstein equation,

$$E_{kin} = h\nu - \varphi_w - E_i, \tag{26}$$

where E_{kin} is the measured kinetic energy of the emitted electron, $h\nu$ is the incident photon energy, φ_w is the work function, and E_i is the energy of the

emitted electron before absorption of the photon energy. Photons with energies below the work-function value cannot (in the absence of potential gradients) produce electron emission. Measurement of the electron emission as a function of photon energy therefore constitutes a means of determining the work function. The work function obtained from photoemission data is not a thermodynamic quantity; these experiments are conducted isothermally but still involve the passage of current.

5. CONCLUSIONS

Electrical potentials are defined in terms of the work of moving a charged test particle from a reference location to the point of interest. The test particle, the physical character of the locations to and from which the particle is moved, and the nature of the work involved can be arbitrarily chosen. The potential can therefore be arbitrarily defined.

The arbitrariness (and the need for careful definition) cancels in thermodynamic calculations between phases of identical composition. Careful definition of potential is needed, however, for characterization of local potential differences between phases of dissimilar composition. The cavity potential is a preferred definition of local electrical state because it has meaning in all phases and can be measured.

Chapter 6. The Equilibrated Liquid-Junction Photovoltaic Cell

Statistical-mechanical and macroscopic-transport models have been used to characterize the semiconductor electrode in the liquid-junction photovoltaic cell. The model of the semiconductor (whether statistical or macroscopic in approach) can be coupled to models of the semiconductor-electrolyte interface and other parts of the cell to describe the cell behavior. Both mathematical approaches relate the electrical potential to concentrations of charged species in the semiconductor through Poisson's equation. Statistical-mechanical models yield these concentrations in terms of the Fermi energy, a statistical parameter (see, e.g., Grove[20] or Sze[21]); macroscopic models rely on material balances to generate the necessary equations.

The object of this work is to identify the relationships between statistical-mechanical and macroscopic-transport models of the semiconductor in the liquid-junction photovoltaic cell. Parameters characteristic of the statistical-mechanical model are be compared to parameters characteristic of the macroscopic-transport model. This comparison is possible through comparison of the equilibrated cell.

A mathematical model of the liquid-junction photovoltaic cell is presented in Chapter 2 in which macroscopic-transport equations describing the semiconductor and the electrolyte were coupled with a kinetic model of the semiconductor-electrolyte interface. In this approach, interfacial equilibrium constants characterize the equilibrated liquid-junction cell. This model forms the basis of the comparison presented here. Calculation of interfacial equilibrium constants in terms of system and statistical parameters is presented.

A wealth of information concerning semiconductor, electrolytic, and interfacial properties is incorporated within interfacial equilibrium constants. The equilibrium (non-illuminated) condition will be examined in section 2 to identify the relationships among the interfacial equilibrium constants and these system properties. The equilibrium relationships are conveniently studied through a statistical-mechanical approach.

1. STATISTICAL-MECHANICAL MODEL

The distribution of electrons within an equilibrated semiconductor has been calculated from statistical considerations.[20,21] The most probable distribution is assumed to be the one which can be obtained in the greatest number of ways subject to the constraints of the system. For electrons in a crystal, the significant constraints are that the electrons are indistinguishable and that no state can contain more than one electron (the Pauli exclusion principle). A system described in this manner is characterized by the Fermi-Dirac distribution function:

$$\frac{n_i}{g_i} = \left[1 + \exp[(E_i - E_f)/kT]\right]^{-1}, \qquad (1)$$

where n_i is the number of electrons within an energy level E_i with degeneracy g_i. The Fermi energy E_f is a statistical parameter defined as the energy at which the probability of occupancy is one half. Calculation of electron and hole concentrations in terms of the Fermi energy is presented in section 2.1.

1.1. Fermi Energy

The Fermi energy has the characteristics of a thermodynamic property, the electrochemical potential (see equation (2) in Chapter 2). The relationship between the Fermi energy (which appears in the Fermi-Dirac

distribution function) and the electrochemical potential of electrons can be obtained from statistical-mechanical arguments.[178]

The statistical analog of entropy is

$$S = k \sum_i \ln W_i \,, \tag{2}$$

where W_i is the probability of occupation of a state i. For a Fermi-Dirac system,

$$W_i = \frac{g_i!}{n_i!(g_i - n_i)!} \,, \tag{3}$$

where n_i is the number of particles in the state i with degeneracy g_i and energy E_i. Through application of Stirling's approximation and the Fermi-Dirac expression for the occupation of state i, the entropy becomes

$$S = k \sum_i g_i \left[\ln[1 + \exp(\frac{E_i - E_f}{kT})] - \frac{(E_i - E_f)}{kT} \right] + k \sum_i n_i \frac{(E_i - E_f)}{kT} \,. \tag{4}$$

The total number of electrons in the system and the total energy of the system are

$$N_T = \sum_i n_i \,, \tag{5a}$$

and

$$E = \sum_i n_i E_i \,, \tag{5b}$$

respectively. The entropy is expressed in terms of these system properties as

$$S = k \sum_i g_i \ln\left[1 + \exp(\frac{E_i - E_f}{k} - T)\right] - \sum_i \frac{g_i E_i}{T} + \sum_i \frac{g_i E_f}{T} + \frac{E}{T} - \frac{N_T E_f}{T} \,. \tag{6}$$

The partial derivative of the entropy with respect to the total electron concentration with temperature, system energy, and concentrations of

other species held constant is

$$\left[\frac{\partial S}{\partial N_T} \right]_{T,E,n_{j \neq T}} = - \frac{E_f}{T} . \tag{7}$$

The electrochemical potential, expressed in terms of the entropy, is given by

$$\mu_i = \left[\frac{\partial G}{\partial N_T} \right]_{P,T,n_{j \neq T}} = - T \left[\frac{\partial S}{\partial N_T} \right]_{V,E,n_{j \neq T}} . \tag{8}$$

The Fermi energy and the electrochemical potential of electrons are therefore related by

$$E_f = \mu_{e^-} + \left[\frac{\partial S}{\partial V} \right]_{E,n_i} \left[\frac{\partial V}{\partial N_T} \right]_{T,E,n_{j \neq T}} , \tag{9}$$

where the electrochemical potential and the Fermi energy are given the same units of energy, e.g., eV. Under the assumption that the semiconductor volume is independent of electron concentration, the Fermi energy is equivalent to the electrochemical potential of electrons and can be related to the electrochemical potential of conduction electrons by a constant. Similar arguments can be used to define individual Fermi energies for valence-band and conduction-band electrons.

1.2. Activity Coefficients

The Fermi-Dirac distribution function (equation (1)) is frequently assumed to be adequately represented by a Boltzmann distribution (see Grove[20] or Sze[21] and see equation (30)). Assumption of the Boltzmann distribution is consistent with the transport development presented in Chapter 2. Use of the more general Fermi-Dirac distribution enters into the transport development through introduction of individual ionic activity coefficients: one for electrons and one for holes.

Through Fermi-Dirac statistics the concentration of conduction electrons is given by

$$n = \int_{E_c}^{\infty} \frac{N(E)}{1 + \exp[(E-E_f)/kT]}\, dE \,, \tag{10}$$

and the concentration of holes by

$$p = \int_{E_o}^{E_v} \left[1 - \frac{1}{1 + \exp[(E-E_f)/kT]}\right] N(E)dE \,. \tag{11}$$

If the distribution of available energy levels is narrow, the valence and conduction electrons can be characterized by single-valued energy levels, E_v (the highest energy level of the valence band) and E_c (the lowest energy level of the conduction band), respectively. Thus;

$$n = \frac{1}{1 + \exp[(E_c-E_f)/kT]} \int_{E_c}^{\infty} N(E)dE \,, \tag{12}$$

or

$$n = \frac{N_c}{1 + \exp[(E_c-E_f)/kT]} \,; \tag{13}$$

where N_c is the concentration of conduction-energy sites for electrons. A similar term, N_v, is defined as the concentration of valence-band sites.

From the definition of the electrochemical potential, the chemical activity,

$$a_i = c_i f_i \,, \tag{14}$$

can be expressed as

$$a_i = \exp\left[\frac{\mu_i - \mu_i^{\circ} - z_i F\Phi}{kT}\right] . \tag{15}$$

In equation (13), the concentration of conduction electrons is given as a function of the Fermi energy level. The energy E_c in this equation depends upon potential as

$$E_c = E_c^{*} + z_i F\, \Phi \,, \tag{16}$$

where E_c^{*} is a constant, independent of potential. The electrochemical

potential of conduction electrons and the Fermi Energy are related by an arbitrary constant (see section 2.1);

$$\mu_{e^-} = E_f + \mu^*_{e^-} . \tag{17}$$

Equations (38) through (42) can be combined to yield

$$f_{e^-} = \frac{\exp[(\mu^*_{e^-} - \mu^\circ_{e^-} + E^*_c)/kT]}{N_c} \left[\frac{1}{1 - n/N_c}\right] . \tag{18}$$

The secondary reference state quantities, E^*_c, $\mu^*_{e^-}$, and $\mu^\circ_{e^-}$, are chosen to allow the activity coefficient to approach unity as the concentration of conduction electrons approaches zero. Thus, the activity coefficient is obtained as a function of composition;

$$f_{e^-} = \frac{1}{1 - n/N_c} , \tag{19}$$

The activity coefficient of conduction electrons is presented in Figure 1 as a function of dimensionless concentration n/N_c.

A similar activity coefficient can be obtained for the holes as

$$f_{h^+} = \frac{1}{1 - p/N_v} . \tag{20}$$

The assumption of unity activity coefficients is in harmony with the assumption of of the Boltzmann limits to the Fermi-Dirac distribution. Use of the Fermi-Dirac distribution results in activity coefficients that are functions of concentration.

1.3. Interfacial Energy Levels

The equilibrium fractional occupation of surface sites at the interface is related to the energy of the sites through Fermi-Dirac statistics:

$$\Theta_i = \frac{1}{1 + e^{(E_i - E_f)/kT}} , \tag{21}$$

where the Fermi energy is that calculated for the bulk of the semiconductor

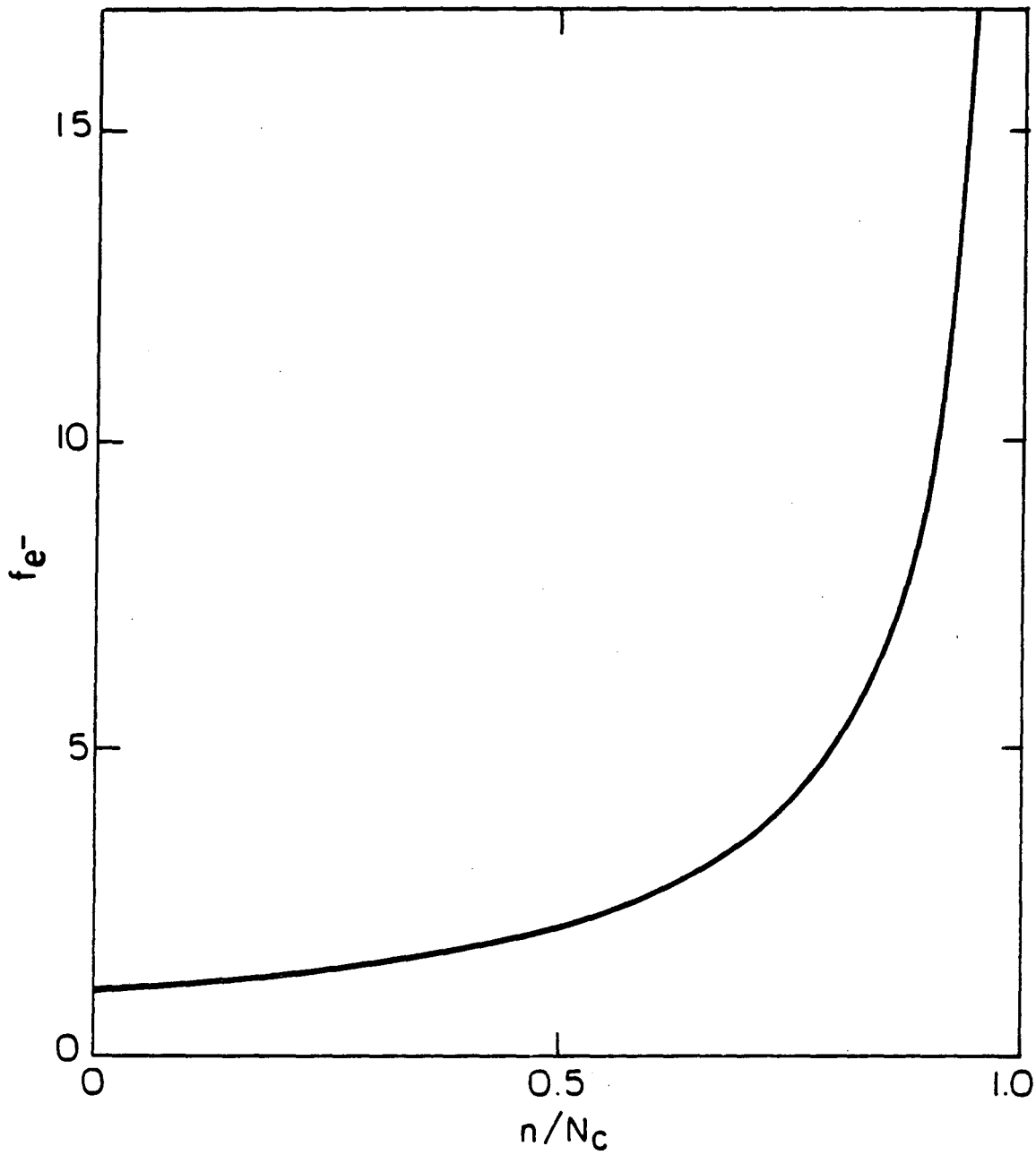

Figure 1. The activity coefficient of conduction electrons as a function of dimensionless concentration.

(see equation (37)). Selection of energy levels for three separate types of surface states (E_v^s, E_t^s, and E_c^s) and concentration of ISS sites (Γ_v , Γ_t , Γ_c) leads to adsorbed electron concentrations as

$$\Theta_v = \frac{\gamma_v}{\Gamma_v} = \frac{1}{1 + e^{(E_v^s - E_f)/kT}}, \tag{22a}$$

$$\Theta_t = \frac{\gamma_t}{\Gamma_t} = \frac{1}{1 + e^{(E_t^s - E_f)/kT}}, \tag{22b}$$

and

$$\Theta_c = \frac{\gamma_c}{\Gamma_c} = \frac{1}{1 + e^{(E_c^s - E_f)/kT}}. \tag{22c}$$

The energy levels presented here depend on the electrical potential (see equation (16)).

An equivalent formulation cannot be used to describe the distribution of adsorbed ions at the IHP; the energy levels E_i of different ionic species are not clearly related, and an equilibrium Fermi energy E_f must be defined for each individual species in the absence of kinetic equilibrium constraints. The Fermi energies so defined do not have a clear relationship with the Fermi energy established in the semiconductor.

A kinetic argument is used instead to establish the equilibrium distribution of ions adsorbed in the IHP. The rate of adsorption of a species i (see Chapter 2) is expressed by

$$\begin{aligned} r_i = {} & k_{f,i} \exp\left[\frac{-z_i(1-\beta_l)F\Delta\Phi_l}{RT}\right]\gamma_i \\ & - k_{b,i} \exp\left[\frac{z_i \beta_l F\Delta\Phi_l}{RT}\right] c_i(\Gamma_{ihp} - \sum_k \gamma_k) . \end{aligned} \tag{23}$$

At equilibrium the net reaction rate is zero, and the concentration of species i at the inner Helmholtz plane is

$$\frac{\gamma_i}{\Gamma_{ihp}} = \frac{k_{b,i}}{k_{f,i}} \exp[\frac{z_i F \Delta\Phi_l}{RT}] c_i (1 - \sum_k \frac{\gamma_k}{\Gamma_{ihp}}) , \tag{24}$$

or

$$\frac{\gamma_i}{\Gamma_{ihp}} = c_i (1 - \sum_k \frac{\gamma_k}{\Gamma_{ihp}}) e^{-\Delta E_i / RT} , \tag{25}$$

where

$$\Delta E_i = -z_i F \Delta\Phi_l + RT \ln(\frac{k_{f,i}}{k_{b,i}}) . \tag{26}$$

The fractional occupation of the IHP by a species i in terms of the adsorption energies ΔE_k is derived from an extension of equation (25) to be

$$\frac{\gamma_i}{\Gamma_{ihp}} = \frac{c_i e^{-\Delta E_i / RT}}{1 + \sum_k c_k e^{-\Delta E_k / RT}} . \tag{27}$$

The equilibrium fractional occupation of the IHP by a single species i, $\gamma_{i,(s)}$, corresponds to that given by the Langmuir adsorption isotherm (see, e.g., Delahay[102]) as

$$\frac{\gamma_{i,(s)}}{\Gamma_{ihp} - \gamma_{i,(s)}} = a_i e^{-\Delta E_i / RT} , \tag{28}$$

where a_i is the activity of the ionic species in the bulk of the solution, and

$$\Delta E_i = \Delta G^o_{ads} , \tag{29}$$

the "standard" free energy of adsorption. The "standard" free energy of adsorption is dependent upon the equilibrium potential difference between the IHP and the OHP.

The equilibrium concentration of adsorbed electrons is therefore obtained in terms of equilibrium site energies and the semiconductor Fermi energy. The equilibrium concentrations of adsorbed ions are obtained in terms of concentrations adjacent to the interface and adsorption energies. The coupling between the semiconductor and the electrolyte under equilibrium conditions can be expressed in terms of the interfacial

equilibrium constants discussed in Chapter 2. The calculation of these equilibrium constants in terms of system properties is presented in the following section.

2. CALCULATION OF EQUILIBRIUM CONDITIONS

The condition of equilibrium is defined by the equality of the electrochemical potential (or equivalently of the Fermi energy) of a given species at any point in the system. At equilibrium and in the absence of corrosion, the interfacial reactions have a zero net rate. The thermal generation of electron-hole pairs in the bulk of the semiconductor is exactly balanced by recombination. Potential and concentration variations in the system do exist within this framework and are caused by the presence of a charge-laden interface. Under the assumption of local equilibration, the presence of a counterelectrode can be neglected. The cell can therefore be examined in terms of its major components: the semiconductor, the solution, and the semiconductor-solution interface. Equilibration with the counterelectrode can be considered subsequently.

2.1. Semiconductor

The statistical-mechanical approach can be used to calculate the equilibrium condition of the semiconductor. The approach presented in this section is described elsewhere[20,21,69,178] and is presented here for completeness.

Under the assumption that the activity coefficients of electrons and holes are given by equations (19) and (20), respectively, the equilibrium concentrations of electrons and holes are given by

$$n = (N_c - n)\exp[-(E_c - E_f)/kT], \tag{30}$$

and

$$p = (N_v - p)\exp[(E_v - E_f)/kT]\,, \tag{31}$$

respectively. The Fermi energy is a sufficient indicator of equilibrium conditions since the electrons and holes are chemically equilibrated.*

The product of the electron and hole concentrations is

$$np = (N_c - n)(N_v - n)\exp(-E_g/kT)\,, \tag{32}$$

where E_g is the semiconductor band-gap energy. Under the assumption that the ratios n/N_c and p/N_v are much less than one (i.e., the activity coefficients for electrons and holes have a value of one), the product np is a function of the semiconductor properties, E_g, N_c, and N_v. For a given semiconductor,

$$np = n_i^2\,, \tag{33}$$

where n_i is called the intrinsic concentration.

Consider a region of the semiconductor far from an interface and where, therefore, the imposition of electroneutrality is valid. The condition of electroneutrality is that

$$p^o + (N_d - N_a) - n^o = 0\,, \tag{34}$$

where n^o is the bulk electron concentration, $(N_d - N_a)$ represents the background charge (doping level), and p^o is the bulk hole concentration. The donors are assumed to be completely ionized. This assumption is consistent with the assumption of unity activity coefficients for electrons and holes.

Substitution of equation (33) into equation (34) leads to the bulk electron concentration as a function of the background charge and the

* Under non-equilibrium conditions, a single Fermi energy does not sufficiently specify the semiconductor. Individual Fermi energies or individual electrochemical potentials must be defined in this case to characterize each species, holes and electrons.

intrinsic concentration.

$$n^o = \frac{1}{2}[(N_d - N_a) + ((N_d - N_a)^2 + 4n_i^2)^{1/2}] . \quad (35)$$

The intrinsic concentration is determined via equation (32) as a function of system properties.

The Fermi energy in the bulk of the semiconductor referenced to the conduction-band energy is

$$E_f = E_c + kT \ln(\frac{n}{N_c}) , \quad (36)$$

or

$$E_f = E_c^* - F\Phi + kT \ln(\frac{n}{N_c}) . \quad (37)$$

The Fermi energy is the statistical equivalent of the electrochemical potential of electrons in the semiconductor (see equation (9)), and is constant throughout the semiconductor at equilibrium. A value for the Fermi energy, valid throughout the semiconductor, can be calculated through equation (37) for the semiconductor far from an interface where the electron concentration is n^o and the potential Φ is zero. This value is useful for evaluating equilibrium conditions at the interface (see equation (22)).

From equation (2) of Chapter 2 (or equivalently from equations (16), (30), and (31)) the equilibrium concentrations of electrons and holes are given as functions of potential by

$$N = n \exp(-\Phi F / RT) = constant , \quad (38)$$

and

$$P = p \exp(\Phi F / RT) = constant . \quad (39)$$

The potential distribution in the semiconductor is related to the charge distribution by Poisson's equation. Upon incorporation of equations (38)

and (39), Poisson's equation can be written as

$$\frac{d^2\Phi}{dy_{sc}^2} = -\frac{F}{\varepsilon_{sc}}\left[Pe^{-\Phi/RT} - Ne^{\Phi/RT} + (N_d - N_a)\right]. \tag{40}$$

A boundary condition in the bulk is

$$\Phi \to 0 \quad as \quad y_{sc} \to \infty, \tag{41}$$

and therefore

$$\frac{d\Phi}{dy_{sc}} \to 0 \quad as \quad y_{sc} \to \infty. \tag{42}$$

These conditions allow N and P to be determined in the bulk of the semiconductor. At the interface ($y_{sc} = y_{oss}$), an electric field is present due to charge adsorbed onto the semiconductor-solution interface. This electric field can be related to system variables as

$$E_{oss} = -\frac{(\Phi_{oss} - \Phi_{iss})}{\delta_1}. \tag{43}$$

Integration of Poisson's equation yields

$$E_{oss} = \pm\left\{\frac{2RT}{\varepsilon_{sc}}\left[N(e^{\Phi_{oss}F/RT} - 1) + P(e^{-\Phi_{oss}F/RT} - 1) - (N_d - N_a)\right]\right\}, \tag{44}$$

where the potential at the OSS is given as a function of the electric field at the OSS. An iterative solution to equation (44) can be obtained via Newton's method.

The relationships developed in this section are coupled with those developed for the solution and the interface to specify concentration and potential variables in the bulk of the semiconductor, the bulk of the solution, and at the interface. Evaluation of these variables in the region between the bulk of the semiconductor and the interface is not a necessary part of this analysis and can be accomplished by numerical solution of the equations presented in Chapter 2.

2.2. Electrolyte

The equations governing the solution are, as in the semiconductor, Poisson's equation and material balances (equations (14) and (13) respectively in Chapter 2). Under equilibrium conditions, the material balance equations can be replaced by the equality of electrochemical potential of species i throughout the solution. This condition can be expressed as

$$C_i = c_i e^{z_i \Phi F / RT} = constant . \tag{45}$$

The boundary condition for Poisson's equation states that the potential tends to zero far from the interface. The potential defined in this manner differs by a constant from the potential used to define the electrical state in the semiconductor. The constant in equation (45) is equal to the bulk ion concentration, therefore

$$c_i = c_{i,bulk} e^{-z_i \Phi F / RT} . \tag{46}$$

This result is in harmony with assumption of the Boltzmann concentration distribution.

Poisson's equation can be integrated to obtain the electric field at the OHP in terms of the potential at the OHP. The electric field is given by

$$E_{ohp} = - \frac{(\Phi_{ihp} - \Phi_{ohp})}{\delta_3} . \tag{47}$$

Therefore;

$$(\Phi_{ihp} - \Phi_{ohp}) = \pm \delta_3 \left\{ \frac{2RT}{\varepsilon_3} \left[\sum_i c_{i,bulk} (e^{-z_i \Phi F / RT} - 1) \right] \right\}^{1/2} , \tag{48}$$

where the root chosen has the same sign as the potential at the OHP (see chapter 7 in reference (99)).

2.3. Interfacial Reaction-Rate Constants

The potential is related to the charge adsorbed at the inner surface states and the inner Helmholtz plane by Gauss's law, presented in equations (26) and (27) of Chapter 2. The concentrations of electrons at the inner surface states are given in terms of the Fermi energy by equation (22) and the concentrations of ions at the inner Helmholtz plane by equation (25).

The remaining parameter needed to solve the equations presented for the equilibrated system is the OSS potential. One could choose a parameter subject to experimental measurement, such as the difference between the cavity potential in the bulk of the electrolytic solution and in the bulk of the semiconductor (or between Φ_{isc} and Φ_{iss}). The choice of parameter is arbitrary, and such measurements can be used with either choice for comparison to the whole model.

The equations presented for the equilibrated liquid-junction cell can be solved by systematic and consecutive calculations to obtain equilibrium concentrations and potentials. The interfacial equilibrium constants can be calculated subsequently as functions of the equilibrium interfacial concentrations and potentials from

$$K_l = \exp[-\frac{F}{RT}\Delta\Phi_l]\prod_i c_i^{-s_{i,l}}, \qquad (49)$$

as presented in the steady-state development (Chapter 2).

2.4. Counterelectrode

The distribution of potential within an electrochemical system cannot be determined from thermodynamic equilibrium considerations alone. The cell potential (as measured with leads of identical composition) can be calculated for an equilibrated system, but the potential distribution within

the cell requires additional experimental characterization. The microscopic model of the cell must yield the same equilibrium cell voltage as obtained from thermodynamics; therefore, for a given model of the semiconductor-electrolyte interface, the equilibrium potential drop across the counterelectrode-electrolyte interface is given by

$$V^{o}_{sol/ce} = V^{o}_{cell} - V^{o}_{m/sc} - V^{o}_{sc/sol} - V^{o}_{ce/m} , \qquad (50)$$

where V^{o}_{cell} is the equilibrium cell voltage obtained from thermodynamic calculations and $V^{o}_{j/k}$ are the equilibrium potential drops obtained from the model for each interface j/k in the system.

3. CONCLUSIONS

Statistical-mechanical and macroscopic-transport models of a semiconductor are related through equilibrium parameters. The Fermi energy of a semiconductor, for example, is equivalent to the electrochemical potential of electrons. The assumption of Boltzmann distributions for electron and hole concentrations in the statistical model is in harmony with the assumption of unity activity coefficients for electrons and holes in the macroscopic model. Use of the more general Fermi-Dirac concentration distribution leads to activity coefficients for electrons and holes that are functions of concentration..

The semiconductor and electrolyte of a liquid-junction photovoltaic cell are related under equilibrium conditions by interfacial equilibrium constants (see Chapter 2), and their values can be determined in terms of system and statistical parameters. The Fermi energy and interfacial energy levels enter into the calculation of these interfacial equilibrium constants through the calculation of concentrations of adsorbed electrons. The concentrations of adsorbed ionic species are related to adsorption energies

(which are dependent upon the equilibrium potential difference between the semiconductor and the electrolyte) and concentrations of ionic species adjacent to the interface.

The equilibrium condition for a semiconductor in contact with an electrolytic solution can be determined in terms of the coupled macroscopic-transport and statistical-mechanical models. The equilibrium potentials and concentrations are obtained in the bulk of the semiconductor, the semiconductor-electrolyte interface, and in the bulk of the solution in terms of the semiconductor band gap, dopant concentration, permittivity, and concentrations of conduction and valence-band sites; the solution permittivity, bulk ionic concentrations, and energies of adsorption; the concentrations and energies of interfacial sites; the distance between the planes of charge at the interface (OSS, ISS, IHP, and OHP); and the potential of the solution side of the interface (OHP). This equilibrium information is incorporated within the equilibrium constants for interfacial reactions used in the macroscopic-transport model of the liquid-junction photovoltaic cell.

Chapter 7. Experimental Methods for Characterization of Liquid-Junction Photovoltaic Cells

A mathematical model of the liquid-junction photovoltaic cell has been presented in Chapter 2. This model incorporates a microscopic model of the semiconductor-electrolyte interface coupled with macroscopic models of the other elements of the cell. The parameters that characterize the system have well-defined physical meaning, but some interfacial parameters are not directly measurable. A measure of the validity of the microscopic model of the semiconductor-electrolyte interface can be obtained by comparison to carefully chosen experiments. These experiments are designed to characterize the electrochemical system and to verify the applicability of the mathematical model.

Characterization of electrochemical systems is carried out through "in-situ" methods and "ex-situ" methods, where the parameters measured are considered to be independent of environment (or dependent in a known way). "In-situ" methods are used to obtain characteristic potential differences, current-potential curves, and capacitance data. "Ex-situ" methods are used to measure bulk transport and kinetic properties. This paper describes some of these experimental methods.

1. IN-SITU METHODS

This section describes some of the experimental approaches used to characterize the liquid-junction photovoltaic cell.

1.1. Potentials

Potentials characterize the electrical state of a given location relative to a reference electrical state. Potentials have meaning only in terms of a

difference, and this potential difference is proportional to the work of moving a charged test particle from the reference location to the point of interest. The test particle, the physical character of the locations to and from which the particle is moved, and the nature of the work involved can be arbitrarily chosen. The potential can therefore be arbitrarily defined.

The arbitrariness (and the need for careful definition) of the potential cancels in thermodynamic calculations of potential differences between phases of identical composition. The cell potential under equilibrium conditions can be calculated and measured directly.[99]

The distribution of potential within an electrochemical system cannot be determined from thermodynamic equilibrium considerations alone. The equilibrium cavity-potential drop across each interface can be measured (see Chapter 5) or calculated from mathematical models (see Chapter 6) under the constraint that the sum of equilibrium potential drops through the cell equal the appropriate thermodynamic quantity.

1.2. Current-Voltage Characteristics

Measurement of current-potential curves[42,105,178,179] for the liquid-junction photovoltaic cell provides a means of comparison of mathematical model and experiment.[87-90,180,181] Species in the semiconductor frequently limit the electrochemical reaction, and this makes characterization of ionic mass transfer less crucial. Use of the rotating disk is still recommended to aid in the characterization of the experimental system and to eliminate spurious effects. The equations governing mass transfer in a rotating disk system have been developed and are presented elsewhere.[182-184]

1.3. Capacitance

Capacitance experiments yield an over-all impedance for the electrochemical cell. The experimental impedance for solid electrodes has been observed to depend upon frequency.[102] The details of such measurements are presented elsewhere.[185] Electrochemical Photocapacitance Spectroscopy[186,187] has been used to determine energy levels for deep traps and surface sites for electrons. The capacitance at a given frequency is measured as a function of incident photon energy. Discontinuities in the capacitance curve indicate the energy of the site.

Quantitative interpretation of experimental impedance results depends upon a postulated mathematical model of the cell. Two models are presented below.

1.3.1. Mott-Schottky Model. Mott[188] and Schottky[189] used an idealized view of the semiconductor-electrolyte interface to derive a relationship between the capacitance of the space charge region and system parameters (see also Gerischer[89]);

$$\frac{1}{C^2} = \frac{2}{A\varepsilon e(N_d - N_a)}\left(V - V_{fb} - \frac{kT}{e}\right) \quad (1)$$

Given ε, the permittivity of the semiconductor, and A, the surface area of the interface, the flat-band potential, V_{fb}, and the effective donor or acceptor density, $(N_d - N_a)$, can be found.

The Mott-Schottky model is based upon the assumptions[190] that:

1. there is no resistance in the semiconductor or electrolyte bulk,
2. no faradaic charge transfer occurs at the interface (the electrode is ideally polarizable),
3. there are no surface sites for electrons,

4. no specific adsorption occurs at the inner Helmholtz plane,

5. the semiconductor permittivity is constant,

6. only one kind of donor is present, and that donor is completely ionized (uniform background charge),

7. any defect distribution in the semiconductor is homogeneous, and

8. the interface can be represented by a one-dimensional model.

Experimental results for a system that follows the Mott-Schottky relationship are presented in Figure 1 (data from Horowitz[191]). Under the assumption that the term, kT/e, can be neglected ($kT/e = 0.026\ V$ at room temperatures), the flat-band potential is obtained from the intercept at infinite capacity, and the doping level is obtained from the slope. Further discussion of the Mott-Schottky model is presented by Pleskov.[192]

1.4. **Microscopic Models.** A microscopic model of the semiconductor-electrolyte interface, or of the entire liquid-junction cell (see Chapter 2), can yield values of the cell impedance which can be compared to the experimental results. This approach depends upon numerical computations and lacks the simple elegance of the model discussed above, but it also can be free of the restrictive assumptions which limit the Mott-Schottky model.

The differential capacitance of a given component of the cell is given by

$$C = -\left(\frac{\partial q}{\partial \Phi}\right)_{\mu} \qquad (2)$$

A circuit analog of the semiconductor-electrolyte interface in the liquid-junction photovoltaic cell is presented in Figure 2. Each interface generates a contribution to the cell impedance, although some can be neglected. From a model of this sort, an effective system capacity can be calculated and compared to experiment.

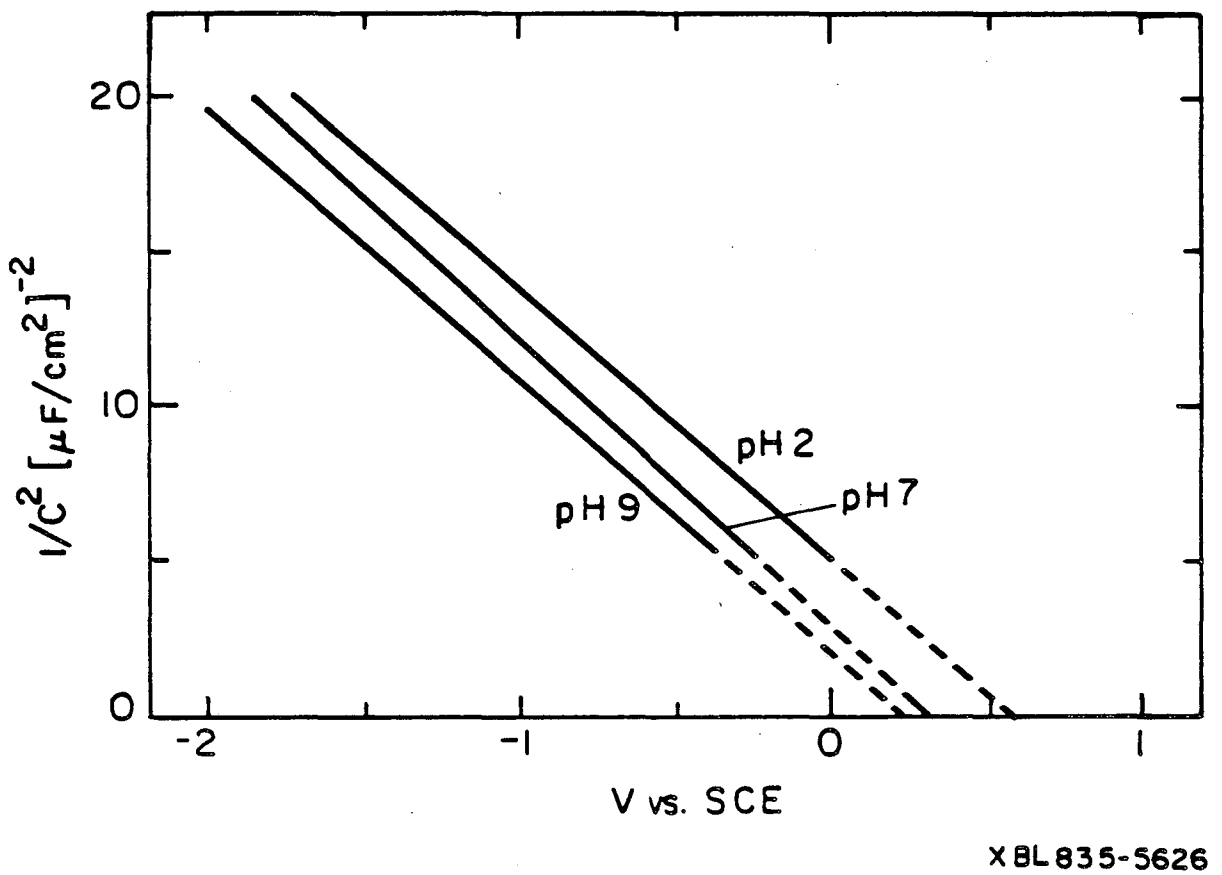

Figure 1. Mott-Schottky plot of p-type GaP in buffered solution at pH=2, 7, and 9. [191]

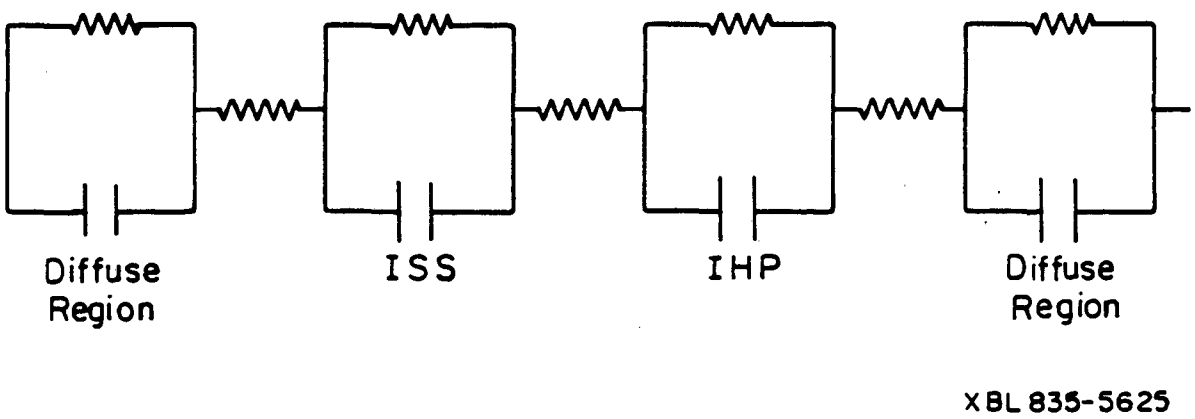

Figure 2. Circuit analog to a semiconductor-electrolyte interface.

2. EX-SITU MEASUREMENTS

Bulk transport and kinetic properties can be assessed outside of the electrochemical cell. Such measurements are dependent upon the ability to isolate phenomena which can be described by equations incorporating the desired physical property. The accuracy of the measured property is dependent upon both the validity (and generality) of the governing equations and the experimental design.

2.1. Semiconductor Properties

The semiconductor properties of interest in the model of the liquid-junction cell (see Chapter 2) are the electron and hole mobilities, u_- and u_+ respectively, the bulk electron and hole concentrations, n^o and p^o respectively, the dopant concentration $(N_d - N_a)$, the band gap $(E_c - E_v)$, the homogeneous recombination rate constant k_{rec} (or the lifetime τ_o), the dielectric permittivity ε, and the optical absorption coefficient α. The measurements described below are related to the determination of these parameters.

2.1.1. Electrical Conductivity. In the limit of infinite dilution, the conductivity of the semiconductor is related to the concentrations and mobilities of the charge carrying species by

$$\sigma = e^2(u_-n + u_+p)\,, \tag{3}$$

where e is the electronic charge, and n and p are the concentrations of electrons and holes, respectively. Direct measurements of the conductivity can be made. The main sources of error are contact resistances, which can be reduced by inducing currents with alternating or rotating magnetic fields or by measuring the potential drop across a sample with high impedance

probes.[193] Completely contactless measurement schemes can be limited, however, by sensitivity, linearity, or geometrical constraints.[194]

The conductivity varies significantly with temperature. The mobility is constant from 0 to 100 K, and conductivity increases in this range are due to increases in the carrier concentrations. Above 100 K and below the onset of intrinsic conduction (300 to 400 K), the conductivity decreases with temperature due to a decrease in the carrier mobility.[195] The value of the forbidden energy gap can be determined from the variation of the conductivity with temperature within an intrinsic semiconductor.[101] The value obtained in this manner is subject to errors due to the uncertainty of having an intrinsic condition and the variation of the mobility and band gap with temperature.

Conductivity measurements at a given temperature yield information about the product of mobility and concentration. Additional experiments are needed to separate these quantities.

2.1.2. Hall Effect. The interaction of magnetic and electrical fields allows an experimental characterization of the semiconductor (or metal) bulk. An electric field is used to drive a current through a sample, as shown in Figure 3, and a magnetic field is applied in the direction normal to flow. A transverse potential develops, counteracting a carrier concentration gradient in that direction. (The current and the electric field vectors are not in the same direction in the presence of a transverse magnetic field.)[100,196] This phenomenon is called the Hall Effect,[196] and the proportionality constant relating the transverse potential V_H, the current density i, the sample width W, and the magnetic field H is the Hall coefficient R_H.

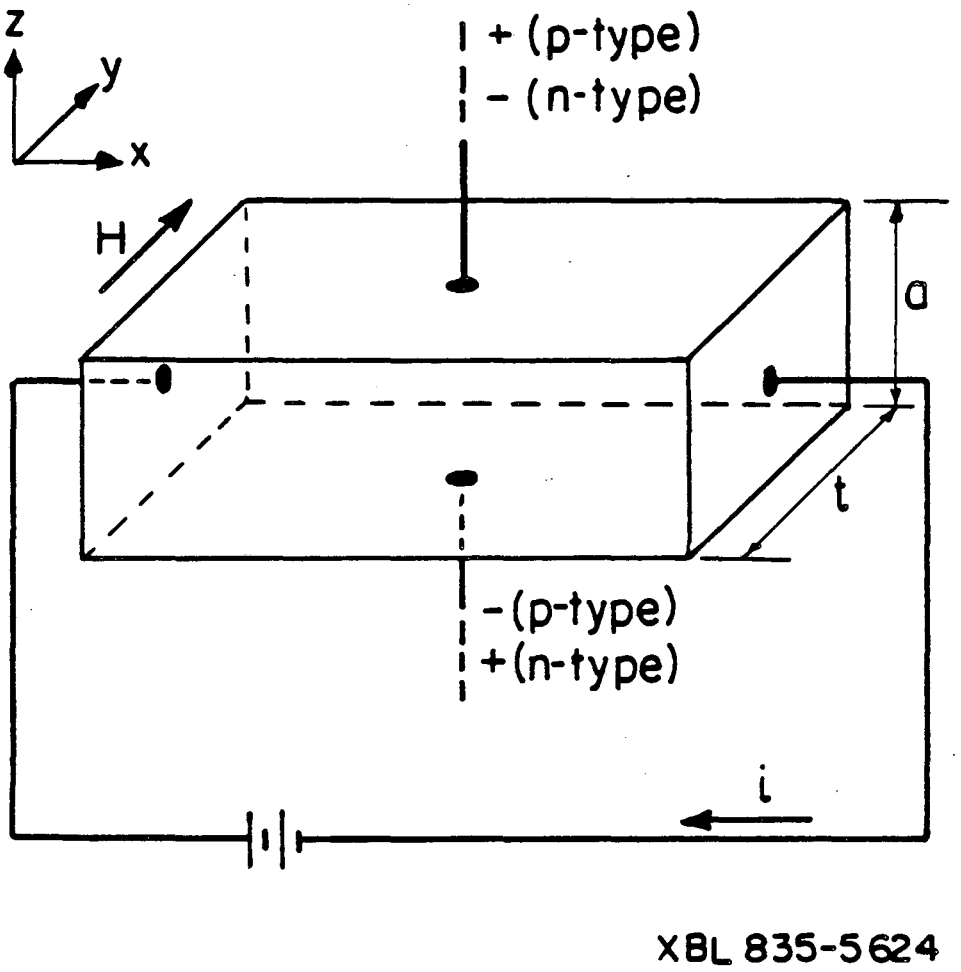

Figure 3. Scheme for measurement of Hall effect.[196]

$$V_H = R_H i H W \,. \tag{4}$$

If the Hall constant is negative, electrons are the majority carriers (n-type); if positive, holes are the majority carriers (p-type).

The Hall coefficient is related to carrier concentrations by

$$R_{H-} = -\frac{1}{ne} \tag{5a}$$

if electrons are the only mobile species present and by

$$R_{H+} = \frac{1}{pe} \tag{5b}$$

if holes are the only mobile species present. The expression for the Hall coefficient when both are present is given by[21,197]

$$R_H = \frac{1}{e}\left[\frac{u_+^2 p - u_-^2 n}{(u_- n + u_+ p)^2}\right]. \tag{6}$$

Measurement of the Hall coefficient and the conductivity gives the mobility of the major carrier species. The temperature dependence of the Hall coefficient provides information about the energy and concentrations of acceptor and/or donor ions and trap states. The interpretation of Hall measurements in terms of dopant parameters, however, is not unique.[198] Donor addition can be used to verify an interpretation of Hall measurements.

2.1.3. Drift and Photodecay Measurements. The direct measurement of the response of a semiconductor to a pulse of light provides information about the mobility and the recombination rate. A typical apparatus is presented in Figure 4. A long filament of the semiconducting material has an electric field applied to it. A local increase in carrier concentration (above the equilibrium values) is caused by a short burst of illumination. The carriers are separated by the electric field. As the pulse of carriers moves, it is diminished by recombination, and it spreads due to diffusion processes. The

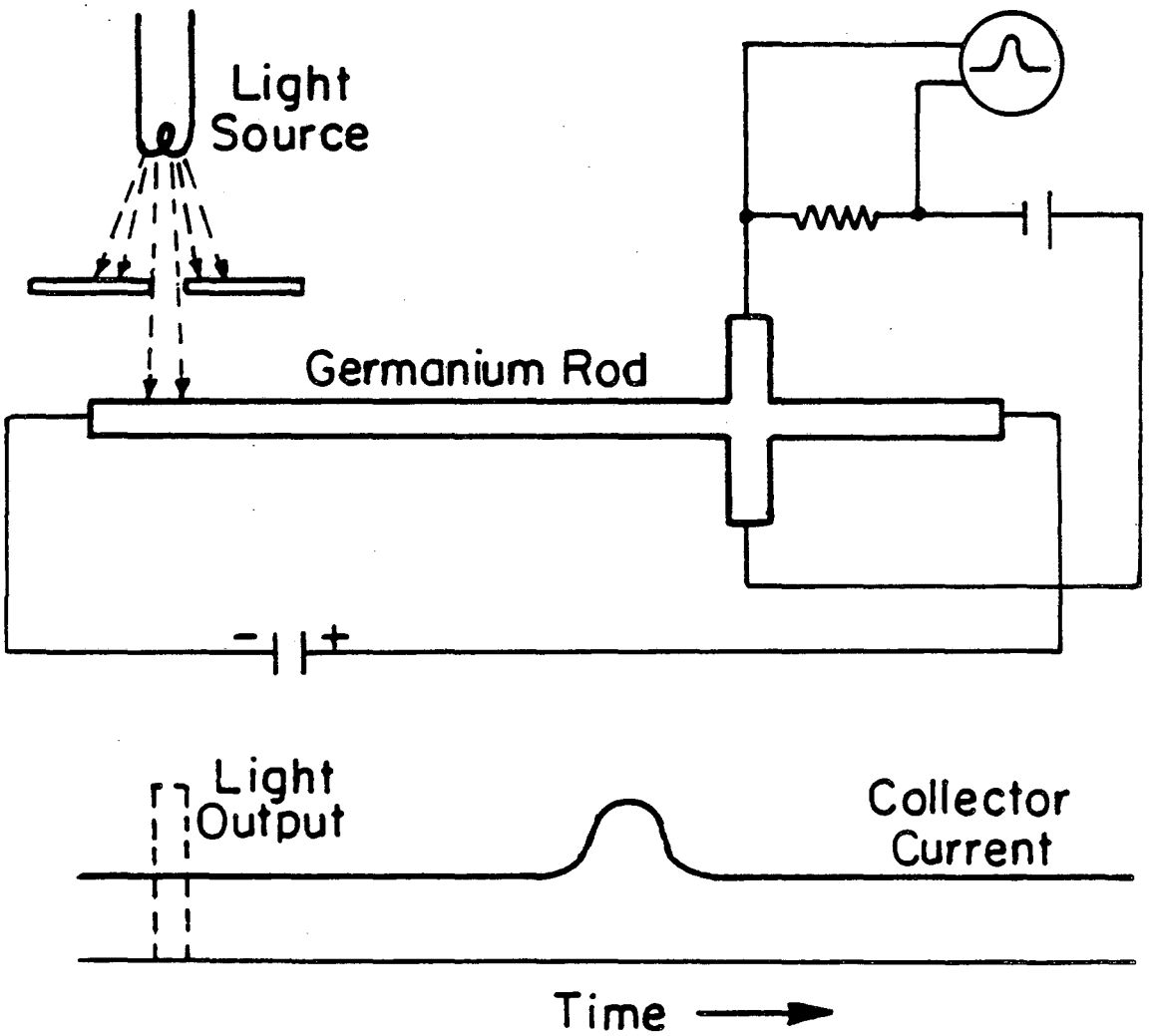

Figure 4. Scheme for measurement of drift mobilities and recombination constants.[196]

arrival of the pulse at the cross arm increases the current at this arm. The time for the pulse to move a known distance in the known electric field is a direct measure of the mobility, and the rate of decrease of the signal area with time (obtained by varying the distance between light source and collector) gives the lifetime.

The mobility measured in drift experiments does not agree at high temperatures with the mobility measured in Hall experiments. This difference is due to inconsistencies in the assumptions made concerning recombination.

Direct measure of the change in photoconductivity with time after a homogeneously distributed pulse of light is also used to measure the lifetime.[199] The conductivity of the sample as a function of time t is related to the lifetime τ by

$$\sigma = \sigma_{dark} + (\sigma_{illum} - \sigma_{dark}) \exp(-\frac{t}{\tau}) . \qquad (7)$$

The conductivity in the dark σ_{dark} and under illumination σ_{illum} are measured, and the conductivity in the dark after an extended period of illumination is measured as a function of time to get the time constant τ.

2.1.4. Seebeck Effect. Thermoelectric characteristics of semiconductors are used to provide information on the energy of majority carriers, and, indirectly, the electron or hole concentrations. A temperature difference between the two ends of a semiconductor gives rise to a potential difference $Q\,\Delta T$, where Q is called the thermoelectric power.[199] The thermoelectric power measured in this way in an n-type semiconductor is related to the energy barrier overcome by the carriers by

$$Q\,\Delta T = (E_c - E_f) + 2kT , \qquad (8)$$

where E_c is the conduction band energy and E_f is the Fermi energy. The

analysis of the Seebeck effect (or the related Peltier effect in which a temperature difference is caused by a potential difference) is not straightforward. There is no thermodynamic basis for the interpretation of this effect.

2.1.5. Dielectric Permittivity The dielectric permittivity ε relates the displacement vector in Maxwell's theory of electromagnetism[170,200] to the electric field. It is a real quantity (see Appendix A). The complex permittivity, used in the study of optics, is related to the permittivity by

$$\varepsilon' = \varepsilon - \frac{j\sigma}{\omega}, \tag{9}$$

where j is $\sqrt{-1}$ and ω is the angular frequency associated with the electromagnetic radiation.

The index of refraction, the ratio of the speed of light in a given medium to the speed of light in vacuum, is a real number. A complex index of refraction n' is given by

$$n' = n(1 - jk), \tag{10}$$

where k is the absorption index (equal to zero in vacuum). Through Maxwell's equations, the complex index of refraction is related to the complex permittivity by

$$n' = \left[\frac{\varepsilon'}{\varepsilon_o}\right]^{1/2}, \tag{11}$$

where ε_o is the permittivity of vacuum, $\varepsilon_o = 8.8542\times10^{-14}$ C/V-cm. The matching of real and imaginary parts yields

$$n^2 = \frac{\varepsilon(1 - k^2)}{\varepsilon_o}, \tag{12a}$$

and

$$n^2 = \frac{\sigma}{\omega k \varepsilon_o} . \qquad (12b)$$

The dielectric constant ($\varepsilon/\varepsilon_o$) is typically obtained from equation (12a) under the assumption that $k << 1$.[69,101,201]

The absorption of light also provides a convenient measure of the band-gap energy of a semiconductor. Semiconductors are transparent to light below the band-gap energy. A sharp increase in the absorption coefficient is therefore observed for photons greater than the band-gap energy.

2.1.6. Surface Techniques Surface analysis techniques such as electron microscopy, LEED, Auger, and ESCA[202] can provide clues to the structure of the semiconductor surface, and thus allow estimates of interfacial parameters. (See also Many et al.[203]) Interfaces are in general strongly dependent upon environment; a semiconductor-vacuum interface is vastly different from a semiconductor-electrolyte interface. Use of ex-situ surface analysis techniques provides a guide, however, in estimating interfacial parameters.

2.2. Electrolytic Properties

The properties of interest in the electrolytic solution are the bulk-solution ionic concentrations and diffusion coefficients and the solution permittivity. Solution concentrations can be obtained from standard analytical chemistry techniques,[204,205] and the permittivity of the solution can be measured in the manner discussed above.

Ionic diffusion coefficients are related to ionic mobilities by the Nernst-Einstein relationship,

$$D_i = RT\,u_i \quad . \tag{13}$$

Ionic diffusion coefficients are not generally reported in the literature, but they can be obtained from values of the equivalent ionic conductance which are reported (see Newman[99]).

The equivalent ionic conductance is related to ionic mobility by

$$\lambda_i = |z_i| F^2 u_i \quad . \tag{14}$$

The ionic diffusion coefficients can be calculated from the equivalent ionic conductance by

$$D_i = \frac{RT\lambda_i}{|z_i| F^2} \quad . \tag{15}$$

Equivalent ionic conductances are determined by measuring the equivalent conductance

$$\Lambda = \lambda_- + \lambda_+ \tag{16}$$

and the transference number t_+ for solutions of single salts and extrapolating the values so obtained to infinite dilution. The transference number is related to the ionic conductances by

$$t_+ = \frac{\lambda_+}{\lambda_- + \lambda_+} \quad . \tag{17}$$

Equations (16) and (17) yield λ_+ and λ_-.

Discussion of mass transfer and diffusion coefficients is presented by Bird et al.[206] and Reid et al.[207]

3. CONCLUSIONS

The mathematical modeling of the liquid-junction photovoltaic cell must depend upon a model of the semiconductor-electrolyte interface. Experiments can be designed to obtain information for comparison to the model; this comparison serves to verify the applicability of the model of the interface.

"Ex situ" measurements are used to obtain bulk transport and kinetic properties, and "in situ" measurements are used to verify the applicability of an interfacial model. Current-potential and capacitance characteristics can be coupled with measurement of cavity potential differences between bulk phases.

Notation

1. Roman Characters

a	radius of sphere, cm
a_i	relative activity of species i, mol/cm^3
c_i	molar concentration of species i, mol/cm^3
D_i	diffusivity of species i, cm^2/s
E	photon energy, eV
E_f	Fermi energy, eV
E_i	energy of species or site i, eV
ΔE_i	ionic adsorption energy, J/mol
f_i	molar activity coefficient of species i
F	Faraday's constant, 96,487 C/equiv
g_i	degeneracy of energy i, mol/cm^3
G	Gibbs free energy, J
G_{th}	rate of thermal electron-hole pair generation, mol/s-cm^3
G_L	rate of photo electron-hole pair generation, mol/s-cm^3
i	current density, mA/cm^2
i_o	exchange current density, mA/cm^2
k	Boltzmann constant, 1.3805×10^{-23} J/K
$k_{f,l}$	forward reaction rate constant for reaction l
$k_{b,l}$	backward reaction rate constant for reaction l
k_k	rate constants for homogeneous reaction k
K_l	equilibrium constant for reaction l
m	solar absorption coefficient, 1/cm

M_i	symbol for chemical formula of species i
n	number of electrons involved in electrode reaction
n	electron concentration, mol/cm^3
n_i	intrinsic electron concentration, mol/cm^3
N	total site concentration, mol/cm^3
N_a	total bulk electron-acceptor concentration, mol/cm^3
N_d	total bulk electron-donor concentration, mol/cm^3
N_i	flux of species i, mol/cm^{2}s
p	hole concentration, mol/cm^3
$p_{i,l}$	heterogeneous reaction order
P	pressure, bar
$q_{i,l}$	heterogeneous reaction order
q_o	incident solar flux, mol/s-cm^2
r_l	heterogeneous reaction rate, mol/s-cm^2
R	universal gas constant, 8.3143 J/mol-K
R_i	net rate of production of species i, mol/s-cm^3
R_{rec}	net rate of electron-hole recombination, mol/s-cm^3
s_i	stoichiometric coefficient of species i in an electrode reaction
S	entropy, J/K
T	absolute temperature, K
u_i	mobility of species i, cm^{2}mol/Js
V	potential drop across depletion layer, V
W	depletion layer thickness, cm
W_i	probability of occupation of state i

y distance variable, cm

z_i charge number of species i

2. Greek Characters

α "real" chemical potential, J/mol

β symmetry factor

γ_k surface concentration of energy or species k, mol/cm^2

Γ_k total surface-site concentration of energy or species k, mol/cm^2

δ_k distance between interfacial planes (gap denoted by k), cm

ε permittivity, C/V-cm

η photon efficiency

η_k total overpotential at interface k, V

Θ fractional occupation of surface sites

κ conductivity, mho/cm

λ Debye length, cm

μ_i electrochemical potential of species i, J/mol

ρ_{j-k} reflectance associated with interface $j-k$

φ Galvani (inner) electrical potential, V

φ_w work function, V

Φ electrical potential, V

χ surface potential, V

ψ cavity (Volta or outer) potential, V

3. Superscripts

o equilibrium

ϑ	secondary reference state at infinite dilution
*	secondary reference state in semiconductor

4. Subscripts

bulk	associated with the bulk
c	associated with conduction band in semiconductor
CE	associated with the counterelectrode
cell	associated with the cell
e^-	relating to electrons
h^+	relating to holes
ihp	associated with inner Helmholtz plane
iss	associated with inner surface states
k	dummy subscript
l	associated with reaction *l*
o	equilibrium value or initial value
ohp	associated with outer Helmholtz plane
oss	associated with outer surface states
sc	associated with semiconductor
sol	associated with solution
t	associated with trap band in semiconductor
v	associated with valence band in semiconductor
1	associated with the region between the OSS and the ISS
2	associated with the region between the ISS and the IHP
3	associated with the region between the IHP and the OHP

References

[1] Fujishima, Akira, and Kenichi Honda, "Electrochemical Photolysis of Water at a Semiconductor Electrode," *Nature*, *238* (1972), 37-38.

[2] Manassen, J., D. Cahen, and G. Hodes, "Electrochemical, Solid State, Photochemical, and Technological Aspects of Photoelectrochemical Energy Converters," *Nature*, *263* (1976), 97-100.

[3] Bard, Allen J., "Photoelectrochemistry and Heterogeneous Photocatalysis at Semiconductors," *Journal of Photochemistry*, *10* (1979), 59-75.

[4] Ehrenreich, H. and J. H. Martin, "Solar Photovoltaic Energy," *Physics Today*, *32*, 9 (1979), 25-32.

[5] Wrighton, Mark S., "Photoelectrochemical Conversion of Optical Energy to Electricity and Fuels," *Accounts of Chemical Research*, *12* (1979), 303-310.

[6] Gerischer, Heinz, "Heterogeneous Electrochemical Systems for Solar Energy Conversion," *Pure and Applied Chemistry*, *52* (1980), 2649-2667.

[7] Bard, Allen J., "Photoelectrochemistry," *Science*, *207* (1980), 139-144.

[8] Heller, Adam, "Conversion of Sunlight into Electrical Power and Photoassisted Electrolysis of Water in Photoelectrochemical Cells," *Accounts of Chemical Research*, *14* (1981), 154-162.

[9] Green, Mino, "Electrochemistry of the Semiconductor-Electrolyte Interface," Chapter 5 in *Modern Aspects of Electrochemistry*, Volume 2, J. O'M Bockris, editor, Academic Press Inc., New York, 1959.

[10] Gerischer, Heinz, "Semiconductor Electrode Reactions," Chapter 4 in *Advances in Electrochemistry and Electrochemical Engineering*, Volume 1, Paul Delahay, editor, Interscience Publishers, New York, 1961.

[11] Archer, M.D., "Electrochemical Aspects of Solar Energy Conversion," *Journal of Applied Electrochemistry*, *5* (1975), 17-38.

[12] Rajeshwar, K., P. Singh, and J. DuBow, "Energy Conversion in Photoelectrochemical Systems: A review," *Electrochimica Acta*, *23* (1975), 1117-1144.

[13] Harris, L. A., and R. H. Wilson, "Semiconductors for Photoelectrolysis," *Annual Reviews in Materials Science*, *8* (1978), 99-134.

[14] Nozik, Arthur, J., "Photoelectrochemistry: Applications to Solar Energy Conversion," *Annual Reviews in Physical Chemistry*, *29* (1978), 189-222.

[15] Tomkiewicz, M., and H. Fay, "Photoelectrolysis of Water with Semiconductors," *Applied Physics*, *18* (1979), 1-28.

[16] Wilson, R.H., "Electron Transfer Processes at the Semiconductor-

Electrolyte Interface," *CRC Critical Reviews in Solid State and Materials Science*, (1980), 1-41.

[17] Memming, R., "Solar Energy Conversion by Photoelectrochemical Processes," *Electrochimica Acta*, *25* (1980), 77-88.

[18] Morrison, S. Roy, *Electrochemistry at Semiconductor and Oxidized Metal Electrodes*, Plenum Press, New York, 1980.

[19] Khan, Shahed U. M., and John O'M. Bockris, "Photoelectrochemical Kinetics and Related Devices," Chapter 3 in *Modern Aspects of Electrochemistry*, Volume 14, J. O'M. Bockris, B. E. Conway, and R. E. White, editors, Plenum Press, New York, 1982.

[20] Grove, A. S., *Physics and Technology of Semiconductor Devices*, John Wiley and Sons, New York, 1967.

[21] Sze, S. M., *Physics of Semiconductor Devices*, Wiley-Interscience, New York, 1969.

[22] Hovel, Harold J., "Solar Cells," Volume 11 of *Semiconductors and Semimetals*, R. K. Willardson and Albert C. Beer, editors, Academic Press, New York, 1975.

[23] Wagner, Sigurd, "Physico-Chemical Problems in Photovoltaic Research," *Berichte der Bunsengesellschaft fur Physikalische Chemie*, *84* (1980), 991-995.

[24] Hovel, Harold J., "Photovoltaic Materials and Devices for Terrestrial Solar Energy Applications," *Solar Energy Materials*, *2* (1980), 277-312.

[25] Russak, Michael A., Joseph Reichman, Horst Witzke, S. K. Deb, and S. N. Chen, "Thin Film CdSe Photoanodes for Electrochemical Photovoltaic Solar Cells," *Journal of the Electrochemical Society*, *127* (1980), 725-733.

[26] Kazacos, M. Skyllas, and B. Miller, "Electrodeposition of CdSe Films from Selenosulfite Solution," *Journal of the Electrochemical Society*, *127* (1980), 2378-2381.

[27] Liu, Chin-Hsin J., Judith Olsen, David R. Saunders, and Jui H. Wang, "Photoactivation of CdSe Films for Photoelectrochemical Cells," *Journal of the Electrochemical Society*, *128* (1981), 1224-1228.

[28] Pratt, Dexter R., Margaret E. Langmuir, Robert A. Boudreau, and R. David Rauh, "Chemically Deposited CdSe Thin Films for Photoelectrochemical Cells," *Journal of the Electrochemical Society*, *128* (1981), 1627-1629.

[29] Rajeshwar, K., L. Thompson, P. Singh, R. C. Kainthla, and K. L. Chopra, "Photoelectrochemical Characterization of CdSe Thin Film Anodes," *Journal of the Electrochemical Society*, *128* (1981), 1744-1750.

[30] Reichman, Joseph, and Michael A. Russak, "Properties of CdSe Thin

Films for Photoelectrochemical Cells," *Journal of the Electrochemical Society*, *128* (1981), 2025-2029.

[31] Liu, Chin-Hsin J., and Jui H. Wang, "Spray-Pyrolyzed Thin Film CdSe Photoelectrochemical Cells," *Journal of the Electrochemical Society*, *129* (1982), 719-722.

[32] Reichman, J., and M. A. Russak, "Improved Efficiency of n-CdSe Thin-Film Photoelectrodes by Zinc Surface Treatment," *Journal of Applied Physics*, *53* (1982), 708-711.

[33] Houston, G. J., J. F. McCann, and D. Haneman, "Optimizing the Photoelectrochemical Performance of Electrodeposited CdSe Semiconductor Electrodes," *Journal of Electroanalytical Chemistry*, *134* (1982), 37-47.

[34] Miller, B., A. Heller, M. Robbins, S. Menezes, K. C. Chang, and J. Thomson, Jr., "Solar Conversion Efficiency of Pressure-Sintered Cadmium Selenide Liquid-Junction Cells," *Journal of the Electrochemical Society*, *124* (1977), 1019-1021.

[35] Heller, A., K. C. Chang, and B. Miller, "Spectral Response and Efficiency Relations in Semiconductor Liquid Junction Solar Cells," *Journal of the Electrochemical Society*, *124* (1977), 697-700.

[36] Miller, Barry, and Adam Heller, "Semiconductor Liquid Junction Solar Cells Based on Anodic Sulphide Films," *Nature*, *262* (1976), 680-681.

[37] Peter, L. M., "The Photoelectrochemical Properties of Anodic Cadmium Sulphide Films," *Electrochimica Acta*, *23* (1978), 1073-1080.

[38] Tsou, C. C., and J. R. Cleveland, "Polycrystalline Thin-Film CdSe Liquid Junction Photovoltaic Cell," *Journal of Applied Physics*, *51* (1980), 455-458.

[39] Heller, A., B. Miller, Shirley S. Chu, and Y. T. Lee, "7.3% Efficient Thin-Film, Polycrystalline n-GaAs Semiconductor Liquid Junction Solar Cell," *Journal of the American Chemical Society*, *101* (1979), 7633-7634.

[40] Johnston, Jr., W. D., H. J. Leamy, B. A. Parkinson, A. Heller, and B. Miller, "Effect of Ruthenium Ions on Grain Boundaries in Gallium Arsenide Thin Film Photovoltaic Devices," *Journal of the Electrochemical Society*, *127* (1980), 90-95.

[41] Noufi, Rommel, and Dennis Tench, "High Efficiency GaAs Photoanodes," *Journal of the Electrochemical Society*, *127* (1980), 188-190.

[42] Heller, Adam, and B. Miller, "Photoelectrochemical Solar Cells: Chemistry of the Semiconductor-Liquid Junction," Chapter 12 in *Interfacial Photoprocesses: Energy Conversion and Synthesis, Advances in Chemistry Series*, *184*, Mark S. Wrighton, editor, American Chemical Society, Washington D. C., 1980.

[43] Parkinson, B. A., A. Heller, and B. Miller, "Enhanced Photoelectrochemical Solar-Energy Conversion by Gallium-Arsenide Surface

Modification," *Applied Physics Letters*, *33* (1978), 521-523.

[44] Gerischer, H., "On the Stability of Semiconductor Electrodes Against Photodecomposition," *Journal of Electroanalytical Chemistry*, *82* (1977), 133-143.

[45] Gerischer, Heinz, "Photoelectrochemical Solar Cells," in *Proceedings of the 2nd Electrochemical Photovoltaic Solar Energy Conference*, R. van Overstraeten and W. Palz, editors, D. Reidel, Boston, 1979, 408-431.

[46] Gartner, Wolfgang W., "Depletion-Layer Photoeffects in Semiconductors," *Physical Review*, *116* (1959), 84-87.

[47] Butler, M. A., "Photoelectrolysis and Physical Properties of the Semiconducting Electrode WO_3," *Journal of Applied Physics*, *48* (1977), 1914-1920.

[48] Kautek, W., H. Gerischer, and H. Tributsch, "The Role of Carrier Diffusion and Indirect Optical Transitions in the Photoelectrochemical Behavior of Layer Type d-Band Semiconductors," *Journal of the Electrochemical Society*, *127* (1980), 2471-2478.

[49] Williams, Larry McClease, *Structural and Photoelectrochemical Properties of Plasma Deposited Titanium Dioxide*, PhD thesis, University of California, Berkeley, December, 1982 (LBL-14994).

[50] Wilson, Ronald H., "A Model for the Current-Voltage Curve of Photoexcited Semiconductor Electrodes," *Journal of Applied Physics*, *48* (1977), 4292-4297.

[51] Wilson, Ronald H., "A Model for the Current-Voltage Curve of Photoexcited Semiconductor Electrodes," *Semiconductor Liquid-Junction Solar Cells*, Adam Heller, editor, The Electrochemical Society, Princeton, N.J., 1977.

[52] Albery, W. John, Phillip N. Bartlett, Andrew Hamnett, and Martin P. Dare-Edwards, "The Transport and Kinetics of Minority Carriers in Illuminated Semiconductor Electrodes," *Journal of the Electrochemical Society*, *128* (1981), 1492-1501.

[53] Reichman, J., "The Current-Voltage Characteristics of Semiconductor-Electrolyte Junction Photovoltaic Cells," *Applied Physics Letters*, *36* (1980), 574-577.

[54] Reichman, J., "Collection Efficiency of Low-Mobility Solar Cells," *Applied Physics Letters*, *38* (1981), 251-253.

[55] Reiss, Howard, "Photocharacteristics for Electrolyte-Semiconductor Junctions," *Journal of the Electrochemical Society*, *125* (1978), 937-949.

[56] Ahlgren, William L., "Analysis of the Current-Voltage Characteristics of Photoelectrolysis Cells," *Journal of the Electrochemical Society*, *128* (1981), 2123-2128.

[57] McCann, J. F., and D. Haneman, "Recombination Effects on Current-Voltage Characteristics of Illuminated Surface Barrier Cells," *Journal of the Electrochemical Society*, *129* (1982), 1134-1145.

[58] McCann, J. F., S. Hinckley, and D. Haneman, "An Analysis of the Current-Voltage Characteristics of Thin-Film Front Wall Illuminated and Back Wall Illuminated Liquid Junction and Schottky Barrier Solar Cells," *Journal of Electroanalytical Chemistry*, *137* (1982), 17-37.

[59] Heusler, K. E., and M. Schulze, "Electron-Transfer Reactions at Semiconducting Anodic Niobium Oxide Films," *Electrochimica Acta*, *20* (1975), 237-244.

[60] Williams, Fred, and A. J. Nozik, "Irreversibilities in the Mechanism of Photoelectrolysis," *Nature*, *271* (1978), 137-139.

[61] Ahmed, Syed M., and H. Gerischer, "Influence of Crystal Surface Orientation on Redox Reactions at Semiconducting MoS_2," *Electrochimica Acta*, *24* (1979), 705-711.

[62] Aruchamy, A., and Mark S. Wrighton, "A Comparison of the Interface Energetics for n-Type Cadmium Sulfide- and Cadmium Telluride-Nonaqueous Electrolyte Junctions," *Journal of Physical Chemistry*, *84* (1980), 2848-2854.

[63] Bard, Allen J., Andrew B. Bocarsly, Fu-Ren F. Fan, Erick G. Walton, and Mark S. Wrighton, "The Concept of Fermi Level Pinning at Semiconductor-Liquid Junctions. Consequences for Energy Conversion Efficiency and Selection of Useful Solution Redox Couples in Solar Devices," *Journal of the American Chemical Society*, *102* (1980), 3671-3677.

[64] Fan, Fu-Ren F., and Allen J. Bard, "Semiconductor Electrodes. 24. Behavior and Photoelectrochemical Cells Based on p-Type GaAs in Aqueous Solutions," *Journal of the American Chemical Society*, *102* (1980), 3677-3683.

[65] Bocarsly, Andrew B., Dana C. Bookbinder, Raymond N. Dominey, Nathan S. Lewis, and Mark S. Wrighton, "Photoreduction at Illuminated p-Type Semiconducting Silicon Photoelectrodes. Evidence for Fermi Level Pinning," *Journal of the American Chemical Society*, *102* (1980), 3683-3688.

[66] Garrett, C. G. B., and W. H. Brattain, "Physical Theory of Semiconductor Surfaces," *Physical Review*, *99* (1955), 376-387.

[67] Johnson, E. O., "Large-Signal Surface Photovoltage Studies with Germanium," *Physical Review*, *111* (1958), 153-166.

[68] Many, A., Y. Goldstein, and N. B. Grover, *Semiconductor Surfaces*, North-Holland Publishing Co., Amsterdam, 1965.

[69] Gerischer, Heinz, "Semiconductor Electrochemistry," chapter 5 in *Physical Chemistry: An Advanced Treatise*, Volume IX, H. Eyring, editor, Academic Press, New York, 1970.

[70] Morrison, S. R., *The Chemical Physics of Surfaces*, Plenum Press, New

York, 1977.

[71] Bockris, J. O'M., and K. Uosaki, "The Theory of the Light-Induced Evolution of Hydrogen at Semiconductor Electrodes," *Journal of the Electrochemical Society*, *125* (1978), 223-227.

[72] Memming, R., "The Role of Energy Levels in Semiconductor-Electrolyte Solar Cells," *Journal of the electrochemical Society*, *125* (1978), 117-123.

[73] Memming, R., "Charge Transfer Processes at Semiconductor Electrodes," in *Electroanalytical Chemistry*, Allen J. Bard, editor, Marcel Dekker, Inc., New York, 1981, 1-84.

[74] Frese, Jr., Karl W., "A Study of Rearrangement Energies of Redox Species," *Journal of Physical Chemistry*, *85* (1981), 3911-3916.

[75] Kautek, W., and H. Gerischer, "A Kinetic Derivation of the Photovoltage for Electrochemical Solar Cells Employing Small-Band-Gap Semiconductors," *Electrochimica Acta*, *27* (1982) 355-358.

[76] Rajeshwar, K., "Charge Transfer in Photoelectrochemical Devices via Interface States: Unified Model and Comparison with Experimental Data," *Journal of the Electrochemical Society*, *129* (1982), 1003-1008.

[77] Chazalviel, J.-N., "Electrochemical Transfer via Surface States: A New Formulation for the Semiconductor-Electrolyte Interface," *Journal of the Electrochemical Society*, *129* (1982) 963-969.

[78] Singh, P., K. Rajeshwar, R. Singh, and J. DuBow, "Estimation of Series Resistance Losses and Ideal Fill Factors for Photoelectrochemical Cells," *Journal of the Electrochemical Society*, *128* (1981), 1396-1398.

[79] McCann, J. F., S. P. S. Badwal, and J. Pezy, "The Electrical Analogue of an n-SnO_2-1M NaOH-Pt Cell," *Journal of Electroanalytical Chemistry*, *118* (1981), 115-130.

[80] McCann, J. F., and S. P. S. Badwal, "Equivalent Circuit Analysis of the Impedance Response of Semiconductor-Electrolyte-Counterelectrode Cells," *Journal of the Electrochemical Society*, *129* (1982), 551-559.

[81] Macdonald, J. Ross, "Accurate Solution of an Idealized One-Carrier Metal-Semiconductor Junction Problem," *Solid-State Electronics*, *5* (1962), 11-37.

[82] De Mari, A., "An Accurate Numerical Steady-State One-Dimensional Solution of the p-n Junction," *Solid-State Electronics*, *11* (1968), 33-58.

[83] De Mari, A., "An Accurate Numerical Steady-State One-Dimensional Solution of the p-n Junction under Arbitrary Transient Conditions," *Solid-State Electronics*, *11* (1968), 1021-1053.

[84] Choo, Seok Cheow, "Numerical Analysis of a Forward-Biased Step-Junction p-i-n Diode," *IEEE Transactions on Electron Devices*, *ED-18* (1971),

574-586.

[85] Choo, Seok Cheow, "Theory of a Forward-Biased Diffused-Junction p-l-n Rectifier-Part 1: Exact Numerical Solution," *IEEE Transactions on Electron Devices, ED-19* (1972), 954-966.

[86] Sutherland, J. E., and J. R. Hauser, "A Computer Analysis of Heterojunction and Graded Composition Solar Cells," *IEEE Transactions on Electron Devices, ED-24* (1977), 363-372.

[87] Laser, Daniel, and Allen J. Bard, "Semiconductor Electrodes: VII. Digital Simulation of Charge Injection and the Establishment of the Space Charge Region in the Absence and Presence of Surface States," *Journal of the Electrochemical Society, 123* (1976), 1828-1832.

[88] Laser, Daniel, and Allen J. Bard, "Semiconductor Electrodes: VIII. Digital Simulation of Open-Circuit Photopotentials," *Journal of the Electrochemical Society, 123* (1976), 1833-1837.

[89] Laser, Daniel, and Allen J. Bard, "Semiconductor Electrodes: IX. Digital Simulation of the Relaxation of Photogenerated Free Carriers and Photocurrents," *Journal of the Electrochemical Society, 123* (1976), 1837-1842.

[90] Laser, Daniel, "Modes of Charge Transfer at an Illuminated Semiconductor Electrode: a Digital Simulation," *Journal of the Electrochemical Society, 126* (1979), 1011-1014.

[91] Leary, D. J., J. O. Barnes, and A. G. Jordan, "Calculation of Carrier Concentration in Polycrystalline Films as a Function of Surface Acceptor State Density: Application for ZnO Gas Sensors," *Journal of the Electrochemical Society, 129* (1982), 1382-1386.

[92] Davis, James A., Robert O. James, and James O. Leckie, "Surface Ionization and Complexation at the Oxide-Water Interface: I. Computation of Electrical Double Layer Properties in Simple Electrolytes," *Journal of Colloid and Interface Science, 63* (1978), 480-499.

[93] Davis, James A., and James O. Leckie, "Surface Ionization and Complexation at the Oxide-Water Interface: II. Surface Properties of Amorphous Iron Oxyhydroxide and Adsorption of Metal Ions," *Journal of Colloid and Interface Science, 67* (1978), 91-107.

[94] Davis, James A., and James O. Leckie, "Surface Ionization and Complexation at the Oxide-Water Interface: 3. Adsorption of Ions," *Journal of Colloid and Interface Science, 74* (1980), 32-43.

[95] Grahame, David C., "The Electrical Double Layer and the Theory of Electrocapillarity," *Chemical Reviews, 41* (1947), 441-501.

[96] Dewald, J. F., "Semiconductor Electrodes," Chapter 17 in *Semiconductors*, N. B. Hannay, editor, Reinhold Publishing Corporation, New York, 1959.

[97] Sparnaay, Marcus Johannes, *The Electrical Double Layer*, Pergamon Press, New York, 1972.

[98] Parsons, Roger, "Equilibrium Properties of Electrified Interphases," Chapter 3 in *Modern Aspects of Electrochemistry*, Volume 1, John O'M Bockris, editor, Academic Press, New York, 1954, 103-179.

[99] Newman, John, *Electrochemical Systems*, Prentice-Hall, Inc., Englewood Cliffs, New Jersey, 1973.

[100] Moll, John L., *Physics of Semiconductors*, McGraw-Hill Book Company, New York, 1964.

[101] Smith, R. A., *Semiconductors*, Cambridge University Press, London, 1959.

[102] Delahay, Paul, *Double Layer and Electrode Kinetics*, Interscience Publishers, New York, 1965.

[103] Orazem, Mark E., and John Newman, "Theoretical Analysis of Liquid-Junction Photovoltaic Cells," 159th meeting of *the Electrochemical Society*, Minneapolis, Minnesota, May 14, 1981.

[104] Newman, John, "Numerical Solution of Coupled, Ordinary Differential Equations," *Industrial and Engineering Chemistry Fundamentals*, *7* (1968), 514-517.

[105] Chang, K. C., A. Heller, B. Schwartz, S. Menezes, and B. Miller, "Stable Semiconductor Liquid-Junction Cell with 9% Solar to Electrical Conversion Efficiency," *Science*, *196* (1977), 1097-1098.

[106] Ellis, Arthur B., Jeffrey M. Bolts, Steven W. Kaiser, and Mark S. Wrighton, "Study of n-Type Gallium Arsenide- and Gallium Phosphide-Based Photoelectrochemical Cells. Stabilization by Kinetic Control and Conversion of Optical Energy to Electricity," *Journal of the American Chemical Society*, *99* (1977), 2848-2854.

[107] Wrighton, Mark S., Jeffrey M. Bolts, Andrew B. Bocarsly, Michael C. Palazzotto, and Erick G. Walton, "Stabilization of n-Type Semiconductors to Photoanodic Dissolution: II-VI and III-V Compound Semiconductors and Recent Results for n-Type Silicon," *Journal of Vacuum Science Technology*, *15* (1978), 1429-1435.

[108] Nakato, Yoshihiro, Nobuyuki Takamori, and Hiroshi Tsubomura, "A Composite Semiconductor Photoanode for Water Electrolysis," *Nature*, *295* (1982), 312-313.

[109] Gissler, W., P. L. Lensi, and S. Pizzini, "Electrochemical Investigation of an Illuminated TiO_2 Electrode," *Journal of Applied Electrochemistry*, *6* (1976), 9-13.

[110] Kung, H. H., H. S. Jarrett, A. W. Sleight, and A. Ferretti, "Semiconducting Oxide Anodes in Photoassisted Electrolysis of Water,"

Journal of Applied Physics, *48* (1977), 2463-2469.

[111] Belloni, Jacqueline, Genevieve Van Amerongen, Michel Herlem, Jean-Lou Sculfort, and Rudolf Heindl, "Photocurrents from Semiconductor-Liquid Ammonia Junctions," *Journal of Physical Chemistry*, *84* (1980), 1269-1270.

[112] Dare-Edwards, M. P., A. Hamnett, and J. B. Goodenough, "The Efficiency of Photogeneration of Hydrogen at P-Type III/V Semiconductors," *Journal of Electroanalytical Chemistry*, *119* (1981) 109-123.

[113] Butler, M. A., R. D. Nasby, and Rod K. Quinn, "Tungsten Trioxide as an electrode for Photoelectrolysis of Water," *Solid State Communications*, *19* (1976), 1011-1014.

[114] Ellis, Arthur B., Steven W. Kaiser, and Mark S. Wrighton, "Semiconducting Potassium Tantalate Electrodes. Photoassistance Agents for the Efficient Electrolysis of Water," *Journal of Physical Chemistry*, *80* (1976), 1325-1328.

[115] Memming, R., "A Rotating Platinum-Semiconductor Ring-Disc Electrode for Analysis of Photoelectrochemical Processes," *Berichte der Bunsengesellschaft fur Physikalische Chemie*, *81* (1977), 732-735.

[116] Gerischer, H. and J. Gobrecht, "On the Power-Characteristics of Electrochemical Solar Cells," *Berichte der Bunsengesellschaft fur Physikalische Chemie*, *80* (1976), 327-330.

[117] Vanden Berghe, R. A. L., W. P. Gomes, and F. Cardon, "Some Aspects of the Anodic Behavior of CdS Single Crystals in Indifferent Electrolyte Solutions," *Berichte der Bunsengesellschaft fur Physikalische Chemie*, *77* (1973), 289-293.

[118] Oman, Henry, and Joseph W. Gelzer, "Solar Cells and Arrays," in *Energy Technology Handbook*, Douglas M. Considine, editor, McGraw Hill, New York, 1977, 6.56-6.80.

[119] Loferski, Joseph J., "Theoretical Considerations Governing the Choice of the Optimum Semiconductor for Photovoltaic Solar Energy Conversion," *Journal of Applied Physics*, *27* (1956), 777-784.

[120] Loferski, Joseph J., "Recent Research on Photovoltaic Solar Energy Converters," *Proceedings of the IEEE*, (1963) 667-674.

[121] Wysocki, J. J., "Photon Spectrum Outside the Earth's Atmosphere," *Solar Energy*, *6* (1962) 104.

[122] Wolf, M., "Limitations and Possibilities for Improvement of Photovoltaic Solar Energy Converters, Part I: Considerations for Earth's Surface Operation," *Proceedings of the IRE*, *48* (1960), 1246-1263.

[123] Shockley, William, and Hans J. Queisser, "Detailed Balance Limit of Efficiency of p-n Junction Solar Cells," *Journal of Applied Physics*, *32* (1961), 510-519.

[124] Heller, Adam, Barry Miller, and F. A. Thiel, "11.5 % Solar Conversion Efficiency in the Photocathodically Protected p-InP/V^{3+}-V^{2+}-HCl Semiconductor Liquid-Junction Cell," *Applied Physics Letters*, *38* (1981), 282-284.

[125] Menezes, S., A. Heller, and B. Miller, "Metal Filmed-Semiconductor Photoelectrochemical Cells," *Journal of the Electrochemical Society*, *127* (1980), 1268-1273.

[126] Frese, K. W., Jr., M. J. Madou, and S. R. Morrison, "Investigation of Photoelectrochemical Corrosion of Semiconductors: III. Effects of Metal Layers on the Stability of GaAs," *Journal of the Electrochemical Society*, *128* (1981), 1939-1943.

[127] Noufi, Rommel, Dennis Tench, and Leslie F. Warren, "Protection of n-GaAs Photoanodes with Photoelectrochemically Generated Polypyrrole Films," *Journal of the Electrochemical Society*, *127* (1980), 2310-2311.

[128] Noufi, Rommel, Dennis Tench, and Leslie F. Warren, "Protection of Semiconductor Photoanodes with Photoelectrochemically Generated Polypyrrole Films," *Journal of the Electrochemical Society*, *128* (1981), 2596-2599.

[129] Skotheim, Terje, Ingemar Lundstrom, and Jiri Prejza, "Stabilization of n-Si Photoanodes to Surface Corrosion in Aqueous Electrolyte with a Thin Film of Polypyrrole," *Journal of the Electrochemical Society*, *128* (1981), 1625-1626.

[130] Fan. Fu-Ren F., Bob L. Wheeler, Allen J. Bard, and Rommel N. Noufi, "Semiconductor Electrodes XXXIX. Techniques for Stabilization of n-Silicon Electrodes in Aqueous Solution Photoelectrochemical Cells," *Journal of the Electrochemical Society*, *128* (1981), 2042-2045.

[131] Bull, Randy A., Fu-Ren F. Fan, Allen J. Bard, "Polymer Films on Electrodes VII. Electrochemical Behavior at Polypyrrole-Coated Platinum and Tantalum Electrodes," *Journal of the Electrochemical Society*, *129* (1982), 1009-1015.

[132] Skotheim, Terje, L.-G. Petersson, O. Inganas, and Ingemar Lundstrom, "Photoelectrochemical Behavior of n-Si Electrodes Protected with Pt-Polypyrrole," *Journal of the Electrochemical Society*, *129* (1982), 1737-1741.

[133] White, Henry S., Hector D. Abruna, and Allen J. Bard, "Semiconductor Electrodes XLI. Improvement of Performance of n-WSe_2 Electrodes by Electrochemical Polymerization of o-Phenylenediamine at Surface Imperfections," *Journal of the Electrochemical Society*, *129* (1982), 265-271.

[134] Iles, P. A., "Evolution of Silicon Solar Cell Design," *9th IEEE Photovoltaic Specialists Conference*, Silver Springs, MD, 1972, 1-5.

[135] Parkinson, Bruce, "An Evaluation of Various Configurations for Photoelectrochemical Photovoltaic Solar Cells," *Solar Cells*, *6* (1982), 177-189.

[136] Mitchell, Kim W., "Status of New Thin-Film Photovoltaic Technologies," *Annual Reviews in Materials Science*, *12* (1982), 401-415.

[137] Fleck, R. N., D. N. Hanson, and C. W. Tobias, "Numerical Evaluation of Current Distribution in Electrochemical Systems," *Lawrence Berkeley Laboratory Report*, UCRL-11612, 1964.

[138] Kasper, Charles, "The Theory of the Potential and the Technical Practice of Electrodeposition: I. The General Problem and the Cases of Uniform Flow," *Transactions of the Electrochemical Society*, *77* (1940), 353-363.

[139] Kasper, Charles, "The Theory of the Potential and the Technical Practice of Electrodeposition: II. Point-Plane and Line-Plane Systems," *Transactions of the Electrochemical Society*, *77* (1940), 365-384.

[140] Kasper, Charles, "The Theory of the Potential and the Technical Practice of Electrodeposition: III. Linear Polarization on Some Line-Plane Systems," *Transactions of the Electrochemical Society*, *78* (1940), 131-146.

[141] Kasper, Charles, "The Theory of the Potential and the Technical Practice of Electrodeposition: IV. The Flow Between and to Circular Cylinders," *Transactions of the Electrochemical Society*, *78* (1940), 147-161.

[142] Kasper, Charles, "The Theory of the Potential and the Technical Practice of Electrodeposition: V. The Two-Dimensional Rectangular Enclosures," *Transactions of the Electrochemical Society*, *82* (1942), 153-185.

[143] Moulton, H. Fletcher, "Current Flow in Rectangular Conductors," *Proceedings of the London Mathematical Society (Ser. 2)*, *3* (1905), 104-110.

[144] Bowman, F., *Introduction to Elliptic Functions with Applications*, John Wiley and Sons, Inc., New York, 1953.

[145] Churchill, Ruel V., *Complex Variables and Applications*, 2nd edition, McGraw-Hill Book Company, New York, 1960.

[146] Copson, E. T., *An Introduction to the Theory of Functions of a Complex Variable*, Oxford University Press, London, 1935.

[147] Byrd, Paul F., and Morris D. Friedman, *Handbook of Elliptic Integrals for Engineers and Scientists*, 2nd edition, Springer-Verlag, Berlin, New York, 1971.

[148] Abramowitz, Milton, and Irene A. Stegun, *Handbook of Mathematical Functions*, Dover Publications, Inc., New York, 1964.

[149] Jarzebski, Z. M., and J. P. Marton, "Physical Properties of SnO_2 Materials: I. Preparation and Defect Structure," *Journal of the Electrochemical Society*, *123* (1976), 199C-205C.

[150] Jarzebski, Z. M., and J. P. Marton, "Physical Properties of SnO_2 Materials: II. Electrical Properties," *Journal of the Electrochemical Society*,

123 (1976), 299C-310C.

[151] Jarzebski, Z. M., and J. P. Marton, "Physical Properties of SnO_2 Materials: III. Optical Properties," *Journal of the Electrochemical Society*, *123* (1976), 333C-346C.

[152] Canfield, Duane, and S. Roy Morrison, "Electrochemical Storage Cell Based on Polycrystalline Silicon," *Lawrence Berkeley Laboratory Report*, LBL-14639, 1982.

[153] Weaver, N. L., R. Singh, K. Rajeschwar, P. Singh, and J. DuBow, "Economic Analysis of Photoelectrochemical Cells," *Solar Cells*, *3* (1981), 221-232.

[154] Newman, John, "Resistance for Flow of Current to a Disk," *Journal of the Electrochemical Society*, *113* (1966), 501-502.

[155] Miksis, Joseph J., Jr., and John Newman, "Primary Resistances for Ring-Disk Electrodes," *Journal of the Electrochemical Society*, *123* (1976), 1030-1036.

[156] Pierini, Peter, and John Newman, "Potential Distribution for Disk Electrodes in Axisymmetric Cylindrical Cells," *Journal of the Electrochemical Society*, *126* (1979), 1348-1352.

[157] Hine, Fumio, Shiro Yoshizawa, and Shinzo Okada, "Effect of the Walls of Electrolytic Cells on Current Distribution," *Journal of the Electrochemical Society*, *103* (1956), 186-193.

[158] Wagner, Carl, "Calculation of the Current Distribution at Electrodes involving Slots," *Plating*, *48* (1961), 997-1002.

[159] Newman, John, "The Fundamental Principles of Current Distribution in Electrochemical Cells," in *Electroanalytical Chemistry*, A. J. Bard, editor, volume 6 (1973), 187-352.

[160] Parsons, Roger, "Manual of Symbols and Terminology for Physicochemical Quantities and Units: Appendix III, Electrochemical Nomenclature," *Pure and Applied Chemistry*, *37* (1974), 501-516.

[161] Maxwell, James Clerk, *An Elementary Treatise on Electricity*, 2nd edition, (edited by William Garnett), Oxford University Press, London, 1888.

[162] Guggenheim, E. A., "The Conceptions of Electrical Potential Difference between Two Phases and the Individual Activities of Ions," *The Journal of Physical Chemistry*, *33* (1929), 842-849.

[163] Smyrl, William H., and John Newman, "Potentials of Cells with Liquid Junctions," *The Journal of Physical Chemistry*, *72* (1968), 4660-4671.

[164] Trasatti, Sergio, "The Work Function in Electrochemistry," in *Advances in Electrochemistry and Electrochemical Engineering*, Volume 10, Heinz Gerischer and Charles W. Tobias, editors, John Wiley and Sons, New York,

1977.

[165] Trasatti, Sergio, "The Electrode Potential," Chapter 2 in *Comprehensive Treatise of Electrochemistry, Volume 1: The Double Layer*, John O'M. Bockris, Brian E. Conway, and Ernest Yeager, editors, Plenum Press, New York, 1980.

[166] Bonciocat, N., "Individual Activity Coefficients of Ionic Species from Electrochemical Measurements on Non-Isothermal Systems," 27th meeting of the *International Society of Electrochemistry*, Zurich, Switzerland, September 11, 1976.

[167] Szabo, Z. G., L. Barcza, L. Ladanyi, and I. Ruff, "Single Ion Activity Coefficients in Concentrated Aqueous Hydrochloric Acid Solutions," 27th meeting of the *International Society of Electrochemistry*, Zurich, Switzerland, September 11, 1976.

[168] Struck, Bernd Dieter, "Is it Possible to Approach Individual Ion Activity Coefficients," 27th meeting of the *International Society of Electrochemistry*, Zurich, Switzerland, September 11, 1976.

[169] Taylor, Paul B., "Electromotive Force of the Cell with Transference and Theory of Interdiffusion of Electrolytes," *The Journal of Physical Chemistry*, *31* (1927), 1478-1500.

[170] Maxwell, James Clerk, *A Treatise on Electricity and Magnetism*, Volume 1, Clarendon Press, Oxford, 1892.

[171] Llopis, J., "Surface Potential at Liquid Interfaces," Chapter 2 in *Modern Aspects of Electrochemistry*, Volume 6, J. O'M. Bockris and B. E. Conway, editors, Plenum Press, New York, 1971, 91-153.

[172] Kenrick, Frank B., "Die Potentialsprunge zwischen Gasen und Flussigkeiten," *Zeitschrift fur Physikalische Chemie*, *19* (1896), 625.

[173] Frumkin, A., "Phasengrenzkrafte und Adsorption an der Trennungsflache Luft | Losung anorganischer Elektrolyte," *Zeitschrift fur Physikalische Chemie*, *109* (1924), 34.

[174] Randles, J. E. B., "The Real Hydration Energies of Ions," *Transactions of the Faraday Society*, *52* (1956), 1573.

[175] Bockris, John O'M., and Amulya Reddy, *Modern Electrochemistry*, Volume 2, Plenum Press, New York, 1970.

[176] Herring, Conyers, and M. H. Nichols, "Thermionic Emission," *Reviews of Modern Physics*, *21* (1949), 185-270.

[177] Feuerbacher, B., B. Fitton, and R. F. Willis, "Introduction," Chapter 1 in *Photoemission and the Electronic Properties of Surfaces*, B. Feuerbacher, B. Fitton, and R. F. Willis, editors, John Wiley and Sons, New York, 1978.

[178] Hannay, N. B., "Semiconductor Principles," Chapter 1 in

Semiconductors, N. B. Hannay, editor, Rheinhold Publishing Corporation, New York, 1959.

[178] Kohl, Paul A., and Allen J. Bard, "Semiconductor Electrodes: XVII. Electrochemical Behavior of n- and p-Type InP Electrodes in Acetonitrile Solutions," *Journal of the Electrochemical Society*, *126* (1979), 598-608.

[179] Fan Fu-Ren F., Henry S. White, Bob Wheeler, and Allen J. Bard, "Semiconductor Electrodes: XXIX. High Efficiency Photoelectrochemical Solar Cells with n-WSe_2 Electrodes in an Aqueous Iodide Medium," *Journal of the Electrochemical Society*, *127* (1980), 518-520.

[180] Hirano Katsuhiko, and Allen J. Bard, "Semiconductor Electrodes: XXVIII. Rotating Ring-Disk Electrode Studies of Photo-oxidation of Acetate and Iodide at n-TiO_2," *Journal of the Electrochemical Society*, *127* (1980) 1056-1059.

[181] Wilson, R. H., "Observation and Analysis of Surface States on TiO_2 Electrodes in Aqueous Electrolytes," *Journal of the ELectrochemical Society*, *127* (1980), 228-234.

[182] Levich, Veniamin G., *Physicochemical Hydrodynamics*, Prentice-Hall, Inc., Englewood Cliffs, N. J., 1962.

[183] Riddiford, A. C., "The Rotating Disk System," *Advances in Electrochemistry and Electrochemical Engineering*, Volume 4, Paul Delahay and Charles W. Tobias, editors, John Wiley and Sons, New York, 1966.

[184] Cochran, W. G., "The Flow to a Rotating Disc," *Proceedings of the Cambridge Philosophical Society*, *30* (1934), 365-375.

[185] Gileadi, E., E. Kirowa-Eisner, J. Penciner, *Interfacial Electrochemistry: An Experimental Approach*, Addison-Wesley Publishing Company, Inc., Reading, Massachusetts, 1975.

[186] Haak, R., and D. Tench, "Characterization of II-VI Compounds by Electrochemical Photocapacitance Spectroscopy," 163rd Meeting of the *Electrochemical Society*, San Francisco, California, May 9, 1983.

[187] Haak, R., and D. Tench, "Characterization of GaAs by Electrochemical Photocapacitance Spectroscopy," 163rd Meeting of the *Electrochemical Society*, San Francisco, California, May 9, 1983.

[188] Mott, N. F., "The Theory of Crystal Rectifiers," *Proceedings of the Royal Society (London), Series A*, *171* (1939), 27-38.

[189] Schottky, W., "Zur Halbleitertheorie der Sperrschicht und Spitzengleichrichter," *Zeitschrift fur Physik*, *113* (1939), 367-414, and "Vereinfachte und erweiterte Theorie der Randschicht-gleichrichter," *Zeitschrift fur Physik*, *118* (1942), 539-592.

[190] Cardon, F., and W. P. Gomes, "On the Determination of the Flat-Band Potential of a Semiconductor in Contact with a Metal or an Electrolyte from

the Mott-Schottky Plot," *Journal of Physics, D: Applied Physics, 11* (1978), L63-L67.

[191] Horowitz, G., "Flatband Potential of a p-Type Phosphide Electrode," *Journal of Applied Physics, 49* (1978), 3571-3573.

[192] Pleskov, Yu. V., "Electric Double Layer on Semiconductor Electrodes," Chapter 6 in *Comprehensive Treatise of Electrochemistry, Volume 1: The Double Layer*, John O'M. Bockris, Brian E. Conway, and Ernest Yeager, editors, Plenum Press, New York, 1980.

[193] Ioffe, A. F., *Physics of Semiconductors*, Academic Press Inc., New York, 1960.

[194] Miller, G. L., D. A. H. Robinson, and S. D. Ferris, "Non-Destructive Electrical Test Methods for Semiconductor Materials," in *Semiconductor Characterization Techniques*, Peter A. Barnes and George A. Rozgonyi, editors, The Electrochemical Society, Princeton, N. J., 1978, 1-31.

[195] Hannay, N. B., "Semiconductor Principles," Chapter 1 in *Semiconductors*, N. B. Hannay, editor, Rheinhold Publishing Corporation, New York, 1959.

[196] Hall, E. H., "On a New Action of the Magnet on Electric Currents," *American Journal of Mathematics, 2* (1879), November, 287-291.

[197] Omar, M. Ali, *Elementary Solid State Physics: Principles and Applications*, Addison-Wesley Publishing Company, Menlo Park, California, 1975.

[198] Larrabee, R. D., "Interpretation of Hall Measurements," in *Semiconductor Characterization Techniques*, Peter A. Barnes and George A. Rozgonyi, editors, The Electrochemical Society, Princeton, N. J., 1978, 71-80.

[199] Shulman, R. G., "Recombination and Trapping," Chapter 11 in *Semiconductors*, N. B. Hannay, editor, Rheinhold Publishing Corporation, New York, 1959.

[200] Sommerfeld, Arnold, *Electrodynamics*, translated by Edward G. Ramberg, Academic Press Inc., Publishers, New York, 1952.

[201] Hrostowski, H. J., "Infrared Absorption of Semiconductors," Chapter 10 in *Semiconductors*, N. B. Hannay, editor, Rheinhold Publishing Corporation, New York, 1959.

[202] Chang, C. C., "Electronics Materials Evaluation Using Auger Electron Spectroscopy and Other Supportive Analytical Techniques," in *Semiconductor Characterization Techniques*, Peter A. Barnes and George A. Rozgonyi, editors, The Electrochemical Society, Princeton, N. J., 1978, 106-135.

[203] Many, A., Y. Goldstein, and N. B. Grover, *Semiconductor Surfaces*, Interscience Publishers, New York, 1965.

[204] Skoog, Douglas A., and Donald M. West, *Fundamentals of Analytical Chemistry*, 2nd edition, Holt, Rinehart, and Winston, Inc., New York, 1969.

[205] Taras, M. J., "*Standard Methods for the Examination of Water and Wastewater*," 13th edition, American Public Health Association, Washington, D. C., 1971.

[206] Bird, R Byron, Warren E. Stewart, and Edwin N. Lightfoot, *Transport Phenomena*, John Wiley and Sons, New York, 1960.

[207] Reid, Robert C., John M. Prausnitz, and Thomas K. Sherwood, *The Properties of Gases and Liquids*, 3rd edition, McGraw-Hill Book Company, New York, 1977.

[208] White, Ralph Edward, *Simultaneous Reactions on a Rotating-Disk Electrode*, PhD thesis, University of California, Berkeley, March 1977 (LBL-6094).

[209] White, Ralph, Charles M. Mohr, Jr., Peter Fedkiw, and John Newman, "The Fluid Motion Generated by a Rotating Disk: A Comparison of Solution Techniques," *Lawrence Berkeley Laboratory Report*, LBL-3910, November 1975.

Appendix A. Application of Maxwell's Equations to Electrochemical Systems

The electromagnetic principles presented by Maxwell[170,200] are a foundation for the characterization of electrical systems. The object of this section is to present the relationship between Maxwell's equations and the macroscopic transport equations used in electrochemical systems analysis.[99] The relationships among the complex permittivity, the complex index of refraction, and the permeability used in Poisson's equation will also be presented.

1. Macroscopic Transport Equations

Maxwell's equations are used here as a starting point. In differential form,

$$\nabla \cdot E = \frac{\rho}{\varepsilon}, \tag{A-1}$$

$$\nabla \cdot B = 0, \tag{A-2}$$

$$\nabla \times E = -\frac{\partial B}{\partial t}, \tag{A-3}$$

and

$$\nabla \times B = \mu i + \mu\varepsilon \frac{\partial E}{\partial t}, \tag{A-4}$$

where E is the electric field (related to the electric potential by $E = -\nabla\Phi$), ρ is the charge density, ε is the permittivity (defined by $D = \varepsilon E$ where D is the displacement vector), B is the magnetic field, μ is the permeability, and i is the electrical current density. The magnetic pole density was assumed to be zero.

Equation (A-1) is Poisson's equation, which is used directly in the macroscopic development. Under the assumption that the permittivity and

the permeability are constant, the divergence of equation (A-4) yields

$$\nabla\cdot(\nabla\times B) = \mu\nabla\cdot i + \mu\varepsilon\,\frac{\partial}{\partial t}(\nabla\cdot E)\,, \tag{A-5}$$

which may be rewritten as

$$0 = F\sum_i z_i(\nabla\cdot N_i + \frac{\partial c_i}{\partial t})\,, \tag{A-6}$$

where the electric current was expressed in terms of the individual ionic fluxes N_i as

$$i = F\sum_i z_i N_i\,, \tag{A-7}$$

and the charge density was introduced from equation (A-1) in terms of individual ion concentrations as

$$\rho = F\sum_i z_i c_i\,. \tag{A-8}$$

A material balance for a species i yields

$$\nabla\cdot N_i + \frac{\partial c_i}{\partial t} = R_i\,. \tag{A-9}$$

where R_i is the homogeneous generation term for species i. Conservation of charge provides that $\sum_i z_i R_i = 0$; thus equation (A-6) follows from multiplying equation (A-9) by z_i and summing over all species i. The development presented above does not involve assumptions concerning the magnetic field. In the presence of a magnetic field, macroscopic equations may be used in conjunction with equations (A-2) and (A-3).

Macroscopic transport equations are therefore consistent with Maxwell's equations. Equations (A-1) and (A-9) are used frequently in the macroscopic analysis of electrochemical systems. The total flux of a species i in a dilute solution is given[99] in terms of migrational, diffusional, and convective contributions by

$$N_i = - z_i u_i F c_i \nabla\Phi - D_i \nabla c_i + c_i v \ , \qquad \text{(A-10)}$$

where v is the bulk phase velocity.

2. Complex Permittivity

The curl of equation (A-3) yields

$$\nabla\times(\nabla\times E) = - \nabla\times(\frac{\partial B}{\partial t}) \ , \qquad \text{(A-11a)}$$

or

$$\nabla(\nabla\cdot E) - \nabla^2 E = - \frac{\partial}{\partial t}(\nabla\times B) \ . \qquad \text{(A-11b)}$$

The time derivative of equation (A-4) is

$$\frac{\partial}{\partial t}(\nabla\times B) = \mu \frac{\partial i}{\partial t} + \mu\varepsilon \frac{\partial^2 E}{\partial t^2} \ . \qquad \text{(A-12)}$$

Equations (A-11b) and (A-12) can be combined to eliminate the magnetic field B;

$$\nabla(\nabla\cdot E) - \nabla^2 E = - \mu \frac{\partial i}{\partial t} - \mu\varepsilon \frac{\partial^2 E}{\partial t^2} \ . \qquad \text{(A-13)}$$

In the absence of concentration gradients and with $\rho = 0$, the electric current is related to the electric field by the conductivity, i.e.,

$$i = \sigma E \ , \qquad \text{(A-14)}$$

thus equation (A-13) becomes

$$\nabla^2 E = \mu\sigma \frac{\partial E}{\partial t} + \mu\varepsilon \frac{\partial^2 E}{\partial t^2} \ . \qquad \text{(A-15)}$$

A general form for the electric field associated with electromagnetic radiation is

$$E = E_m e^{j\omega t} \ , \qquad \text{(A-16)}$$

where E_m is the maximum value of the electric field, j is $\sqrt{-1}$, and ω is the angular frequency associated with the radiation. Introduction of equation (A-16) into equation (A-15) yields

$$\nabla^2 E_m = -\mu\omega^2(\varepsilon - \frac{j\sigma}{\omega})E_m \,. \tag{A-17}$$

It is convenient to define a complex permittivity ε' such that

$$\varepsilon' = \varepsilon - \frac{j\sigma}{\omega} \,. \tag{A-18}$$

The imaginary term disappears in vacuum ($\sigma = 0$), and the right hand term of equation (A-17) becomes zero in a stationary electric field ($\omega = 0$).

3. Complex Index of Refraction

The velocity of the electromagnetic radiation is a constant given by

$$v = (\mu\varepsilon)^{-1/2} \,, \tag{A-19}$$

or in vacuum,

$$c = (\mu_o \varepsilon_o)^{-1/2} \,. \tag{A-20}$$

The index of refraction is defined as the ratio of the velocity of light in vacuum to the velocity of light in the given medium:

$$n = \frac{c}{v} \,. \tag{A-21}$$

Substitution of equation (A-21) into equation (A-17) results in

$$\left[n^2 - \frac{\mu j\sigma}{\mu_o \varepsilon_o \omega}\right] = \left[\frac{\mu(\varepsilon - \frac{j\sigma}{\omega})}{\mu_o \varepsilon_o}\right], \tag{A-22}$$

or, with $\mu = \mu_o$,

$$(n')^2 = \frac{\varepsilon'}{\varepsilon_o} \,, \tag{A-23}$$

where

$$(n')^2 = n^2 - j\frac{\mu\sigma}{\mu_o \varepsilon_o \omega} \,. \tag{A-24}$$

The complex permittivity is related to the complex index of refraction by equation (A-23), and to the permittivity by equation (A-18). The complex index of refraction is related to the index of refraction by equation (A-24), which is frequently written as

$$n' = n(1 - jk) , \qquad \text{(A-25)}$$

where k is the absorption index (equal to zero in vacuum).

Appendix B. Computer Program Documentation

Brief descriptions, program listings, and data input files are presented for the computer programs presented in this dissertation. Program **LJCMPY** performs the calculations for the modeling and optimization of the liquid-junction photovoltaic cell, and program **RCALC** performs the calculations for the primary current distribution and resistance of a slotted-electrode cell.

1. PROGRAM LJCMPY

The following program was written to solve the coupled equations (see Chapter 2) which govern the liquid-junction photovoltaic cell. The program also allows calculation of cell performance by coupling the one-dimensional model with primary resistance calculations (see Chapters 3 and 4). The input data include parameters for the semiconductor, the semiconductor-electrolyte interface, the electrolyte, and the counterelectrode. These parameters and their units are defined within comments in the subroutine **READ**. The cell characteristics are calculated for input values of illumination and current density. Output control parameters are defined within comments in the main program listing. A sample input file is presented after the program listing.

The governing equations were written in finite-difference form and properly linearized. The equations are written in dimensionless form. Numerical accuracy was enhanced by definition of concentration variables that are uniform under equilibrium conditions. The concentration and potential variables in the semiconductor are

$$AN(J) = \frac{n}{N_d - N_a} e^{-\frac{F\Phi}{RT}},$$

$$P(J) = \frac{p}{N_d - N_a} e^{\frac{F\Phi}{RT}},$$

and

$$PHI(J) = \frac{F\Phi}{RT},$$

where the index J marks the location. The corresponding variables in the electrolyte are

$$CSOL(I,J) = \frac{c_i}{c_{i,\infty}} e^{\frac{z_i F \Phi}{RT}}$$

and

$$PHI(J) = \frac{F\Phi}{RT} .$$

Under equilibrium conditions, the dimensionless potential varies in the semiconductor from zero to around 40.

Numerical accuracy was further improved by partial decoupling of the three equations governing the semiconductor. Separate variables were defined for the charge density, RHO(J), the electron flux, FN(J), and the hole flux, FP(J). Five equations govern the solution with four ionic species. These were written as seven equations, with separate variables defined for the flux of species 3, F3(J), and the flux of species 4, F4(J). Twenty eight equations are written for the semiconductor-electrolyte interface, involving 21 variables that appear only at that location. These are decomposed to seven equations involving the bulk phase variables in a local inversion routine, **LOCINV**. A general method for local inversion is presented by White.[208]

A description of the routines **BAND** and **MATINV** is presented by Newman[104] and by White *et al.*[209]

```
      PROGRAM LJCMPY (INPUT,OUTPUT)
C
C        PROGRAM FOR CALCULATING POTENTIAL AND CURRENT CHARACTERISTICS
C        OF THE LIQUID-JUNCTION PHOTOVOLTAIC CELL.
C        PROGRAM INCLUDES 13 REACTION STEPS AT THE SEMICONDUCTOR-
C        SOLUTION INTERFACE.
C
      DIMENSION ERR(9),RMOD(13)
      COMMON/BA/ N,NJ,A(7,7),B(7,7),C(7,250),D(7,15),G(7),X(7,7),Y(7,7)
      COMMON/LI/ AA(28,28),BB(28,28),CC(28,1),DD(28,28),GG(28)
      COMMON/LI2/ AM(28,28),BM(28,28),DM(28,28),GM(28)
      COMMON/SC/ PHI(250),P(250),AN(250),DFN(250),DFP(250),FN(250),
     1   FP(250),RHO(250),D2(250)
      COMMON/RUN/ EX,H,H2,HD2,EXH,NJJ,INDEX(7,250),KERR,ERRSUB,IJ
      COMMON/IN/ ALM,DELT,BD,SO,CURRNT,QII,SPOSN,TET,ANI2,DSC,DSOL,MSOL
      COMMON/IN2/ BE,B3,RSC,GSC,RSOLN,GSOLN,GV,GT,GC,SI,DEL1,DEL3
      COMMON/SOL/ CBULK(4),Z(4),CSOL(4,250),F(4),HS,DC(4,250),XP(4)
      COMMON/FLUX/ F3(250),F4(250)
      COMMON/IFC/ RATE(13),EQUIL(13),S(13,13),CONC(13),RXN(13),RXS(13)
     1   ,CIF(5)
      COMMON/IFC2/ PHISS,PHISC,PHIHP,BKISS
      COMMON/SMQ/ SMQ,QI,QSL,SMQL
      COMMON/CHG/ SQL(250)
      COMMON/STOP/ NSTOP
      COMMON/M/ MODE,MRPRNT,MREAL,MERROR,MPARAM
      COMMON/CONV/ CL,CPOT,CCHG,COND
      COMMON/CE/ DIST,EXCOB,NREACT,CLIM3,CLIM4
      COMMON/OPT/ MOPT,SFLUX,ACE,RESIR
      COMMON/INIT/ PHIOSS,PHIOHP,CELECQ,CHOLEQ,MDIM,DPOT1,DPOT2,DPOT3
     1   ,FRACVQ,FRACTQ,FRACCQ,FRAC3Q,FRAC4Q,FUOV,FUOT,FUOC,FUOIHP
      COMMON/END/ CURAN(40),VOLT(40),VNOT(40),VWIR(40),VWCE(40)
     1   ,CHGISS(40),CHGIHP(40),CHG(40)
     2   ,POWER1(40),POWER2(40),POWER3(40),POWER4(40)
C     TRACE SUBPROGRAM TIME
  200 FORMAT( * J=*,I3,* G =*,7(E10.2))
  400 FORMAT( * INDEX:*,7(I10))
  100 FORMAT( 4(I3))
  101 FORMAT( 4(F10.5))
  102 FORMAT( I3)
  103 FORMAT( 2(I3))
C
C        ERREQN    LIMITING VALUE FOR THE DIFFERENCE BETWEEN FORWARD AND
C           BACKWARD REACTION RATES. NET REACTION RATES LESS THAN ERREQN
C           ARE SET EQUAL TO ZERO.
C        ERRSUB    LIMITING VALUE FOR G(I) RELATIVE TO THE BIGGEST TERM
C           IN THE EQUATION.
C
      ERREQN = 0.
      ERRSUB = 1.0E-09
C
C        H,HS    MESH INTERVALS FOR THE SEMICONDUCTOR AND THE SOLUTION
```

```
C           RESPECTIVELY.                                    (DEBYE LENGTHS)
C        DSC,DSOL   DISTANCE FROM THE INTERFACE TO THE CURRENT-COLLECTOR
C          AND INTO THE SOLUTION RESPECTIVELY.              (DEBYE LENGTHS)
C
      READ 101,H,HS,DSC,DSOL
      IJ = DSOL/HS + 2.1
      NJ = DSC/H + FLOAT(IJ) + 0.1
      N = 7
      NJJ = NJ - 1
      IJJ = IJ-1
      H2 = H**2
C
C        DIST    DISTANCE FROM COUNTERELECTRODE TO OUTER POINT OF
C           SOLUTION.                                        (CM)
C        EXCOB    BUTLER-VOLMER EXCHANGE CURRENT DENSITY FOR COUNTER-
C           ELECTRODE REACTION WITH NO MASS-TRANSFER LIMITATIONS.
C                                                            (MA/CM2)
C        CLIM3,CLIM4    MASS-TRANSFER LIMITING CURRENTS FOR SPECIES 3 AN
C           AND 4 AT COUNTERELECTRODE.                       (MA/CM2)
C        NREACT    ELECTRON-TRANSFER NUMBER FOR COUNTERELECTRODE
C           REACTION                                         (DIMENSIONLESS)
C
      READ 101,DIST,EXCOB,CLIM3,CLIM4
      READ 102,NREACT
C
C        ERRMAX    MAXIMUM CONVERGENCE ERROR ALLOWED.
C        NDATA    NUMBER OF DATA SETS.
C        NPRINT    ITERATION AFTER WHICH ALL G(I) ARE TO BE PRINTED.
C        JPRINT    ITERATION AFTER WHICH ALL INTERMEDIATE RESULTS ARE TO
C           BE PRINTED.
C        JCMAX    MAXIMUM NUMBER OF ITERATIONS ALLOWED.
C        NCOUNT,JCOUNT    DUMMY COUNTERS .
C
      ERRMAX = 1.0E-06
      READ 100,NDATA,NPRINT,JPRINT,JCMAX
C
C        MRPRNT = 0 SUPPRESSES PRINTING OF RESULTS AT EACH MESH POINT.
C        MERROR = 0 SUPPRESSES PRINTING OF CONVERGENCE CRITERIA.
C        MPARAM = 0 SUPPRESSES PRINTING OF INPUT PARAMETERS AFTER THE
C           FIRST DATA SET AND LIMITS THE NUMBER OF PARAMETERS READ FOR
C           EACH SUCCESSIVE DATA SET.
C        MPARAM = 1 ALLOWS READING AND PRINTING OF A COMPLETE SET OF
C           PARAMETERS FOR EACH NEW DATA SET.
C        MREAL  = 0 YIELDS PRINTING OF COMPUTER VARIABLES FOR
C           SEMICONDUCTOR CONCENTRATIONS.
C        MREAL  = 1 YIELDS PRINTING OF REAL CONCENTRATIONS, NORMALIZED
C           TO THE BACKGROUND CHARGE.
C
      READ 100,MRPRNT,MERROR,MPARAM,MREAL
C
C        MSOL = 0;  ILLUMINATION AT ELECTROLYTE-SEMICONDUCTOR INTERFACE
```

```
C         MSOL = 1;  ILLUMINATION AT SEMICONDUCTOR-CURRENT COLLECTOR
C            INTERFACE
C         MOPT = 0;  DO NOT CALL OPTIMIZATION ROUTINES
C         MOPT = 1;  CALL OPTIM1
C         MOPT = 2;  CALL OPTIM2
C         MOPT = 3;  CALL OPTIM3
C
      READ 103,MSOL,MOPT
C
      DLIM1 = 5.0
      DLIM2 = 1.0
      UP1 = EXP(DLIM1)-1.0
      DN1 = 1.0-EXP(-DLIM1)
      UP2 = EXP(DLIM2)-1.0
      DN2 = 1.0-EXP(-DLIM2)
      NCOUNT = 0
      NSTOP = 0
    1 CALL READ(NCOUNT)
C
      DSC = 1689.*DEL1
      NJ = DSC/H + FLOAT(IJ) + 0.1
      NJJ = NJ - 1
C
      NCOUNT = NCOUNT + 1
C     MRPRNT = 0
C     IF(NCOUNT.EQ.1) MRPRNT = 1
C     IF(NCOUNT.EQ.2) MRPRNT = 1
C     IF(NCOUNT.EQ.31) MRPRNT = 1
C     IF(NCOUNT.EQ.17) MRPRNT = 1
      EXH = EXP(-ALM*H)
      HD2 = (H*DELT)**2
      SMQ = 0.
C
C        INITIALIZATION OF VARIABLES
C
      IF(NCOUNT.GT.2) GO TO 10
      QS = 3.0*SO - 1.0E-06
      QG = 32.0*EXP(-5.*SO)
      ANQ = .5E-27
      PQ = ANI2/ANQ
      IF(MDIM.EQ.4) QS = PHIOHP
      EXSO = EXP(-5.6*SO)
      IF(MDIM.EQ.4) QG = -PHIOSS*EXSO
      IF(MDIM.EQ.4) ANQ = CELECQ
      IF(MDIM.EQ.4) PQ = CHOLEQ
         DO 5 J = 1,IJ
         PHI(J) = QS*(1.0 - EXP(-(J-1)*HS))
         F3(J) = 0.
         F4(J) = 0.
              DO 5 I = 1,4
              CSOL(I,J) = CBULK(I)
```

```
            DC(I,J) = 0.
    5    CONTINUE
         LCT = 0
            DO 6 J = IJ,NJ
            PHI(J) = QG*(1.0 - EXP(-LCT*H))
            P(J) = PQ + 1.0*SO
            AN(J) = ANQ + SO*0.1E-07
            DFN(J) = 0.
            DFP(J) = 0.
            FN(J) = 0.
            FP(J) = 0.
            RHO(J) = -1.0
            D2(J) = 0.
            LCT = LCT+1
    6    CONTINUE
         CIF(1) = 0.0005 + 0.0025*SO
         CONC(4) = GV - CIF(1)
         CIF(2) = 0.00005 + 0.00025*SO
         CONC(6) = GT - CIF(2)
         CIF(3) = 0.00005 + 0.00025*SO
         CONC(8) = GC - CIF(3)
         CIF(4) = 0.01193 - 0.016*SO
         CIF(5) = 0.01193 - 0.016*SO
         CONC(11) = 1. - CIF(4) - CIF(5)
         IF(MDIM.EQ.4) CIF(1) = FRACVQ*GV
         IF(MDIM.EQ.4) CIF(2) = FRACTQ*GT
         IF(MDIM.EQ.4) CIF(3) = FRACCQ*GC
         IF(MDIM.EQ.4) CIF(4) = FRAC3Q
         IF(MDIM.EQ.4) CIF(5) = FRAC4Q
         IF(MDIM.EQ.4) CONC(4) = FUOV*GV
         IF(MDIM.EQ.4) CONC(6) = FUOT*GT
         IF(MDIM.EQ.4) CONC(8) = FUOC*GC
         IF(MDIM.EQ.4) CONC(11) = FUOIHP
         DP1 = 0.04
         DP2 = 0.0
         DP3 = 0.8*PHI(IJ-1)
         IF(MDIM.EQ.4) DP1 = DPOT1
         IF(MDIM.EQ.4) DP2 = DPOT2
         IF(MDIM.EQ.4) DP3 = DPOT3
         PHISC = PHI(IJ) - DP1
         PHIHP = PHI(IJ-1) + DP3
         PHISS = PHIHP + DP2
            DO 7 L=1,13
            RXN(L) = 0.
    7    CONTINUE
C
C        CALCULATION OF EQUATION COEFFICIENTS AT EACH MESH POINT
C
   10 JCOUNT = 0
      MERROR = 0
      KERR = 0
```

```
   15 IF(JCOUNT.GE.JCMAX) GO TO 65
      JCOUNT = JCOUNT + 1
      PHI(NJ+1) = 2.*PHI(NJ) - PHI(NJ-1)
      IF(JCOUNT.GE.NPRINT) KERR = 1
      IF(JCOUNT.GE.JPRINT) CALL PRINT(NCOUNT)
      IF(JCOUNT.GE.(NPRINT-2)) MERROR = 1
         DO 20 I=1,N
              DO 20 K=1,N
              X(I,K) = 0.
              Y(I,K) = 0.
   20    CONTINUE
      J = 0
   30 J = J + 1
         DO 35 I=1,N
         G(I) = 0.
         INDEX(I,J) = 0
              DO 35 K=1,N
              A(I,K) = 0.
              B(I,K) = 0.
              D(I,K) = 0.
   35    CONTINUE
      IF(J.GT.1) GO TO 40
      CALL BC1(J)
      GO TO 50
   40 IF(J.GT.IJ) GO TO 45
      IF(J.LT.IJJ) CALL SOLN(J)
      IF(J.EQ.IJJ) CALL INTRFC(J)
      GO TO 50
   45 IF(J.LT.NJ) CALL SC(J)
      IF(J.EQ.NJ) CALL BCNJ(J)
   50 KERRR = 0
         DO 48 L=1,7
   48    IF(G(L).NE.0.0) KERRR = 1
      KERR = 0
      IF(KERRR.EQ.1 .AND. JCOUNT.GT.NPRINT) KERR = 1
      IF(J.LT.(NJ-4) .AND. J.GT.(IJ+5)) KERR = 0
      IF(J.GT.5 .AND. J.LT.(IJ-5)) KERR = 0
      IF(KERR.GT.0) PRINT 200,J,G(1),G(2),G(3),G(4),G(5),G(6),G(7)
      IF(KERR.GT.0) PRINT 400,(INDEX(I,J), I=1,7)
      IF(KERR.GT.0 .AND. J.GE.IJ) PRINT 2001,PHI(J),AN(J),P(J),FN(J),
     1   FP(J),RHO(J)
      IF(KERR.GT.0 .AND. J.LT.IJ) PRINT 2001,PHI(J),(CSOL(I,J), I=1,4)
     1   ,DC(4,J)
 2001 FORMAT( 3X,6(E12.4))
      CALL BAND(J)
      IF(J.LT.NJ) GO TO 30
C
C        CALCULATION OF NEW VALUES FOR VARIABLES
C
      LOC = 1
      NE = N+1
```

```
      NP = 28
      J = IJ
         DO 49 I=NE,NP
         CC(I,1) = GG(I)
            DO 49 K=1,N
            CC(I,1) = CC(I,1) - AA(I,K)*C(K,J-1) - BB(I,K)*C(K,J)
49       CONTINUE
      CC(7,1) = C(7,IJ)
         DO 51 J=1,IJJ
         IF(C(1,J).LT.-DLIM2) C(1,J) = -DLIM2
         IF(C(1,J).GT.DLIM2) C(1,J) = DLIM2
         PHI(J) = PHI(J) + C(1,J)
         F3(J) = F3(J) + C(6,J)
         F4(J) = F4(J) + C(7,J)
              DO 51 I=1,4
              IF(C(I+1,J).LT.-DN2*CSOL(I,J)) C(I+1,J) = -DN2*CSOL(I,J)
              IF(C(I+1,J).GT. UP2*CSOL(I,J)) C(I+1,J) = UP2*CSOL(I,J)
              CSOL(I,J) = CSOL(I,J) + C(I+1,J)
              IF(J.EQ.1) GO TO 51
              DC(I,J-1) = DC(I,J-1) + C(I+1,J) - C(I+1,J-1)
51       CONTINUE
         DO 55 J=IJ,NJ
         FP(J) = FP(J) + C(4,J)
         FN(J) = FN(J) + C(5,J)
         IF(C(6,J).LT.-0.2) C(6,J) = -0.2
         IF(C(6,J).GT.0.2) C(6,J) = 0.2
         RHO(J) = RHO(J) + C(6,J)
         D2(J) = D2(J) + C(7,J)
         IF(C(1,J).LT.-DLIM1) C(1,J) = -DLIM1
         IF(C(1,J).GT.DLIM1) C(1,J) = DLIM1
         IF(C(2,J).GT.UP1*AN(J)) C(2,J) = UP1*AN(J)
         IF(C(2,J).LT.0.) C(2,J) = AN(J)*(EXP(C(2,J)/AN(J))-1.)
         IF(C(2,J).LT.-DN1*AN(J)) C(2,J) = -DN1*AN(J)
         IF(C(3,J).GT.UP1*P(J)) C(3,J) = UP1*P(J)
         IF(C(3,J).LT.-DN1*P(J)) C(3,J) = -DN1*P(J)
         PHI(J) = PHI(J) + C(1,J)
         AN(J) = AN(J) + C(2,J)
         P(J) = P(J) + C(3,J)
         IF(J.EQ.IJ) GO TO 55
         DFN(J) = DFN(J) + C(2,J) - C(2,J-1)
         DFP(J) = DFP(J) + C(3,J) - C(3,J-1)
55       CONTINUE
      IF(CC(27,1).GT.DLIM2) CC(27,1) = DLIM2
      IF(CC(27,1).LT.-DLIM2) CC(27,1) = -DLIM2
      IF(CC(7,1).GT.DLIM2) CC(7,1) = DLIM2
      IF(CC(7,1).LT.-DLIM2) CC(7,1) = -DLIM2
      IF(CC( 8,1).GT.DN2*CONC(4)) CC( 8,1) = DN2*CONC(4)
      IF(CC( 9,1).GT.DN2*CONC(6)) CC( 9,1) = DN2*CONC(6)
      IF(CC(10,1).GT.DN2*CONC(8)) CC(10,1) = DN2*CONC(8)
      IF(CC(28,1).LT.-DN2*CONC(11)) CC(28,1) = -DN2*CONC(11)
      IF(CC(28,1).GT.UP2*CONC(11)) CC(28,1) = UP2*CONC(11)
```

```
      IF(CC(13,1).LT.-DLIM2) CC(13,1) = -DLIM2
      IF(CC(13,1).GT.DLIM2) CC(13,1) = DLIM2
      PHISS = PHISS + CC(27,1)
      PHIHP = PHIHP + CC(7,1)
         DO 56 I = 1,5
         IF(CC(I+7,1).LT.-DN2*CIF(I)) CC(I+7,1) = -DN2*CIF(I)
         IF(CC(I+7,1).GT.UP2*CIF(I)) CC(I+7,1) = UP2*CIF(I)
         CIF(I) = CIF(I) + CC(I+7,1)
   56    CONTINUE
      CONC(4) = CONC(4) - CC(8,1)
      CONC(6) = CONC(6) - CC(9,1)
      CONC(8) = CONC(8) - CC(10,1)
      PHISC = PHISC + CC(13,1)
      RXN(6) = RXN(6) + CC(14,1)
      RXN(8) = RXN(8) + CC(15,1)
      RXN(9) = RXN(9) + CC(16,1)
      RXN(1) = RXN(1) + CC(17,1)
      RXN(2) = RXN(2) + CC(18,1)
      RXN(3) = RXN(3) + CC(19,1)
      RXN(4) = RXN(4) + CC(20,1)
      RXN(5) = RXN(5) + CC(21,1)
      RXN(7) = RXN(7) + CC(22,1)
      RXN(10) = RXN(10) + CC(23,1)
      RXN(11) = RXN(11) + CC(24,1)
      RXN(12) = RXN(12) + CC(25,1)
      RXN(13) = RXN(13) + CC(26,1)
      CONC(11) = CONC(11) + CC(28,1)
C
C        EVALUATION OF ITERATION ERRORS
C
      ERRSOL = 0.
      IF(ABS(PHI(IJJ)).GT.0.1E-06) ERRSOL = C(1,IJJ)/PHI(IJJ)
      ERPNJ = C(3,NJ)/P(NJ)
      ERRC4 = C(5,IJJ)/CSOL(4,IJJ)
      ERRPHI = C(1,NJ)/PHI(NJ)
      ERRAN = C(2,IJ)/AN(IJ)
      ERRP = C(3,IJ)/P(IJ)
         DO 57 L=1,13
         IF(ABS(RXN(L)).LT.ERREQN*RXS(L)/2.) RXN(L) = 0.
         ERR(L) = 0.
   57    CONTINUE
      IF(RXS(1).NE.0.) ERR(1) = CC(17,1)/RXS(1)
      IF(RXS(2).NE.0.) ERR(2) = CC(18,1)/RXS(2)
      IF(RXS(6).NE.0.) ERR(6) = CC(14,1)/RXS(6)
      IF(RXS(8).NE.0.) ERR(8) = CC(15,1)/RXS(8)
      IF(RXS(9).NE.0.) ERR(9) = CC(16,1)/RXS(9)
      IF(RXS(3).NE.0.) ERR(3) = CC(19,1)/RXS(3)
      IF(RXS(4).NE.0.) ERR(4) = CC(20,1)/RXS(4)
      IF(RXS(5).NE.0.) ERR(5) = CC(21,1)/RXS(5)
      IF(RXS(7).NE.0.) ERR(7) = CC(22,1)/RXS(7)
      RMOD(1) = RXN(1)
```

```
      RMOD(2) = RXN(2)/BD
      RMOD(3) = RXN(3)/BD
      RMOD(4) = RXN(4)
      RMOD(5) = RXN(5)/BD
      RMOD(6) = RXN(6)
      RMOD(7) = RXN(7)
      RMOD(8) = RXN(8)/BE
      RMOD(9) = RXN(9)/BE/B3
      RMOD(10) = RXN(10)
      RMOD(11) = RXN(11)
      RMOD(12) = RXN(12)/BD
      RMOD(13) = RXN(13)/BD
      IF(MERROR.EQ.0) GO TO 60
      PRINT 202,JCOUNT,ERRPHI,ERRAN,ERRP,ERRSOL,ERPNJ,ERRC4
  202 FORMAT( * JCOUNT = *,I3,* ERRPHI  = *,E10.3,* ERRAN   = *,
     1 E10.3,* ERRP    = *,E10.3,/,13X,* ERRSOL  = *E10.3* ERPNJ   = *
     2 E10.3* ERRC4   = *E10.3)
      PRINT 201,(L,ERR(L), L=1,9)
  201 FORMAT( 3(13X,3(* ERR(*,I2,*) = *E10.3)/))
      PRINT 204,(L,RMOD(L), L=1,12)
      PRINT 207,RMOD(13)
  204 FORMAT( 3(* RXN(*,I2,*) =*E13.6,1X))
  207 FORMAT( * RXN(13) =*E13.6,1X/)
  206 FORMAT( 3(* RXS(*,I2,*) =*E13.6,1X))
  208 FORMAT( * RXS(13) =*E13.6,1X/)
      PRINT 203,PHI(NJ),AN(IJ),P(IJ),PHI(IJ-1),FN(IJ),FP(IJ)
  203 FORMAT( * PHI(NJ) =*E13.6* AN(IJ)  =*E13.6* P(IJ)   =*
     1   E13.6,/* PHI(SL) =*E13.6* FN(IJ)  =*E13.6* FP(IJ)  =*
     2   E13.6/)
      PRINT 210,PHISC,PHISS,PHIHP
      PRINT 211,(CIF(L), L=1,5)
      PRINT 212,CONC(4),CONC(6),CONC(8),CONC(11)
  210 FORMAT( * PHISC,SS,HP = *,8X,3(E13.6,1X))
  211 FORMAT( * CIF(I) =*,5(E13.6,1X))
  212 FORMAT( * CONC(I)=*,4(E13.6,1X)/)
   60 IF(ABS(ERRPHI).GT.ERRMAX) GO TO 15
      IF(ABS(ERRSOL).GT.ERRMAX) GO TO 15
      IF(ABS(ERPNJ).GT.ERRMAX) GO TO 15
      IF(ABS(ERRC4).GT.ERRMAX) GO TO 15
      IF(ABS(ERRAN).GT.ERRMAX) GO TO 15
      IF(ABS(ERRP).GT.ERRMAX) GO TO 15
         DO 64 L=1,9
         ERR2 = ERRMAX*1.0E-03
         IF(ABS(RXN(L))/RXS(L).GT.1.0E-03) ERR2 = ERRMAX
         IF(ABS(ERR(L)).GT.ERR2) GO TO 15
   64    CONTINUE
      GO TO 90
   65 PRINT 205,JCOUNT
  205 FORMAT( * SYSTEM DID NOT CONVERGE IN *I3* ITERATIONS*)
   90 IF(JCOUNT.LT.JCMAX) PRINT 221,JCOUNT
  221 FORMAT( /* CONVERGENCE OBTAINED IN *I3* ITERATIONS*/)
```

```
      CALL PRINT(NCOUNT)
      IF(JCOUNT.GE.JCMAX .OR. NSTOP.EQ.1) NCOUNT = NCOUNT-1
      IF(JCOUNT.GE.JCMAX .OR. NSTOP.EQ.1) GO TO 99
      IF(NCOUNT.LT.NDATA) GO TO 1
   99 CONTINUE
      PRINT 600,NCOUNT-1
      PRINT 620,(CURAN(K),VNOT(K),K=2,NCOUNT)
      PRINT 601,NCOUNT-1
      PRINT 620,(CURAN(K),VWIR(K),K=2,NCOUNT)
      PRINT 602,NCOUNT-1
      PRINT 620,(CURAN(K),VWCE(K),K=2,NCOUNT)
      PRINT 603,NCOUNT-2
      PRINT 620,(CURAN(K),VOLT(K),K=3,NCOUNT)
      PRINT 604,NCOUNT-1
      PRINT 620,(CURAN(K),CHGISS(K),K=2,NCOUNT)
      PRINT 605,NCOUNT-1
      PRINT 620,(CURAN(K),CHGIHP(K),K=2,NCOUNT)
      PRINT 606,NCOUNT-1
      PRINT 620,(CURAN(K),CHG(K),K=2,NCOUNT)
      PRINT 607,NCOUNT-1
      PRINT 620,(CURAN(K),POWER1(K),K=2,NCOUNT)
      PRINT 608,NCOUNT-1
      PRINT 620,(CURAN(K),POWER2(K),K=2,NCOUNT)
      PRINT 609,NCOUNT-1
      PRINT 620,(CURAN(K),POWER3(K),K=2,NCOUNT)
      PRINT 610,NCOUNT-2
      IF(MOPT.EQ.4) PRINT 620,(CURAN(K),ACE*POWER4(K),K=3,NCOUNT)
      IF(MOPT.NE.4) PRINT 620,(CURAN(K),POWER4(K),K=3,NCOUNT)
  600 FORMAT( * POTENTIAL; NO CE OR IR*,/,I4)
  601 FORMAT( * POTENTIAL; WITH IR*,/,I4)
  602 FORMAT( * POTENTIAL; WITH CE*,/,I4)
  603 FORMAT( * POTENTIAL; WITH CE AND IR*,/,I4)
  604 FORMAT( * CHARGE ON ISS*,/,I4)
  605 FORMAT( * CHARGE ON IHP*,/,I4)
  606 FORMAT( * CHARGE ON INTERFACE*,/,I4)
  607 FORMAT( * POWER DENSITY; NO CE OR IR*,/,I4)
  608 FORMAT( * POWER DENSITY; WITH IR*,/,I4)
  609 FORMAT( * POWER DENSITY; WITH CE*,/,I4)
  610 FORMAT( * POWER DENSITY; WITH CE AND IR*,/,I4)
  620 FORMAT( 2E15.7)
      STOP
      END



      SUBROUTINE READ(NCOUNT)
C
C        SUBROUTINE FOR INPUT OF DATA AND CALCULATION OF DIMENSIONLESS
C        PARAMETERS.
C
```

```
      COMMON/IN/ ALM,DELT,BD,SO,CURRNT,QII,SPOSN,TET,ANI2,DSC,DSOL,MSOL
      COMMON/IN2/ BE,B3,RSC,GSC,RSOLN,GSOLN,GV,GT,GC,SI,DEL1,DEL3
      COMMON/RUN/ EX,H
      COMMON/SOL/ CBULK(4),Z(4),CSOL(4,250),F(4),HS
      COMMON/IFC/ RATE(13),EQUIL(13),S(13,13)
      COMMON/IFC2/ PHISS,PHISC,PHIHP,BKISS
      COMMON/M/ MODE,MPRINT,MREAL,MERROR,MPARAM
      COMMON/CONV/ CL,CPOT,CCHG,COND
      COMMON/CE/ DIST
      COMMON/OPT/ MOPT,SFLUX,ACE,RESIR
      COMMON/INIT/ PHIOSS,PHIOHP,CELECQ,CHOLEQ,MDIM,DPOT1,DPOT2,DPOT3
     1   ,FRACVQ,FRACTQ,FRACCQ,FRAC3Q,FRAC4Q,FUOV,FUOT,FUOC,FUOIHP
      DIMENSION DIFF(4),RDIM(13),RMOD(13)
  100 FORMAT( 13(F5.1))
  102 FORMAT( I2)
  103 FORMAT( F20.15)
  104 FORMAT( E10.3,F20.15)
  105 FORMAT( 2(F20.15))
  106 FORMAT( 3(F20.15))
  107 FORMAT( 4(E10.3))
  108 FORMAT( 3(E10.3))
  109 FORMAT( 2(E10.3))
  110 FORMAT( 4(F20.15))
  111 FORMAT( E10.3)
C
C        FOR SET CURRENT AT BCNJ(J) (AS CURRNT) ..... MODE=1
C        FOR SET POTENTIAL AT BCNJ(J) (AS CURRNT) ... MODE=2
C        TO READ DIMENSIONLESS PARAMETERS..... MDIM=1
C        TO READ DIMENSIONAL PARAMETERS..... MDIM=2
C        TO READ DIMENSIONAL PARAMETERS AND CALCULATE
C          INTERFACIAL EQUILIBRIUM PARAMETERS..... MDIM=3
C        TO READ DIMENSIONAL PARAMETERS AND CALCULATE
C          PARAMETERS FROM BAND GAP AND INTERFACIAL
C          ISS SITE ENERGIES..... MDIM=4
C
      IF(NCOUNT.EQ.0) GO TO 3
      IF(MPARAM.EQ.0) GO TO 6
      IF(MPARAM.EQ.1) GO TO 5
    3 CONTINUE
      READ 102,MODE
      READ 102,MDIM
      SPOSN = 100.0
      TET = 2.57E-06
      ANI2 = 2.25E-20
C
C                STOCHIOMETRIC COEFFICIENTS
C
      NR = 13
      NC = 13
         DO 4 L=1,NR
         READ 100,(S(I,L), I=1,NC)
```

```
    4    CONTINUE
    5 CONTINUE
      IF(MDIM.GT.1) GO TO 7
C
C     ********************************************************************
C
C                        REACTION PARAMETERS
C
      READ 105,(RATE(L),EQUIL(L), L=1,NR)
      EQUIL(4) = EQUIL(3)/EQUIL(1)/EQUIL(2)/ANI2
      EQUIL(6) = EQUIL(5)/EQUIL(3)
      EQUIL(7) = EQUIL(6)*EQUIL(4)
      EQUIL(10) = EQUIL(1)*EQUIL(4)
      EQUIL(11) = EQUIL(10)/EQUIL(3)
      EQUIL(12) = EQUIL(2)/EQUIL(3)
      EQUIL(13) = EQUIL(12)*EQUIL(4)
      READ 107,GV,GT,GC,SI
C
C                      SOLUTION CHARACTERISTICS
C
      READ 105,(CBULK(I),Z(I), I=1,4)
      READ 105,BE,B3
C
C                    SEMICONDUCTOR CHARACTERISTICS
C
      READ 110,RSC,GSC,RSOLN,GSOLN
      READ 106,DEL1,DEL3,BKISS
      GSC = GSC*DEL1 $ GSOLN = GSOLN*DEL3
      RSC = RSC*DEL1 $ RSOLN = RSOLN*DEL3
      SI = 0.
      READ 110,ALM,DELT,BD,QII
      GO TO 6
C
C     ********************************************************************
C
    7 CONTINUE
C
C                            RATE CONSTANTS
C
C        RDIM(1 AND 2)     INTERFACIAL RATE CONSTANTS      (CM3/MOLE-SEC)
C        RDIM(3, 4, 5, 6, AND 7)    INTERFACIAL RATE CONSTANTS
C                                                         (CM2/MOLE-SEC)
C        RDIM(8 AND 9)     INTERFACIAL RATE CONSTANTS      (1/SEC)
C        RDIM(10, 11, 12, AND 13)    INTERFACIAL RATE CONSTANTS
C                                                         (CM3/MOLE-SEC)
C
      READ 104,(RDIM(L),EQUIL(L), L=1,NR)
C
C                         GENERAL PARAMETERS
C
C        FARAD    FARADAYS CONSTANT                       (C/EQUIV.)
```

```
C        R    IDEAL GAS CONSTANT                                (J/MOLE-K)
C        T    TEMPERATURE                                       (DEGREES K)
C
      FARAD = 96487.
      R = 8.3143
      READ 104,T
C
C                        SOLUTION PARAMETERS
C
C        CBULK(I)    BULK ION CONCENTRATION                    (MOLES/CM3)
C        DIFF(I)    DIFFUSIVITY                                (CM2/SEC)
C        EPSOL    PERMITIVITY                                  (C/V-CM)
C        COND    BULK CONDUCTIVITY                             (1/OHM-CM)
C
      READ 106,(CBULK(I),Z(I),DIFF(I), I=1,4)
      READ 109,EPSOL,COND
      CTOT = CBULK(1)+CBULK(2)+CBULK(3)+CBULK(4)
         DO 8 I=1,4
    8    CBULK(I) = CBULK(I)/CTOT
C
C                      SEMICONDUCTOR PARAMETERS
C
C        DIFFE, DIFFH    ELECTRON AND HOLE DIFFUSIVITIES
C                                                              (CM2/SEC)
C        EPSC    PERMITIVITY                                   (C/V-CM)
C        BKCHG    BACKGROUND CHARGE                            (EQUIV/CM3)
C        ADS    PHOTON ABSOPTIVITY                             (1/CM)
C        EF    PHOTON EFFICIENCY FACTOR                        (DIMENSIONLESS)
C        QINC    INCIDENT PHOTON FLUX                          (MOLES/CM2-SEC)
C        STK2    HOMOGENEOUS RECOMBINATION RATE CONSTANT       (1/SEC)
C        SPOSN   HOMOGENEOUS RECOMBINATION RATE CONSTANT       (DIMENSIONLESS)
C        TKT    HOMOGENEOUS RECOMBINATION RATE CONSTANT        (MOLES/CM3)
C        CINT    INTRINSIC CONCENTRATION                       (MOLES/CM3)
C        QII    CHARGE ADSORBED AT CURRENT COLLECTOR           (MICRO-C/CM2)
C        SO    FRACTION OF INCIDENT RADIATION STRKING SURFACE
C                                                              (DIMENSIONLESS)
C
      READ 105,DIFFE,DIFFH
      READ 109,EPSC,BKCHG
      READ 108,ADS,EF,QINC
      READ 107,STK2,SPOSN,TKT,CINT
      READ 104,QII
C
C                        INTERFACIAL PARAMETERS
C
C        GISS    DENSITY OF SITES AT INNER SURFACE STATES
C                                                              (MOLES/CM2)
C        BKINT    DENSITY OF POSITIVE CHARGE AT INNER SURFACE STATES
C                                                              (EQUIV./CM2)
C        GIHP    DENSITY OF SITES AT INNER HELMHOLTZ PLANE
C                                                              (MOLES/CM2)
```

```
C        GC    FRACTION OF HIGH ENERGY ISS SITES          (DIMENSIONLESS)
C        GT    FRACTION OF INTERMEDIATE ENERGY SITES      (DIMENSIONLESS)
C        GV    FRACTION OF LOW ENERGY SITES               (DIMENSIONLESS)
C        DL1    DISTANCE BETWEEN OSS AND ISS              (CM)
C        DL2    DISTANCE BETWEEN ISS AND IHP              (CM)
C        DL3    DISTANCE BETWEEN IHP AND OHP              (CM)
C
      READ 108,GISS,GIHP,BKINT
      READ 107,GV,GT,GC,SI
      READ 108,DL1,DL2,DL3
      IF(MDIM.LT.3) GO TO 9
      IF(MDIM.EQ.4) GO TO 11
C
C     ***********************************************************************
C
C                    EQUILIBRIUM INTERFACIAL PARAMETERS
C
C        FRACVQ,FRACTQ,FRACCQ    FRACTIONAL OCCUPATION OF LOW, INTERMED-
C           IATE, AND HIGH ENERGY SITES AT THE ISS       (DIMENSIONLESS)
C        FUOV,FUOT,FUOC    FRACTION OF UNOCCUPIED SITES  (DIMENSIONLESS)
C        DPOT1,DPOT2,DPOT3    POTENTIAL DIFFERENCES BETWEEN THE OSS AND
C           THE ISS, THE ISS AND THE IHP AND THE IHP AND THE OHP
C                                                        (V)
C        SUMQ    TOTAL CHARGE SET AT THE INTERFACE       (MICRO-C/CM2)
C        CELECQ,CHOLEQ    CONCENTRATIONS OF ELECTRONS AND HOLES AT THE
C           OSS NORMALIZED TO THE BACKGROUND CHARGE      (DIMENSIONLESS)
C        FRAC3Q,FRAC4Q    FRACTIONAL OCCUPATION OF IHP BY SPECIES
C           3, 4 AND 5                                   (DIMENSIONLESS)
C        C3Q,C4Q    CONCENTRATION OF IONIC SPECIES 3 AND 4 AT THE
C           OHP                                          (MOLES/CM3)
C
      READ 108,FRACVQ,FRACTQ,FRACCQ
      READ 109,FRAC3Q,FRAC4Q
      READ 109,DPOT3,SUMQ
      READ 108,CELECQ,C3Q,C4Q
      FUOV = 1.-FRACVQ
      FUOT = 1.-FRACTQ
      FUOC = 1.-FRACCQ
      FUO3 = 1.-FRAC3Q
      FUO4 = 1.-FRAC4Q
      GO TO 12
C
C     ***********************************************************************
C
C              CALCULATION OF PARAMETERS FROM ENERGY VALUES
C
C        EGAP    SEMICONDUCTOR BAND GAP                    (V)
C        EV,ET,EC    ISS SITE ENERGIES                     (V)
C        EFERMI    FERMI LEVEL                             (V)
C        DGADS3,DGADS4    FREE ENERGIES OF ADSORPTION TO THE
C           IHP                                          (J/MOLE)
```

```
C        EREDOX    REDOX REACTION HALF-CELL POTENTIALS (REFERENCED TO
C           THE NORMAL HYDROGEN ELECTRODE)                    (V)
C        VALN,CONDN    SEMICONDUCTOR VALENCE AND CONDUCTION ENERGY SITE
C           CONCENTRATION                                     (MOLES/CM3)
C        ANEQ    ELECTRON CONCENTRATION IN ABSENCE OF POTENTIAL GRADIENT
C                                                             (MOLES/CM3)
C
   11 READ 108,EGAP,VALN,CONDN
      READ 108,EV,ET,EC
      READ 109,DGADS3,DGADS4
      READ 109,PHIOHP,EHMV
      READ 109,SUMQ,CELECQ
      CINT = SQRT(VALN*CONDN*EXP(-EGAP*FARAD/R/T))
      ANEQ = (BKCHG + SQRT(BKCHG**2 + 4.*CINT**2))/2.
      EFERMI = EGAP + R*T/FARAD*ALOG(ANEQ/CONDN)
      FRACVQ = 1./(1.+EXP((EV-EFERMI)*FARAD/R/T))
      FRACTQ = 1./(1.+EXP((ET-EFERMI)*FARAD/R/T))
      FRACCQ = 1./(1.+EXP((EC-EFERMI)*FARAD/R/T))
      FRAC3Q = CBULK(3)*EXP(-DGADS3/R/T)/
     1   (1.+CBULK(3)*EXP(-DGADS3/R/T))
      FRAC4Q = CBULK(4)*EXP(-DGADS4/R/T)/
     1   (1.+CBULK(4)*EXP(-DGADS4/R/T))
      FUO3 = 1./(1.+CBULK(3)*EXP(-DGADS3/R/T))
      FUO4 = 1./(1.+CBULK(4)*EXP(-DGADS4/R/T))
      FUOV = FRACVQ*EXP((EV-EFERMI)*FARAD/R/T)
      FUOT = FRACTQ*EXP((ET-EFERMI)*FARAD/R/T)
      FUOC = FRACCQ*EXP((EC-EFERMI)*FARAD/R/T)
      PHID = PHIOHP*FARAD/R/T
      C3Q = CBULK(3)*CTOT*EXP(-Z(3)*PHIOHP*FARAD/R/T)
      C4Q = CBULK(4)*CTOT*EXP(-Z(4)*PHIOHP*FARAD/R/T)
      TKSL = SQRT(2.*R*T*CTOT/EPSOL*(CBULK(1)*(EXP(-Z(1)*PHID)-1.)
     1    +CBULK(2)*(EXP(-Z(2)*PHID)-1.)
     2    +CBULK(3)*(EXP(-Z(3)*PHID)-1.)
     3    +CBULK(4)*(EXP(-Z(4)*PHID)-1.)))
      IF(PHIOHP.LE.0.) DPOT3 = -TKSL*DL3
      IF(PHIOHP.GT.0.) DPOT3 = TKSL*DL3
C
C     ******************************************************************
C
   12 CONTINUE
      EX3 = EXP(DPOT3*FARAD/R/T)
      EPSTR = EPSOL
      RAT3 = FRAC3Q/FUO3
      RAT4 = FRAC4Q/FUO4
      FRAC3Q = RAT3/(1.+RAT3+RAT4)
      FRAC4Q = RAT4/(1.+RAT3+RAT4)
      FUOIHP = 1./(1.+RAT3+RAT4)
      BKMIN = (GV*FRACVQ+GT*FRACTQ+GC*FRACCQ)*GISS + SUMQ*1.0E-06/FARAD
     1   - (Z(3)*FRAC3Q+Z(4)*FRAC4Q)*GIHP
      GISS = -(SUMQ*1.0E-06/FARAD - (Z(3)*FRAC3Q+Z(4)*FRAC4Q)*GIHP)
     1   /(GV*FRACVQ+GT*FRACTQ+GC*FRACCQ)
```

```
      DPOT2 = (DPOT3*EPSOL/DL3 - FARAD*GIHP*(Z(3)*FRAC3Q + Z(4)*FRAC4Q))
     1   *DL2/EPSTR
      DPOT1 = (FARAD*(GISS*(GV*FRACVQ+GT*FRACTQ+GC*FRACCQ) - BKINT)
     1   + DPOT2*EPSTR*SQRT(BKCHG*EPSOL/EPSC/CTOT)/DL2)*DL1/EPSC
      IF(DPOT1.GE.0.) PHIOSS = -1.5
      IF(DPOT1.LT.0.) PHIOSS = 1.5
      PEQ = CINT**2/ANEQ
         DO 52 KPOT=1,100
         PHIOLD = PHIOSS
         FOFPOT = EPSC*DPOT1**2/2./R/T/DL1**2/BKCHG - ANEQ/BKCHG*(EXP(
     1      PHIOLD*FARAD/R/T)-1.)- PEQ/BKCHG*(EXP(-PHIOLD*FARAD/R/T)-1.)
     2      + PHIOLD*FARAD/R/T
         DFDPOT = FARAD/R/T*(1.-ANEQ/BKCHG*EXP(PHIOLD*FARAD/R/T)
     1      +PEQ/BKCHG*EXP(-PHIOLD*FARAD/R/T))
         PHIOSS = PHIOLD - FOFPOT/DFDPOT
         IF(ABS((PHIOSS-PHIOLD)/PHIOSS).LT.1.0E-08) GO TO 54
   52    CONTINUE
      PRINT 53,KPOT
   53 FORMAT(* CONVERGENCE NOT OBTAINED FOR PHIOSS IN*,I4,* ITERATIONS*)
      PRINT 55,PHIOSS,PHIOLD
   55 FORMAT(* PHIOSS, PHIOLD =*,2(E20.10))
      STOP
   54 CONTINUE
      CELECQ = ANEQ/BKCHG*EXP(PHIOSS*FARAD/R/T)
      CHOLEQ = CINT**2/CELECQ/BKCHG**2
      EX1 = EXP(DPOT1*FARAD/R/T)
      EX2 = EXP(DPOT2*FARAD/R/T)
      EQUIL(1) = FRACCQ*EX1/FUOC/CELECQ
      EQUIL(2) = FUOV/CHOLEQ/FRACVQ/EX1
      EQUIL(3) = FRACTQ*FUOV/FRACVQ/FUOT
      EQUIL(5) = FRAC4Q*FUOV/FRACVQ/FRAC3Q*EX2
      EQUIL(8) = C3Q*FUOIHP*EX3**(-Z(3))/FRAC3Q/CTOT
      EQUIL(9) = C4Q*FUOIHP*EX3**(-Z(4))/FRAC4Q/CTOT
      PHIOSS = PHIOSS*FARAD/R/T
      PHIOHP = PHIOHP*FARAD/R/T
      DPOT1 = DPOT1*FARAD/R/T
      DPOT2 = DPOT2*FARAD/R/T
      DPOT3 = DPOT3*FARAD/R/T
C
C     ******************************************************************
C
    9 CONTINUE
C
C                  CALCULATION OF DIMENSIONLESS GROUPS
C
C
C                              SOLUTION
C        DEBSOL    DEBYE LENGTH                          (CM)
C        B3    RATIO OF SPECIES 3 AND 4 DIFFUSIVITIES    (DIMENSIONLESS)
C
C                           SEMICONDUCTOR
```

```
C       ANI2    SQUARE OF INTRINSIC CONCENTRATION       (DIMENSIONLESS)
C       TET    HOMOGENEOUS RECOMBINATION RATE CONSTANT  (DIMENSIONLESS)
C       DEBSC    DEBYE LENGTH                           (CM)
C       DIFFL    MINORITY CARRIER DIFFUSION LENGTH      (CM)
C       DELT    RATIO OF DEBYE TO DIFFUSION LENGTH      (DIMENSIONLESS)
C       ALM    RATIO OF DEBYE LENGTH TO SOLAR ABSORPTION LENGTH
C                                                       (DIMENSIONLESS)
C       SFLUX    SOLAR FLUX                             (DIMENSIONLESS)
C       BD    RATIO OF ELECTRON AND HOLE DIFFUSIVITIES  (DIMENSIONLESS)
C
C                            INTERFACE
C       BE    RATIO OF CHARACTERISTIC TRANSPORT RATES FOR SEMICONDUCTOR
C          TO SOLUTION                                  (DIMENSIONLESS)
C       DEL1,DEL3    DISTANCE BETWEEN OSS AND ISS AND BETWEEN IHP AND
C          OHP                                          (DIMENSIONLESS)
C       EPSTR    PERMITTIVITY CHARACTERISTIC OF REGION BETWEEN ISS AND
C          OHP                                          (C/V-CM)
C       DEBSTR    DEBYE LENGTH CHARACTERISTIC OF REGION BETWEEN ISS AND
C          OHP                                          (CM)
C       GSC,RSC,GSOLN,RSOLN    PARAMETERS RELATING CHARGE ADSORBED ON
C          INTERFACE TO POTENTIAL CHANGES ACROSS INTERFACE
C                                                       (DIMENSIONLESS)
C       BKISS    FIXED POSITIVE CHARGE AT ISS           (DIMENSIONLESS)
C
      ANI2 = (CINT/BKCHG)**2
      EQUIL(4) = EQUIL(3)/EQUIL(1)/EQUIL(2)/ANI2
      EQUIL(6) = EQUIL(5)/EQUIL(3)
      EQUIL(7) = EQUIL(6)*EQUIL(4)
      EQUIL(10) = EQUIL(1)*EQUIL(4)
      EQUIL(11) = EQUIL(10)/EQUIL(3)
      EQUIL(12) = EQUIL(2)/EQUIL(3)
      EQUIL(13) = EQUIL(12)*EQUIL(4)
      TET = TKT/BKCHG
      DEBSC = SQRT(R*T*EPSC/FARAD**2/BKCHG)
      DEBSOL = SQRT(R*T*EPSOL/FARAD**2/CTOT)
      IF(MDIM.NE.4) GO TO 13
      RDIM(2) = VALN*RDIM(1)/CONDN/EQUIL(2)
      RDIM(12) = VALN*RDIM(1)/CONDN/EQUIL(12)
      RDIM(13) = VALN*RDIM(1)/CONDN/EQUIL(13)
         DO 16 L=1,NR
         RMOD(L) = RDIM(L)/SQRT(EQUIL(L))
   16    CONTINUE
      RATE(1) = RMOD(1)*GISS*DEBSC/DIFFE
      RATE(2) = RMOD(2)*GISS*DEBSC/DIFFH
      RATE(3) = RMOD(3)*GISS**2*DEBSC/DIFFH/BKCHG
      RATE(4) = RMOD(4)*GISS**2*DEBSC/DIFFE/BKCHG
      RATE(5) = RMOD(5)*GISS*GIHP*DEBSC/DIFFH/BKCHG
      RATE(6) = RMOD(6)*GISS*GIHP*DEBSC/DIFFE/BKCHG
      RATE(7) = RMOD(7)*GISS*GIHP*DEBSC/DIFFE/BKCHG
      RATE(8) = RMOD(8)*GIHP*DEBSOL/DIFF(3)/CTOT
      RATE(9) = RMOD(9)*GIHP*DEBSOL/DIFF(4)/CTOT
```

```
      RATE(10) = RMOD(10)*GISS*DEBSC/DIFFE
      RATE(11) = RMOD(11)*GISS*DEBSC/DIFFE
      RATE(12) = RMOD(12)*GISS*DEBSC/DIFFH
      RATE(13) = RMOD(13)*GISS*DEBSC/DIFFH
      GO TO 14
   13 CONTINUE
      RATE(1) = RDIM(1)*GISS*DEBSC/DIFFE
      RATE(2) = RDIM(2)*GISS*DEBSC/DIFFH
      RATE(3) = RDIM(3)*GISS**2*DEBSC/DIFFH/BKCHG
      RATE(4) = RDIM(4)*GISS**2*DEBSC/DIFFE/BKCHG
      RATE(5) = RDIM(5)*GISS*GIHP*DEBSC/DIFFH/BKCHG
      RATE(6) = RDIM(6)*GISS*GIHP*DEBSC/DIFFE/BKCHG
      RATE(7) = RDIM(7)*GISS*GIHP*DEBSC/DIFFE/BKCHG
      RATE(8) = RDIM(8)*GIHP*DEBSOL/DIFF(3)/CTOT
      RATE(9) = RDIM(9)*GIHP*DEBSOL/DIFF(4)/CTOT
      RATE(10) = RDIM(10)*GISS*DEBSC/DIFFE
      RATE(11) = RDIM(11)*GISS*DEBSC/DIFFE
      RATE(12) = RDIM(12)*GISS*DEBSC/DIFFH
      RATE(13) = RDIM(13)*GISS*DEBSC/DIFFH
   14 B3 = DIFF(3)/DIFF(4)
      BE = DIFFE*BKCHG*DEBSOL/DIFF(3)/CTOT/DEBSC
      BD = DIFFE/DIFFH
      SFLUX = EF*ADS*QINC/BKCHG/STK2
      DIFFL = SQRT(DIFFH/STK2)
      DELT = DEBSC/DIFFL
      ALM = DEBSC*ADS
      DEL1 = DL1/DEBSC
      DEL3 = DL3/DEBSOL
      EPSTR = EPSOL
      DEBSTR = DEBSOL
      GSC = FARAD**2*GISS*DEBSC/R/T/EPSC*DEL1
      RSC = EPSTR*DEBSTR/EPSC/DL2*DEL1
      GSOLN = FARAD**2*DEBSOL*GIHP/R/T/EPSOL*DEL3
      RSOLN = EPSTR*DEBSTR/EPSOL/DL2*DEL3
      BKISS = BKINT/GISS
C
C                          CONVERSION FACTORS
C
C        CL     CONVERTS DIMENSIONLESS ELECTRON FLUX TO UNITS OF (MA/CM2)
C        CPOT     CONVERTS DIMENSIONLESS POTENTIAL TO UNITS OF (MV)
C        CCHG     CONVERTS DIMENSIONLESS CHARGE TO UNITS OF (MICRO-C/CM2)
C
      CL = 1000.*FARAD*BKCHG*DIFFE/DEBSC
      CPOT = 1000./(FARAD/R/T)
      CCHG = 1.0E+06/(FARAD*DEBSC/R/T/EPSC)
      QII = QII/CCHG
C
C     ****************************************************************
C
    6 CONTINUE
      IF(MDIM.EQ.1) CL = 1.263E+09
```

```
      IF(MDIM.EQ.1) CPOT = 25.85
      IF(MDIM.EQ.1) CCHG = 1.621E-02
      IF(MDIM.EQ.1) COND = 0.1214
      IF(NCOUNT.EQ.0 .AND. MOPT.EQ.1) CALL OPTIM1
      IF(NCOUNT.EQ.0 .AND. MOPT.EQ.2) CALL OPTIM2
      IF(NCOUNT.EQ.0 .AND. MOPT.EQ.3) CALL OPTIM3
      READ 105,SO,CURRNT
      IF(MDIM.GT.1) SO = SO*SFLUX
C
C        PRINT INPUT PARAMETERS
C
      PRINT 195
  195 FORMAT(1H1//)
      PRINT 200
  200 FORMAT( 20X,* LIQUID-JUNCTION PHOTOVOLTAIC CELL */)
      IF(MODE.EQ.1) PRINT 201
      IF(MODE.EQ.2) PRINT 202
      IF(MSOL.EQ.0) PRINT 196
      IF(MSOL.EQ.1) PRINT 197
  196 FORMAT( * MSOL = 0      ILLUMINATION AT SEMICONDUCTOR-ELECTROLYTE I
     1NTERFACE*)
  197 FORMAT( * MSOL = 1      ILLUMINATION AT SEMICONDUCTOR-CURRENT COLLE
     1CTOR INTERFACE*)
  201 FORMAT( * MODE = 1      CURRENT SET AT BCNJ(J)*)
  202 FORMAT( * MODE = 2      POTENTIAL SET AT BCNJ(J)*)
      PRINT 203,HS,H,DSOL,DSC
  203 FORMAT( * MESH SIZE;    HS =*,F6.4,*      H =*,F6.4,/,
     1   * DEPTH;      DSOL =*,F6.2,*   DSC =*,F6.2)
      IF(SO.GT.0.) GO TO 10
      PRINT 205
  205 FORMAT( * SEMICONDUCTOR IN THE DARK*)
   10 IF(MODE.EQ.2) GO TO 20
      IF(CURRNT) 20,15,20
   15 PRINT 210
  210 FORMAT( * CELL AT OPEN CIRCUIT*)
   20 CONTINUE
      PRINT 211
  211 FORMAT( /,28X,* INPUT PARAMETERS*)
      IF(NCOUNT.EQ.0) GO TO 19
      IF(MPARAM.EQ.0) GO TO 24
   19 IF(MDIM.EQ.1) GO TO 24
      IF(MDIM.NE.4) GO TO 21
      PRINT 410
      PRINT 415,EV,ET,EC
      PRINT 416,VALN,CONDN
      PRINT 417,EGAP,EFERMI
      PRINT 411,DGADS3,DGADS4,PHIOHP,PHIOSS
  410 FORMAT( * MDIM = 4*17X* INPUT ENERGY LEVELS*/)
  411 FORMAT(* FREE ENERGY OF ADSORPTION OF SPECIES 3 AND 4 ONTO THE IHP
     1  IN J/MOLE*/* AND PHIOHP AND PHIOSS (DIMENSIONLESS)*
     2 /4(E15.4))
```

```
415 FORMAT( * LOW, INTERMEDIATE, AND HIGH ISS SITE ENERGY LEVELS IN V
   1*/3(E15.4))
416 FORMAT( * VALENCE AND CONDUCTION BAND SITE CONCENTRATIONS IN MOLES
   1/CM3*/2(E15.4))
417 FORMAT( * BAND GAP AND FERMI LEVEL IN V*/2(E15.4)/)
 21 IF(MDIM.LE.2) GO TO 22
    IF(MDIM.EQ.3) PRINT 498
    IF(MDIM.EQ.4) PRINT 499
    PRINT 500,FRACVQ,FRACTQ,FRACCQ,GV,GT,GC,GISS,GIHP,FRAC3Q,FRAC4Q,
   1   FUOIHP,SUMQ,BKINT,BKMIN
    PRINT 502,DPOT1,DPOT2,DPOT3,EX1,EX2,EX3
    PRINT 503,CELECQ,CHOLEQ,C3Q,C4Q
498 FORMAT( * MDIM = 3*13X* INPUT EQUILIBRIUM PARAMETERS*/)
499 FORMAT( /23X* EQUILIBRIUM PARAMETERS*/)
500 FORMAT( * FRACTIONAL ISS SITE CONCENTRATIONS (V, T, C)*/3(E15.4)/
   1   * DISTRIBUTION OF SITES (V, T, C)*/3(E15.4)/
   2   * TOTAL ISS AND IHP SITE CONCENTRATION (MOLES/CM2)*/2(E15.4)/
   3   * COMPUTED FRACTIONAL OCCUPATION OF IHP (3, 4, AND VACANT)*
   4    /3(E15.4)/
   5   * TOTAL CHARGE SET AT INTERFACE (MICRO-C/CM2)*/E15.4/
   6   * FIXED POSITIVE CHARGE AT ISS AND MINIMUM FIXED CHARGE (EQUIV/
   7CM2)*/2(E15.4)/)
501 FORMAT( * PROGRAM ABORTED; SURFACE CONCENTRATIONS AT IHP < ZERO*/)
502 FORMAT( * INTERFACIAL POTENTIAL DRIVING FORCES (V)*/3(E15.4)/
   1   * EXP(DPOT(1, 2, 3)FARAD/R/T)*/3(E15.4))
503 FORMAT( * OSS ELECTRON AND HOLE CONCENTRATIONS (DIMENSIONLESS)*/
   1   2(E15.4)/
   2   * OHP CONCENTRATIONS 3 AND 4 (MOLES/CM3)*/2(E15.4)/)
    IF(FRAC4Q.LE.0.) PRINT 501
    IF(FRAC4Q.LE.0.) STOP
 22 IF(NCOUNT.EQ.0) GO TO 23
    IF(MPARAM.EQ.0) GO TO 24
 23 CONTINUE
    PRINT 299
    PRINT 300
    PRINT 301,RDIM(1),RDIM(2)
    PRINT 302,RDIM(3),RDIM(4),RDIM(5),RDIM(6),RDIM(7)
    PRINT 303,RDIM(8),RDIM(9)
    PRINT 298,RDIM(10),RDIM(11),RDIM(12),RDIM(13)
    IF(MDIM.EQ.4) PRINT 297
    IF(MDIM.EQ.4) PRINT 301,RMOD(1),RMOD(2)
    IF(MDIM.EQ.4) PRINT 302,RMOD(3),RMOD(4),RMOD(5),RMOD(6),RMOD(7)
    IF(MDIM.EQ.4) PRINT 303,RMOD(8),RMOD(9)
    IF(MDIM.EQ.4) PRINT 298,RMOD(10),RMOD(11),RMOD(12),RMOD(13)
    PRINT 304
    PRINT 305,FARAD,R,T
    PRINT 306
    PRINT 307,CTOT,EPSOL,COND
    PRINT 308,(DIFF(I), I=1,4)
    PRINT 309
    PRINT 310,DIFFE,DIFFH
```

```
      PRINT 311,EPSC,BKCHG
      PRINT 312,ADS,EF,QINC
      PRINT 313,STK2,SPOSN,TKT,CINT
      PRINT 314
      PRINT 315,GIHP,GISS,BKINT
      PRINT 316,DL1,DL2,DL3
      PRINT 317
      PRINT 318,EPSTR,DEBSTR
      PRINT 319,DEBSOL,DEBSC,DIFFL
      PRINT 320
      PRINT 321,CL,CPOT,CCHG
      PRINT 322
  297 FORMAT( /* RATE CONSTANTS MODIFIED BY ENERGY DIFFERENCES*)
  298 FORMAT( * RATE CONSTANTS 10,11,12 AND 13 IN CM3/MOLE-SEC*
     1   /4(E15.4))
  299 FORMAT( * MDIM > 1*15X*  DIMENSIONAL PARAMETERS*)
  300 FORMAT( /* HETEROGENEOUS REACTION RATE CONSTANTS*)
  301 FORMAT( * RATE CONSTANTS 1 AND 2 IN CM3/MOLE-SEC*/ 2(E15.4))
  302 FORMAT( * RATE CONSTANTS 3,4,5,6, AND 7 IN CM2/MOLE-SEC*/5(E15.4))
  303 FORMAT( * RATE CONSTANTS 8 AND 9 IN 1/SEC*/2(E15.4))
  304 FORMAT( /* GENERAL PARAMETERS*)
  305 FORMAT( * FARADAYS CONSTANT IN C/EQUIV, IDEAL GAS CONSTANT IN J/MO
     1LE-K, AND TEMPERATURE*/* IN DEGREES K*/3(E15.4))
  306 FORMAT( /* SOLUTION PARAMETERS*)
  307 FORMAT( * TOTAL ION CONCENTRATION IN MOLES/CM3, PERMITTIVITY IN C/
     1V-CM, AND CONDUCTIVITY*/* IN 1/OHM-CM*/3(E15.4))
  308 FORMAT( * DIFFUSIVITIES OF ION (I) IN CM2/SEC*/4(E15.4))
  309 FORMAT( /* SEMICONDUCTOR CHARACTERISTICS*)
  310 FORMAT( * ELECTRON AND HOLE DIFFUSIVITIES IN CM2/SEC*/2(E15.4))
  311 FORMAT( * PERMITTIVITY IN C/V-CM AND BACKGROUND CHARGE IN EQUIV/CM
     13*/2(E15.4))
  312 FORMAT( * ABSORPTION COEFF. IN 1/CM, PHOTON EFFICIENCY, AND INCIDE
     1NT FLUX IN*/* MOLES/CM2-SEC*/3(E15.4))
  313 FORMAT( * HOMOGENEOUS RECOMB. RATE CONSTANTS IN 1/SEC, DIMENSIONLE
     1SS, AND MOLES/CM3*/3(E15.4)/* INTRINSIC CONCENTRATION IN MOLES/CM3
     2*/E15.4)
  314 FORMAT( /* INTERFACIAL PARAMETERS*)
  315 FORMAT( * DENSITY OF SITES AT IHP AND ISS IN MOLES/CM2*/2(E15.4)/
     1   * FIXED POSITIVE CHARGE AT ISS IN EQUIV/CM2*/E15.4)
  316 FORMAT( * DISTANCE BETWEEN OSS AND ISS, ISS AND IHP, AND IHP AND O
     1HP IN CM*/3(E15.4))
  317 FORMAT( /* CALCULATED PARAMETERS*)
  318 FORMAT( * PERMITTIVITY (C/V-CM) AND DEBYE LENGTH (CM) CHARACTERIST
     1IC OF REGION */* FROM ISS TO IHP*/2(E15.4))
  319 FORMAT( * DEBYE LENGTH IN SOLUTION AND SEMICONDUCTOR, AND MINORITY
     1 CARRIER DIFFUSION*/* LENGTH IN CM*/3(E15.4))
  320 FORMAT( /* CONVERSION FACTORS*)
  321 FORMAT( * MULTIPLY DIMENSIONLESS VARIABLE BY FACTOR TO GET CURRENT
     1 IN MA/CM2, POTENTIAL*/* IN MV AND CHARGE IN MICRO-C/CM2*/3(E15.4)
     2)
  322 FORMAT( /25X* DIMENSIONLESS GROUPS*)
```

```
 24 PRINT 240
240 FORMAT( /* SEMICONDUCTOR CHARACTERISTICS*)
    IF(MODE.EQ.1) PRINT 215, ALM,DELT,BD,SO,CURRNT
    IF(MODE.EQ.2) PRINT 216, ALM,DELT,BD,SO,CURRNT
215 FORMAT( /* ALM =*,E10.3,*,   DELT =*,E10.3,*,   BD =*,E10.3,
   1   *,   SO =*,E10.3,/,* CURRNT =*,F6.2,* MA/CM2*)
216 FORMAT( /* ALM =*,E10.3,*,   DELT =*,E10.3,*,   BD =*,E10.3,
   1   *,   SO =*,E10.3,/,* CURRNT =*,F6.2,* (POTENTIAL SET AT BCNJ(J)
   2)*)
    IF(MODE.EQ.1) CURRNT = CURRNT/CL
    IF(NCOUNT.EQ.0) GO TO 25
    IF(MPARAM.EQ.0) GO TO 35
 25 CONTINUE
    PRINT 225, SPOSN, TET, ANI2
225 FORMAT( /* SPOSN = *,E10.3,*,   TET = *,E10.3,*,   ANI2 = *,E10.3)
    PRINT 250
250 FORMAT(  /* INTERFACIAL CHARACTERISTICS*/)
       DO 30 L=1,NR
 30    PRINT 255,L,(S(I,L), I=1,NC)
255 FORMAT( * L = *I2* S(I,L) = *,13(F4.1))
    PRINT 260,(L,RATE(L),L,EQUIL(L), L=1,NR)
260 FORMAT( * RATE(*I2*)= *E10.3*   EQUIL(*I2*)= *E14.7)
    IF(MDIM.EQ.4) PRINT 261,MDIM
    IF(MDIM.EQ.3) PRINT 261,MDIM
    IF(MDIM.EQ.2) PRINT 262
261 FORMAT( * MDIM =*I2*   EQUILIBRIUM CONSTANTS CALCULATED FROM INPUT
   1 EQUILIBRIUM PARAMETERS*/)
262 FORMAT( * MDIM = 2   EQUILIBRIUM CONSTANTS ARE INPUT*)
    PRINT 265,GV,GT,GC,SI
265 FORMAT(* GV = *E10.3*   GT = *E10.3*   GC = *E10.3*   SI = *E10.3)
    PRINT 270,RSC,GSC,RSOLN,GSOLN
270 FORMAT( * RSC = *E10.3*   GSC = *E10.3*   RSOLN = *E10.3*   GSOLN
   1= *E10.3)
    PRINT 275, DEL1,DEL3,BKISS
275 FORMAT( * DEL1 = *E10.3*   DEL3 = *E10.3*   BKISS =*E10.3)
    PRINT 280
280 FORMAT( /* SOLUTION CHARACTERISTICS*/)
    PRINT 285,(I,CBULK(I),I,Z(I), I=1,4)
285 FORMAT( * CBULK(*I2*) = *E10.3*   Z(*I2*) = *F3.0)
    PRINT 290,BE,B3
290 FORMAT( * BE =*E10.3*   B3 = *E10.3)
 35 CONTINUE
    PRINT 230
230 FORMAT( //* CONVERGENCE CRITERIA *)
    RETURN
    END



    SUBROUTINE BC1(J)
```

```
C
C        SUBROUTINE FOR CALCULATION OF EQUATION COEFFICIENTS FOR THE
C        BOUNDARY CONDITIONS IN THE SOLUTION (OUTSIDE THE DIFFUSE
C        REGION).
C
      COMMON/BA/ N,NJ,A(7,7),B(7,7),C(7,250),D(7,15),G(7),X(7,7),Y(7,7)
      COMMON/SC/ PHI(250)
      COMMON/RUN/ EX,H,H2,HD2,EXH,NJJ,INDEX(7,250),KERR,ERRSUB
      COMMON/SOL/ CBULK(4),Z(4),CSOL(4,250),F(4),HS,DC(4,250),XP(4)
      COMMON/FLUX/ F3(250),F4(250)
      COMMON/SMQ/ SMQ,QI,QSL,SMQL
      COMMON/CHG/ SQL(250)
C
C        POTENTIAL SET TO ZERO
C
      G(1) = PHI(J)
      B(1,1) = -1.0
      SQL(J) = 0.
C
C        CONCENTRATIONS FOR SPECIES 1 THROUGH 4 SET TO BULK VALUES
C
         DO 5 I=1,4
         SQL(J) = SQL(J) + Z(I)*CSOL(I,J)*EXP(-Z(I)*PHI(J))*HS/3.
         XP(I) = EXP(-Z(I)*(PHI(J)+PHI(J+1))/2.)
         F(I) = -DC(I,J)*XP(I)
         G(I+1) = CSOL(I,J) - CBULK(I)*EXP(Z(I)*PHI(J))
         B(I+1,1) = CBULK(I)*Z(I)*EXP(Z(I)*PHI(J))
         B(I+1,I+1) = -1.
    5    CONTINUE
C
C        CALCULATION OF FLUX FOR SPECIES 3
C
      G(6) = F3(J) + DC(3,J)*XP(3)
      B(6,1) = Z(3)*DC(3,J)*XP(3)*0.5
      D(6,1) = Z(3)*DC(3,J)*XP(3)*0.5
      B(6,4) = XP(3)
      D(6,4) = -XP(3)
      B(6,6) = -1.0
C
C        CALCULATION OF FLUX FOR SPECIES 4
C
      G(7) = F4(J) + DC(4,J)*XP(4)
      B(7,1) = Z(4)*DC(4,J)*XP(4)*0.5
      D(7,1) = Z(4)*DC(4,J)*XP(4)*0.5
      B(7,5) = XP(4)
      D(7,5) = -XP(4)
      B(7,7) = -1.0
C
      RETURN
      END
```

```
      SUBROUTINE SOLN(J)
C
C        SUBROUTINE FOR CALCULATION OF COEFFICIENTS FOR EQUATIONS
C        GOVERNING THE SOLUTION (POISSON'S EQUATION AND MATERIAL
C        BALANCES).
C
      DIMENSION FM(4),XM(4)
      COMMON/BA/ N,NJ,A(7,7),B(7,7),C(7,250),D(7,15),G(7),X(7,7),Y(7,7)
      COMMON/SC/ PHI(250)
      COMMON/RUN/ EX,H,H2,HD2,EXH,NJJ,INDEX(7,250),KERR,ERRSUB
      COMMON/SOL/ CBULK(4),Z(4),CSOL(4,250),F(4),HS,DC(4,250),XP(4)
      COMMON/FLUX/ F3(250),F4(250)
      COMMON/SMQ/ SMQ,QI,QSL,SMQL
      COMMON/CHG/ SQL(250)
C
C        POISSON'S EQUATION
C
      G(1) = PHI(J+1) - 2.*PHI(J) + PHI(J-1)
      A(1,1) = -1.
      B(1,1) = 2.
      D(1,1) = -1.
      BIG = ABS(2.*PHI(J))
      SQL(J) = 0.
         DO 10 I=1,4
         GCON = (HS**2)*Z(I)*CSOL(I,J)*EXP(-Z(I)*PHI(J))
         SQL(J) = SQL(J) + GCON/HS/3.
         G(1) = G(1) + GCON
         IF(ABS(GCON).GT.BIG) BIG = ABS(GCON)
         B(1,1) = B(1,1) + (HS**2)*CSOL(I,J)*EXP(-Z(I)*PHI(J))*Z(I)**2
         B(1,I+1) = -(HS**2)*Z(I)*EXP(-Z(I)*PHI(J))
         XM(I) = XP(I)
         XP(I) = EXP(-Z(I)*((PHI(J)+PHI(J+1))/2.
     1      - (PHI(J+1) - 2.*PHI(J) + PHI(J-1))/8.))
         IF(I.GE.3) GO TO 10
         FM(I) = F(I)
         F(I) = -DC(I,J)*XP(I)
C
C        CONTINUITY OF FLUX FOR SPECIES 1 AND 2
C
         G(I+1) = FM(I) - F(I)
         A(I+1,1) = Z(I)*FM(I)*0.750 + Z(I)*F(I)*0.125
         B(I+1,1) = Z(I)*FM(I)*0.375 - Z(I)*F(I)*0.750
         D(I+1,1) = -Z(I)*F(I)*0.375
         A(I+1,I+1) = -XM(I)
         B(I+1,I+1) = XP(I) - A(I+1,I+1)
         D(I+1,I+1) = -XP(I)
   10    CONTINUE
C
C        CONTINUITY OF FLUX FOR SPECIES 3
C
      G(4) = F3(J-1) - F3(J)
```

```
      A(4,6) = -1.0
      B(4,6) = 1.0
C
C        CONTINUITY OF FLUX FOR SPECIES 4
C
      G(5) = F4(J-1) - F4(J)
      A(5,7) = -1.0
      B(5,7) = 1.0
C
C        CALCULATION OF FLUX FOR SPECIES 3
C
      G(6) = F3(J) + DC(3,J)*XP(3)
      A(6,1) = -Z(3)*DC(3,J)*XP(3)*0.125
      B(6,1) = Z(3)*DC(3,J)*XP(3)*0.750
      D(6,1) = Z(3)*DC(3,J)*XP(3)*0.375
      B(6,4) = XP(3)
      D(6,4) = -XP(3)
      B(6,6) = -1.0
C
C        CALCULATION OF FLUX FOR SPECIES 4
C
      G(7) = F4(J) + DC(4,J)*XP(4)
      A(7,1) = -Z(4)*DC(4,J)*XP(4)*0.125
      B(7,1) = Z(4)*DC(4,J)*XP(4)*0.750
      D(7,1) = Z(4)*DC(4,J)*XP(4)*0.375
      B(7,5) = XP(4)
      D(7,5) = -XP(4)
      B(7,7) = -1.0
C
      IF(ABS(G(1)).LE.BIG*ERRSUB) G(1) = 0.
      RETURN
      END



      SUBROUTINE INTRFC(J)
C
C        SUBROUTINE FOR CALCULATION OF COEFFICIENTS FOR EQUATIONS
C        GOVERNING THE SEMICONDUCTOR-SOLUTION INTERFACE. THE EQUATIONS
C        GOVERNING THE INNER HELMHOLTZ PLANE, THE INNER SURFACE STATES,
C        AND THE OUTER SURFACE STATES ARE WRITTEN HERE.
C
      DIMENSION IE(28)
      COMMON/BA/ N,NJ,A(7,7),B(7,7),C(7,250),D(7,15),G(7),X(7,7),Y(7,7)
      COMMON/LI/ AA(28,28),BB(28,28),CC(28,1),DD(28,28),GG(28)
      COMMON/LI2/ AM(28,28),BM(28,28),DM(28,28),GM(28)
      COMMON/SC/ PHI(250),P(250),AN(250),DFN(250),DFP(250),FN(250),
     1   FP(250),RHO(250),D2(250)
      COMMON/RUN/ EX,H,H2,HD2,EXH,NJJ,INDEX(7,250),KERR,ERRSUB
      COMMON/IN/ ALM,DELT,BD,SO,CURRNT,QII,SPOSN,TET,ANI2,DSC,DSOL,MSOL
```

```
      COMMON/IN2/ BE,B3,RSC,GSC,RSOLN,GSOLN,GV,GT,GC,SI,DEL1,DEL3
      COMMON/SOL/ CBULK(4),Z(4),CSOL(4,250),F(4),HS,DC(4,250),XP(4)
      COMMON/FLUX/ F3(250),F4(250)
      COMMON/IFC/ RATE(13),EQUIL(13),S(13,13),CONC(13),RXN(13),RXS(13)
     1   ,CIF(5)
      COMMON/IFC2/ PHISS,PHISC,PHIHP,BKISS
      COMMON/CHG/ SQL(250)
      COMMON/SMQ/ SMQ,QI,QSL,SMQL
      ERRSUB = 1.0E-09
      NR = 13
      NC = 13
      NP = 28
      NE = N+1
      J = J+1
      EXDIF1 = EXP((PHI(J)-PHISC)/2.)
      EXDIF2 = EXP((PHISS-PHIHP)/2.)
      EXDIF3 = EXP((PHIHP-PHI(J-1))/2.)
      CONC(1) = AN(J)*EXP(PHI(J))
      CONC(2) = P(J)*EXP(-PHI(J))
      CONC(3) = CIF(1)
      CONC(5) = CIF(2)
      CONC(7) = CIF(3)
      CONC(9) = CIF(4)
      CONC(10) = CIF(5)
      CONC(12) = CSOL(3,J-1)*EXP(-Z(3)*PHI(J-1))
      CONC(13) = CSOL(4,J-1)*EXP(-Z(4)*PHI(J-1))
         DO 50 L=1,NR
         RLB = RATE(L)
         RLF = RLB*EQUIL(L)
            DO 25 I=1,NC
            IF(S(I,L)) 5,25,15
 5          IF(CONC(I).GT.0.) GO TO 10
            RLB = 0.
            GO TO 25
10          RLB = RLB*CONC(I)**(-S(I,L))
            GO TO 25
15          IF(CONC(I).GT.0.) GO TO 20
            RLF = 0.
            GO TO 25
20          RLF = RLF*CONC(I)**(S(I,L))
25       CONTINUE
         IF(L.GT.1) GO TO 27
         RLB = RLB*EXDIF1
         RLF = RLF/EXDIF1
         GO TO 45
27       IF(L.GT.2) GO TO 30
         RLB = RLB/EXDIF1
         RLF = RLF*EXDIF1
         GO TO 45
30       IF(L.LE.4) GO TO 45
         IF(L.GT.7) GO TO 35
```

```
      RLB = RLB*EXDIF2
      RLF = RLF/EXDIF2
      GO TO 45
35    IF(L.EQ.8) I = 3
      IF(L.EQ.9) I = 4
      IF(L.GT.9) GO TO 37
      RLB = RLB*EXDIF3**(-Z(I))
      RLF = RLF/EXDIF3**(-Z(I))
      GO TO 45
37    IF(L.GT.11) GO TO 38
      RLB = RLB*EXDIF1
      RLF = RLF/EXDIF1
      GO TO 45
38    RLB = RLB/EXDIF1
      RLF = RLF*EXDIF1
45    RXS(L) = RLF + RLB
50    CONTINUE
   IF(MSOL.EQ.0) EX = SO*EXP(-ALM*H/4.)
   IF(MSOL.EQ.1) EX = SO*EXP(-ALM*H*(FLOAT(NJ)-FLOAT(J)+0.25))
   ANQ = (3.*AN(J) + AN(J+1))/4.
   PQ = (3.*P(J) + P(J+1))/4.
   EXJ = EXP(-(3.*PHI(J) + PHI(J+1))/4.)
   DEN = ANQ/EXJ + SPOSN*PQ*EXJ + TET
   HD2 = HD2/2.
   REC = (ANQ*PQ - ANI2)/DEN
      DO 60 I=1,NP
      IE(I)=0
      GG(I) = 0.
         DO 60 K=1,NP
         AA(I,K) = 0.
         BB(I,K) = 0.
         DD(I,K) = 0.
60    CONTINUE
   FLJ = P(J)*EXP(-PHI(J))
   FLJP1 = P(J+1)*EXP(-PHI(J+1))
   FLJPH = SQRT(FLJ*FLJP1)
   GLJ = AN(J)*EXP(PHI(J))
   GLJP1 = AN(J+1)*EXP(PHI(J+1))
   GLJPH = SQRT(GLJ*GLJP1)
   BANQ = (GLJPH-GLJ)/ALOG(GLJPH/GLJ)
   BPQ = (FLJPH-FLJ)/ALOG(FLJPH/FLJ)
   QI = (PHI(J)-PHISC)/DEL1
   SMQ=H*(1.-(GLJP1-GLJ)/ALOG(GLJP1/GLJ)+(FLJP1-FLJ)/ALOG(FLJP1/FLJ))
C
C     POISSON'S EQUATION EVALUATED AT QUARTER-MESH POINT BETWEEN OSS
C        AND ISS
C
   GG(1) = RHO(J+1)/4. + 3.*RHO(J)/4. - 2.*((PHI(J+1)-PHI(J))/H-QI)/H
   BB(1,1) = -2./H2 - 2./H/DEL1
   DD(1,1) = 2./H2
   BB(1,6) = -3./4.
```

```
      DD(1,6) = -1./4.
      BB(1,13) = 2./H/DEL1
C
C        CONTINUITY OF ELECTICAL CURRENT
C
      GG(2) = (FP(J)-FP(J+1))/BD - FN(J)+FN(J+1)
      BB(2,4) = -1./BD $ DD(2,4) = 1./BD
      BB(2,5) = 1.     $ DD(2,5) = -1.
C
C        MATERIAL BALANCE OF HOLES AT QUARTER-MESH POINT BETWEEN OSS AND
C           ISS
C
      EPS = DEN*(EX-(FP(J+1)-FP(J))/HD2)/ANI2
      IF(ABS(EPS).GT.0.2) GO TO 2100
      REM = ALOG(1+EPS)
      GG(3) = ALOG(ANQ*PQ/ANI2) - REM
      IE(3) = 1
      BB(3,1) = 3.*EPS/(1.+EPS)/DEN*(ANQ/EXJ-SPOSN*PQ*EXJ)/4.
      DD(3,1) = EPS/(1.+EPS)/DEN*(ANQ/EXJ-SPOSN*PQ*EXJ)/4.
      BB(3,2) = -3./ANQ/4. + 3.*EPS/(1.+EPS)/DEN/EXJ/4.
      DD(3,2) = -1./ANQ/4. + EPS/(1.+EPS)/DEN/EXJ/4.
      BB(3,3) = -3./PQ/4. + 3.*EPS/(1.+EPS)/DEN*SPOSN*EXJ/4.
      DD(3,3) = -1./PQ/4. + EPS/(1.+EPS)/DEN*SPOSN*EXJ/4.
      BB(3,4) = DEN/(1.+EPS)/ANI2/HD2
      DD(3,4) = -DEN/(1.+EPS)/ANI2/HD2
      GO TO 2101
 2100 GG(3) = HD2*(EX-REC) + FP(J) - FP(J+1)
      BB(3,1) = -3.*HD2*REC*(ANQ/EXJ-SPOSN*PQ*EXJ)/(DEN*4.)
      DD(3,1) = -HD2*REC*(ANQ/EXJ - SPOSN*PQ*EXJ)/(DEN*4.)
      BB(3,2) = 3.*HD2*(PQ - REC/EXJ)/(DEN*4.)
      DD(3,2) = BB(3,2)/3.
      BB(3,3) = 3.*HD2*(ANQ - REC*SPOSN*EXJ)/(DEN*4.)
      DD(3,3) = HD2*(ANQ - REC*SPOSN*EXJ)/(DEN*4.)
      BB(3,4) = -1. $      DD(3,4) = 1.
 2101 CONTINUE
C
C        RXN(1)   TRANSFER OF CONDUCTION-BAND ELECTRONS TO HIGH-ENERGY
C                 ISS SITES
C
      EPS = RXN(1)/CONC(7)/EXDIF1/RATE(1)
      IF(ABS(EPS).GT.0.01) GO TO 2015
      REM = ALOG(1.+EPS)
      IF(ABS(REM).LT.1.0E-09) REM = EPS*(1.-EPS*(.5-EPS*(1./3.-EPS/4.)))
      GG(4) = ALOG(EQUIL(1)*CONC(1)*CONC(8)/CONC(7)/EXDIF1**2)
     1   -REM
      IE(4) = 1
      BB(4,1) = -1./(1.+EPS)*EPS/2.
      BB(4,2) = -1./AN(J)
      BB(4,10) = 1./CONC(7)+1./CONC(8)-1./(1.+EPS)*EPS/CONC(7)
      BB(4,13) = -1.0+1./(1.+EPS)*EPS/2.
      BB(4,17) = 1./(1.+EPS)/CONC(7)/EXDIF1/RATE(1)
```

```
      GO TO 2014
 2015 GG(4) = RXN(1) - RATE(1)*(EQUIL(1)*CONC(1)*CONC(8)/EXDIF1
     1    -CONC(7)*EXDIF1)
      BB(4,1) = -RXS(1)/2. + RATE(1)*EQUIL(1)*CONC(8)*CONC(1)/EXDIF1
      BB(4,2) = RATE(1)*EQUIL(1)*CONC(8)/EXDIF1*EXP(PHI(J))
      BB(4,10) = -RATE(1)*(EQUIL(1)*CONC(1)/EXDIF1 + EXDIF1)
      BB(4,13) = RXS(1)/2.
      BB(4,17) = -1.0
 2014 CONTINUE
C
C        POTENTIAL SET TO ZERO
C
      GG(5) = PHI(J) $ BB(5,1) = -1.0
C
C        CALCULATION OF CHARGE DENSITY
C
      EXG = EXP(-PHI(J))
      EPS = RHO(J) + P(J)*EXG
      IF(ABS(EPS).GT.0.2) GO TO 2310
      REM = ALOG(1.+EPS)
      IF(ABS(REM).LT.1.0E-09) REM = EPS*(1.-EPS*(.5-EPS*(1./3.-EPS/4.)))
      GG(6) = PHI(J) + ALOG(AN(J)) - REM
      IE(6) = 1
      BB(6,1) = -1. - P(J)*EXG/(1.+EPS)
      BB(6,2) = -1./AN(J)
      BB(6,3) = 1./(1.+EPS)*EXG
      BB(6,6) = 1./(1.+EPS)
      GO TO 2311
 2310 GG(6) = 1.-AN(J)/EXG+P(J)*EXG + RHO(J)
      BB(6,1) = P(J)*EXG+AN(J)/EXG
      BB(6,2) = 1.0/EXG
      BB(6,3) = -EXG
      BB(6,6) = -1.0
 2311 CONTINUE
C
C        POISSON'S EQUATION EVALUATED AT IHP
C
      GG(7) = RSOLN*(PHISS-PHIHP) - PHIHP+PHI(J-1)
     1   +GSOLN*(CONC( 9)*Z(3) + CONC(10)*Z(4))
      AA(7,1) = -1.
      BB(7,7) = 1.+RSOLN
      BB(7,11) = -GSOLN*Z(3)
      BB(7,12) = -GSOLN*Z(4)
      BB(7,27) = -RSOLN
C
C        CONTINUITY OF HOLE FLUX
C
      GG(8) = FP(J)/H + RXN(2) + RXN(12) + RXN(13)
      BB(8,4) = -1./H
      BB(8,18) = -1.0
      BB(8,25) = -1.0
```

```
      BB(8,26) = -1.0
C
C        MATERIAL BALANCE FOR INTERMEDIATE ENERGY LEVEL ISS ELECTRONS
C
      GG(9) = (-RXN(12) + RXN(3))/BD + RXN(4) + RXN(10) - RXN(6)
      BB(9,14) = 1.0
      BB(9,19) = -1.0/BD
      BB(9,20) = -1.0
      BB(9,23) = -1.0
      BB(9,25) = 1.0/BD
C
C        MATERIAL BALANCE FOR HIGH ENERGY LEVEL ISS ELECTRONS
C
      GG(10) = -RXN(13)/BD + RXN(1) + SI*SO - RXN(4) - RXN(7)
      BB(10,17) = -1.0
      BB(10,20) = 1.0
      BB(10,22) = 1.0
      BB(10,26) = 1.0/BD
C
C        MATERIAL BALANCE FOR ADSORBED SPECIES 3 AT IHP
C
      GG(11) = RXN(8) + S(9,5)*BE*(RXN(5)/BD + RXN(6) + RXN(7))
      BB(11,14) = -S(9,5)*BE
      BB(11,15) = -1.0
      BB(11,21) = -S(9,5)*BE/BD
      BB(11,22) = -S(9,5)*BE
C
C        MATERIAL BALANCE FOR ADSORBED SPECIES 4 AT IHP
C
      GG(12) = RXN(9) - B3*BE*(RXN(5)/BD + RXN(6) + RXN(7))
      BB(12,14) = B3*BE
      BB(12,16) = -1.0
      BB(12,21) = B3*BE/BD
      BB(12,22) = B3*BE
C
C        CONTINUITY OF ELECTRON FLUX
C
      GG(13) = FN(J)/H + RXN(1) + RXN(10) + RXN(11)
      BB(13,5) = -1./H
      BB(13,17) = -1.0
      BB(13,23) = -1.0
      BB(13,24) = -1.0
C
C        RXN(6)   CHARGE-TRANSFER WITH INTERMEDIATE ENERGY ISS ELECTRONS
C
      EPS = RXN(6)/CONC(10)/CONC(6)/EXDIF2/RATE(6)
      IF(ABS(EPS).GT.0.2) GO TO 2013
      REM = ALOG(1.+EPS)
      IF(ABS(REM).LT.1.0E-09) REM=EPS*(1.-EPS*(.5-EPS*(1./3.-EPS/4.)))
      GG(14) = ALOG(EQUIL(6)*CONC(5)*S(9,6)*CONC(9)/CONC(10)/CONC(6)/
     1   EXDIF2**2) - REM
```

```
      IE(14) = 1
      BB(14,27) = 1.0-1./(1.+EPS)*EPS/2.
      BB(14,7) = -1.0+1./(1.+EPS)*EPS/2.
      BB(14,9) = -1./CONC(5)-1./CONC(6)+1./(1.+EPS)*EPS/CONC(6)
      BB(14,11) = -1./CONC(9)
      BB(14,12) = 1./CONC(10)-1./(1.+EPS)*EPS/CONC(10)
      BB(14,14) = 1./(1.+EPS)/CONC(10)/CONC(6)/EXDIF2/RATE(6)
      GO TO 2012
 2013 GG(14) = RXN(6) - RATE(6)*(EQUIL(6)*CONC(5)*S(9,6)*CONC(9)/EXDIF2
     1   - CONC(10)*CONC(6)*EXDIF2)
      BB(14,7) = RXS(6)/2.
      BB(14,9) = RATE(6)*(EQUIL(6)*S(9,6)*CONC(9)/EXDIF2 +
     1   CONC(10)*EXDIF2)
      BB(14,11) = RATE(6)*EQUIL(6)*S(9,6)*CONC(5)/EXDIF2
      BB(14,12) = -RATE(6)*CONC(6)*EXDIF2
      BB(14,14) = -1.0
      BB(14,27) = -RXS(6)/2.
 2012 CONTINUE
C
C        RXN(8)   ADSORPTION OF SPECIES 3 TO IHP
C
      EPS = RXN(8)*EXDIF3**(Z(3))/RATE(8)/CONC(11)/CONC(12)
      IF(ABS(EPS).GT.0.2) GO TO 2001 $ REM = ALOG(1.0+EPS)
      IF(ABS(REM).LT.1.0E-9) REM = EPS*(1.-EPS*(.5-EPS*(1./3.-EPS/4.)))
      GG(15)= ALOG(EQUIL(8)*CONC(9)*EXDIF3**(2.*Z(3))/CONC(11)/CONC(12))
     1   -REM
      IE(15) = 1
      AA(15,1) = 1.0/(1.0+EPS)*EPS*Z(3)/2.0
      BB(15,7) = -Z(3) + 1.0/(1.0+EPS)*EPS*Z(3)/2.0
      BB(15,11) = -1.0/CONC(9)
      BB(15,28) = 1.0/CONC(11)-1.0/(1.0+EPS)*EPS/CONC(11)
      AA(15,4) = 1.0/CSOL(3,J-1)-1.0/(1.0+EPS)*EPS/CSOL(3,J-1)
      BB(15,15) = 1.0/(1.0+EPS)*EXDIF3**(Z(3))/RATE(8)/CONC(11)/CONC(12)
      GO TO 2000
 2001 GG(15) = RXN(8) - RATE(8)*(EQUIL(8)*CONC(9)/EXDIF3**(-Z(3))
     1   - CONC(11)*CONC(12)*EXDIF3**(-Z(3)))
      AA(15,1) = -Z(3)*(RXS(8)/2. - RATE(8)*CONC(11)*CONC(12)*EXDIF3**
     1   (-Z(3)))
      AA(15,4) = -RATE(8)*CONC(11)*EXP(-Z(3)*PHI(J-1))*EXDIF3**(-Z(3))
      BB(15,7) = Z(3)*RXS(8)/2.
      BB(15,11) = RATE(8)*EQUIL(8)/EXDIF3**(-Z(3))
      BB(15,15) = -1.0
      BB(15,28) = -RATE(8)*CONC(12)*EXDIF3**(-Z(3))
 2000 CONTINUE
C
C        RXN(9)   ADSORPTION OF SPECIES 4 TO IHP
C
      EPS = RXN(9)*EXDIF3**(Z(4))/RATE(9)/CONC(11)/CONC(13)
      IF(ABS(EPS).GT.0.2) GO TO 2007
      REM = ALOG(1.0+EPS)
      IF(ABS(REM).LT.1.0E-09) REM = EPS*(1.-EPS*(.5-EPS*(1./3.-EPS/4.)))
```

```
      GG(16)=ALOG(EQUIL(9)*CONC(10)*EXDIF3**(2.*Z(4))/CONC(11)/CONC(13))
     1   -REM
      IE(16) = 1
      AA(16,1) = 1.0/(1.0+EPS)*EPS*Z(4)/2.0
      BB(16,7) = -Z(4) + 1.0/(1.0+EPS)*EPS*Z(4)/2.0
      BB(16,28) = 1.0/CONC(11)-1.0/(1.0+EPS)*EPS/CONC(11)
      BB(16,12) = -1.0/CONC(10)
      BB(16,16) = 1.0/(1.0+EPS)*EXDIF3**(Z(4))/RATE(9)/CONC(11)/CONC(13)
      AA(16,5) = 1.0/CSOL(4,J-1)-1.0/(1.0+EPS)*EPS/CSOL(4,J-1)
      GO TO 2006
 2007 GG(16) = RXN(9) - RATE(9)*(EQUIL(9)*CONC(10)/EXDIF3**(-Z(4))
     1    - CONC(11)*CONC(13)*EXDIF3**(-Z(4)))
      AA(16,1) = -Z(4)*(RXS(9)/2. - RATE(9)*CONC(11)*CONC(13)*EXDIF3**
     1   (-Z(4)))
      AA(16,5) = -RATE(9)*CONC(11)*EXP(-Z(4)*PHI(J-1))*EXDIF3**(-Z(4))
      BB(16,7) = Z(4)*RXS(9)/2.
      BB(16,12) = RATE(9)*EQUIL(9)/EXDIF3**(-Z(4))
      BB(16,16) = -1.0
      BB(16,28) = -RATE(9)*CONC(13)*EXDIF3**(-Z(4))
 2006 CONTINUE
C
C        MATERIAL BALANCE FOR LOW ENERGY ISS ELECTRONS
C
      GG(17) = RXN(2) + SI*SO*BD + RXN(3) + RXN(5) - RXN(11)*BD
      BB(17,18) = -1.0
      BB(17,19) = -1.0
      BB(17,21) = -1.0
      BB(17,24) = BD
C
C        RXN(2)   TRANSFER OF LOW-ENERGY ELECTRONS FROM THE ISS TO THE
C                 VALENCE BAND
C
      EPS = RXN(2)/CONC(4)*EXDIF1/RATE(2)
      IF(ABS(EPS).GT.0.2) GO TO 2021
      REM = ALOG(1.+EPS)
      IF(ABS(REM).LT.1.0E-09) REM = EPS*(1.-EPS*(.5-EPS*(1./3.-EPS/4.)))
      GG(18) = ALOG(EQUIL(2)*CONC(2)*CONC(3)/CONC(4)*EXDIF1**2)
     1   -REM
      IE(18) = 1
      BB(18,1) = 1./(1.+EPS)*EPS/2.
      BB(18,3) = -1./P(J)
      BB(18,8) = -1./CONC(3)-1./CONC(4)+1./(1.+EPS)*EPS/CONC(4)
      BB(18,13) = 1.0-1./(1.+EPS)*EPS/2.
      BB(18,18) = 1./(1.+EPS)/CONC(4)*EXDIF1/RATE(2)
      GO TO 2020
 2021 IF(EPS.LT.0.8) GO TO 2026
      REM = ALOG(1.0+1.0/EPS)
      IF(EPS.GT.1.E9) REM = (1.-1./EPS*(.5-1./EPS*(1./3.-.25/EPS)))/EPS
      GG(18) = ALOG(EQUIL(2)*CONC(2)*CONC(3)*RATE(2)*EXDIF1/RXN(2))-REM
      IE(18) = 2
      BB(18,1) = 0.5-0.5/(1.0+EPS)
```

```
      BB(18,3) = -1.0/P(J)
      BB(18,8) = -1.0/CONC(3)-1.0/(1.0+EPS)/CONC(4)
      BB(18,13) = 0.5+0.5/(1.0+EPS)
      BB(18,18) = 1.0/RXN(2)-1.0/RXN(2)/(1.0+EPS)
      GO TO 2020
 2026 GG(18) = RXN(2) - RATE(2)*(EQUIL(2)*CONC(2)*CONC(3)*EXDIF1
     1    - CONC(4)/EXDIF1)
      BB(18,1) = RXS(2)/2. - RATE(2)*EQUIL(2)*CONC(2)*CONC(3)*EXDIF1
      BB(18,3) = RATE(2)*EQUIL(2)*CONC(3)*EXP(-PHI(J))*EXDIF1
      BB(18,8) = RATE(2)*(EQUIL(2)*CONC(2)*EXDIF1 + 1.0/EXDIF1)
      BB(18,13) = -RXS(2)/2.
      BB(18,18) = -1.0
 2020 CONTINUE
C
C        RXN(3)   TRANSFER OF ELECTRONS FROM LOW TO INTERMEDIATE ENERGY
C                 ISS SITES
C
      EPS = RXN(3)/RATE(3)/CONC(5)/CONC(4)
      IF(ABS(EPS).GT.0.2) GO TO 2003 $ REM = ALOG(1.0+EPS)
      IF(ABS(REM).LT.1.0E-9) REM= EPS*(1.0-EPS*(0.5-EPS*(1./3.-EPS/4.)))
      GG(19) = ALOG(EQUIL(3)*CONC(3)*CONC(6)/CONC(5)/CONC(4))-REM
      IE(19) = 1
      BB(19,8) = -1.0/CONC(3)-1.0/CONC(4)+1.0/(1.0+EPS)*EPS/CONC(4)
      BB(19,9) = 1.0/CONC(5)+1.0/CONC(6)-1.0/(1.0+EPS)*EPS/CONC(5)
      BB(19,19) = 1.0/(1.0+EPS)/RATE(3)/CONC(5)/CONC(4)
      GO TO 2002
 2003 GG(19) = RXN(3) - RATE(3)*(EQUIL(3)*CONC(3)*CONC(6)
     1   - CONC(5)*CONC(4))
      BB(19,8) = RATE(3)*(EQUIL(3)*CONC(6) + CONC(5))
      BB(19,9) = -RATE(3)*(EQUIL(3)*CONC(3) + CONC(4))
      BB(19,19) = -1.0
 2002 CONTINUE
C
C        RXN(4)   TRANSFER OF ELECTRONS FROM HIGH TO INTERMEDIATE ENERGY
C                 ISS SITES
C
      EPS = RXN(4)/RATE(4)/CONC(5)/CONC(8)
      IF(ABS(EPS).GT.0.2) GO TO 2005 $ REM = ALOG(1.0+EPS)
      IF(ABS(REM).LT.1.0E-09) REM=EPS*(1.0-EPS*(0.5-EPS*(1./3.-EPS/4.)))
      GG(20) = ALOG(EQUIL(4)*CONC(7)*CONC(6)/CONC(5)/CONC(8)) - REM
      IE(20) = 1
      BB(20,9) = 1.0/CONC(5)+1.0/CONC(6)-1.0/(1.0+EPS)*EPS/CONC(5)
      BB(20,10) = -1.0/CONC(7)-1.0/CONC(8)+1.0/(1.0+EPS)*EPS/CONC(7)
      BB(20,20) = 1.0/(1.0+EPS)/RATE(4)/CONC(5)/CONC(8)
      GO TO 2004
 2005 GG(20) = RXN(4) - RATE(4)*(EQUIL(4)*CONC(7)*CONC(6)
     1   - CONC(5)*CONC(8))
      BB(20,9) = -RATE(4)*(EQUIL(4)*CONC(7) + CONC(8))
      BB(20,10) = RATE(4)*(EQUIL(4)*CONC(6) + CONC(5))
      BB(20,20) = -1.0
 2004 CONTINUE
```

```
C
C        RXN(5)   CHARGE-TRANSFER WITH LOW-ENERGY ISS ELECTRONS
C
      EPS = RXN(5)/CONC(10)/CONC(4)/EXDIF2/RATE(5)
      IF(ABS(EPS).GT.0.2) GO TO 2009
      REM = ALOG(1.+EPS)
      IF(ABS(REM).LT.1.0E-09) REM = EPS*(1.-EPS*(.5-EPS*(1./3.-EPS/4.)))
      GG(21) = ALOG(EQUIL(5)*CONC(3)*S(9,5)*CONC(9)/CONC(10)/CONC(4)/
     1   EXDIF2**2) - REM
      IE(21) = 1
      BB(21,27) = 1.0-1./(1.+EPS)*EPS/2.
      BB(21,7) = -1.0+1./(1.+EPS)*EPS/2.
      BB(21,8) = -1./CONC(3)-1./CONC(4)+1./(1.+EPS)*EPS/CONC(4)
      BB(21,11) = -1./CONC(9)
      BB(21,12) = 1./CONC(10)-1./(1.+EPS)*EPS/CONC(10)
      BB(21,21) = 1./(1.+EPS)/CONC(10)/CONC(4)/EXDIF2/RATE(5)
      GO TO 2008
 2009 GG(21) = RXN(5) - RATE(5)*(EQUIL(5)*CONC(3)*S(9,5)*CONC(9)/EXDIF2
     1   - CONC(10)*CONC(4)*EXDIF2)
      BB(21,27) = -RXS(5)/2.
      BB(21,7) = RXS(6)/2.
      BB(21,8) = RATE(5)*(EQUIL(5)*S(9,5)*CONC(9)/EXDIF2 +
     1   CONC(10)*EXDIF2)
      BB(21,11) = RATE(5)*EQUIL(5)*S(9,5)*CONC(3)/EXDIF2
      BB(21,12) = -RATE(5)*CONC(4)*EXDIF2
      BB(21,21) = -1.0
 2008 CONTINUE
C
C        RXN(7)   CHARGE-TRANSFER WITH HIGH-ENERGY ISS ELECTRONS
C
      EPS = RXN(7)/CONC(10)/CONC(8)/EXDIF2/RATE(7)
      IF(ABS(EPS).GT.0.2) GO TO 2011
      REM = ALOG(1.+EPS)
      IF(ABS(REM).LT.1.0E-09) REM = EPS*(1.-EPS*(.5-EPS*(1./3.-EPS/4.)))
      GG(22) = ALOG(EQUIL(7)*CONC(7)*S(9,7)*CONC(9)/CONC(10)/CONC(8)/
     1   EXDIF2**2) - REM
      IE(22) = 1
      BB(22,27) = 1.0-1./(1.+EPS)*EPS/2.
      BB(22,7) = -1.0+1./(1.+EPS)*EPS/2.
      BB(22,10) = -1./CONC(7)-1./CONC(8)+1./(1.+EPS)*EPS/CONC(8)
      BB(22,11) = -1./CONC(9)
      BB(22,12) = 1./CONC(10)-1./(1.+EPS)*EPS/CONC(10)
      BB(22,22) = 1./(1.+EPS)/CONC(10)/CONC(8)/EXDIF2/RATE(7)
      GO TO 2010
 2011 GG(22) = RXN(7) - RATE(7)*(EQUIL(7)*CONC(7)*S(9,7)*CONC(9)/EXDIF2
     1   - CONC(10)*CONC(8)*EXDIF2)
      BB(22,27) = -RXS(7)/2.
      BB(22,7) = RXS(7)/2.
      BB(22,10) = RATE(7)*(EQUIL(7)*S(9,7)*CONC(9)/EXDIF2 +
     1   CONC(10)*EXDIF2)
      BB(22,11) = RATE(7)*EQUIL(7)*S(9,7)*CONC(7)/EXDIF2
```

```
      BB(22,12) = -RATE(7)*CONC(8)*EXDIF2
      BB(22,22) = -1.0
 2010 CONTINUE
C
C        RXN(10)   TRANSFER OF CONDUCTION-BAND ELECTRONS TO INTERMEDIATE
C                  ENERGY ISS SITES
C
      EPS = RXN(10)/CONC(5)/EXDIF1/RATE(10)
      IF(ABS(EPS).GT.0.2) GO TO 2017
      REM = ALOG(1.+EPS)
      IF(ABS(REM).LT.1.0E-09) REM = EPS*(1.-EPS*(.5-EPS*(1./3.-EPS/4.)))
      GG(23) = ALOG(EQUIL(10)*CONC(1)*CONC(6)/CONC(5)/EXDIF1**2)
     1   -REM
      IE(23) = 1
      BB(23,1) = -1./(1.+EPS)*EPS/2.
      BB(23,2) = -1./AN(J)
      BB(23,9) = 1./CONC(5)+1./CONC(6)-1./(1.+EPS)*EPS/CONC(5)
      BB(23,13) = -1.0+1./(1.+EPS)*EPS/2.
      BB(23,23) = 1./(1.+EPS)/CONC(5)/EXDIF1/RATE(10)
      GO TO 2016
 2017 GG(23) = RXN(10) - RATE(10)*(EQUIL(10)*CONC(1)*CONC(6)/EXDIF1
     1   - CONC(5)*EXDIF1)
      BB(23,1) = -RXS(10)/2. + RATE(10)*EQUIL(10)*CONC(1)*CONC(6)/EXDIF1
      BB(23,2) = RATE(10)*EQUIL(10)*CONC(6)/EXDIF1*EXP(PHI(J))
      BB(23,9) = -RATE(10)*(EQUIL(10)*CONC(1)/EXDIF1 + EXDIF1)
      BB(23,13) = RXS(10)/2.
      BB(23,23) = -1.0
 2016 CONTINUE
C
C        RXN(11)   TRANSFER OF CONDUCTION-BAND ELECTRONS TO LOW-ENERGY
C                  ISS SITES
C
      EPS = RXN(11)/CONC(3)/EXDIF1/RATE(11)
      IF(ABS(EPS).GT.0.2) GO TO 2019
      REM = ALOG(1.+EPS)
      IF(ABS(REM).LT.1.0E-09) REM=EPS*(1.-EPS*(.5-EPS*(1./3.-EPS/4.)))
      GG(24) = ALOG(EQUIL(11)*CONC(1)*CONC(4)/CONC(3)/EXDIF1**2)
     1   -REM
      IE(24) = 1
      BB(24,1) = -1./(1.+EPS)*EPS/2.
      BB(24,2) = -1./AN(J)
      BB(24,8) = 1./CONC(3)+1./CONC(4)-1./(1.+EPS)*EPS/CONC(3)
      BB(24,13) = -1.0+1./(1.+EPS)*EPS/2.
      BB(24,24) = 1./(1.+EPS)/CONC(3)/EXDIF1/RATE(11)
      GO TO 2018
 2019 GG(24) = RXN(11) - RATE(11)*(EQUIL(11)*CONC(1)*CONC(4)/EXDIF1
     1   - CONC(3)*EXDIF1)
      BB(24,1) = -RXS(11)/2. + RATE(11)*EQUIL(11)*CONC(1)*CONC(4)/EXDIF1
      BB(24,2) = RATE(11)*EQUIL(11)*CONC(4)/EXDIF1*EXP(PHI(J))
      BB(24,8) = -RATE(11)*(EQUIL(11)*CONC(1)/EXDIF1 + EXDIF1)
      BB(24,13) = RXS(11)/2.
```

```
      BB(24,24) = -1.0
 2018 CONTINUE
C
C        RXN(12)   TRANSFER OF INTERMEDIATE-ENERGY ELECTRONS FROM THE
C                  ISS TO THE VALENCE BAND
C
      EPS = RXN(12)/CONC(6)*EXDIF1/RATE(12)
      IF(ABS(EPS).GT.0.2) GO TO 2023
      REM = ALOG(1.+EPS)
      IF(ABS(REM).LT.1.0E-09) REM = EPS*(1.-EPS*(.5-EPS*(1./3.-EPS/4.)))
      GG(25) = ALOG(EQUIL(12)*CONC(2)*CONC(5)/CONC(6)*EXDIF1**2)
     1   -REM
      IE(25) = 1
      BB(25,1) = 1./(1.+EPS)*EPS/2.
      BB(25,3) = -1./P(J)
      BB(25,9) = -1./CONC(5)-1./CONC(6)+1./(1.+EPS)*EPS/CONC(5)
      BB(25,13) = 1.0-1./(1.+EPS)*EPS/2.
      BB(25,25) = 1./(1.+EPS)/CONC(6)*EXDIF1/RATE(12)
      GO TO 2022
 2023 IF(EPS.LT.0.8) GO TO 2027
      REM = ALOG(1.0+1.0/EPS)
      IF(EPS.GT.1.E9) REM = (1.-1./EPS*(.5-1./EPS*(1./3.-.25/EPS)))/EPS
      GG(25)=ALOG(EQUIL(12)*CONC(2)*CONC(5)*RATE(12)*EXDIF1/RXN(12))-REM
      IE(25) = 2
      BB(25,1) = 0.5-0.5/(1.0+EPS)
      BB(25,3) = -1.0/P(J)
      BB(25,9) = -1.0/CONC(5)-1.0/(1.0+EPS)/CONC(6)
      BB(25,13) = 0.5+0.5/(1.0+EPS)
      BB(25,25) = 1.0/RXN(12)-1.0/RXN(12)/(1.0+EPS)
      GO TO 2022
 2027 GG(25) = RXN(12) - RATE(12)*(EQUIL(12)*CONC(2)*CONC(5)*EXDIF1
     1   - CONC(6)/EXDIF1)
      BB(25,1) = RXS(12)/2. - RATE(12)*EQUIL(12)*CONC(2)*CONC(5)*EXDIF1
      BB(25,3) = RATE(12)*EQUIL(12)*CONC(5)*EXDIF1*EXP(-PHI(J))
      BB(25,9) = RATE(12)*(EQUIL(12)*CONC(2)*EXDIF1 + 1.0/EXDIF1)
      BB(25,13) = -RXS(12)/2.
      BB(25,25) = -1.0
 2022 CONTINUE
C
C        RXN(13)   TRANSFER OF HIGH-ENERGY ELECTRONS FROM THE ISS TO THE
C                  VALENCE BAND
C
      EPS = RXN(13)/CONC(8)*EXDIF1/RATE(13)
      IF(ABS(EPS).GT.0.2) GO TO 2025
      REM = ALOG(1.+EPS)
      IF(ABS(REM).LT.1.0E-09) REM = EPS*(1.-EPS*(.5-EPS*(1./3.-EPS/4.)))
      GG(26) = ALOG(EQUIL(13)*CONC(2)*CONC(7)/CONC(8)*EXDIF1**2)
     1   -REM
      IE(26) = 1
      BB(26,1) = 1./(1.+EPS)*EPS/2.
      BB(26,3) = -1./P(J)
```

```
      BB(26,10) = -1./CONC(7)-1./CONC(8)+1./(1.+EPS)*EPS/CONC(7)
      BB(26,13) = 1.0-1./(1.+EPS)*EPS/2.
      BB(26,26) = 1./(1.+EPS)/CONC(8)*EXDIF1/RATE(13)
      GO TO 2024
 2025 IF(EPS.LT.0.8) GO TO 2028
      REM = ALOG(1.0+1.0/EPS)
      IF(EPS.GT.1.E9) REM = (1.-1./EPS*(.5-1./EPS*(1./3.-.25/EPS)))/EPS
      GG(26)=ALOG(EQUIL(13)*CONC(2)*CONC(7)*RATE(13)*EXDIF1/RXN(13))-REM
      IE(26) = 2
      BB(26,1) = 0.5-0.5/(1.0+EPS)
      BB(26,3) = -1.0/P(J)
      BB(26,10) = -1.0/CONC(7)-1.0/(1.0+EPS)/CONC(8)
      BB(26,13) = 0.5+0.5/(1.0+EPS)
      BB(26,26) = 1.0/RXN(13)-1.0/RXN(13)/(1.0+EPS)
      GO TO 2024
 2028 GG(26) = RXN(13) - RATE(13)*(EQUIL(13)*CONC(2)*CONC(7)*EXDIF1
     1   - CONC(8)/EXDIF1)
      BB(26,1) = RXS(13)/2. - RATE(13)*EQUIL(13)*CONC(2)*CONC(7)*EXDIF1
      BB(26,3) = RATE(13)*EQUIL(13)*CONC(7)*EXDIF1*EXP(-PHI(J))
      BB(26,10) = RATE(13)*(EQUIL(13)*CONC(2)*EXDIF1 + 1.0/EXDIF1)
      BB(26,13) = -RXS(13)/2.
      BB(26,26) = -1.0
 2024 CONTINUE
C
C        POISSON'S EQUATION EVALUATED AT ISS
C
      GG(27) = PHI(J)-PHISC - RSC*(PHISS-PHIHP) - GSC*(CONC(3)+CONC(5)
     1   +CONC(7)-BKISS)
      BB(27,1) = -1.
      BB(27,7) = -RSC
      BB(27,8) =  GSC
      BB(27,9) =  GSC
      BB(27,10) =  GSC
      BB(27,13) = 1.
      BB(27,27) = RSC
C
C        CALCULATION OF VACANT IHP SITES
C
      GG(28) = 1.0 - CONC(11) - CIF(4) - CIF(5)
      BB(28,11) = 1.0
      BB(28,12) = 1.0
      BB(28,28) = 1.0
C
C
      BIG = ABS(2.*PHI(J+1)/H/H)
      IF(ABS(RHO(J+1)/4.).GT.BIG) BIG = ABS(RHO(J+1)/4.)
      IF(ABS(RHO(J)*3./4.).GT.BIG) BIG = ABS(RHO(J)*3./4.)
      IF(ABS(QI/H*2.).GT.BIG) BIG = ABS(QI/H*2.)
      IF(ABS(GG(1)).LE.BIG*ERRSUB) GG(1) = 0.
C
      BIG = ABS(FP(J)/H)
```

```
      IF(ABS(RXN(2)).GT.BIG) BIG = ABS(RXN(2))
      IF(ABS(RXN(12)).GT.BIG) BIG = ABS(RXN(12))
      IF(ABS(RXN(13)).GT.BIG) BIG = ABS(RXN(13))
      IF(ABS(GG(8)).LE.BIG*ERRSUB) GG(8) = 0.
C
      BIG = ABS((-RXN(12)+RXN(3))/BD)
      IF(ABS(RXN(4)).GT.BIG) BIG = ABS(RXN(4))
      IF(ABS(RXN(10)).GT.BIG) BIG = ABS(RXN(10))
      IF(ABS(RXN(6)).GT.BIG) BIG = ABS(RXN(6))
      IF(ABS(GG(9)).LE.BIG*ERRSUB) GG(9) = 0.
C
      BIG = ABS(RXN(13)/BD)
      IF(ABS(RXN(1)).GT.BIG) BIG = ABS(RXN(1))
      IF(ABS(SI*SO).GT.BIG) BIG = ABS(SI*SO)
      IF(ABS(RXN(4)).GT.BIG) BIG = ABS(RXN(4))
      IF(ABS(RXN(7)).GT.BIG) BIG = ABS(RXN(7))
      IF(ABS(GG(10)).LE.BIG*ERRSUB) GG(10) = 0.
C
      BIG = ABS(BE*(RXN(5)/BD+RXN(6)+RXN(7)))
      IF(ABS(RXN(8)).GT.BIG) BIG = ABS(RXN(8))
      IF(ABS(GG(11)).LE.BIG*ERRSUB) GG(11) = 0.
C
      BIG = ABS(B3*BE*(RXN(5)/BD+RXN(6)+RXN(7)))
      IF(ABS(RXN(9)).GT.BIG) BIG = ABS(RXN(9))
      IF(ABS(GG(12)).LE.BIG*ERRSUB) GG(12) = 0.
C
      BIG = ABS(FN(J)/H)
      IF(ABS(RXN(1)).GT.BIG) BIG = ABS(RXN(1))
      IF(ABS(RXN(10)).GT.BIG) BIG = ABS(RXN(10))
      IF(ABS(RXN(11)).GT.BIG) BIG = ABS(RXN(11))
      IF(ABS(GG(13)).LE.BIG*ERRSUB) GG(13) = 0.
C
      BIG = ABS(SI*SO*BD)
      IF(ABS(RXN(2)).GT.BIG) BIG = ABS(RXN(2))
      IF(ABS(RXN(3)).GT.BIG) BIG = ABS(RXN(3))
      IF(ABS(RXN(5)).GT.BIG) BIG = ABS(RXN(5))
      IF(ABS(RXN(11)*BD).GT.BIG) BIG = ABS(RXN(11)*BD)
      IF(ABS(GG(17)).LE.BIG*ERRSUB) GG(17) = 0.
C
      HD2 = (H*DELT)**2
      J = J-1
         DO 1 I=1,NP
         GM(I) = 0.
            DO 1 K=1,NP
            AM(I,K) = 0.
            BM(I,K) = 0.
            DM(I,K) = 0.
    1    CONTINUE
      QSL = (PHIHP-PHI(J))/DEL3
C
C        POISSON'S EQUATION EVALUATED AT QUARTER-MESH POINT BETWEEN IHP
```

```
C           AND OHP
C
      GM(1) = HS*QSL-PHI(J)+PHI(J-1)
      AM(1,1) = -1.
      BM(1,1) = 1. + HS/DEL3
      BIG = ABS(HS*QSL)
      IF(ABS(PHI(J)).GT.BIG) BIG = ABS(PHI(J))
      HS2 = HS**2
      SQL(J) = 0.
         DO 62 I=1,4
         SQL(J) = SQL(J) + HS*Z(I)*CSOL(I,J)*EXP(-Z(I)*PHI(J))/3.
         EXJ = EXP(-Z(I)*(3.*PHI(J)+PHI(J-1))/4.)
         CQ = (3.*CSOL(I,J) + CSOL(I,J-1))/4.
         GM(1) = GM(1) + Z(I)*CQ*EXJ*(HS2)/2.0
         IF(ABS(Z(I)*CQ*EXJ*HS2/2.).GT.BIG) BIG= ABS(Z(I)*CQ*EXJ*HS2/2.)
         AM(1,1) = AM(1,1) + (Z(I)**2)*CQ*EXJ/8.*(HS2)
         BM(1,1) = BM(1,1) + (Z(I)**2)*CQ*EXJ/8.*3.*(HS2)
         AM(1,I+1) = -Z(I)*EXJ/8.*(HS2)
         BM(1,I+1) = -Z(I)*EXJ/8.*3.*(HS2)
   62    CONTINUE
      DM(1,7) = -HS/DEL3
C
C        FLUX OF SPECIES 1 SET EQUAL TO ZERO
C
      GM(2) = F(1)
      AM(2,1) = Z(1)*F(1)*0.750
      BM(2,1) = Z(1)*F(1)*0.375
      AM(2,2) = -XP(1)
      BM(2,2) = XP(1)
C
C        FLUX OF SPECIES 2 SET EQUAL TO ZERO
C
      GM(3) = F(2)
      AM(3,1) = Z(2)*F(2)*0.750
      BM(3,1) = Z(2)*F(2)*0.375
      AM(3,3) = -XP(2)
      BM(3,3) = XP(2)
C
C        FLUX OF SPECIES 3 SET EQUAL TO THE RATE OF ADSORPTION TO IHP
C
      GM(4) = F3(J)/HS + RXN(8)
      BM(4,6) = -1.0/HS
      DM(4,15) = -1.0
C
C        FLUX OF SPECIES 4 SET EQUAL TO THE RATE OF ADSORPTION TO IHP
C
      GM(5) = F4(J)/HS + RXN(9)
      BM(5,7) = -1.0/HS
      DM(5,16) = -1.0
C
C        CONTINUITY OF FLUX FOR SPECIES 3
```

```
C
      GM(6) = F3(J-1) - F3(J)
      AM(6,6) = -1.0
      BM(6,6) = 1.0
C
C        CONTINUITY OF FLUX FOR SPECIES 4
C
      GM(7) = F4(J-1) - F4(J)
      AM(7,7) = -1.0
      BM(7,7) = 1.0
C
      IF(ABS(GM(1)).LE.BIG*ERRSUB) GM(1) = 0.
C
      IF(KERR.EQ.0) GO TO 1000
      PRINT 205, (I,I=1,NP)
      PRINT 205, (IE(I),I=1,NP)
  205 FORMAT (28I2)
      PRINT 204,NP,N
      PRINT 202,(I,I=1,10)
      PRINT 201,(GG(I),I=1,NP)
      PRINT 203
      PRINT 201,(GM(I),I=1,N)
      PRINT 203
      PRINT 206,PHI(J),(CSOL(I,J),I=1,4),DC(4,J)
  206 FORMAT( 2X,6(E12.4))
  201 FORMAT( 10E8.1)
  202 FORMAT( 10(3X,I3,2X))
  203 FORMAT( /)
  204 FORMAT( /,18X,* GG(I),  I = 1,*,I3,* / GM(I),  I = 1,*,I2,/)
 1000 CONTINUE
      CALL LOCINV(NE,NP)
         DO 65 I=1,N
         G(I) = GM(I)
            DO 65 K=1,N
            A(I,K) = AM(I,K)
            B(I,K) = BM(I,K)
            D(I,K) = DM(I,K)
   65    CONTINUE
      IF(KERR.GT.0) PRINT 200,J,G(1),G(2),G(3),G(4),G(5),G(6),G(7)
  200 FORMAT( * J=*,I3,* G =*,7(E10.2))
      CALL BAND(J)
      J = J+1
         DO 70 I=1,N
         G(I) = GG(I)
            DO 70 K=1,N
            A(I,K) = AA(I,K)
            B(I,K) = BB(I,K)
            D(I,K) = DD(I,K)
   70    CONTINUE
      IF(MSOL.EQ.0) EX = SO
      ERRSUB = 1.0E-09
```

```
      RETURN
      END



      SUBROUTINE SC(J)
C
C        SUBROUTINE FOR CALCULATION OF COEFFICIENTS FOR EQUATIONS
C        GOVERNING THE SEMICONDUCTOR (POISSON'S EQUATION AND MATERIAL
C        BALANCES).
C
      COMMON/BA/ N,NJ,A(7,7),B(7,7),C(7,250),D(7,15),G(7),X(7,7),Y(7,7)
      COMMON/SC/ PHI(250),P(250),AN(250),DFN(250),DFP(250),FN(250),
     1   FP(250),RHO(250),D2(250)
      COMMON/RUN/ EX,H,H2,HD2,EXH,NJJ,INDEX(7,250),KERR,ERRSUB
      COMMON/IN/ ALM,DELT,BD,SO,CURRNT,QII,SPOSN,TET,ANI2,DSC,DSOL,MSOL
      COMMON/SMQ/ SMQ
      FLJ = P(J)*EXP(-PHI(J))
      FLJP1 = P(J+1)*EXP(-PHI(J+1))
      FLJM1 = P(J-1)*EXP(-PHI(J-1))
      GLJ = AN(J)*EXP(PHI(J))
      GLJP1 = AN(J+1)*EXP(PHI(J+1))
      GLJM1 = AN(J-1)*EXP(PHI(J-1))
      SQ=H*(1.-(GLJP1-GLJ)/ALOG(GLJP1/GLJ)+(FLJP1-FLJ)/ALOG(FLJP1/FLJ))
      SMQ = SMQ + SQ
      IF(MSOL.EQ.0) EX = EX*EXH
      IF(MSOL.EQ.1) EX = SO*EXP(-ALM*H*(FLOAT(NJ)-FLOAT(J)))
      XM=EXP(-.5*(PHI(J)+PHI(J-1))+(PHI(J+1)-2.*PHI(J)+PHI(J-1))/8.)
      EXJ = EXP(-PHI(J))
      DEN = AN(J)/EXJ+SPOSN*P(J)*EXJ+TET
C
C        CALCULATION OF CHARGE DENSITY
C
      EPS=RHO(J) + P(J)*EXJ
      IF(ABS(EPS).GT.0.2) GO TO 10
      INDEX(1,J) = 1
      REM=ALOG(1.+EPS)
      IF(ABS(REM).LT.1.0E-09) REM=EPS*(1.-EPS*(.5-EPS*(1./3.-EPS/4.)))
      G(1) = PHI(J) + ALOG(AN(J)) - REM
      B(1,1) = -1. - P(J)*EXJ/(1.+EPS)
      B(1,2) = -1./AN(J)
      B(1,3) = 1./(1.+EPS)*EXJ
      B(1,6) = 1./(1.+EPS)
      GO TO 11
   10 G(1) = 1.-AN(J)/EXJ+P(J)*EXJ + RHO(J)
      B(1,1) = P(J)*EXJ+AN(J)/EXJ
      B(1,2) = 1.0/EXJ
      B(1,3) = -EXJ
      B(1,6) = -1.0
   11 CONTINUE
```

```
C
C        CONTINUITY OF ELECTRICAL CURRENT
C
      G(2) = (FP(J)-FP(J+1))/BD-FN(J)+FN(J+1)
      B(2,5) = 1.0
      D(2,5) = -1.0
      B(2,4) = -1.0/BD
      D(2,4) = 1.0/BD
C
C        MATERIAL BALANCE FOR HOLES
C
      EPS=DEN*(EX-(FP(J+1)-FP(J))/HD2)/ANI2
      IF(ABS(EPS).GT.0.2) GO TO 20
      INDEX(3,J) = 1
      REM=ALOG(1+EPS)
      G(3) = ALOG(AN(J)*P(J)/ANI2) - REM
      B(3,1) = EPS/(1.+EPS)/DEN*(AN(J)/EXJ-SPOSN*P(J)*EXJ)
      B(3,2) = -1./AN(J) + EPS/(1.+EPS)/DEN/EXJ
      B(3,3) = -1./P(J) + EPS/(1.+EPS)/DEN*SPOSN*EXJ
      B(3,4) = DEN/(1.+EPS)/ANI2/HD2
      D(3,4) = -DEN/(1.+EPS)/ANI2/HD2
      GO TO 21
   20 REC = (AN(J)*P(J)-ANI2)/DEN
      G(3) = HD2*(EX-REC)+FP(J)-FP(J+1)
      B(3,4) = -1.0
      D(3,4) = 1.0
      B(3,1) = -HD2*REC*(AN(J)/EXJ-SPOSN*P(J)*EXJ)/DEN
      B(3,2) = HD2*(P(J)-REC/EXJ)/DEN
      B(3,3) = HD2* (AN(J)-REC*SPOSN*EXJ) /DEN
   21 CONTINUE
C
C        CALCULATION OF HOLE FLUX
C
      G(4) = FP(J)+DFP(J)*XM
      B(4,4) = -1.0
      B(4,3) = -XM
      A(4,3) = XM
      B(4,1) = DFP(J)*XM*0.75
      D(4,1) = -DFP(J)*XM*0.125
      A(4,1) = DFP(J)*XM*0.375
C
C        CALCULATION OF ELECTRON FLUX
C
      G(5) = FN(J)+DFN(J)/XM
      B(5,5) = -1.0
      B(5,2) = -1.0/XM
      A(5,2) = 1.0/XM
      B(5,1) = -DFN(J)/XM*0.75
      D(5,1) = DFN(J)/XM*0.125
      A(5,1) = -DFN(J)/XM*0.375
C
```

```
C        POISSON'S EQUATION
C
      G(6) = H2*RHO(J) - PHI(J-1) + 2.*PHI(J) - PHI(J+1)
      A(6,1) = 1.0
      B(6,1) = -2.0
      D(6,1) = 1.0
      B(6,6) = -H2
C
C        DUMMY EQUATION
C
      G(7) = D2(J) $ B(7,7) = -1.0
C
      BIG = ABS(H2*(RHO(J)))
      IF(ABS(2.*PHI(J)).GT.BIG) BIG = ABS(2.*PHI(J))
      IF(ABS(G(6)).LE.BIG*ERRSUB) G(6) = 0.
C
      RETURN
      END



      SUBROUTINE BCNJ(J)
C
C        SUBROUTINE FOR CALCULATION OF EQUATION COEFFICIENTS FOR
C        BOUNDARY CONDITIONS AT THE SEMICONDUCTOR-CURRENT COLLECTOR
C        INTERFACE.
C
      COMMON/BA/ N,NJ,A(7,7),B(7,7),C(7,250),D(7,15),G(7),X(7,7),Y(7,7)
      COMMON/SC/ PHI(250),P(250),AN(250),DFN(250),DFP(250),FN(250),
     1   FP(250),RHO(250),D2(250)
      COMMON/RUN/ EX,H,H2,HD2,EXH,NJJ,INDEX(7,250),KERR,ERRSUB
      COMMON/IN/ ALM,DELT,BD,SO,CURRNT,QII,SPOSN,TET,ANI2,DSC,DSOL,MSOL
      COMMON/M/ MODE
      IF(MSOL.EQ.0) EX = EX*EXP(-0.75*ALM*H)
      IF(MSOL.EQ.1) EX = SO*EXP(-ALM*H/4)
      XM=EXP(-.5*(PHI(J)+PHI(J-1)))
      FPP = 0.
      HD2 = HD2/2.
      ANQ = (3.*AN(J) + AN(J-1))/4.
      PQ = (3.*P(J) + P(J-1))/4.
      EXJ = EXP(-(3.*PHI(J) + PHI(J-1))/4.)
      DEN = ANQ/EXJ + PQ*EXJ*SPOSN + TET
C
C        CALCULATION OF CHARGE DENSITY
C
      EPS=RHO(J) + P(J)*EXJ
      IF(ABS(EPS).GT.0.2) GO TO 5
      INDEX(1,J) = 1
      REM=ALOG(1.+EPS)
      IF(ABS(REM).LT.1.0E-09) REM=EPS*(1.-EPS*(.5-EPS*(1./3.-EPS/4.)))
      G(1) = PHI(J) + ALOG(AN(J)) - REM
```

```
      B(1,1) = -1. - P(J)*EXJ/(1.+EPS)
      B(1,2) = -1./AN(J)
      B(1,3) = 1./(1.+EPS)*EXJ
      B(1,6) = 1./(1.+EPS)
      GO TO 6
    5 G(1) = 1.-AN(J)/EXJ+P(J)*EXJ + RHO(J)
      B(1,1) = P(J)*EXJ+AN(J)/EXJ
      B(1,2) = 1.0/EXJ
      B(1,3) = -EXJ
      B(1,6) = -1.0
    6 CONTINUE
      IF(MODE.NE.1) GO TO 10
C
C        MODE=1      CURRENT SET
C
      G(2) = CURRNT*H - FP(J)/BD + FN(J)
      B(2,4) = 1./BD $ B(2,5) = -1.0
   10 CONTINUE
C
C        MODE=2      POTENTIAL AT CURRENT COLLECTOR SET
C
      IF(MODE.NE.2) GO TO 20
      G(2) = PHI(J) - CURRNT $ B(2,1) = -1.0
   20 CONTINUE
C
C        MATERIAL BALANCE FOR HOLES EVALUATED AT QUARTER-MESH POINT
C
      EPS=DEN*(EX-(FPP-FP(J))/HD2)/ANI2
      IF(ABS(EPS).GT.0.2) GO TO 7
      INDEX(3,J) = 1
      REM=ALOG(1+EPS)
      G(3) = ALOG(ANQ*PQ/ANI2) - REM
      A(3,1) = EPS/(1.+EPS)/DEN*(ANQ/EXJ-SPOSN*PQ*EXJ)/4.
      B(3,1) = 3.*EPS/(1.+EPS)/DEN*(ANQ/EXJ-SPOSN*PQ*EXJ)/4.
      A(3,2) = -1./ANQ/4. + EPS/(1.+EPS)/DEN/EXJ/4.
      B(3,2) = -3./ANQ/4. + 3.*EPS/(1.+EPS)/DEN/EXJ/4.
      A(3,3) = -1./PQ/4. + EPS/(1.+EPS)/DEN*SPOSN*EXJ/4.
      B(3,3) = -3./PQ/4. + 3.*EPS/(1.+EPS)/DEN*SPOSN*EXJ/4.
      B(3,4) = DEN/(1.+EPS)/ANI2/HD2
      GO TO 8
    7 REC = (ANQ*PQ - ANI2)/DEN
      G(3) = HD2*(EX-REC) + FP(J) - FPP
      A(3,1) = -HD2*REC*(ANQ/EXJ-SPOSN*PQ*EXJ)/DEN/4.
      B(3,1) = -HD2*REC*(ANQ/EXJ-SPOSN*PQ*EXJ)/DEN/4.*3.
      A(3,2) = HD2*(PQ-REC/EXJ)/DEN/4.
      B(3,2) = A(3,2)*3.
      A(3,3) = HD2*(ANQ-REC*SPOSN*EXJ)/DEN/4.
      B(3,3) = HD2*(ANQ-REC*SPOSN*EXJ)/DEN/4.*3.
      B(3,4) = -1.
    8 CONTINUE
      HD2 = (H*DELT)**2
```

```
C
C        CALCULATION OF HOLE FLUX
C
      G(4) = FP(J)+DFP(J)*XM
      A(4,1) = DFP(J)*XM*0.5
      B(4,1) = DFP(J)*XM*0.5
      A(4,3) = XM
      B(4,3) = -XM
      B(4,4) = -1.0
C
C        CALCULATION OF ELECTRON FLUX
C
      G(5) = FN(J)+DFN(J)/XM
      B(5,1) = -DFN(J)/XM*0.5 $ A(5,1) = B(5,1)
      B(5,2) = -1.0/XM
      A(5,2) = 1.0/XM
      B(5,5) = -1.0
C
C        POISSON'S EQUATION EVALUATED AT QUARTER-MESH POINT
C
      G(6) = RHO(J-1)/4. + 3.*RHO(J)/4. - 2.*(QII-(PHI(J)-PHI(J-1))/H)/H
      A(6,1) = 2.0/H2
      B(6,1) = -2.0/H2
      A(6,6) = -1./4.
      B(6,6) = -3./4.
C
C        DUMMY EQUATION
C
      G(7) = D2(J) $ B(7,7) = -1.0
C
      BIG = ABS(3.*RHO(J)/4.)
      IF(ABS(2./H2*PHI(J)).GT.BIG) BIG = ABS(2./H2*PHI(J))
      IF(ABS(G(6)).LE.BIG*ERRSUB) G(6) = 0.
C
      RETURN
      END



      SUBROUTINE LOCINV(NE,NP)
C
C        SUBROUTINE FOR INVERSION OF (NP) EQUATIONS INVOLVING (NP-NE)
C        LOCAL VARIABLES (THAT APPEAR AT ONLY ONE POINT) TO (NE)
C        EQUATIONS. VALUES FOR A LOCAL VARIABLE (I) AT LOCATION (LOC)
C        CAN BE OBTAINED FROM
C
C           CC(I,LOC) = GG(I,LOC) - AA(I,K)*C(K,J-1) - BB(I,K)*C(K,J)
C
C        WHERE SUMMATION OVER SUBSCRIPT K=1,N IS IMPLIED.
C
      DIMENSION ID(28)
```

```
      COMMON/BA/ N,NJ
      COMMON/LI/ AA(28,28),BB(28,28),CC(28,1),DD(28,28),GG(28)
      COMMON/LI2/ AM(28,28),BM(28,28),DM(28,28),GM(28)
  100 FORMAT( * DETERM=0 IN SUBROUTINE LOCINV*)
          DO 10 I=NE,NP
   10     ID(I) = 0
          DO 80 NN=NE,NP
          BMAX = 1.01
             DO 40 I=NE,NP
             IF(ID(I).NE.0) GO TO 40
             BNEXT = 0.
             BTRY = 0.
                DO 30 J=NE,NP
                IF(ID(J).NE.0) GO TO 30
                IF(ABS(BB(I,J)).LE.BNEXT) GO TO 30
                BNEXT = ABS(BB(I,J))
                IF(BNEXT.LE.BTRY) GO TO 30
                BNEXT = BTRY
                BTRY = ABS(BB(I,J))
                JC = J
   30           CONTINUE
             IF(BNEXT.GE.BMAX*BTRY) GO TO 40
             BMAX = BNEXT/BTRY
             IROW = I
             JCOL = JC
   40        CONTINUE
          IF(ID(JC).EQ.0) GO TO 42
          DETERM = 0.
          PRINT 100
          RETURN
   42     ID(JCOL) = 1
          IF(JCOL.EQ.IROW) GO TO 60
   50        DO 55 J=1 ,NP
             SAVE = BB(IROW,J)
             BB(IROW,J) = BB(JCOL,J)
             BB(JCOL,J) = SAVE
             IF(J.GT.N) GO TO 55
             SAVE = AA(IROW,J)
             AA(IROW,J) = AA(JCOL,J)
             AA(JCOL,J) = SAVE
             SAVE = DD(IROW,J)
             DD(IROW,J) = DD(JCOL,J)
             DD(JCOL,J) = SAVE
   55        CONTINUE
          SAVE = GG(IROW)
          GG(IROW) = GG(JCOL)
          GG(JCOL) = SAVE
   60     F = 1./BB(JCOL,JCOL)
             DO 70 J=1 ,NP
             BB(JCOL,J) = BB(JCOL,J)*F
             IF(J.GT.N) GO TO 70
```

```
         AA(JCOL,J) = AA(JCOL,J)*F
         DD(JCOL,J) = DD(JCOL,J)*F
70       CONTINUE
      GG(JCOL) = GG(JCOL)*F
         DO 80 I=1 ,NP
         IF(I-JCOL) 75,80,75
75       F = BB(I,JCOL)
         FM = DM(I,JCOL)
         GG(I) = GG(I) - F*GG(JCOL)
         IF(I.LE.N) GM(I) = GM(I) - FM*GG(JCOL)
            DO 80 J=1 ,NP
            BB(I,J) = BB(I,J) - F*BB(JCOL,J)
            IF(J.EQ.JCOL) BB(I,J) = 0.0
            IF(I.LE.N) DM(I,J) = DM(I,J) - FM*BB(JCOL,J)
            IF(I.LE.N .AND. J.EQ.JCOL) DM(I,J) = 0.0
            IF(J.GT.N) GO TO 80
            AA(I,J) = AA(I,J) - F*AA(JCOL,J)
            DD(I,J) = DD(I,J) - F*DD(JCOL,J)
            IF(I.GT.N) GO TO 80
            BM(I,J) = BM(I,J) - FM*AA(JCOL,J)
80    CONTINUE
   RETURN
   END



   SUBROUTINE BAND(J)
   DIMENSION E(7,8,250)
   COMMON/BA/ N,NJ,A(7,7),B(7,7),C(7,250),D(7,15),G(7),X(7,7),Y(7,7)
101 FORMAT (15H DETERM=0 AT J=,I4)
   IF (J-2)  1,6,8
 1 NP1 = N + 1
   DO 2 I=1,N
   D(I,2*N+1) = G(I)
   DO 2 L=1,N
   LPN = L + N
 2 D(I,LPN) = X(I,L)
   CALL MATINV(N,2*N+1,DETERM)
   IF (DETERM)  4,3,4
 3 PRINT 101, J
 4 DO 5 K=1,N
   E(K,NP1,1) = D(K,2*N+1)
   DO 5 L=1,N
   E(K,L,1) = - D(K,L)
   LPN = L + N
 5 X(K,L) = - D(K,LPN)
   RETURN
 6 DO 7 I=1,N
   DO 7 K=1,N
   DO 7 L=1,N
 7 D(I,K) = D(I,K) + A(I,L)*X(L,K)
```

```
 8 IF (J-NJ)  11,9,9
 9 DO 10 I=1,N
   DO 10 L=1,N
   G(I) = G(I) - Y(I,L)*E(L,NP1,J-2)
   DO 10 M=1,N
10 A(I,L) = A(I,L) + Y(I,M)*E(M,L,J-2)
11 DO 12 I=1,N
   D(I,NP1) = - G(I)
   DO 12 L=1,N
   D(I,NP1) = D(I,NP1) + A(I,L)*E(L,NP1,J-1)
   DO 12 K=1,N
12 B(I,K) = B(I,K) + A(I,L)*E(L,K,J-1)
   CALL MATINV(N,NP1,DETERM)
   IF (DETERM)  14,13,14
13 PRINT 101, J
14 DO 15 K=1,N
   DO 15 M=1,NP1
15 E(K,M,J) = - D(K,M)
   IF (J-NJ)  20,16,16
16 DO 17 K=1,N
17 C(K,J) = E(K,NP1,J)
   DO 18 JJ=2,NJ
   M = NJ - JJ + 1
   DO 18 K=1,N
   C(K,M) = E(K,NP1,M)
   DO 18 L=1,N
18 C(K,M) = C(K,M) + E(K,L,M)*C(L,M+1)
   DO 19 L=1,N
   DO 19 K=1,N
19 C(K,1) = C(K,1) + X(K,L)*C(L,3)
20 RETURN
   END
```

```
   SUBROUTINE MATINV(N,M,DETERM)
   DIMENSION ID(7)
   COMMON/BA/ K,NJ,A(7,7),B(7,7),C(7,250),D(7,15)
   DETERM=1.01  $ DO 1 I=1,N
 1 ID(I)=0 $ DO 18 NN=1,N $ BMAX=1.1 $ DO 6 I=1,N
   IF(ID(I).NE.0) GOTO 6 $ BNEXT=0.0 $ BTRY=0.0 $ DO 5 J=1,N
   IF(ID(J).NE.0) GOTO 5 $ IF(ABS(B(I,J)).LE.BNEXT) GOTO 5
   BNEXT=ABS(B(I,J)) $ IF(BNEXT.LE.BTRY) GOTO 5 $ BNEXT=BTRY
   BTRY=ABS(B(I,J)) $ JC=J
 5 CONTINUE $ IF(BNEXT.GE.BMAX*BTRY) GOTO 6
   BMAX=BNEXT/BTRY $ IROW=I $ JCOL=JC
 6 CONTINUE $ IF(ID(JC).EQ.0) GOTO 8 $ DETERM=0.0 $ RETURN
 8 ID(JCOL)=1 $ IF(JCOL.EQ.IROW) GOTO 12 $ DO 10 J=1,N
   SAVE=B(IROW,J) $ B(IROW,J)=B(JCOL,J)
10 B(JCOL,J)=SAVE $ DO 11 K=1,M $ SAVE=D(IROW,K)
   D(IROW,K)=D(JCOL,K)
```

```
 11  D(JCOL,K)=SAVE
 12  F=1.0/B(JCOL,JCOL) $ DO 13 J=1,N
 13  B(JCOL,J)=B(JCOL,J)*F $ DO 14 K=1,M
 14  D(JCOL,K)=D(JCOL,K)*F $ DO 18 I=1,N $ IF(I.EQ.JCOL) GO TO 18
     F=B(I,JCOL) $ DO 16 J=1,N
 16  B(I,J)=B(I,J)-F*B(JCOL,J) $ DO 17 K=1,M
 17  D(I,K)=D(I,K)-F*D(JCOL,K)
 18  CONTINUE $ RETURN $ END



      SUBROUTINE OPTIM1
C
C         SUBROUTINE FOR DETERMINATION OF CELL DESIGN EFFECTS. THE CELL
C         INCLUDES A TRANSLUSCENT PLATE WITH THICKNESS "XGLASS" (CM)
C         AND MEAN ABSORPTION COEFFICIENT "AGLASS" (1/CM), A SOLUTION
C         DEPTH OF "XSOLN" (CM) WITH MEAN ABSORPTION COEFFICIENT "ASOLN"
C         (1/CM), AND A WIRE GRID COUNTERELECTRODE WITH ELEMENT RADIUS
C         "RCE" (CM) AND A SPACING "SPAC" (CM).
C         THE SEMICONDUCTOR IS ILLUMINATED FROM THE ELECTROLYTE SIDE.
C         THE REFLECTIVITIES OF THE AIR/GLASS INTERFACE "RHOAG,"
C         THE GLASS/ELECTROLYTE INTERFACE "RHOGS," AND THE
C         ELECTROLYTE/SEMICONDUCTOR INTERFACE "RHOSSC" ARE INCLUDED.
C         THE EFFECTIVE SOLAR FLUX, THE RATIO OF COUNTERELECTRODE TO
C         SEMICONDUCTOR AREA, AND THE ELECTROLYTIC RESISTANCE ARE
C         CALCULATED.
C
      COMMON/IN/ ALM,DELT,BD,SO,CURRNT,QII,SPOSN,TET,ANI2,DSC,DSOL,MSOL
      COMMON/IN2/ BE,B3,RSC,GSC,RSOLN,GSOLN,GV,GT,GC,SI,DEL1,DEL3
      COMMON/CONV/ CL,CPOT,CCHG,COND
      COMMON/CE/ DIST
      COMMON/OPT/ MOPT,SFLUX,ACE,RESIR
  100 FORMAT( 4(E10.3))
  105 FORMAT( 5(E10.3))
      READ 100,RCE,SPAC,XGLASS,XSOLN
      READ 105,AGLASS,ASOLN,RHOAG,RHOGS,RHOSSC
C
C        MODIFICATION OF SOLAR FLUX
C
      SFLUXO = SFLUX
      SFLUX = SFLUX*(1.-RHOAG)*EXP(-AGLASS*XGLASS)*(1.-RHOGS)
     1   *EXP(-ASOLN*XSOLN)*(1.-2.*RCE/SPAC)*(1.-RHOSSC)
      QRATIO = SFLUX/SFLUXO
      CERAT = SPAC/RCE/2.
C
C        CALCULATION OF THE RATIO OF COUNTERELECTRODE TO SEMICONDUCTOR
C        AREA
C
      PI = 3.141592654
      ACE = SPAC/2./PI/RCE
C
```

```
C         CALCULATION OF POTENTIAL DROP IN SOLUTION
C
      PG = XSOLN
      Y = DIST
      X = SPAC/2.
      NCOUNT = 0
    5 NCOUNT = NCOUNT + 1
      B = DIST + RCE
      A = SPAC/2.
      TERM1 = COSH(PI/SPAC*(Y+B)) - COS(PI/SPAC*(X+A))
      TERM2 = COSH(PI/SPAC*(Y-B)) - COS(PI/SPAC*(X+A))
      TERM3 = COSH(PI/SPAC*(Y+B)) - COS(PI/SPAC*(X-A))
      TERM4 = COSH(PI/SPAC*(Y-B)) - COS(PI/SPAC*(X-A))
      RESPT = 0.25/PI/COND*(ALOG(TERM1/TERM2) + ALOG(TERM3/TERM4))
      SUM = 0.
         DO 10 N=1,100
         FN = FLOAT(N)
         REMAIN = 0.25/PI/COND*EXP(-FN*PI*PG/SPAC)/FN
     1      *SINH(FN*PI*B/SPAC)*SINH(FN*PI*Y/SPAC)*COS(FN*PI*A/SPAC)
     2      *COS(FN*PI*X/SPAC)/COSH(FN*PI*PG/SPAC)
         SUM = SUM + REMAIN
         IF(ABS(REMAIN/SUM).LT.1.0E-06) GO TO 15
   10    CONTINUE
      PRINT 300,FN,RESPT,SUM
  300 FORMAT( //* IR CALCULATION DID NOT CONVERGE IN*,F4.0,* ITERATIONS*
     1   /* PROGRAM STOPPED*/* RESIR =*,E10.3,* SUM = *,E10.3)
      STOP
   15 IF(NCOUNT.EQ.1) RESIR = RESPT + SUM
      IF(NCOUNT.EQ.2) RESTST = RESPT + SUM
      X = SPAC/2. + RCE
      Y = DIST + RCE
      IF(NCOUNT.EQ.1) GO TO 5
      ERROR = (RESIR-RESTST)/RESIR
      PRINT 204
      PRINT 202
      PRINT 200,RCE,SPAC,XGLASS,XSOLN,CERAT
      PRINT 203
      PRINT 200,AGLASS,ASOLN,RHOAG,RHOGS,RHOSSC
      PRINT 201
      PRINT 200,QRATIO,ACE,RESIR,ERROR,FN
  203 FORMAT( // * AGLASS (1/CM),    ASOLN (1/CM),  RHO; AIR/GLASS,   GL
     1ASS/SOLN,    SOLN/SEMI*)
  202 FORMAT( // *    CE RADIUS (CM), CE SPACING (CM), XGLASS (CM),  XSO
     1LN (CM),   CERAT (L/D)*)
  201 FORMAT( // *       QRATIO,          ACE,     RESIR (OHM-CM2), (ERRO
     1R IN RESIR), ITERATION*)
  204 FORMAT( //, 26X,* OPTIMIZATION OF SYSTEM 1*)
  200 FORMAT( 1X,5(E15.5))
      RETURN
      END
```

```
      SUBROUTINE OPTIM2
C
C         SUBROUTINE FOR DETERMINATION OF CELL DESIGN EFFECTS. THE CELL
C         INCLUDES A TRANSLUSCENT PLATE WITH THICKNESS "XGLASS" (CM)
C         AND MEAN ABSORPTION COEFFICIENT "AGLASS" (1/CM), A SOLUTION
C         DEPTH OF "XSOLN" (CM) WITH MEAN ABSORPTION COEFFICIENT "ASOLN"
C         (1/CM), AND A SLOTTED SEMICONDUCTOR.
C         THE SEMICONDUCTOR IS ILLUMINATED FROM THE ELECTROLYTE SIDE.
C         THE REFLECTIVITY OF THE AIR/GLASS INTERFACE "RHOAG,"
C         THE OVER-ALL REFLECTIVITY OF THE GLASS/METAL AND
C         METAL/ELECTROLYTE INTERFACES "RHOGS," AND THE REFLECTIVITY OF
C         THE ELECTROLYTE/SEMICONDUCTOR INTERFACE "RHOSSC" ARE INCLUDED.
C         THE EFFECTIVE SOLAR FLUX, THE RATIO OF COUNTERELECTRODE TO
C         SEMICONDUCTOR AREA, AND THE ELECTROLYTIC RESISTANCE ARE
C         CALCULATED.
C
      COMMON/IN/ ALM,DELT,BD,SO,CURRNT,QII,SPOSN,TET,ANI2,DSC,DSOL,MSOL
      COMMON/IN2/ BE,B3,RSC,GSC,RSOLN,GSOLN,GV,GT,GC,SI,DEL1,DEL3
      COMMON/CONV/ CL,CPOT,CCHG,COND
      COMMON/CE/ DIST
      COMMON/OPT/ MOPT,SFLUX,ACE,RESIR
  100 FORMAT( 6(E10.3))
  105 FORMAT( 5(E10.3))
      READ 105,THICK,ABLONG,TALL,GAP,WKRES
      READ 100,AGLASS,ASOLN,RHOAG,RHOGS,RHOSSC,XGLASS
C
C        MODIFICATION OF SOLAR FLUX
C
      XSOLN = TALL
      SFLUXO = SFLUX
      SFLUX = SFLUX*(1.-RHOAG)*EXP(-AGLASS*XGLASS)*(1.-RHOGS)
     1   *EXP(-ASOLN*XSOLN)*(1.-RHOSSC)
      QRATIO = SFLUX/SFLUXO
C
C        CALCULATION OF THE RATIO OF COUNTERELECTRODE TO SEMICONDUCTOR
C        AREA
C
      ACE = ABLONG/(ABLONG+GAP)
C
C        CALCULATION OF POTENTIAL DROP IN SOLUTION
C
      RESIR = WKRES*ABLONG/COND
C
      PRINT 204
      PRINT 202
      PRINT 200,THICK,ABLONG,TALL,GAP,XGLASS
      PRINT 203
      PRINT 200,AGLASS,ASOLN,RHOAG,RHOGS,RHOSSC
      PRINT 201
      PRINT 200,QRATIO,ACE,WKRES,RESIR
  203 FORMAT( // * AGLASS (1/CM),    ASOLN (1/CM),  RHO; AIR/GLASS, GLAS
```

```
     1S/SOLN,    SOLN/SEMI*)
  202 FORMAT( // *  THICKNESS (CM),   LENGTH OF AB (CM),  HEIGHT (CM),
     1    GAP (CM), XGLASS (CM)*)
  201 FORMAT( // *        QRATIO,         ACE,          WKRES,
     1 RESIR (OHM-CM2)*)
  204 FORMAT( //, 26X,* OPTIMIZATION OF SYSTEM 4*)
  200 FORMAT( 1X,5(E15.5))
      RETURN
      END


      SUBROUTINE OPTIM3
C
C         SUBROUTINE FOR DETERMINATION OF CELL DESIGN EFFECTS.  THE CELL
C         INCLUDES A TRANSLUSCENT PLATE WITH THICKNESS "XGLASS" (CM),
C         MEAN ABSORPTION COEFFICIENT "AGLASS" (1/CM), AND RESISTIVITY
C         "RESGLS" (OHM-CM2), A SOLUTION DEPTH OF "XSOLN" (CM),
C         AND A GRID CURRENT-COLLECTOR WITH ELEMENT HALF-WIDTH
C         "RCB" (CM) AND A SPACING "SPAC" (CM).  THE SEMICONDUCTOR IS
C         ILLUMINATED FROM THE CURRENT-COLLECTOR SIDE.
C         THE REFLECTIVITIES OF THE AIR/GLASS INTERFACE "RHOAG"
C         AND THE GLASS/SEMICONDUCTOR INTERFACE "RHOGSC" ARE INCLUDED.
C         THE EFFECTIVE SOLAR FLUX, THE RATIO OF COUNTERELECTRODE TO
C         SEMICONDUCTOR AREA, AND THE ELECTROLYTIC RESISTANCE ARE
C         CALCULATED.
C
      COMMON/IN/ ALM,DELT,BD,SO,CURRNT,QII,SPOSN,TET,ANI2,DSC,DSOL,MSOL
      COMMON/IN2/ BE,B3,RSC,GSC,RSOLN,GSOLN,GV,GT,GC,SI,DEL1,DEL3
      COMMON/CONV/ CL,CPOT,CCHG,COND
      COMMON/CE/ DIST
      COMMON/OPT/ MOPT,SFLUX,ACE,RESIR
  100 FORMAT( 4(E10.3))
  105 FORMAT( 5(E10.3))
      READ 100,RCB,SPAC,XGLASS,XSOLN
      READ 100,AGLASS,RESGLS,RHOAG,RHOGSC
C
C        MODIFICATION OF SOLAR FLUX
C
      SFLUXO = SFLUX
      SFLUX = SFLUX*(1.-RHOAG)*EXP(-AGLASS*XGLASS)*(1.-RHOGSC)
     1   *(1.-RCB/SPAC)
      QRATIO = SFLUX/SFLUXO
      CERAT = SPAC/RCB
C
C        CALCULATION OF THE RATIO OF COUNTERELECTRODE TO SEMICONDUCTOR
C        AREA
C
      ACE = 1.0
C
C        CALCULATION OF POTENTIAL DROP IN SOLUTION
C
```

```
      RESSOL = XSOLN/COND
C
C        CALCULATION OF POTENTIAL DROP IN CURRENT COLLECTOR
C
      EKOEK1 = SPAC/XGLASS
      EMK1 = 0.
      PI = 3.141592654
      IF(EKOEK1.GE.1.) GO TO 19
      EK1OEK = 1./EKOEK1
      EMK = 0.
      DO 10 NCNT=1,40
      FNCNT = FLOAT(NCNT)
      EMKOLD = EMK
      EMK = 16.*EXP(-PI*EK1OEK-EMKOLD/2.-252./768.*EMKOLD**2)
      ERROR = ABS((EMK-EMKOLD)/(EMK+1.0E-10))
      IF(ERROR.LE.1.0E-08) GO TO 11
   10 CONTINUE
      PRINT 300,FNCNT,ERROR
   11 EMK1 = 1.-EMK
      GO TO 23
   19 DO 20 NCNT=1,40
      FNCNT = FLOAT(NCNT)
      EMK1OD = EMK1
      EMK1 = 16.*EXP(-PI*EKOEK1-EMK1OD/2.-252./768.*EMK1OD**2)
      ERROR = ABS((EMK1-EMK1OD)/(EMK1+1.0E-10))
      IF(ERROR.LE.1.0E-08) GO TO 21
   20 CONTINUE
      PRINT 300,FNCNT,ERROR
  300 FORMAT( * CALCULATION OF EMK1 IN SUBROUTINE OPTIM3 DID NOT CONVERG
     1E*/* IN * F4.0 * ITERATIONS (ERROR = * E10.3 *)*)
      STOP
   21 EMK = 1.-EMK1
   23 EKSPAC = EK(EMK1)
C
      U = RCB*EKSPAC/SPAC
      INDEX = 0
      IF(EMK1.LT.0.0001) GO TO 30
      EMKNEW = EMK
   25 IF(EMKNEW.GT.0.9999) GO TO 35
      INDEX = INDEX + 1
      SQTEMK = SQRT(EMKNEW)
      EMKNEW = 4.*SQTEMK/(1.+SQTEMK)**2
      PARAM1 = (1.-SQTEMK)/(1.+SQTEMK)
      UNEW = U/(1.+PARAM1)
      SNNEW = TANH(UNEW) + (1.-EMKNEW)/4./(SINH(UNEW))**2*(SINH(UNEW)
     1   *COSH(UNEW)-UNEW)
      CNNEW = 1./SINH(UNEW) - (1.-EMKNEW)/4.*TANH(UNEW)/SINH(UNEW)
     1   *(SINH(UNEW)*COSH(UNEW)-UNEW)
      DNNEW = 1./SINH(UNEW) + (1.-EMKNEW)/4.*TANH(UNEW)/SINH(UNEW)
     1   *(SINH(UNEW)*COSH(UNEW)+UNEW)
      SN = (1.+PARAM1)*SNNEW*CNNEW/DNNEW
```

```
      IF (INDEX.GE.20) GO TO 35
      GO TO 25
C
   30 SN = TANH(U) + EMK1/4./(SINH(U))**2*(SINH(U)*COSH(U)-U)
   35 EML = EMK*(SN)**2
      EKL1 = EK(EML)
      EML1 = 1.-EML
      EKL = EK(EML1)
C
      RESCB = SPAC*RESGLS*EKL1/EKL
C
      RESIR = RESSOL + RESCB


      PRINT 204
      PRINT 202
      PRINT 200,RCB,SPAC,XGLASS,XSOLN,CERAT
      PRINT 203
      PRINT 200,AGLASS,RESGLS,RHOAG,RHOGSC
      PRINT 201
      PRINT 200,QRATIO,ACE,RESSOL,RESCB,RESIR
      PRINT 205
      PRINT 200,EMK,EMK1,EKSPAC,EKOEK1
      PRINT 206
      PRINT 200,EML,EML1,EKL,EKL1
      IF (INDEX.EQ.0) GO TO 50
  203 FORMAT( // * AGLASS (1/CM), RESGLS (OHM-CM2), RHO; AIR/GLASS,   GL
     1ASS/SEMI*)
  202 FORMAT( // *    CC WIDTH (CM),  CC SPACING (CM), XGLASS (CM),  XSO
     1LN (CM),   CC RATIO (L/D)*)
  201 FORMAT( // *       QRATIO,         ACE,   RESSOL (OHM-CM2), RESCB
     1(OHM-CM2) RESIR (OHM-CM2)*)
  205 FORMAT( // *        EMK,          EMK1,           EKSPAC,       EK
     1OEK1*)
  206 FORMAT( // *        EML,          EML1,           EKL,           E
     1KL1*)
  204 FORMAT( //, 26X,* OPTIMIZATION OF SYSTEM 3*)
  200 FORMAT( 1X,5(E15.5))
      IF (INDEX.EQ.0) GO TO 50
      PRINT 220,INDEX,EMKNEW
      IF (INDEX.GE.20) PRINT 310
  310 FORMAT( * CAUTION; LANDEN SERIES DID NOT MEET SPECIFICATIONS FOR E
     1MK.*)
  220 FORMAT( /* USED LANDEN SERIES TO CALCULATE SN(UEMK);*
     1   /*    INDEX = *I4*, EMKNEW = *E15.8)
   50 CONTINUE
      RETURN
      END


      FUNCTION EK(EM1)
```

```
C
C        FUNCTION CALCULATES COMPLETE ELLIPTIC INTEGRALS OF THE FIRST
C        KIND WITH COMPLEMENTARY MODULUS AS A PARAMETER.
C
      IF(EM1.NE.0.) GO TO 10
      PRINT 200
  200 FORMAT( * PROGRAM STOPPED IN FUNCTION EK(EM1). *
     1   /* COMPLEMENTARY MODULUS EQUAL TO ZERO.*)
      STOP
   10 EK = 1.38629436112 + EM1*(0.09666344259 + EM1*(0.03590092383 +
     1   EM1*(0.03742563713 + EM1*0.01451196212)))
     2   - ALOG(EM1)*(0.5 + EM1*(0.12498593597 + EM1*(0.06880248576 +
     3   EM1*(0.03328355346 + EM1*0.00441787012))))
      RETURN
      END



      SUBROUTINE PRINT(NCOUNT)
C
C        SUBROUTINE FOR MANIPULATING AND PRINTING RESULTS OF PROGRAM
C        LJCMPY
C
      DIMENSION RXNMOD(14),CR(4)
      COMMON/SC/ PHI(250),P(250),AN(250),DFN(250),DFP(250),FN(250),
     1   FP(250)
      COMMON/RUN/ EX,H,H2,HD2,EXH,NJJ,INDEX(7,250),KERR,ERRSUB,IJ
      COMMON/IN/ ALM,DELT,BD,SO,CURRNT,QII,SPOSN,TET,ANI2
      COMMON/IN2/ BE,B3,RSC,GSC,RSOLN,GSOLN,GV,GT,GC,SI,DEL1,DEL3
      COMMON/SOL/ CBULK(4),Z(4),CSOL(4,250),F(4),HS,DC(4,250)
      COMMON/FLUX/ F3(250),F4(250)
      COMMON/IFC/ RATE(13),EQUIL(13),S(13,13),CONC(13),RXN(13),RXS(13)
     1   ,CIF(5)
      COMMON/IFC2/ PHISS,PHISC,PHIHP,BKISS
      COMMON/SMQ/ SMQ,QI,QSL,SMQL
      COMMON/CHG/ SQL(250)
      COMMON/M/ MODE,MRPRNT,MREAL
      COMMON/CONV/ CL,CPOT,CCHG,COND
      COMMON/CE/ DIST,EXCOB,NREACT,CLIM3,CLIM4
      COMMON/OPT/ MOPT,SFLUX,ACE,RESIR
      COMMON/STOP/ NSTOP
      COMMON/END/ CURAN(40),VOLT(40),VNOT(40),VWIR(40),VWCE(40)
     1   ,CHGISS(40),CHGIHP(40),CHG(40)
     2   ,POWER1(40),POWER2(40),POWER3(40),POWER4(40)
  190 FORMAT( *   J*,10X,*PHI(J)*,10X,*CSOL(I)*,10X,*CR(I)*
     1   ,6X,*F(I)/HS*, 8X,*I*)
  195 FORMAT( /* INTERFACE...*/ 15X,*PHISC*,
     1    10X,*PHISS*, 9X,*PHIHP*)
         DO 2 I=1,4
         F(I) = 0.
    2    CONTINUE
```

```
      NJ = NJJ + 1
C
C        ZPOT    LIQUID-JUNCTION VOLTAGE AT EQUILIBRIUM  (DIMENSIONLESS)
C        DIST    DISTANCE BETWEEN ELECTRODES             (CM)
C        COND    BULK ELECTROLYTE CONDUCTIVITY           (1./OHM-CM)
C        EXCOB    BUTLER-VOLMER EXCHANGE-CURRENT DENSITY FOR
C          REACTION AT COUNTERELECTRODE WITH NO MASS-TRANSFER
C          LIMITATIONS                                   (MA/CM2)
C        NREACT    NUMBER OF ELECTRONS TRANSFERED IN REACTION AT
C          COUNTERELECTRODE                              (EQUIV./MOLE)
C        CLIM3,CLIM4    MASS-TRANSFER LIMITING CURRENTS FOR SPECIES 3
C          AND 4 AT COUNTERELECTRODE                     (MA/CM2)
C        RMSC    THE RATIO OF ELECTRON CONCENTRATIONS IN THE METAL
C          CURRENT-COLLECTOR TO THAT IN THE SEMICONDUCTOR
C
      IF(NCOUNT.EQ.1) ZPOT = 45.6052*CPOT
      IF(NCOUNT.GT.1) GO TO 6
      PRINT 140
      PRINT 141,DIST,COND
      PRINT 142,EXCOB,NREACT
      PRINT 143,CLIM3,CLIM4
  140 FORMAT( /* ELECTROLYTE AND COUNTERELECTRODE CHARACTERISTICS*)
  141 FORMAT( /* DIST  =*F9.4* CM*15X*COND   =*F9.4* 1/OHM-CM*)
  142 FORMAT( * EXCOB =*F9.4* MA/CM2*11X*NREACT =*I4,5X* EQUIV./MOLE*)
  143 FORMAT( * CLIM3 =*F9.4* MA/CM2*11X*CLIM4  =*F9.4* MA/CM2*/)
    6 CONTINUE
C
C        CALCULATION OF TOTAL CELL VOLTAGE INCLUDING SEMICONDUCTOR,
C        COUNTERELECTRODE, AND SOLUTION RESISTANCE CONTRIBUTIONS.
C
      VLJ = -(PHI(NJ) - PHISC + PHISS - PHI(1))*CPOT
      IF(MODE.EQ.1) CURRENT = CURRNT*CL
      IF(MODE.EQ.2) CURRENT = (FP(IJ)/BD-FN(IJ))/H*CL
      IF(SO.NE.0.) GO TO 7
      IF(CURRENT.NE.0.) GO TO 7
      ZPOT = -VLJ
    7 VIR = DIST*CURRENT/COND
      IF(MOPT.NE.0) VIR = CURRENT*RESIR
      IJJ = IJ - 1
      C3 = -F3(IJJ)/HS/BE*CL
      C4 = -F4(IJJ)/HS/BE/B3*CL
      IF(CURRENT.EQ.0.) C3 = 0.
      IF(CURRENT.EQ.0.) C4 = 0.
      IF(MOPT.NE.0) C3 = C3*ACE
      IF(MOPT.NE.0) C4 = C4*ACE
C
      BETA = 0.50
      IF((1.+C3/CLIM3)/(1.+C4/CLIM4).LE.1.0E-10) PRINT 300
      IF((1.+C3/CLIM3)/(1.+C4/CLIM4).LE.1.0E-10) NSTOP = 1
      IF((1.+C3/CLIM3)/(1.+C4/CLIM4).LE.1.0E-10) RETURN
      ETACE = CPOT/(FLOAT(NREACT))*ALOG((1.+C3/CLIM3)/(1.+C4/CLIM4))
```

```
      DO 15 K=1,100
      GOFETA = (1.+C4/CLIM4)*EXP((1.-BETA)*FLOAT(NREACT)*ETACE/CPOT)
     1    - SQRT(1.+C3/CLIM3)*EXP(-BETA*FLOAT(NREACT)*ETACE/CPOT)
     2    + CURRENT/EXCOB
      GPRIME = (1.+C4/CLIM4)*EXP((1.-BETA)*FLOAT(NREACT)*ETACE/CPOT)
     1    *(1.-BETA)*FLOAT(NREACT)/CPOT
     2    + SQRT(1.+C3/CLIM3)*EXP(-BETA*FLOAT(NREACT)*ETACE/CPOT)
     3    *BETA*FLOAT(NREACT)/CPOT
      ETANEW = ETACE - GOFETA/GPRIME
      PRINT 1010,K,ETACE,ETANEW
      IF(ABS(ETANEW-ETACE).LT.1.0E-05) GO TO 16
      ETACE = ETANEW
 1010 FORMAT( * K=*,I4,*   ETACE=*,F12.7,*  ETANEW=*,F12.7)
   15    CONTINUE
   16 ETACE = ETANEW
C
  300 FORMAT( * COUNTERELECTRODE LIMITING CURRENT EXCEEDED*)
      RMSC = 1.
      VMSC = -CPOT*ALOG(RMSC)
      VEQ = ZPOT
      VCE = -ETACE + VEQ
      VTOT = VMSC + VLJ + VIR + VCE
      VCALC1 = VLJ + VEQ
      VCALC2 = VCALC1 + VIR
      VCALC3 = VCALC1 - ETACE
      VNOT(NCOUNT) = VCALC1
      POWER1(NCOUNT) = -VCALC1*CURRENT/100.
      VWIR(NCOUNT) = VCALC2
      POWER2(NCOUNT) = -VCALC2*CURRENT/100.
      VWCE(NCOUNT) = VCALC3
      POWER3(NCOUNT) = -VCALC3*CURRENT/100.
      VOLT(NCOUNT) = VTOT
      CURAN(NCOUNT) = -CURRENT
C
C        CALCULATION OF CHARGE DISTRIBUTION IN SEMICONDUCTOR, ISS, IHP,
C        AND SOLUTION.
C
      NI = IJ/2 - 1
      SUM = SQL(1) + SQL(2*NI+1)
         DO 3 K=1,NI
         SUM = SUM + 4.*SQL(2*K)
         IF(K.EQ.NI) GO TO 3
         SUM = SUM + 2.*SQL(2*K+1)
    3    CONTINUE
      QSL = -QSL*RSC*DEL3/RSOLN/DEL1
      SMQL = SUM*RSC*DEL3/RSOLN/DEL1
      QISS = -(CIF(1)+CIF(2)+CIF(3)-BKISS)*GSC/DEL1
      QIHP = (CIF(4)*Z(3) + CIF(5)*Z(4))*GSOLN*RSC/RSOLN/DEL1
      SUMQ = (QISS + QIHP)*CCHG
      CHGISS(NCOUNT) = QISS*CCHG
      CHGIHP(NCOUNT) = QIHP*CCHG
```

```
      CHG(NCOUNT) = SUMQ
      DPHDYZ = (4.*PHI(2)-3.*PHI(1)-PHI(3))*RSC*DEL3/RSOLN/DEL1/HS/2.
      QSL = QSL - DPHDYZ
      QISL = (PHISS - PHIHP)*RSC/DEL1
      EN1 = QI + QISS + QIHP + QSL
      EN2 = SMQ + QISS + QIHP + SMQL
      POWER = -CURRENT*VTOT/100.
      POWER4(NCOUNT) = POWER
C
C         PRINTING OF RESULTS
C
      PRINT 176,CURRENT,VTOT,SUMQ,POWER,VCALC1,VCALC2,VCALC3
      PRINT 177,QI,SMQ
      PRINT 178,QISS,QISS
      PRINT 179,QIHP,QIHP
      PRINT 180,QSL,SMQL
      PRINT 181,EN1,EN2
      PRINT 182,DPHDYZ
      PRINT 183,QISL
      PRINT 191
      PRINT 189,VMSC
      PRINT 184,VLJ
      PRINT 185,VIR
      PRINT 186,VCE
      PRINT 187,VTOT
  176 FORMAT( * CURRENT = *,F6.2,* MA/CM2;  CELL VOLTAGE = *,F6.1,* MV;
     1 SURFACE CHRG = *,E10.3,/* CHARGE IN UNITS OF MICRO-C/CM2*/
     2 * POWER DENSITY = *,F6.2,* W/M2*,/
     3 * CELL VOLTAGE (NO IR OR CE EFFECTS) = *,F6.2,* MV*/
     4 * CELL VOLTAGE (WITH IR, NO CE)      = *,F6.2,* MV*/
     4 * CELL VOLTAGE (WITH CE, NO IR)      = *,F6.2,* MV*/)
  177 FORMAT( * CHARGE IN SEMICONDUCTOR; DERIVATIVE, INTEGRAL...*2(F9.5,
     12X))
  178 FORMAT( * CHARGE ON INNER SURFACE STATES.................*F9.5,
     13X,E13.6)
  179 FORMAT( * CHARGE ON INNER HELMHOLTZ PLANE................*F9.5,
     13X,E13.6)
  180 FORMAT( * CHARGE IN SOLUTION; DERIVATIVE, INTEGRAL........*2(F9.5,
     12X))
  181 FORMAT( * OVERALL ELECTRONEUTRALITY CHECK; SUM EQUALS.....*2(F9.5,
     12X))
  182 FORMAT( /* POTENTIAL DERIVATIVE AT J=1.....................*F9.5)
  183 FORMAT( * POTENTIAL DERIVATIVE BETWEEN ISS AND IHP........*F9.5)
  191 FORMAT( /* TOTAL CELL VOLTAGE = (COUNTERELECTRODE) - (SEMICONDUCTO
     1R CURRENT-COLLECTOR)*)
  189 FORMAT( * METAL-SEMICONDUCTOR JUNCTION VOLTAGE............*F9.2
     1* MV*)
  184 FORMAT( * LIQUID-JUNCTION VOLTAGE.........................*F9.2
     1* MV*)
  185 FORMAT( * IR DROP IN SOLUTION.............................*F9.2
     1* MV*)
```

```
186 FORMAT( * COUNTERELECTRODE VOLTAGE.....................*F9.2
   1* MV*)
187 FORMAT( * TOTAL CELL VOLTAGE...........................*F9.2
   1* MV*)
    PRINT 188
188 FORMAT( //* SOLUTION...*)
    PRINT 190
    YSOL = 0.
150 FORMAT(/,I4,6X,4(E13.6,2X),I4)
155 FORMAT( 3( 25X,3(E13.6,2X),I4/))
    IL = 1
    IF(IJJ.GT.5) IL = IJJ - 1
    IF(MRPRNT.EQ.1) IL = 1
    PHIDIF = PHISS - PHISC
       DO 5 J=IL,IJJ
          DO 4 I=1,4
          CR(I) = CSOL(I,J)*EXP(-Z(I)*PHI(J))
          IF(I.GE.3) GO TO 4
          IF(J.EQ.1) GO TO 4
          IF(J.EQ.2) F(I) = -DC(I,J-1)*EXP(-Z(I)*((PHI(J-1)
   1         +PHI(J))/2.-(PHI(J-1)-2.*PHI(J)+PHI(J+1))/8.))/HS/BE
          IF(J.GT.2) F(I) = -DC(I,J-1)*EXP(-Z(I)*((PHI(J-1)
   1         +PHI(J))/2.-(PHI(J)-2.*PHI(J-1)+PHI(J-2))/8.))/HS/BE
  4       CONTINUE
       F(3) = F3(J)/HS/BE
       F(4) = F4(J)/HS/BE/B3
       I = 1
       PHIMOD = PHI(J)
       IF(MREAL.EQ.1) F(1) = F(1)*CL
       IF(MREAL.EQ.1) F(2) = F(2)*CL
       IF(MREAL.EQ.1) F(3) = F(3)*CL
       IF(MREAL.EQ.1) F(4) = F(4)*CL
       IF(MREAL.EQ.1) PHIMOD = (PHI(J) - PHIDIF - PHI(NJ))*CPOT
       PRINT 150,J,PHIMOD,CSOL(1,J),CR(1),F(1),I
       PRINT 155,(CSOL(I,J),CR(I),F(I),I, I=2,4)
       YSOL = YSOL + HS
  5    CONTINUE
     PHISCP = PHISC
     PHISSP = PHISS
     PHIHPP = PHIHP
     IF(MREAL.EQ.1) PHISCP = (PHISC - PHI(NJ))*CPOT
     IF(MREAL.EQ.1) PHISSP = PHISC
     IF(MREAL.EQ.1) PHIHPP = (PHIHP - PHIDIF - PHI(NJ))*CPOT
     PRINT 165,PHISCP,PHISSP,PHIHPP
165 FORMAT( * INTERFACE...*,/* PHISC,SS,HP = *,8X,3(E13.6,1X))
     PRINT 166,(CIF(I),I=1,5)
166 FORMAT( * CIF(I) =*,5(E13.6,1X))
     RXNMOD(1) = RXN(1)
     RXNMOD(2) = RXN(2)/BD
     RXNMOD(3) = RXN(3)/BD
     RXNMOD(4) = RXN(4)
```

```
      RXNMOD(5) = RXN(5)/BD
      RXNMOD(6) = RXN(6)
      RXNMOD(7) = RXN(7)
      RXNMOD(8) = RXN(8)/BE
      RXNMOD(9) = RXN(9)/BE/B3
      RXNMOD(10) = RXN(10)
      RXNMOD(11) = RXN(11)
      RXNMOD(12) = RXN(12)/BD
      RXNMOD(13) = RXN(13)/BD
      RXNMOD(14) = SI*SO
      IF(MREAL.NE.1) GO TO 9
         DO 9 L=1,14
         RXNMOD(L) = RXNMOD(L)*CL
    9    CONTINUE
      PRINT 167,(L,RXNMOD(L), L=1,12)
      PRINT 168,RXNMOD(13),RXNMOD(14)
  167 FORMAT( 3(* RXN(*,I2,*)=*,E13.6,2X))
  168 FORMAT( * RXN(13)=*E13.6,2X,* RXN(14)=*E13.6)
      PRINT 196
  196 FORMAT( //* SEMICONDUCTOR...*)
      PRINT 200
  200 FORMAT( *  J *,6X,*AN(J)*,10X,*P(J)*
     1,11X,*PHI(J)*,8X,*FP(J)/H*,9X,*FN(J)/H*)
      YSC = 0.
      LJ = IJ + 2
      IF(MRPRNT.EQ.1) LJ = NJ
         DO 10 J=IJ,LJ
         FPOH = FP(J)/H/BD
         FNOH = FN(J)/H
         IF(MREAL.EQ.1) FPOH = FPOH*CL
         IF(MREAL.EQ.1) FNOH = FNOH*CL
         IF(MREAL.EQ.1) PHIMOD = (PHI(J)-PHI(NJ))*CPOT
         PR = P(J)/EXP(PHI(J))
         ANR = AN(J)*EXP(PHI(J))
         IF(MREAL.EQ.1) PRINT 205,J,ANR,PR,PHIMOD,FPOH,FNOH
         IF(MREAL.EQ.0) PRINT 205,J,AN(J),P(J),PHI(J),FPOH,FNOH
         YSC = YSC + H
   10    CONTINUE
  205 FORMAT( I4,1X,5(E13.6,2X))
      IF(MREAL.EQ.0) PRINT 206
      IF(MREAL.EQ.1) PRINT 207
      IF(MREAL.EQ.1) PRINT 208
      IF(MREAL.EQ.0) PRINT 209
  206 FORMAT( * AN(J) AND P(J) ARE COMPUTER VARIABLES; PR = P(J)/EXP(PHI
     1(J))*)
  207 FORMAT( * AN(J) AND P(J) ARE REAL CONCENTRATIONS, NORMALIZED TO TH
     1E BACKGROUND CHARGE*/
     2   * POTENTIALS REFERENCED TO CURRENT-COLLECTOR   (MV)*)
  208 FORMAT( * ALL FLUXES AND REACTION RATES ARE IN UNITS OF ELECTRON F
     1LUX    (MA/CM2)*)
  209 FORMAT( * ALL FLUXES AND REACTION RATES ARE IN UNITS OF ELECTRON F
```

```
     1LUX    (DIMENSIONLESS)*)
      PRINT 210
210 FORMAT( // )
      RETURN
      END
```

```
0.2         0.2         10.0          10.0
1.00       100.0        20.0          80.0
 1
30 41 41 40
 0  0  0  1
 0  0
1
4
1.  0.   0.   0.   0.   0.   -1.  1.   0.   0.   0.   0.   0.
0.  1.   1.   -1.  0.   0.   0.   0.   0.   0.   0.   0.   0.
0.  0.   1.   -1.  -1.  1.   0.   0.   0.   0.   0.   0.   0.
0.  0.   0.   0.   -1.  1.   1.   -1.  0.   0.   0.   0.   0.
0.  0.   1.   -1.  0.   0.   0.   0.   0.5  -1.  0.   0.   0.
0.  0.   0.   0.   1.   -1.  0.   0.   0.5  -1.  0.   0.   0.
0.  0.   0.   0.   0.   0.   1.   -1.  0.5  -1.  0.   0.   0.
0.  0.   0.   0.   0.   0.   0.   0.   1.   0.   -1.  -1.  0.
0.  0.   0.   0.   0.   0.   0.   0.   0.   1.   -1.  0.   -1.
1.  0.   0.   0.   -1.  1.   0.   0.   0.   0.   0.   0.   0.
1.  0.   -1.  1.   0.   0.   0.   0.   0.   0.   0.   0.   0.
0.  1.   0.   0.   1.   -1.  0.   0.   0.   0.   0.   0.   0.
0.  1.   0.   0.   0.   0.   1.   -1.  0.   0.   0.   0.   0.
0.100E+24 1.
0.100E+24 2.
0.100E+28 3.
0.100E+28 4.
0.100E+28 5.
0.100E+28 6.
0.100E+28 7.
0.100E+22 8.
0.100E+22 9.
0.100E+24 10.
0.100E+24 11.
0.100E+24 12.
0.100E+24 13.
300.
0.002800              1.0                0.00001957
0.001000             -1.0                0.00005260
0.0001               -2.0                0.00001000
0.0008               -2.0                0.00001000
 0.693E-11 0.300E-00
 222.0                6.46
 0.106E-11 0.996E-07
 0.440E+06 3.735E-01 7.139E-07
 0.189E+13 0.100E+03 0.256E-12 0.149E-16
 0.
 0.166E-08 1.200E-13 0.000E+00
 3.334E-01 3.333E-01 3.333E-01 0.000E+00
 0.100E-07 0.200E-07 0.200E-07
 1.400E+00 1.160E-05 7.800E-07
 1.300E+00 1.400E+00 1.500E+00
 0.000E+00 0.000E+00
```

```
 5.930E-03 0.500E+00
-1.298E-01 5.828E-15
    0.0                 0.0
    1.0                 0.0
    1.0                -1.0
    1.0                -2.0
    1.0                -3.0
    1.0                -5.0
    1.0                -9.0
    1.0                -11.0
    1.0                -12.0
    1.0                -14.0
    1.0                -16.0
    1.0                -18.0
    1.0                -19.0
    1.0                -20.0
    1.0                -21.0
    1.0                -21.5
    1.0                -22.0
    1.0                -22.5
    1.0                -22.7
    1.0                -22.9
    1.0                -23.0
    1.0                -23.1
    1.0                -23.2
    1.0                -23.3
    1.0                -23.4
    1.0                -24.0
    1.0                -24.5
    1.0                -25.0
    1.0                -25.2
    1.0                -25.4
    1.0                -25.5
    1.0                -25.6
```

2. PROGRAM RCALC

This program was written to calculate the primary resistance and current distributions along the electrodes for a slotted-electrode cell. The Schwarz-Christoffel transformation is the basis of this work, and the appropriate equations are presented in Chapter 4.

Input program control parameters are defined in the main program listing. The correspondence between program variables and the variables defined in Chapter 4 is given below. A sample input data file and output are presented after the program listing.

AHGTH = $\mathrm{Re}\{C - B\}$

ALNGTH = $\mathrm{Im}\{B - A\}$

AT = a

ATOLD = initial guess for at

AZ = A

BT = b

BTOLD = initial guess for bt

BZ = B

CT = c

CTOLD = initial guess for ct

CZ = C

DT = d

DTOLD = initial guess for dt

DZ = D

GAP = $\mathrm{Im}\{-D\}$

$$\text{WIDTH} = \text{Re}\{A\}$$

```
      PROGRAM RCALC (INPUT,OUTPUT)
C
C         PROGRAM FOR CALCULATION OF PRIMARY CURRENT DISTRIBUTION
C         AND CELL RESISTANCE FOR A SLOTTED ELECTRODE ABOVE A
C         PLANAR ELECTRODE (BOTH FACING THE SAME DIRECTION) USING THE
C         SCHWARZ-CHRISTOFFEL TRANSFORMATION.
C
      DIMENSION NPEG(3)
      COMMON/TRANS/ AT,BT,CT,DT,AZI,BZI,CZI,DZI
      COMMON/TRANS2/ NATSND
      COMMON/WMAX/ WIMAX
      COMMON/CURR/ AZIMAG,BZIMAG,CZIMAG,DZIMAG,SUMAB,RESCD,MPLOT,WOVRAZ
      COMMON N,B(3,4),C(3),G(3)
      COMPLEX AZ,BZ,CZ,DZ
      COMPLEX AZWDTH,BZWDTH,CZWDTH,DZWDTH
      COMPLEX AZWANT,BZWANT,CZWANT,DZWANT
  100 FORMAT(6I3)
  102 FORMAT(4E10.3)
  200 FORMAT( //,* CALCULATION OF PRIMARY CURRENT DISTRIBUTION AND CELL
     1RESISTANCE*/* FOR A SYSTEM OF THE GENERAL SHAPE;*//,14X,*D*,
     2* _____ C*/,15X,* |*,28X,*|*,/,15X,* |*
     3,28X,*|*,/,15X,* |*,4X,*A _____|*/,15X,
     4* |*,6X,*|*,4X,*ELECTRODE AB*,7X,*B*,/,15X,* |*,6X,
     5*|_____*,/,15X,* |*,28X,*|*,/,15X,* |*,28X,*|*,/,
     615X,* |_____|*/,24X,*ELECTRODE -C-D*/)
  201 FORMAT( * SHAPE PARAMETERS;*,5X,*HALF-WIDTH (0A) =*,F12.4,/
     1,27X,*LENGTH (AB) =*,F12.4,/
     1,27X,*HEIGHT (BC) =*,F12.4,/
     1,25X,*GAP (CD)-(AB) =*,F12.4,/)
  400 FORMAT(//,* CALCULATION OF Z-DOMAIN PARAMETERS FROM T-DOMAIN PARAM
     1ETERS*,/* NATMAX=*I8,/)
  210 FORMAT( /* PARAMETERS IN T-DOMAIN*/ * AT=*E18.9,12X,F18.6
     1   /* BT=*E18.9,12X,F18.6
     2   /* CT=*E18.9,12X,F18.6
     3   /* DT=*E18.9,12X,F18.6)
  205 FORMAT( /* PARAMETERS IN Z-DOMAIN*/ * AZ=*2E12.5,6X,2F12.6
     1   /* BZ=*2E12.5,6X,2F12.6
     2   /* CZ=*2E12.5,6X,2F12.6
     3   /* DZ=*2E12.5,6X,2F12.6)
  300 FORMAT( * CONVERGENCE NOT ACHIEVED IN*, I4,* ITERATIONS*)
  301 FORMAT( * CONVERGENCE ACHIEVED IN*, I4,* ITERATIONS*)
  801 FORMAT( * CURRENT DISTRIBUTION ALONG ELECTRODE CD*)
  802 FORMAT( * CURRENT DISTRIBUTION ALONG ELECTRODE AB*)
  803 FORMAT( * ASYMPTOTIC CURRENT DISTRIBUTION ALONG ELECTRODE CD*)
  804 FORMAT( * ASYMPTOTIC CURRENT DISTRIBUTION ALONG ELECTRODE AB*)
 1000 FORMAT( * TARGET *, 4E15.6)
 1001 FORMAT( * G, B'S *, 4E15.6)
 1002 FORMAT( / * ICOUNT *, I4)
 1003 FORMAT( * C'S    *, 15X,3E15.6)
 1004 FORMAT( * TOLD'S *, 4E15.6)
 1005 FORMAT( * ZN'S   *, 4E15.6)
```

```
 1007 FORMAT( * NPEG'S *, 20X,3(I5,10X))
      PRINT 200
C
C        MPLOT = 0 ALLOWS PRINTING OF CURRENT DISTRIBUTION WITH LABLED
C           FORMAT.
C        MPLOT = 1 ALLOWS PRINTING OF CURRENT DISTRIBUTION IN UNLABELED
C           FORMAT FOR EASE IN COMPUTER-ASSISTED PLOTTING.
C        MDIST = 0 SUPRESSES CALCULATION OF CURRENT DISTRIBUTION.
C        MDIST = 1 ALLOWS CALCULATION OF CURRENT DISTRIBUTION.
C        MIT   = 0 SUPRESSES PRINTING OF CALCULATED VALUES DURING
C           ITERATION FOR T-PARAMETERS FROM INPUT Z-PARAMETERS.
C        MIT   = 1 ALLOWS PRINTING OF CALCULATED VALUES DURING
C           ITERATION FOR T-PARAMETERS FROM INPUT Z-PARAMETERS.
C        MSCALE = 0 SUPRESSES ADJUSTMENT OF POSITION VARIABLE FOR THE AB
C           ELECTRODE SUCH THAT THE ELECTRODE BEGINS AT 0.
C        MSCALE = 1 ADJUSTS POSITION VARIABLE FOR THE AB ELECTRODE
C           SUCH THAT THE ELECTRODE BEGINS AT A.
C        MASYMP = 0 SUPRESSES PRINTING OF ASYMPTOTIC SOLUTIONS FOR
C           CURRENT DISTRIBUTION.
C        MASYMP = 1 ALLOWS PRINTING OF ASYMPTOTIC SOLUTIONS FOR
C           CURRENT DISTRIBUTION.
C        IMAX     MAXIMUM NUMBER OF ITERATIONS ALLOWED.
C
      READ 100,MPLOT,MDIST,MIT,MSCALE,MASYMP,IMAX
      READ 102,WIDTH,ALNGTH,AHGTH,GAP
      READ 102,ATOLD,BTOLD,CTOLD,DTOLD
      PRINT 201,WIDTH,ALNGTH,AHGTH,GAP
      AZWANT = CMPLX(WIDTH,0.)
      BZWANT = CMPLX(WIDTH,ALNGTH)
      CZWANT = CMPLX(WIDTH+AHGTH,ALNGTH)
      DZWANT = CMPLX(WIDTH+AHGTH,-GAP)
      N=3
      ICOUNT = 0
      AZTG = REAL(AZWANT)
      BZTG = AIMAG(BZWANT)
      CZTG = REAL(CZWANT-BZWANT)
      DZTG = AIMAG(DZWANT-CZWANT)
      IF(MIT.EQ.1) PRINT 1000, AZTG,BZTG,CZTG,DZTG
C
    1 ICOUNT = ICOUNT + 1
      IF(MIT.EQ.1) PRINT 1002,ICOUNT
      IF(MIT.EQ.1) PRINT 1004,ATOLD,BTOLD,CTOLD,DTOLD
      AT = ATOLD
      BT = BTOLD
      CT = CTOLD
      DT = DTOLD
      CALL TRANSZ
      WOVRAZ = WIDTH/AZI
      AZN = WIDTH
      BZN = BZI*WOVRAZ
      CZN = CZI*WOVRAZ
```

```
      DZN = DZI*WOVRAZ
      DELBT = (CT-BT)/100.
      IF((BT-AT).LT.(CT-BT)) DELBT = (BT-AT)/100.
      DELCT = (DT-CT)/100.
      IF((CT-BT).LT.(DT-CT)) DELCT = (CT-BT)/100.
      DELDT = (DT-CT)/100.
      BT = BTOLD + DELBT
      CALL TRANSZ
      WTEMP = WIDTH/AZI
      BZNP1B = BZI*WTEMP
      CZNP1B = CZI*WTEMP
      DZNP1B = DZI*WTEMP
      BT = BTOLD - DELBT
      CALL TRANSZ
      WTEMP = WIDTH/AZI
      BZNM1B = BZI*WTEMP
      CZNM1B = CZI*WTEMP
      DZNM1B = DZI*WTEMP
      BT = BTOLD
      CT = CTOLD + DELCT
      CALL TRANSZ
      WTEMP = WIDTH/AZI
      BZNP1C = BZI*WTEMP
      CZNP1C = CZI*WTEMP
      DZNP1C = DZI*WTEMP
      CT = CTOLD - DELCT
      CALL TRANSZ
      WTEMP = WIDTH/AZI
      BZNM1C = BZI*WTEMP
      CZNM1C = CZI*WTEMP
      DZNM1C = DZI*WTEMP
      CT = CTOLD
      DT = DTOLD + DELDT
      CALL TRANSZ
      WTEMP = WIDTH/AZI
      BZNP1D = BZI*WTEMP
      CZNP1D = CZI*WTEMP
      DZNP1D = DZI*WTEMP
      DT = DTOLD - DELDT
      CALL TRANSZ
      WTEMP = WIDTH/AZI
      BZNM1D = BZI*WTEMP
      CZNM1D = CZI*WTEMP
      DZNM1D = DZI*WTEMP
      DT = DTOLD
C
      DBZDBT = -(BZNM1B - BZNP1B)/DELBT/2.
      DBZDCT = -(BZNM1C - BZNP1C)/DELCT/2.
      DBZDDT = -(BZNM1D - BZNP1D)/DELDT/2.
      DCZDBT = -(CZNM1B - CZNP1B)/DELBT/2.
      DCZDCT = -(CZNM1C - CZNP1C)/DELCT/2.
```

```
      DCZDDT = -(CZNM1D - CZNP1D)/DELDT/2.
      DDZDBT = -(DZNM1B - DZNP1B)/DELBT/2.
      DDZDCT = -(DZNM1C - DZNP1C)/DELCT/2.
      DDZDDT = -(DZNM1D - DZNP1D)/DELDT/2.
C
      G(1) = BZTG - BZN
      B(1,1) = DBZDBT
      B(1,2) = DBZDCT
      B(1,3) = DBZDDT
      G(2) = CZTG - CZN
      B(2,1) = DCZDBT
      B(2,2) = DCZDCT
      B(2,3) = DCZDDT
      G(3) = DZTG - DZN
      B(3,1) = DDZDBT
      B(3,2) = DDZDCT
      B(3,3) = DDZDDT
      IF(MIT.EQ.1) PRINT 1001,(G(L),B(L,1),B(L,2),B(L,3),L=1,3)
C
      CALL SOLVEQ
      IF(MIT.EQ.1) PRINT 1003,(C(K),K=1,3)
         DO 15, K=1,3
   15    NPEG(K) = 0
      IF(C(1).GT.(CT-BT)*0.499) C(1) = (CT-BT)*0.499
      IF(C(1).GT.(CT-BT)*0.499) NPEG(1) = 1
      IF(C(1).LT.-(BT-AT)*0.999) C(1) = -(BT-AT)*0.499
      IF(C(1).LT.-(BT-AT)*0.999) NPEG(1) = 1
      IF(C(2).GT.(DT-CT)*0.499) C(2) = (DT-CT)*0.499
      IF(C(2).GT.(DT-CT)*0.499) NPEG(2) = 1
      IF(C(2).LT.-(CT-BT)*0.499) C(2) = -(CT-BT)*0.499
      IF(C(2).LT.-(CT-BT)*0.499) NPEG(2) = 1
      IF(C(3).GT.DT) C(3) = DT
      IF(C(3).GT.DT) NPEG(3) = 1
      IF(C(3).LT.-(DT-CT)*0.499) C(3) = -(DT-CT)*0.499
      IF(C(3).LT.-(DT-CT)*0.499) NPEG(3) = 1
      IF(MIT.EQ.1) PRINT 1007,(NPEG(K),K=1,3)
      IF(MIT.EQ.1) PRINT 1003,(C(K),K=1,3)
      BTOLD = BTOLD + C(1)
      CTOLD = CTOLD + C(2)
      DTOLD = DTOLD + C(3)
      IF(MIT.EQ.1) PRINT 1005,AZN,BZN,CZN,DZN
C
      IF(ICOUNT.GE.IMAX) GO TO 50
      IF(ICOUNT.GE.IMAX-4) MIT = 1
      IF(ABS(G(1)).GT.1.0E-06) GO TO 1
      IF(ABS(G(2)).GT.1.0E-06) GO TO 1
      IF(ABS(G(3)).GT.1.0E-06) GO TO 1
      PRINT 301,ICOUNT
      GO TO 51
C
   50 PRINT 300,ICOUNT
```

```
 51 AZWDTH = CMPLX(AZN,0.)
    BZWDTH = AZWDTH + CMPLX(0.,BZN)
    CZWDTH = BZWDTH + CMPLX(CZN,0.)
    DZWDTH = CZWDTH + CMPLX(0.,DZN)
    AZ = CMPLX(WIDTH/WOVRAZ,0.)
    BZ = AZ + CMPLX(0.,BZN/WOVRAZ)
    CZ = BZ + CMPLX(CZN/WOVRAZ,0.)
    DZ = CZ + CMPLX(0.,DZN/WOVRAZ)
    BT = BTOLD
    CT = CTOLD
    DT = DTOLD
    PRINT 400,NATSND
    PRINT 210, AT,AT,BT,BT,CT,CT,DT,DT
    PRINT 205, AZ,AZWDTH,BZ,BZWDTH,CZ,CZWDTH,DZ,DZWDTH
    CALL TRANSW
    AZIMAG = AIMAG(AZ)
    BZIMAG = AIMAG(BZ)
    CZIMAG = AIMAG(CZ)
    DZIMAG = AIMAG(DZ)
    IF(MPLOT.EQ.1 .AND. MDIST.EQ.1) PRINT 801
    CALL DISTCD(MDIST,CURCD)
    IF(MSCALE.EQ.1) DZADJ = DZIMAG
    IF(MSCALE.EQ.0) DZADJ = 0.
    IF(MPLOT.EQ.1 .AND. MDIST.EQ.1) PRINT 802
    IF(MDIST.EQ.1) CALL DISTAB(NATSND,DZADJ,CURAB)
    IF(MASYMP.EQ.1 .AND. MDIST.EQ.1) PRINT 803
    IF(MASYMP.EQ.1) CALL ASYMPT(CURCD,AHGTH,ALNGTH+GAP)
    IF(MASYMP.EQ.1 .AND. MDIST.EQ.1) PRINT 804
    IF(MASYMP.EQ.1 .AND. MDIST.EQ.1) CALL ASYMPT(CURAB,AHGTH,ALNGTH)
    STOP
    END



    SUBROUTINE TRANSZ
C
C       ROUTINE FOR CALCULATION OF CONSTANTS IN THE Z-DOMAIN FROM
C       CONSTANTS IN THE T-DOMAIN USING THE SCHWARZ-CHRISTOFFEL
C       TRANSFORMATION.
C
    COMMON/TRANS/ AT,BT,CT,DT,AZI,BZI,CZI,DZI
    COMMON/TRANS2/ NATSND
    NATMAX = 100
    AZI = 0.
    BZI = 0.
    CZI = 0.
    DZI = 0.
  1 NATMAX = NATMAX*2
    IF(NATMAX.GT.6500) PRINT 100,NATMAX/2
    IF(NATMAX.GT.6500) STOP
100 FORMAT( * CONVERGENCE NOT ACHIEVED FOR NATMAX =*, I6,* IN TRANSZ*)
```

```
IF(NATMAX.GT.6500) GO TO 99
AZOLD = AZI
BZOLD = BZI
CZOLD = CZI
DZOLD = DZI
HAT = AT/FLOAT(NATMAX)
HBT = SQRT(BT-AT)/FLOAT(NATMAX)
HCT1 = SQRT((CT-BT)/2.)/FLOAT(NATMAX)
HCT2 = HCT1
HDT1 = SQRT((DT-CT)/2.)/FLOAT(NATMAX)
HDT2 = HDT1
T4A = -HAT
U4B = -HBT
U4C1 = -HCT1
U4C2 = -HCT2
U4D1 = -HDT1
U4D2 = -HDT2
T2A = 0.
U2B = 0.
U2C1 = 0.
U2C2 = 0.
U2D1 = 0.
U2D2 = 0.
SUM4A = 0.
SUM4B = 0.
SUM4C1 = 0.
SUM4C2 = 0.
SUM4D1 = 0.
SUM4D2 = 0.
SUM2A = 0.
SUM2B = 0.
SUM2C1 = 0.
SUM2C2 = 0.
SUM2D1 = 0.
SUM2D2 = 0.
MAX = NATMAX/2-1
   DO 10,N=1,MAX
   T4A = T4A + 2.*HAT
   U4B = U4B + 2.*HBT
   T4B = BT-U4B**2
   U4C1 = U4C1 + 2.*HCT1
   U4C2 = U4C2 + 2.*HCT2
   T4C1 = BT+U4C1**2
   T4C2 = CT-U4C2**2
   U4D1 = U4D1 + 2.*HDT1
   U4D2 = U4D2 + 2.*HDT2
   T4D1 = CT+U4D1**2
   T4D2 = DT-U4D2**2
   T2A = T2A + 2.*HAT
   U2B = U2B + 2.*HBT
   T2B = BT-U2B**2
```

```
      U2C1 = U2C1 + 2.*HCT1
      U2C2 = U2C2 + 2.*HCT2
      T2C1 = BT+U2C1**2
      T2C2 = CT-U2C2**2
      U2D1 = U2D1 + 2.*HDT1
      U2D2 = U2D2 + 2.*HDT2
      T2D1 = CT+U2D1**2
      T2D2 = DT-U2D2**2
      SUM4A = SUM4A + FA(T4A)
      SUM4B = SUM4B + FB(T4B)*2.
      SUM4C1 = SUM4C1 + 2.*FB(T4C1)
      SUM4C2 = SUM4C2 + 2.*FC(T4C2)
      SUM4D1 = SUM4D1 - 2.*FC(T4D1)
      SUM4D2 = SUM4D2 + 2.*FD(T4D2)
      SUM2A = SUM2A + FA(T2A)
      SUM2B = SUM2B + FB(T2B)*2.
      SUM2C1 = SUM2C1 + 2.*FB(T2C1)
      SUM2C2 = SUM2C2 + 2.*FC(T2C2)
      SUM2D1 = SUM2D1 - 2.*FC(T2D1)
      SUM2D2 = SUM2D2 + 2.*FD(T2D2)
10    CONTINUE
     AZI = HAT/3.*(FA(0.) + 4.*(SUM4A+FA(T4A+2.*HAT)) + 2.*SUM2A)
     BZI = HBT/3.*(2.*FB(BT) + 4.*(SUM4B+2.*FB(BT-(U4B+2.*HBT)**2))
    1    + 2.*SUM2B + 2.*FB(AT))
     CZI = HCT1/3.*(2.*FB(BT) + 4.*(SUM4C1+2.*FB(BT+(U4C1+2.*HCT1)**2))
    1    + 2.*SUM2C1 + 2.*FB((BT+CT)/2.))
    2    + HCT2/3.*(2.*FC(CT) + 4.*(SUM4C2+2.*FC(CT-(U4C2+2.*HCT2)**2))
    3    + 2.*SUM2C2 + 2.*FC((BT+CT)/2.))
     DZI = HDT1/3.*(-2.*FC(CT)+4.*(SUM4D1-2.*FC(CT+(U4D1+2.*HDT1)**2))
    1    + 2.*SUM2D1 - 2.*FC((CT+DT)/2.))
    2    + HDT2/3.*(2.*FD(DT) + 4.*(SUM4D2+2.*FD(DT-(U4D2+2.*HDT2)**2))
    3    + 2.*SUM2D2 + 2.*FD((CT+DT)/2.))
     IF(ABS((AZOLD-AZI)/AZI).GT.1.0E-04) GO TO 1
     IF(ABS((BZOLD-BZI)/BZI).GT.1.0E-04) GO TO 1
     IF(ABS((CZOLD-CZI)/CZI).GT.1.0E-04) GO TO 1
     IF(ABS((DZOLD-DZI)/DZI).GT.1.0E-04) GO TO 1
99   NATSND = NATMAX
     RETURN
     END

     FUNCTION FA(T)
     COMMON/TRANS/ AT,BT,CT,DT,AZI,BZI,CZI,DZI
     IF(T.EQ.AT) GO TO 5
     FA = SQRT(AT*AT-T*T)/SQRT(BT*BT-T*T)/SQRT(CT*CT-T*T)/
    1    SQRT(DT*DT-T*T)
     RETURN
   5 FA = 0.
     RETURN
     END
```

```
      FUNCTION FB(T)
      COMMON/TRANS/ AT,BT,CT,DT,AZI,BZI,CZI,DZI
      IF(T.EQ.AT) GO TO 5
      FB = SQRT(T*T-AT*AT)/SQRT(BT+T)/SQRT(CT*CT-T*T)/SQRT(DT*DT-T*T)
      RETURN
    5 FB = 0.
      RETURN
      END


      FUNCTION FC(T)
      COMMON/TRANS/ AT,BT,CT,DT,AZI,BZI,CZI,DZI
      IF(T.EQ.AT) GO TO 5
      FC = SQRT(T*T-AT*AT)/SQRT(T*T-BT*BT)/SQRT(CT+T)/SQRT(DT*DT-T*T)
      RETURN
    5 FC = 0.
      RETURN
      END


      FUNCTION FD(T)
      COMMON/TRANS/ AT,BT,CT,DT,AZI,BZI,CZI,DZI
      IF(T.EQ.AT) GO TO 5
      FD = -SQRT(T*T-AT*AT)/SQRT(T*T-BT*BT)/SQRT(T*T-CT*CT)/SQRT(DT+T)
      RETURN
    5 FD = 0.
      RETURN
      END


      SUBROUTINE TRANSW
C
C         ROUTINE FOR CALCULATION OF GEOMETRIC RESISTANCE FOR THE
C         RECTANGULAR CELL IN THE W-DOMAIN FROM CONSTANTS IN THE
C         T-DOMAIN USING THE SCHWARZ-CHRISTOFFEL TRANSFORMATION.
C
      COMMON/TRANS/ AT,BT,CT,DT,AZI,BZI,CZI,DZI
      COMMON/WMAX/ WIMAX
      COMPLEX AZ,BZ,CZ,DZ
  400 FORMAT(//,* CALCULATION OF W-DOMAIN EFFECTIVE RESISTANCE FROM T-DO
     1MAIN PARAMETERS*,/* NATMAX=*I8,/)
C 202 FORMAT( * N=*I3,* T4C1=*E11.5* T2C1=*E11.5* SUM4C1=*E11.5
C    1   * SUM2C1=*E11.5)
C 203 FORMAT( 6X,* T4C2=*E11.5* T2C2=*E11.5* SUM4C2=*E11.5
C    1   * SUM2C2=*E11.5)
  210 FORMAT( /* PARAMETERS IN T-DOMAIN*/ * WIMAX=*E12.5,18X,F12.6)
      NATMAX = 10
      WIMAX = 0.
```

```
    1 NATMAX = NATMAX*2
      WOLD = WIMAX
      HCT1 = SQRT((CT+AT)/2.)/FLOAT(NATMAX)
      HCT2 = HCT1
      U4C1 = -HCT1
      U4C2 = -HCT2
      U2C1 = 0.
      U2C2 = 0.
      SUM4C1 = 0.
      SUM4C2 = 0.
      SUM2C1 = 0.
      SUM2C2 = 0.
      MAX = NATMAX/2-1
         DO 10,N=1,MAX
         U4C1 = U4C1 + 2.*HCT1
         U4C2 = U4C2 + 2.*HCT2
         T4C1 = -CT+U4C1**2
         T4C2 = AT-U4C2**2
         U2C1 = U2C1 + 2.*HCT1
         U2C2 = U2C2 + 2.*HCT2
         T2C1 = -CT+U2C1**2
         T2C2 = AT-U2C2**2
         SUM4C1 = SUM4C1 + 2.*FBW(T4C1)
         SUM4C2 = SUM4C2 + 2.*FCW(T4C2)
         SUM2C1 = SUM2C1 + 2.*FBW(T2C1)
         SUM2C2 = SUM2C2 + 2.*FCW(T2C2)
C        PRINT 202,N,T4C1,T2C1,SUM4C1,SUM2C1
C        PRINT 203,T4C2,T2C2,SUM4C2,SUM2C2
   10    CONTINUE
      WIMAX = HCT1/3.*(2.*FBW(-CT) +
     1   4.*(SUM4C1+2.*FBW(-CT+(U4C1+2.*HCT1)**2)) + 2.*SUM2C1 +
     2   2.*FBW((AT-CT)/2.)) + HCT2/3.*(2.*FCW(AT) +
     3   4.*(SUM4C2+2.*FCW(AT-(U4C2+2.*HCT2)**2)) + 2.*SUM2C2 +
     4   2.*FCW((AT-CT)/2.))
      IF(ABS((WOLD-WIMAX)/WIMAX).GT.1.0E-04) GO TO 1

      PRINT 400,NATMAX
      PRINT 210, WIMAX,WIMAX
      RETURN
      END



      FUNCTION FBW(T)
      COMMON/TRANS/ AT,BT,CT,DT,AZI,BZI,CZI,DZI
      FBW =  1./SQRT(AT-T)/SQRT(BT-T)/SQRT(DT+T)
      RETURN
      END
```

```
      FUNCTION FCW(T)
      COMMON/TRANS/ AT,BT,CT,DT,AZI,BZI,CZI,DZI
      FCW = 1./SQRT(BT-T)/SQRT(DT+T)/SQRT(CT+T)
      RETURN
      END



      SUBROUTINE DISTAB(NATSND,DZADJ,CURAB)
C
C         ROUTINE FOR CALCULATION OF CURRENT DISTRIBUTION AT THE
C         ELECTRODE AZ-BZ.
C
      COMMON/TRANS/ AT,BT,CT,DT,AZI,BZI,CZI,DZI
      COMMON/WMAX/ WIMAX
      COMMON/CURR/ AZIMAG,BZIMAG,CZIMAG,DZIMAG,SUMAB,RESCD,MPLOT,WOVRAZ
  198 FORMAT( 2(3X,E13.5),10X,*INF*)
  199 FORMAT( 10X,*T*,15X,*Z*,13X,*CURRENT*)
  201 FORMAT( 3(3X,E13.5))
  400 FORMAT(//,* CALCULATION OF CURRENT DISTRIBUTION ALONG THE ELECTROD
     1E A-B*,/* NATMAX=*I8)
  600 FORMAT( I4)
  620 FORMAT( 2E15.7)
      NATMAX = 800
      IF(NATSND.GT.1600) NATMAX = NATSND/2
      IF(MPLOT.EQ.0) PRINT 400,NATMAX
      IF(MPLOT.EQ.1) PRINT 600,(2*NATMAX+1)
      HBT = ((BT-AT)/2.)**(1.5)/FLOAT(NATMAX)
      CURAVG = SUMAB/(BZIMAG-AZIMAG)
      TNM2 = AT
      UNM1 = HBT
      UN = 2.*HBT
      TNM1 = UNM1**(2./3.) + AT
      TN = UN**(2./3.) + AT
      ZNM2 = 0.
      ZNM1 = ZNM2 + HBT/9.*(FAT(TNM2)+4.*FAT((TNM2+TNM1)/2.)+FAT(TNM1))
      ZN = ZNM2 + 2.*HBT/9.*(FAT(TNM2)+4.*FAT(TNM1)+FAT(TN))
      CURNM1 = 1./WIMAX*SQRT(BT+TNM1)*SQRT(CT-TNM1)*SQRT(DT-TNM1)
     1   /(TNM1-AT)/SQRT(AT+TNM1)/CURAVG
      CURN = 1./WIMAX*SQRT(BT+TN)*SQRT(CT-TN)*SQRT(DT-TN)
     1   /(TN-AT)/SQRT(AT+TN)/CURAVG
      IF(MPLOT.EQ.0) PRINT 199
      IF(MPLOT.EQ.0) PRINT 198,TNM2,ZNM2
      IF(MPLOT.EQ.1) PRINT 620,(ZNM2-DZADJ)*WOVRAZ,1.0E+20
      IF(MPLOT.EQ.0) PRINT 201,TNM1,ZNM1,CURNM1
      IF(MPLOT.EQ.0) PRINT 201,TN,ZN,CURN
      IF(MPLOT.EQ.1) PRINT 620,(ZNM1-DZADJ)*WOVRAZ,CURNM1
      IF(MPLOT.EQ.1) PRINT 620,(ZN-DZADJ)*WOVRAZ,CURN
      MAX = NATMAX/2-1
```

```
      DO 10,N=1,MAX
      TNM2 = TN
      TNM3 = TNM1
      UNM1 = UNM1 + 2.*HBT
      UN = UN + 2.*HBT
      TNM1 = UNM1**(2./3.) + AT
      TN = UN**(2./3.) + AT
      ZNM2 = ZN
      ZNM3 = ZNM1
      ZNM1 = ZNM3 + 2.*HBT/9.*(FAT(TNM3)+4.*FAT(TNM2)+FAT(TNM1))
      ZN = ZNM2 + 2.*HBT/9.*(FAT(TNM2)+4.*FAT(TNM1)+FAT(TN))
      CURNM1 = 1./WIMAX*SQRT(BT+TNM1)*SQRT(CT-TNM1)*SQRT(DT-TNM1)
     1    /(TNM1-AT)/SQRT(AT+TNM1)/CURAVG
      CURN = 1./WIMAX*SQRT(BT+TN)*SQRT(CT-TN)*SQRT(DT-TN)
     1    /(TN-AT)/SQRT(AT+TN)/CURAVG
      IF(MPLOT.EQ.0) PRINT 201,TNM1,ZNM1,CURNM1
      IF(MPLOT.EQ.0) PRINT 201,TN,ZN,CURN
      IF(MPLOT.EQ.1) PRINT 620,(ZNM1-DZADJ)*WOVRAZ,CURNM1
      IF(MPLOT.EQ.1) PRINT 620,(ZN-DZADJ)*WOVRAZ,CURN
10    CONTINUE
   HBT = SQRT((BT-AT)/2.)/FLOAT(NATMAX)
   TNM2 = TN
   UNM1 = SQRT((BT-AT)/2.) - HBT
   UN = UNM1 - HBT
   TNM1 = BT-UNM1**2
   TN = BT-UN**2
   ZNM2 = ZN
   ZNM1 = ZNM2 + HBT/3.*(FB(TNM2)+4.*FB((TNM2+TNM1)/2.)+FB(TNM1))
   ZN = ZNM2 + 2.*HBT/3.*(FB(TNM2)+4.*FB(TNM1)+FB(TN))
   CURNM1 = 1./WIMAX*SQRT(BT+TNM1)*SQRT(CT-TNM1)*SQRT(DT-TNM1)
  1   /(TNM1-AT)/SQRT(AT+TNM1)/CURAVG
   CURN = 1./WIMAX*SQRT(BT+TN)*SQRT(CT-TN)*SQRT(DT-TN)
  1   /(TN-AT)/SQRT(AT+TN)/CURAVG
   IF(MPLOT.EQ.0) PRINT 201,TNM1,ZNM1,CURNM1
   IF(MPLOT.EQ.0) PRINT 201,TN,ZN,CURN
   IF(MPLOT.EQ.1) PRINT 620,(ZNM1-DZADJ)*WOVRAZ,CURNM1
   IF(MPLOT.EQ.1) PRINT 620,(ZN-DZADJ)*WOVRAZ,CURN
      DO 20,N=1,MAX
      TNM2 = TN
      TNM3 = TNM1
      UNM1 = UNM1 - 2.*HBT
      UN = UN - 2.*HBT
      TNM1 = BT - UNM1**2
      TN = BT - UN**2
      ZNM2 = ZN
      ZNM3 = ZNM1
      ZNM1 = ZNM3 + 2.*HBT/3.*(FB(TNM3)+4.*FB(TNM2)+FB(TNM1))
      ZN = ZNM2 + 2.*HBT/3.*(FB(TNM2)+4.*FB(TNM1)+FB(TN))
      CURNM1 = 1./WIMAX*SQRT(BT+TNM1)*SQRT(CT-TNM1)*SQRT(DT-TNM1)
     1    /(TNM1-AT)/SQRT(AT+TNM1)/CURAVG
      CURN = 1./WIMAX*SQRT(BT+TN)*SQRT(CT-TN)*SQRT(DT-TN)
```

```
     1       /(TN-AT)/SQRT(AT+TN)/CURAVG
             IF(MPLOT.EQ.0) PRINT 201,TNM1,ZNM1,CURNM1
             IF(MPLOT.EQ.0) PRINT 201,TN,ZN,CURN
             IF(MPLOT.EQ.1) PRINT 620,(ZNM1-DZADJ)*WOVRAZ,CURNM1
             IF(MPLOT.EQ.1) PRINT 620,(ZN-DZADJ)*WOVRAZ,CURN
    20       CONTINUE
C
         CURAB = CURN
         RETURN
         END



         FUNCTION FAT(T)
         COMMON/TRANS/ AT,BT,CT,DT,AZI,BZI,CZI,DZI
         FAT = SQRT(AT+T)/SQRT(BT*BT-T*T)/SQRT(CT*CT-T*T)/
        1   SQRT(DT*DT-T*T)
         RETURN
         END



         SUBROUTINE DISTCD(MDIST,CURCD)
C
C            ROUTINE FOR CALCULATION OF CURRENT DISTRIBUTION, TOTAL
C            CURRENT, AND CELL RESISTANCE AT THE ELECTRODE (-CZ)-(-DZ).
C
         COMMON/TRANS/ AT,BT,CT,DT,AZI,BZI,CZI,DZI
         COMMON/WMAX/ WIMAX
         COMMON/CURR/ AZIMAG,BZIMAG,CZIMAG,DZIMAG,SUMAB,RESCD,MPLOT,WOVRAZ
  220 FORMAT( /* CELL RESISTANCE (EVALUATED AT CD) =*,E13.5,/)
  400 FORMAT(//,* CALCULATION OF CURRENT DISTRIBUTION ALONG THE ELECTROD
     1E (-C)-(-D)*,/* NATMAX=*I8,/)
  600 FORMAT( I4)
  620 FORMAT( 2E15.7)
  198 FORMAT( I4,4(3X,E13.5))
  199 FORMAT( 3X,*N*,10X,*T*,15X,*Z*,13X,*CURRENT*,8X,*INTEGRAL*)
  200 FORMAT( I4,4(3X,E13.5),3X,I4)
  201 FORMAT( 4X,3(3X,E13.5))
  310 FORMAT( * CONVERGENCE NOT ACHIEVED BY *I4* ITERATIONS.*
     1   /* TOLD=* E13.5, *    TNEW=* E13.5)
         NATMAX = 100
         SUMAB = 0.
         CURAVG = 1.
         NPRINT = 0
    1  IF(NPRINT.EQ.0) NATMAX = NATMAX*2
         IF(NATMAX.GT.6500) PRINT 100,NATMAX/2
         IF(NATMAX.GT.6500) STOP
  100 FORMAT( * CONVERGENCE NOT ACHIEVED FOR NATMAX =*, I6,* IN DISTCD*)
         IF(NATMAX.GT.6500) NPRINT = 1
         IF(NPRINT.EQ.1) RESCD = 1./SUMAB
```

```
      IF(NPRINT.EQ.1) PRINT 220, RESCD
      IF(MDIST.EQ.0 .AND. NPRINT.EQ.1) CURCD = CURN
      IF(MDIST.EQ.0 .AND. NPRINT.EQ.1) RETURN
      MSWICH = 0
      MS = 0
      IF(MPLOT.EQ.0 .AND. NPRINT.EQ.1) PRINT 400,NATMAX
      IF(MPLOT.EQ.1 .AND. NPRINT.EQ.1) PRINT 600,NATMAX+1
      MAX = NATMAX/2-1
      SOLD = SUMAB
      HBT = (-CZIMAG+DZIMAG)/FLOAT(NATMAX)
      ZNM2 = 0.
      ZNM1 = HBT
      ZN = 2.*HBT
      TNM2 = -DT
      TNM10 = -DT + (DT-CT)/2000./FLOAT(NATMAX)
      TNO = -DT + (DT-CT)/1000./FLOAT(NATMAX)
         DO 13,K=1,100
         KPR = K
         TNM1 = -DT + ( - 3.*(ZNM1-ZNM2)/(FDT(TNM2)+
     1      4.*FDT((TNM2+TNM10)/2.)+FDT(TNM10)))**2
         TN = -DT + ( - 3.*(ZN-ZNM2)/(FDT(TNM2)+
     1      4.*FDT(TNM1)+FDT(TNO)))**2
         IF(ABS((TN-TNO)/TN).LT.1.0E-10.AND.ABS((TNM1-TNM10)/TNM1)
     1      .LT.1.0E-10) GO TO 14

         TNM10 = TNM1
   13    TNO = TN
      PRINT 310,KPR,TNO,TN
   14 CONTINUE
      SUMAB = HBT/3./WIMAX*(FBCUR2(TN)+4.*FBCUR2(TNM1)
     1   +FBCUR2(TNM2))
      CURNM1 = 1./WIMAX*SQRT(-BT-TNM1)*SQRT(CT-TNM1)*SQRT(DT-TNM1)
     1   /(TNM1-AT)/SQRT(-AT-TNM1)/CURAVG
      CURN = 1./WIMAX*SQRT(-BT-TN)*SQRT(CT-TN)*SQRT(DT-TN)
     1   /(TN-AT)/SQRT(-AT-TN)/CURAVG
      KN=2
      KNOO = 0
      TNOO = -DT
      ZNOO = 0.
      CURNOO = -1./WIMAX*SQRT(DT-BT)*SQRT(CT+DT)*SQRT(DT+DT)
     1   /(DT+AT)/SQRT(DT-AT)/CURAVG
      SUMOO = 0.
      IF(MPLOT.EQ.0 .AND. NPRINT.EQ.1) PRINT 199
      IF(MPLOT.EQ.0 .AND. NPRINT.EQ.1) PRINT 198,KNOO,TNOO,-ZNOO*WOVRAZ
     1   ,CURNOO,SUMOO
      IF(MPLOT.EQ.0 .AND. NPRINT.EQ.1) PRINT 201,TNM1,-ZNM1*WOVRAZ
     1   ,CURNM1
      IF(MPLOT.EQ.0 .AND. NPRINT.EQ.1) PRINT 200,KN,TN,-ZN*WOVRAZ,CURN
     1   ,SUMAB,KPR
      IF(MPLOT.EQ.1 .AND. NPRINT.EQ.1) PRINT 620,-ZNOO*WOVRAZ,CURNOO
      IF(MPLOT.EQ.1 .AND. NPRINT.EQ.1) PRINT 620,-ZNM1*WOVRAZ,CURNM1
```

```
      IF(MPLOT.EQ.1 .AND. NPRINT.EQ.1) PRINT 620,-ZN*WOVRAZ,CURN
         DO 20,N=1,MAX
         KN = 2*(N+1)
         ZNM2 = ZN
         ZNM3 = ZNM1
         ZNM1 = ZNM1 + 2.*HBT
         ZN = ZN + 2.*HBT
         TNM2 = TN
         TNM3 = TNM1
         TNO = TN + (DT-CT)/1000./FLOAT(NATMAX)
         TNM10 = TNM1 + (DT-CT)/1000./FLOAT(NATMAX)
            DO 15,K=1,100
            KPR = K
            IF(TNM2.GT.((-DT-CT)/2.)) GO TO 12
            TNM1 = -DT + (SQRT(DT+TNM3) - 3.*(ZNM1-ZNM3)/(FDT(TNM3)+
     1         4.*FDT(TNM2)+FDT(TNM10)))**2
            TN = -DT + (SQRT(DT+TNM2) - 3.*(ZN-ZNM2)/(FDT(TNM2)+
     1         4.*FDT(TNM1)+FDT(TNO)))**2
            GO TO 9
   12       IF(MSWICH.EQ.0) TNM1=-CT-(SQRT(-CT-TNM2) + 3.*(ZNM1-ZNM2)
     1         /(FCT(TNM2)+4.*FCT((TNM2+TNM10)/2.)+FCT(TNM10)))**2
            IF(MSWICH.EQ.0) GO TO 19
            TNM1 = -CT - (SQRT(-CT-TNM3) + 3.*(ZNM1-ZNM3)/(FCT(TNM3)+
     1         4.*FCT(TNM2)+FCT(TNM10)))**2
   19       TN = -CT - (SQRT(-CT-TNM2) + 3.*(ZN-ZNM2)/(FCT(TNM2)+
     1         4.*FCT(TNM1)+FCT(TNO)))**2
            MS = 1
    9       IF(ABS((TN-TNO)/TN).LT.1.0E-10.AND.ABS((TNM1-TNM10)/TNM1)
     1         .LT.1.0E-10) GO TO 16
            TNM10 = TNM1
   15       TNO = TN
         PRINT 310,KPR,TNO,TN
   16    CONTINUE
         IF(MS.EQ.1) MSWICH = 1
         SUMAB = SUMAB + HBT/3./WIMAX*
     1      (FBCUR2(TN)+4.*FBCUR2(TNM1)+FBCUR2(TNM2))
         CURNM1 = 1./WIMAX*SQRT(-BT-TNM1)*SQRT(CT-TNM1)*SQRT(DT-TNM1)
     1      /(TNM1-AT)/SQRT(-AT-TNM1)/CURAVG
         CURN = 1./WIMAX*SQRT(-BT-TN)*SQRT(CT-TN)*SQRT(DT-TN)
     1      /(TN-AT)/SQRT(-AT-TN)/CURAVG
         IF(MPLOT.EQ.0 .AND. NPRINT.EQ.1) PRINT 201,TNM1,-ZNM1*WOVRAZ
     1      ,CURNM1
         IF(MPLOT.EQ.0 .AND. NPRINT.EQ.1) PRINT 200,KN,TN,-ZN*WOVRAZ
     1      ,CURN,SUMAB
     1      ,KPR
         IF(MPLOT.EQ.1.AND.NPRINT.EQ.1) PRINT 620,-ZNM1*WOVRAZ,CURNM1
         IF(MPLOT.EQ.1 .AND. NPRINT.EQ.1) PRINT 620,-ZN*WOVRAZ,CURN
   20    CONTINUE
C
      IF(NPRINT.EQ.1) GO TO 2
      IF(ABS((SOLD-SUMAB)/SUMAB).LT.1.0E-04) NPRINT = 1
```

```
      CURAVG = SUMAB/(DZIMAG-CZIMAG)
      GO TO 1
    2 CURCD = CURN
      RETURN
      END



      FUNCTION FBCUR2(T)
      COMMON/TRANS/ AT,BT,CT,DT,AZI,BZI,CZI,DZI
      IF(T.LT.AT) GO TO 5
      FBCUR2 = SQRT(BT+T)*SQRT(CT-T)*SQRT(DT-T)/(T-AT)/SQRT(AT+T)
      RETURN
    5 FBCUR2 = SQRT(-BT-T)*SQRT(CT-T)*SQRT(DT-T)/(T-AT)/SQRT(-AT-T)
      RETURN
      END



      FUNCTION FDT(T)
      COMMON/TRANS/ AT,BT,CT,DT,AZI,BZI,CZI,DZI
      IF(T.EQ.AT) GO TO 5
      FDT = SQRT(-AT*AT+T*T)/SQRT(-BT*BT+T*T)/SQRT(-CT*CT+T*T)/
     1   SQRT(DT-T)
      RETURN
    5 FDT = 0.
      RETURN
      END



      FUNCTION FCT(T)
      COMMON/TRANS/ AT,BT,CT,DT,AZI,BZI,CZI,DZI
      IF(T.EQ.AT) GO TO 5
      FCT = SQRT(-AT*AT+T*T)/SQRT(-BT*BT+T*T)/SQRT(DT*DT-T*T)/
     1   SQRT(CT-T)
      RETURN
    5 FCT = 0.
      RETURN
      END



      SUBROUTINE SOLVEQ
      COMMON N,B(3,4),C(3),G(3)
  100 FORMAT( * PIVOT IS TOO SMALL. PIVOT =*,E12.5)
          DO 5 K=1,N
    5     B(K,N+1)=G(K)
      K=1
      NP1=N+1
          DO 70 IROW=1,N
```

```
      K=K+1
      ISWAP=IROW
      IF(K.GT.N) GO TO 51
         DO 50 IN=K,N
         IF(ABS(B(ISWAP,IROW))-ABS(B(IN,IROW)).GE.0.) GO TO 50
         ISWAP=IN
 50      CONTINUE
 51   CONTINUE
      IF(ISWAP.EQ.IROW) GO TO 99
         DO 92 J=1,NP1
         TEMP=B(IROW,J)
         B(IROW,J)=B(ISWAP,J)
 92      B(ISWAP,J)=TEMP
 99   PIVOT=B(IROW,IROW)
      IF(ABS(PIVOT)-1.0E-12) 27,27,28
 27   PRINT 100,PIVOT
      STOP
 28      DO 10 J=1,NP1
 10      B(IROW,J)=B(IROW,J)/PIVOT
         DO 20 I=1,N
         IF(I.EQ.IROW) GO TO 20
         RATIO=B(I,IROW)
            DO 18 J=1,NP1
 18         B(I,J)=B(I,J)-B(IROW,J)*RATIO
 20      CONTINUE
 70   CONTINUE
      DO 72, K=1,N
 72   C(K)=B(K,N+1)
   RETURN
   END



   SUBROUTINE ASYMPT(CURZMX,ZIMAX,ZRMAX)
600 FORMAT( I4)
620 FORMAT( 2E15.7)
   PI = 3.14159265358979
   NMAX = 200
   ANU = PI/2./ZIMAX
   PRINT 600, NMAX
   DELZR = ZRMAX/(NMAX-1)
   ZR = -DELZR
      DO 10 K=1,NMAX
      ZR = ZR + DELZR
      VAR = ANU*(ZR-ZRMAX)
      CURDST = CURZMX*(EXP(VAR)+EXP(-VAR))/2.
 10   PRINT 620,ZR,CURDST
   RETURN
   END
```

```
 0   0   0   0   0 40
1.000e-06 1.500e+01 3.000e+01 5.000e+00
1.000e+00 1.958e+03 1.960e+03 2.027e+03
```

CALCULATION OF PRIMARY CURRENT DISTRIBUTION AND CELL RESISTANCE
FOR A SYSTEM OF THE GENERAL SHAPE;

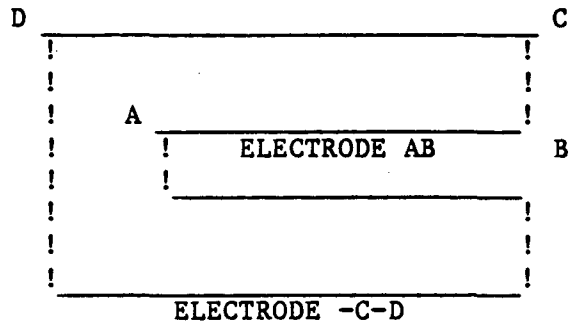

SHAPE PARAMETERS; HALF-WIDTH (0A) = .0000
LENGTH (AB) = 15.0000
HEIGHT (BC) = 30.0000
GAP (CD)-(AB) = 5.0000

CONVERGENCE ACHIEVED IN 8 ITERATIONS

CALCULATION OF Z-DOMAIN PARAMETERS FROM T-DOMAIN PARAMETERS
NATMAX= 400

PARAMETERS IN T-DOMAIN

AT=	.100000000E+01	1.000000
BT=	.188013153E+04	1880.131532
CT=	.202461487E+04	2024.614874
DT=	.204604066E+04	2046.040661

PARAMETERS IN Z-DOMAIN

AZ=	.10084E-09	0.	.000001	0.
BZ=	.10084E-09	.15126E-02	.000001	15.000000
CZ=	.30252E-02	.15126E-02	30.000001	15.000000
DZ=	.30252E-02	-.50420E-03	30.000001	-5.000000

CALCULATION OF W-DOMAIN EFFECTIVE RESISTANCE FROM T-DOMAIN PARAMETERS
NATMAX= 40

PARAMETERS IN T-DOMAIN

WIMAX=	.28548E-02	.002855

CELL RESISTANCE (EVALUATED AT CD) = .25659E+01

This report was done with support from the Department of Energy. Any conclusions or opinions expressed in this report represent solely those of the author(s) and not necessarily those of The Regents of the University of California, the Lawrence Berkeley Laboratory or the Department of Energy.

Reference to a company or product name does not imply approval or recommendation of the product by the University of California or the U.S. Department of Energy to the exclusion of others that may be suitable.

TECHNICAL INFORMATION DEPARTMENT
LAWRENCE BERKELEY LABORATORY
UNIVERSITY OF CALIFORNIA
BERKELEY, CALIFORNIA 94720